TRANSPORTATION RESEARCH
RECORD

No. 1482

Pavement Design, Management, and Performance

Pavement Design and Analysis

A peer-reviewed publication of the Transportation Research Board

TRANSPORTATION RESEARCH BOARD
NATIONAL RESEARCH COUNCIL

NATIONAL ACADEMY PRESS
WASHINGTON, D.C. 1995

Transportation Research Record 1482
ISSN 0361-1981
ISBN 0-309-06120-2
Price: $30.00

Subscriber Category
IIB pavement design, management, and performance

Printed in the United States of America

Sponsorship of Transportation Research Record 1482

GROUP 2—DESIGN AND CONSTRUCTION OF TRANSPORTATION FACILITIES
Chairman: Michael G. Katona, U.S. Air Force Armstrong Laboratory

Pavement Management Section
Chairman: Albert J. Bush III, U.S. Army Corps of Engineers Waterways Experiment Station

Committee on Rigid Pavement Design
Chairman: Gary Wayne Sharpe, Kentucky Transportation Cabinet
Don R. Alexander, Mark W. Bintlzer, Brian T. Bock, Larry J. Buttler, Lawrence W. Cole, Judith B. Corley-Lay, Kathleen T. Hall, John E. Hunt, Anastasios M. Ioannides, Walter P. Kilareski, Starr D. Kohn, Roger M. Larson, Jo A. Lary, Brian R. McWaters, Theodore L. Neff, William Albert Nokes, Mauricio R. Poblete, Robert J. Risser, Jr., Wayne J. Seiler, Mark B. Snyder, Shiraz D. Tayabji, Mang Tia, John P. Zaniewski, Dan G. Zollinger

Committee on Flexible Pavement Design
Chairman: Newton C. Jackson
Secretary: Stephen B. Seeds, Nichols Consulting Engineers
Uno Arebratt, Gilbert Y. Baladi, Elton R. Brown, Stephen F. Brown, George R. Cochran, N. F. Coetzee, Judith B. Corley-Lay, Jean Francois Corte, Raymond A. Forsyth, W. Charles Greer, Jr., Jerry J. Hajek, John P. Hallin, R. Gary Hicks, Richard W. May, Kenneth H. McGhee, Brian R. McWaters, William Albert Nokes, Cesar A. V. Queiroz, Lutfi Raad, Cheryl Allen Richter, F. Chris Rust, Peter Sebaaly, Gary Wayne Sharpe

Transportation Research Board Staff
Robert E. Spicher, Director, Technical Activities
D. W. Dearasaugh, Engineer of Design
Nancy A. Ackerman, Director, Reports and Editorial Services

Sponsorship is indicated by a footnote at the end of each paper. The organizational units, officers, and members are as of December 31, 1994.

Transportation Research Record 1482

Contents

Foreword v

Faulting Performance Modeling for Undoweled Plain Concrete Pavements 1
Khaled Ksaibati and Rick Staigle

Nationwide Field Investigation of Continuously Reinforced Concrete Pavements 7
Shiraz D. Tayabji, Peter J. Stephanos, and Dan G. Zollinger

Estimating Load Transfer From Measured Joint Efficiency in Concrete Pavements 19
Yu T. Chou

Three-Dimensional Finite-Element Analysis of Jointed Concrete Pavement With Discontinuities 26
Waheed Uddin, Robert M. Hackett, Ajith Joseph, Zhou Pan, and Alfred B. Crawley

Pavement–Falling Weight Deflectometer Interaction Using Dynamic Finite-Element Analysis 33
S. Nazarian and K. M. Boddapati

Viscoelastic Analysis of Hot Mix Asphalt Pavement Structures 44
G. M. Rowe, S. F. Brown, M. J. Sharrock, and M. G. Bouldin

DIPLOMAT: Analysis Program for Bituminous and Concrete Pavements 52
Lev Khazanovich and Anastasios M. Ioannides

Analytical Procedures in Nondestructive Testing Pavement Evaluation 61
Per Ullidtz and N. F. Coetzee

General Axle Load Equivalency Factors 67
Jerry J. Hajek

Accelerated Dynamic Loading of Flexible Pavements at the Canterbury Accelerated Pavement Testing Indoor Facility 79
Bryan D. Pidwerbesky

Strain Response and Performance of Subgrades and Flexible Pavements Under Various Loading Conditions 87
Bryan D. Pidwerbesky

Comparison of AASHTO and ROADHOG Flexible Pavement Overlay Design Procedures 94
Kevin D. Hall and Quintin B. Watkins

Inverted Flexible Pavement Response and Performance 102
Erol Tutumluer and Richard D. Barksdale

Sensitivity Analysis of Input Parameters for Pavement Design and Reliability 111
Brian M. Killingsworth and Dan G. Zollinger

Assessment of Computer Programs for Analysis of Flexible Pavement Structure 123
Dar-Hao Chen, Musharraf Zaman, Joakim Laguros, and Alan Soltani

Foreword

The 15 papers in this volume were peer-reviewed by two TRB committees. The first 4 are sponsored by the Committee on Rigid Pavement Design, and the final 11 were reviewed by the Committee on Flexible Pavement Design. Most of the papers were presented at the 1995 TRB Annual Meeting during three sessions sponsored by the respective committees.

Ksaibati and Staigle discuss the development of a statistical model to predict faulting generated from actual field performance of numerous undoweled plain concrete pavement test sections. Tayabji et al. present key findings from a field investigation of continuously reinforced concrete pavements throughout the United States. Chou recommends that the relationship between joint efficiency and load transfer for jointed plain concrete pavements be based on the ratio of the concrete slab size to the radius of relative stiffness. Uddin et al. study the effects of discontinuities on deflection response of jointed nonreinforced concrete pavements through the use of the three-dimensional finite-element model, ABAQUS.

Nazarian and Boddapati use a finite-element program to investigate the significance of nonuniform pressure distribution and the dynamic effects from the use of a falling weight deflectometer for pavement evaluation. Rowe et al. present a method for predicting fatigue cracking and permanent deformation of flexible\ pavements involving dissipated energy fatigue criterion based on viscoelastic materials characterization. Khazanovich and Ioannides introduce a new computer program to analyze both flexible and rigid pavements using layered elastic theory extended to multilayered systems incorporating elastic plates and spring beds in addition to isotropic layers. Ullidtz and Coetzee provide an overview of pavement evaluation using nondestructive testing with emphasis on problems encountered and critical issues in connection with validation of backcalculation results. Hajek proposes general axle load equivalency factors for pavement design that are independent of pavement-related variables and axle configurations. Piderbesky is the author of two papers relating to research efforts on mostly thin-surfaced unbound granular pavements in New Zealand. The first paper described the development of an indoor accelerated pavement testing facility and presents results therefrom. The second paper discusses pavement response and performance, noting that measured resilient strains can be significantly higher than those predicted by flexible pavement design models. Hall and Watkins compare the ROADHOG flexible pavement overlay design procedure with that presented in the *AASHTO Guide for Design of Pavement Structures*, 1993. Tutumluer and Barksdale report on laboratory testing of inverted flexible pavements consisting of an unstabilized crushed stone layer between a lower cement stabilized base and an upper asphalt concrete surfacing. Killingsworth and Zollinger conduct a sensitivity analysis of various input parameters on the resulting pavement design and the level of reliability. Chen et al. compare five computer programs for flexible pavement design and analysis, report results, and suggest the program they consider most appropriate for routine structural analysis.

Faulting Performance Modeling for Undoweled Plain Concrete Pavements

KHALED KSAIBATI AND RICK STAIGLE

Data on factors causing faulting in undoweled plain concrete pavements were collected. A large number of concrete pavement test sections located in southern Wyoming were included in the experiment. Extensive field data were collected on all test sections. These data included faulting over a 4-year period, traffic applications, construction information, annual precipitation, and drainage conditions. The most important factors causing faulting were identified and a statistical model with high R^2 was then generated to predict faulting.

Joints in concrete pavements are susceptible to different distress types and severities. Among these distresses are faulting, spalling, and corner cracking along joints. These distresses occur even though pavement sections are designed according to standard practices and conventional codes. Eventually joint repairs are necessary, which are a costly procedure that accounts for a major portion of rehabilitation contracts.

There are two main types of joints in portland concrete cement (PCC) pavements: doweled and undoweled. The main difference between these two joints is the method used in transferring the load of a moving vehicle from one slab to the next. Doweled joints transfer the loading through the dowels, which provides a smooth transfer (*1*). Undoweled joints transfer the loadings through the aggregate interlock (*2*). The type of joint will influence the amount of joint faulting.

Faulting is defined as the difference in elevation across a joint (*3*). Faulting is a nuisance to the driving public because it can set up a resonance in the vehicle, which leads to driver discomfort (*4*). It is generally recognized that accumulated equivalent single-axle loads (ESALs) are the most important factor in predicting the rate and amount of faulting on a specific project. Other factors that are commonly used to predict faulting are

- Environmental factors,
- Average joint width,
- Edge support,
- Subgrade soil classification, and
- Presence of positive drainage.

The following faulting performance model was recently developed for undoweled joints by Ioannides et al. (*1*):

$$\text{Fault} = \text{ESAL}^{0.3157}[0.4531 + 0.3367\omega^{0.3322} - 0.5376(100\,\delta_c)^{-0.008437} + 0.0009092\,FI^{0.5998} + 0.004654\,\text{ERODF} - 0.03608\,\text{EDGESUP} - 0.01087\,\text{SOILCRS} - 0.009467\,\text{DRAIN}]$$

statistics: $R^2 = 0.55$

where

ESAL = cumulative 18-kip equivalent single-axle load applications,
ω = width of joint opening,
δ_c = Westergaard corner deflection,
FI = mean air-freezing index,
ERODF = erodibility factors for the base and subbase material from 2.5 for granular material to 0.5 for lean concrete,
EDGESUP = numerical indicator of type of edge support (e.g., 0, if no support exists, and 1, if edge beam/tied shoulder exists),
SOILCRS = numerical indicator of AASHTO subgrade soil classification (e.g., 0, if A-4 to A-7, and 1, if A-1 to A-3), and
DRAIN = numerical indicator of drainage provided (e.g., 0, if no edge subdrains exist, and 1, if edge subdrains exist).

This formula was developed on the basis of faulting data collected from several states with different construction practices.

In this research project, conducted by the University of Wyoming and the Wyoming Department of Transportation (DOT), faulting of undoweled concrete pavements with similar characteristics was monitored over several years. Performance faulting models were later developed to predict faulting based on traffic level, subdrainage characteristics, and pavement thickness.

DESIGN OF EXPERIMENT

Figure 1 presents a summary of the data collection and overall analysis strategies followed. All test sections included in the experiment were located on I-80 in Wyoming. Faulting and other relevant data were collected on all test sections between 1989 and 1993. All data were later summarized in a computerized data base. Performance models were then developed to predict pavement faulting.

CHARACTERISTICS OF TEST SECTIONS

Table 1 shows general information on all test sections. These data include the beginning and ending milepost for each project, the construction date, and the thicknesses of concrete layers.

Interstate 80 traverses Wyoming on an east-west axis across the southern end of the state. There are slightly over 644 centerline km on Interstate 80. Of this total, approximately 161 km are paved with concrete. All of the concrete constructed on I-80 is undoweled plain jointed PCC. This type of pavement is susceptible to pumping and rocking from the action of wheel loads. The resultant movement and loss of fines can result in increased faulting, cracking, and corner breaking.

University of Wyoming, P.O. Box 3295, University Station, Laramie, Wyo. 82071.

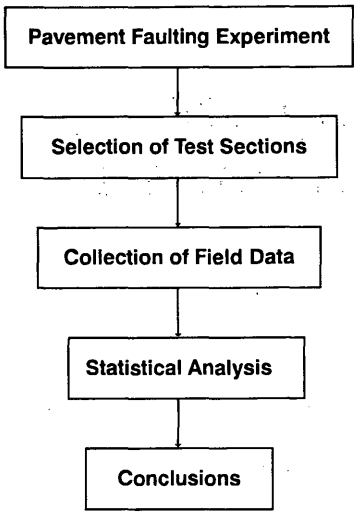

FIGURE 1 Data collection and analysis strategies.

The climate in this region is classified as "dry, hard freeze spring thaw." Annual precipitation is variable but ranges only from 230 to 380 mm. All of the projects included in the experiment are 11.6 m wide with the exception of a few PCC inlays. As shown in Table 1, pavement thicknesses vary from 254 to 318 mm. Joint width and spacing are similar for all projects. All the projects have tied shoulders with the exception of the inlays. To date, none of the projects show any significant types of distress besides faulting.

DATA COLLECTION

Faulting measurements were collected on all test sections in 1989, 1991, and 1993. Table 2 summarizes these measurements. Typically, the first 10 slabs of every mile were evaluated for faulting and other types of pavement distress. Faulting measurements were taken 0.3 m into the pavement from the shoulder. Slabs lower on the leave side of the joint were recorded as positive faulting. The average fault was determined by summing the absolute values of the fault measurements and dividing by the number of measurements.

TABLE 1 General Information on Test Sections

Project	Beginning Milepost	Ending Milepost	Construction Date	Pavement Thickness mm
I-80 W	0.0	2.9	1991	292
I-80 E	0.0	2.9	1991	292
I-80 W	6.9	12.3	1992	305
I-80 E	6.9	12.3	1992	305
I-80 W	17.7	22.7	1991	318
I-80 E	17.7	22.7	1992	318
I-80 W	22.7	28.0	1988	267
I-80 E	22.7	28.0	1988	267
I-80 E	130.0	138.0	1986	254
I-80 E	258.6	263.4	1989	254
I-80 E	263.4	270.0	1988	254
I-80 E	270.0	275.6	1989	254
I-80 W	258.6	269.4	1990	254
I-80 W	269.4	275.6	1990	254
I-80 W	2.9	6.9	1985	254
I-80 E	2.9	6.9	1986	254
I-80 W	86.4	92.2	1987	305
I-80 E	86.4	92.2	1987	305
I-80 W	92.2	101.7	1987	305
I-80 E	92.2	101.7	1987	305
I-80 W	393.4	400.5	1985	254
I-80 E	393.4	400.5	1985	254
I-80 W	382.3	393.4	1987	254
I-80 E	382.3	393.4	1987	254
I-80 W	378.1	382.3	1989	254
I-80 E	378.1	382.3	1989	254
I-80 W	372.4	378.1	1988	254
I-80 E	372.4	378.1	1988	254
I-80 W	212.4	216.2	1990	279
I-80 E	212.4	216.2	1991	279
I-80 W	358.3	360.0	1992	254
I-80 E	358.3	360.0	1991	254

TABLE 2 Faulting Data on Test Sections

Project	Beginning Milepost	Ending Milepost	1989 Fault mm	1991 Fault mm	1993 Fault mm
I-80 W	0.0	2.9	*	*	0.1
I-80 E	0.0	2.9	*	*	0.1
I-80 W	6.9	12.3	*	*	0.1
I-80 E	6.9	12.3	*	*	0.2
I-80 W	17.7	22.7	*	0.5	0.6
I-80 E	17.7	22.7	*	*	0.5
I-80 W	22.7	28.0	0.2	0.6	1.9
I-80 E	22.7	28.0	0.2	0.4	1.0
I-80 E	130.0	138.0	*	*	3.0
I-80 E	258.6	263.4	*	*	2.3
I-80 E	263.4	270.0	0.4	*	1.7
I-80 E	270.0	275.6	*	*	2.5
I-80 W	258.6	269.4	*	*	0.8
I-80 W	269.4	275.6	*	*	1.2
I-80 W	2.9	6.9	1.8	2.2	3.0
I-80 E	2.9	6.9	1.5	1.6	2.2
I-80 W	86.4	92.2	0.7	1.6	2.5
I-80 E	86.4	92.2	0.9	*	2.1
I-80 W	92.2	101.7	0.5	1.5	1.5
I-80 E	92.2	101.7	0.7	*	2.3
I-80 W	393.4	400.5	1.6	1.5	1.8
I-80 E	393.4	400.5	1.2	2.1	2.6
I-80 W	382.3	393.4	1.4	1.6	2.0
I-80 E	382.3	393.4	1.3	1.1	1.6
I-80 W	378.1	382.3	*	1.0	1.4
I-80 E	378.1	382.3	*	0.7	1.9
I-80 W	372.4	378.1	0.5	0.7	1.2
I-80 E	372.4	378.1	0.7	1.1	1.5
I-80 W	212.4	216.2	*	*	0.7
I-80 E	212.4	216.2	*	*	0.5
I-80 W	358.3	360.0	*	*	0.5
I-80 E	358.3	360.0	*	*	0.7

* Section built after measurement or faulting data not available.

Two devices were used in collecting faulting data. The Wyoming DOT's fault meter, which was built in house based on a design originating with the California DOT, was used to measure faulting through 1992. This device is equipped with a K-D Tools dial gauge accurate to a thousandth of an inch. The 1993 fault data were collected using the SHRP modified Georgia digital fault meter, which is currently under evaluation by the Strategic Highway Research Program (SHRP). The SHRP modified Georgia digital fault meter uses a linear variable differential transformer, which measures the values to the nearest millimeter.

To ensure that the devices were producing equivalent results, comparison studies were performed. Direct comparison readings were taken at 418 transverse joints with both fault meters. Statistical analysis revealed that the Georgia meter measurements were slightly higher than the Wyoming DOT's meter measurements. Although statistically different, the variations were of such a small magnitude that there was no practical difference.

The repeatability of both meters was checked by raising and lowering each fault meter on the same site five times at a number of locations. Computed variations indicated that both fault meters provided repeatable results.

Other information needed in this research was collected from the Wyoming DOT data files. This information included the cumulative number of ESALs on each project, annual precipitation, and drainage conditions. As shown in Table 3, the accumulated traffic on the test sections varied between 2.66×10^5 and 5.41×10^6. Table 4 shows the annual precipitation and drainage conditions for all test sections. Annual precipitation varied slightly from 230 to 380 mm. About half of the test sections had edge drains, and the other half had no drainage.

TABLE 3 Accumulated Traffic Applications on Test Sections

Project	Beginning Milepost	Ending Milepost	ESAL's
I-80 W	0.0	2.9	1.38E+06
I-80 E	0.0	2.9	1.38E+06
I-80 W	6.9	12.3	4.34E+05
I-80 E	6.9	12.3	4.34E+05
I-80 W	17.7	22.7	2.17E+06
I-80 E	17.7	22.7	1.30E+06
I-80 W	22.7	28.0	3.72E+06
I-80 E	22.7	28.0	3.72E+06
I-80 E	130.0	138.0	5.41E+06
I-80 E	258.6	263.4	2.67E+06
I-80 E	263.4	270.0	3.43E+06
I-80 E	270.0	275.6	2.67E+06
I-80 W	258.6	269.4	1.90E+06
I-80 W	269.4	275.6	1.90E+06
I-80 W	2.9	6.9	6.64E+06
I-80 E	2.9	6.9	5.76E+06
I-80 W	86.4	92.2	4.78E+06
I-80 E	86.4	92.2	4.78E+06
I-80 W	92.2	101.7	5.36E+06
I-80 E	92.2	101.7	5.36E+06
I-80 W	393.4	400.5	3.85E+06
I-80 E	393.4	400.5	3.85E+06
I-80 W	382.3	393.4	2.83E+06
I-80 E	382.3	393.4	2.83E+06
I-80 W	378.1	382.3	1.80E+06
I-80 E	378.1	382.3	1.80E+06
I-80 W	372.4	378.1	2.31E+06
I-80 E	372.4	378.1	2.31E+06
I-80 W	212.4	216.2	1.90E+06
I-80 E	212.4	216.2	1.14E+06
I-80 W	358.3	360.0	2.66E+05
I-80 E	358.3	360.0	7.97E+05

DATA ANALYSIS

All data collected in this research project were summarized in a computerized data base. The statistical analysis performed aimed at (a) identifying the most important factors behind pavement faulting and (b) incorporating these parameters in a regression model to predict pavement faulting. The following five independent factors were considered in this experiment: accumulated ESALs, pavement thicknesses, pavement ages, average annual precipitation, and existence of edge drain. A stepwise regression analysis was performed on the data to identify the significant factors behind faulting. The 1993 faulting data were used in this analysis. As expected, pavement age and accumulated ESALs were highly correlated. The analysis also indicated that ESALs are better predictors of faulting than pavement age. Therefore, the age factor was dropped from the analysis. The factor of annual precipitation was found insignificant and was eliminated. This left the independent variables of ESALs, pavement thickness, and drainage to be used in the prediction model. After considering varieties of regression models, the following equation was found to yield the highest R^2 value:

$$\text{faulting} = 3.49 + 3.62E-07 * \text{ESAL} - 0.0107 * \text{thickness} - 0.324 * \text{drainage}$$

where

faulting = predicted faulting (mm),
ESAL = cumulative 18-kip equivalent single-axle load applications,
thickness = pavement thickness (mm), and
drainage = numerical indicator of drainage provided (e.g., 0, if no edge drains exist, and 1, if edge drains exist).

The R^2 value for this equation was 79.4 percent, and the individual variables were significant to the $\alpha = 0.1$ level. The standard error of estimates for this model can be found in Table 5. The model indicates the importance of edge drains on reducing faulting.

The developed model was used to compare predicted and actual faulting for the 1993 data. This comparison is presented in Figure 2. It is clear that the developed model predicted actual fault measurements very successfully.

TABLE 4 Subdrainage (Edge Drain) and Annual Precipitation

Project	Beginning Milepost	Ending Milepost	Annual Precipitation mm	Edge Drains
I-80 W	0.0	2.9	280	yes
I-80 E	0.0	2.9	280	yes
I-80 W	6.9	12.3	280	yes
I-80 E	6.9	12.3	280	yes
I-80 W	17.7	22.7	280	yes
I-80 E	17.7	22.7	280	yes
I-80 W	22.7	28.0	254	yes
I-80 E	22.7	28.0	254	yes
I-80 E	130.0	138.0	229	yes
I-80 E	258.6	263.4	330	yes
I-80 E	263.4	270.0	330	yes
I-80 E	270.0	275.6	330	no
I-80 W	258.6	269.4	330	yes
I-80 W	269.4	275.6	330	no
I-80 W	2.9	6.9	280	no
I-80 E	2.9	6.9	280	no
I-80 W	86.4	92.2	229	no
I-80 E	86.4	92.2	229	no
I-80 W	92.2	101.7	229	no
I-80 E	92.2	101.7	229	no
I-80 W	393.4	400.5	381	no
I-80 E	393.4	400.5	381	no
I-80 W	382.3	393.4	381	no
I-80 E	382.3	393.4	381	no
I-80 W	378.1	382.3	381	no
I-80 E	378.1	382.3	381	no
I-80 W	372.4	378.1	381	no
I-80 E	372.4	378.1	381	no
I-80 W	212.4	216.2	280	yes
I-80 E	212.4	216.2	280	yes
I-80 W	358.3	360.0	381	yes
I-80 E	358.3	360.0	381	yes

CONCLUSIONS

Faulting is a serious problem in concrete pavements that can lead to other pavement deficiencies. Among these are driver discomfort, corner break, and spalling. In this research project, data on factors related to faulting in undoweled concrete pavements were collected and analyzed. The following conclusions can be made from this experiment:

- The limited variation in annual precipitation did not influence the faulting in test sections included in this experiment.
- The most important factor in predicting pavement faulting is the accumulated traffic applications. ESALs and pavement age were found to be highly correlated, which resulted in dropping the pavement age from the analysis.
- Pavements with edge drains have lower faulting than pavements without edge drains. Further analysis and more data will be

TABLE 5 Standard Error of Estimates for Predictive Model

	Standard Error of Estimates
Intercept	0.89192061
ESAL	0.00000005
Thickness	0.00328903
Drainage	0.17500666

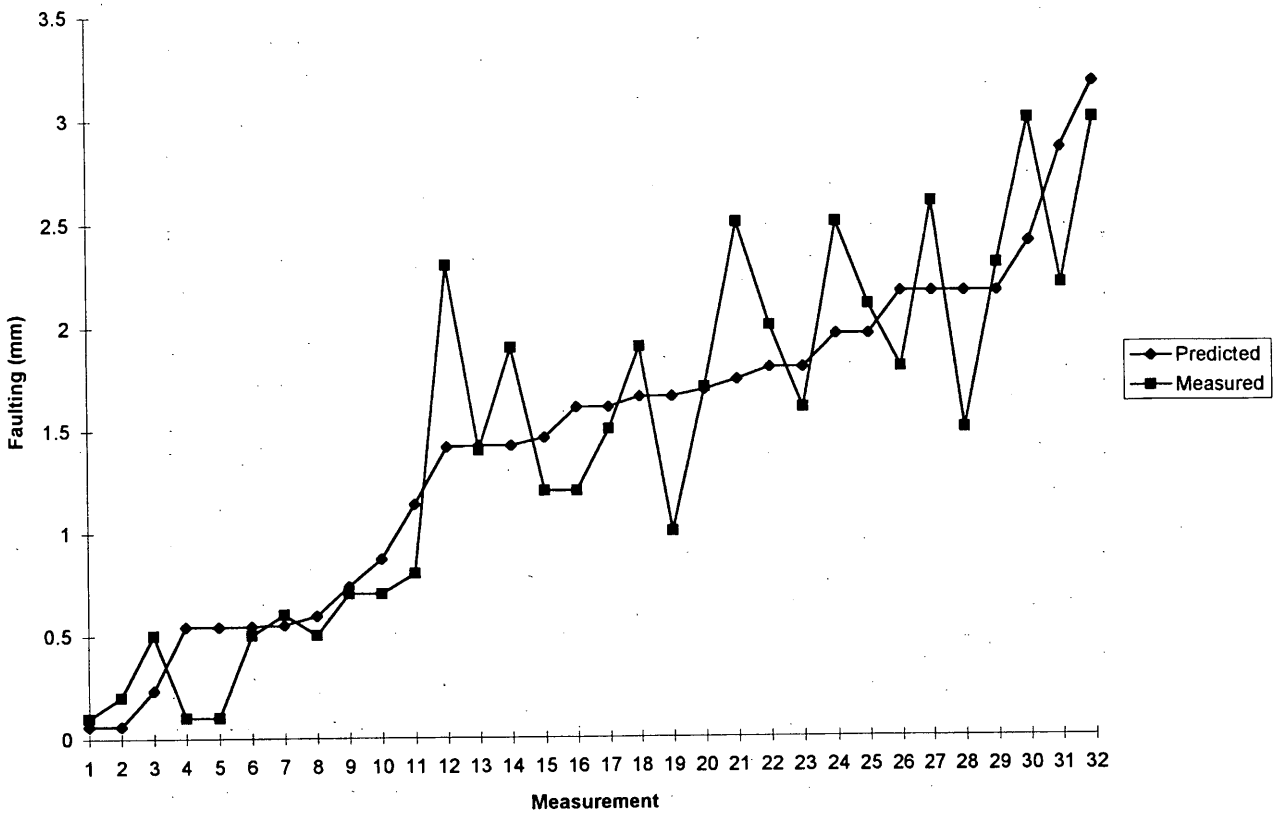

FIGURE 2 Predicted and measured faulting.

needed to determine whether the reduction in faulting can make the installation of edge drains cost effective.

- As expected, it was found that thicker pavements will have lower faulting.
- A regression model with a good R^2 was developed to predict pavement faulting based on the accumulated traffic, pavement thickness, and drainage type. Such a model can be used to predict the expected pavement faulting during the pavement design process.

ACKNOWLEDGMENTS

This study was funded by Wyoming DOT. The authors express their appreciation to Mike Farrar and Andrew Beamer of the Wyoming DOT for their cooperation.

REFERENCES

1. Ioannides, A. M., Y. Lee, and M. I. Darter. Control of Faulting Through Joint Load Transfer Design. In *Transportation Research Record 1286,* TRB, National Research Council, Washington, D.C., 1990.
2. Ioannides, A. M., and G. T. Korovesis. Aggregate Interlock: A Pure-Shear Load Transfer Mechanism. In *Transportation Research Record 1286,* TRB, National Research Council, Washington, D.C., 1990.
3. Shahin, M., and S. D. Kohn. *Pavement Maintenance Management for Roads and Parking Lots.* Technical Report M-294. U.S. Army Corps of Engineers, Champaign, Ill., 1981.
4. Yoder, E. J., and M. W. Witczak. *Principles of Pavement Design,* 2nd ed. John Wiley and Sons, Inc., New York, 1975.

Publication of this paper sponsored by Committee on Rigid Pavement Design.

Nationwide Field Investigation of Continuously Reinforced Concrete Pavements

SHIRAZ D. TAYABJI, PETER J. STEPHANOS, AND DAN G. ZOLLINGER

There are over 48,300 km of continuously reinforced concrete (CRC) pavements in the United States. Many of these pavements are more than 20 years old and have provided excellent performance over the years. Much of the CRC pavement technology has developed through experience. This and the recent use of new design features (i.e., tied concrete shoulder, permeable cement treated base, and epoxy-coated steel) identified a need to conduct a study to evaluate performance of existing CRC pavement sections. A national pooled-fund study administered by FHWA aimed at updating the state of the art of the design, construction, maintenance, and rehabilitation of CRC pavements was recently completed. As part of the study, a comprehensive field investigation of 23 in-service CRC pavements was conducted to study the effects of various design and construction features on performance of CRC pavements. The investigation included crack mapping and distress survey, profile and roughness measurement, falling weight deflectometer testing, and materials sampling and testing for 305 m long in-service test sections. The key findings of the field investigation program as they relate to CRC pavement design and construction are presented.

Continuously reinforced concrete (CRC) pavement is portland cement concrete (PCC) pavement with continuous longitudinal steel reinforcement with no intermediate transverse expansion or contraction joints. The continuous joint-free length of CRC pavements can extend to several thousand meters with breaks provided only at structures. Terminal anchorage is provided at the ends of the CRC pavement to restrain length changes due to temperature variations and drying shrinkage of concrete. The CRC pavements develop a random cracking pattern with cracks generally spaced at about 0.9 to 2.4 m. The cracking pattern is governed by the environment conditions at the time of construction, the amount of steel, and concrete strength. The steel reinforcement restrains the opening of the cracks. Also, the higher the amount of steel reinforcement, the more closely spaced the cracks will be. Most of the cracks form shortly after construction but additional cracking may develop over the next few years as a result of continued drying shrinkage of concrete, temperature variations, and traffic loading.

A major concern with CRC pavement is punchout distress. Other distresses associated with punchouts include spalling along transverse cracks and faulting. Other leading causes of CRC pavement failure are wide (and spalled) transverse cracks due to steel rupture and spalling of concrete due to steel corrosion in the presence of heavy deicing salt applications in the northern states. The punchout distress is related to crack spacing, pavement thickness, poor foundation support, and heavy truck loadings. The repair of punchout distress typically consists of full-depth patches. With time, as the number of full-depth patches increases, the pavement may be resurfaced with asphalt concrete or PCC or it may be reconstructed.

This paper presents the results of a field investigation conducted as part of a recent study administered by FHWA aimed at updating the state of the art of the design, construction, maintenance, and rehabilitation of CRC pavements (*1,2*). Because CRC pavement performance is influenced significantly by crack spacing, the data analysis and evaluation were focused on a more detailed review of the crack-spacing–related data.

Shiraz D. Tayabji, Transportation Technologies USA, Inc., 9030 Red Branch Road, Suite 230, Columbia, Md. 21045. Peter J. Stephanos, PCS/Law Engineering, Inc., 12104 Indian Creek Court, Suite A, Beltsville, Md. 20705. Dan G. Zollinger, Texas Transportation Institute, College Station, Tex. 77843-3135.

FIELD INVESTIGATION DETAILS

The specific objective of the field investigation was to conduct necessary field investigations and laboratory testing of existing CRC pavement sections and to evaluate the effect of standard and new design features on CRC pavement performance. After a detailed evaluation of available project sites in conjunction with participating state highway agencies, 23 project sites were selected. At each site, performance of a representative 305-m-long section was evaluated using visual condition surveys, profile measurements, falling weight deflectometer testing, and corrosion-related testing. In addition, concrete cores were obtained for strength, stiffness (modulus of elasticity), and coefficient of thermal expansion testing. Samples of base, subbase, and subgrade were also obtained for material characterization. For each project site, available inventory-type data related to design, construction, maintenance, performance, and traffic were collected from state agencies.

Test Section Details

The list of the test sections selected for field evaluation is given in Table 1. As shown in Table 1, the selected test sections incorporate a broad range of attributes of interest:

- Design thickness—ranging from 203 to 330 mm,
- Epoxy-coated reinforcement—three sections,
- Permeable base—two sections,
- Age—ranging from 0.3 to 22 years,
- Subgrade—both coarse and fine-grained soils,
- Base—CTB, LCB, ATB, and granular,
- Steel amount—0.45 to 0.7 percent,
- Steel placement—tube fed and chairs,

TABLE 1 Final List of Test Sections

Test Section ID	Route	Age as of Fall 1991 Testing, years	Climatic Region	Terminal Joint Type	Design Thickness, mm	Subgrade Type (AASHTO)	Base Type	Outside Shoulder Type	Long. Steel Amount, %	Steel Placement Method	Epoxy Coated Steel	1,991 2-Way AADT	Design Lane Cumul. ESALs upto 9/91
IL-1	US51	0	wet-freeze	wide flange	254	A-7-6	perm. ctb	pcc	0.70	chair	no	na	180,000
IL-2	I72	15	wet-freeze	lug	203	A-6	ctb	ac	0.59	tube	no	7,500	4,800,000
IL-3	US36	20	wet-freeze	lug	203	A-7-5	atb	ac	0.60	chair	no	17,700	4,800,000
IL-4	I55	20	wet-freeze	lug	203	A-7-5	atb	ac	0.60	tube	no	17,700	13,700,000
IL-5	US50	5	wet-freeze	wide flange	203	A-7-5	lcb	pcc	0.70	chair	no	na	300,000
IA-1	I29	20	wet-freeze	lug	203	A-2-6	ctb	ac	0.65	tube	no	7,500	3,700,000
IA-2	I80	22	wet-freeze	lug	203	A-6	atb	ac	0.65	tube	no	12,700	8,850,000
IA-3	I380	15	wet-freeze	lug	203	A-6	atb	pcc	0.65	tube	no	27,700	5,300,000
OK-1	I40	4	wet-no freeze	wide flange	229	A-6	atb	pcc	0.50	chair	no	13,000	na
OK-2	US69	5	wet-no freeze	wide flange	229	A-6	atb	pcc	0.50	chair	no	8,000	na
OK-3	I35	3	wet-no freeze	wide flange	254	A-4	atb	pcc	0.50	chair	yes	21,000	na
OK-4	US69	7	wet-no freeze	wide flange	229	A-6	soil-asphalt	pcc	0.50	chair	no	9,000	na
OK-5	I40	2	wet-no freeze	wide flange	254	A-2-6	perm. ctb	pcc	0.61	chair	no	12,000	na
OR-1	I5	7	wet-no freeze	wide flange	330	A-4	granular	ac	0.60	tube	no	29,700	11,300,000
OR-2	I5	4	wet-no freeze	wide flange	254	A-4	ctb	ac	0.60	tube	no	30,300	3,000,000
OR-3	I205	20	wet-no freeze	lug	203	A-6	ctb	ac	0.54	tube	no	59,000	30,000,000
PA-1	I180	15	wet-freeze	wide flange	229	A-2-4	granular	ac	0.45	tube	no	9,000	5,500,000
PA-2	I81	22	wet-freeze	lug	229	A-2-4	granular	pcc	0.55	chair	no	13,700	32,000,000
WI-1	I43	18	wet-freeze	lug	203	A-2-4	granular	ac	0.65	chair	no	10,900	2,290,000
WI-2	I90	6	wet-freeze	wide flange	254	A-4	granular	pcc	0.67	tube	yes	31,400	2,530,000
WI-3	I90/94	7	wet-freeze	lug	254	A-4	granular	pcc	0.67	tube	yes	35,100	3,960,000
WI-4	I90/94	7	wet-freeze	na	254	A-2-4	granular	pcc	0.67	tube	no	42,600	4,180,000
WI-5	I90/94	16	wet-freeze	lug	203	A-1-a	granular	ac	0.61	chair	no	26,900	na

Note: ESALs = 80 kN equivalent single-axle loads.

- Shoulder type—11 asphalt concrete and 12 PCC, and
- Climatic region—wet-freeze (15 sections) and wet-no freeze (8 sections).

All field testing was performed during fall 1991.

Field Data Collection and Analysis Plan

The field data collection program was aimed at collecting data on the current condition of each 305-m-long representative test section. The following activities were completed at most of the test sections:

1. Visual condition survey
   - –Crack and distress mapping along the 305-m section,
   - –Joint width measurements (for cracks located within a 30.5-m subsection), and
   - –Windshield survey of adjacent 8.1 km of pavement;
2. Nondestructive deflection testing using a falling weight deflectometer (FWD)
   - –Basin testing (slab interior—midslab between cracks) at a spacing of 87.6 m along the 305-m length of the section, and
   - –Testing at crack locations (midslab and edge) (for cracks located within a 30.5-m subsection);
3. Profile testing using a South Dakota–type profiler
4. Corrosion-related testing
   - –Corrosion potential measurement, and
   - –Examination of steel bars (cores);
5. Coring and shallow borings
   - –Concrete testing (laboratory testing): splitting tensile strength, modulus of elasticity, coefficient of thermal expansion, and chloride content determination.
   - –Material characterization: Atterberg limits and particle size distribution.
6. Reinforcing steel location survey
7. Photographic and video imaging

All field testing was accomplished during 1 day of testing. The details of field data collection procedures used are given elsewhere (*1*).

Deflection Testing Data Analysis

Deflection data from the basin testing were used to backcalculate the radius of relative stiffness l, modulus of subgrade reaction k, and slab rigidity D, for the pavement at each test location. l and D are defined as follows:

$$l = [(Eh^3/12(1 - \mu^2)k]^{0.25}$$

where

E = concrete modulus of elasticity,
h = slab thickness,
μ = concrete Poisson's ratio, and
k = modulus of subgrade reaction.

and

$$D = Eh^3/12(1 - \mu^2)$$

Program ILLI-BACK (*3*) was used for this purpose. The backcalculation was performed for all three load levels used. Backcalculated data indicate that the radius of relative stiffness values computed for each of the three load levels at each test location were almost identical. Therefore, in subsequent data analysis, only the data for the nominal 9,000-lb load were used. For edge testing, no corrections were made for the boundary conditions (free edge). Thus, the backcalculated values computed using ILLI-BACK actually represent the effective or equivalent radius of relative stiffness, modulus of subgrade reaction, or slab rigidity, as appropriate.

Data Analysis for Deflection Testing at Cracks and Along Edge

A review of the data obtained from deflection testing at cracks indicated that edge deflections were almost twice as large as midslab deflections for early morning and midafternoon testing. However, the backcalculated radius of relative stiffness along the edge was not always proportionately less than along the midslab. Thus, care must be exercised in interpreting the backcalculated relative stiffness values without considering maximum deflections for edge testing. The radius of relative stiffness values was backcalculated without accounting for the edge boundary condition (free edge or tied shoulder). Thus, these values represent effective values and are used primarily to allow comparison of overall pavement stiffness along the edge to the overall pavement stiffness along midslab (interior) locations and to identify whether tied shoulder has any effect on the overall pavement stiffness along the edge. Also, as expected, afternoon testing produced lower deflections at the midslab and edge locations. In early morning, the slab edge is curled upward because of a cooler slab surface resulting in a slight loss of support along the free edges. In midafternoon, the reverse is true and the slab edge is either in contact with the base and subbase or is close to contact because of the downward curl along the slab edge.

Summary of Test Data

One of the major concerns at the beginning of the field study was the availability and reliability of data related to traffic along the test sections. Reliable traffic data were unavailable for many of the test sections—in most cases because the reliable traffic data did not exist or the required traffic data e.g., ESALs were not maintained by the agency. This is not unusual; the same problem has been encountered on many similar pavement data collection programs, including the Long-Term Pavement Performance (LTPP) program. For the LTPP program, the state agencies have initially provided the best estimates of the ESALs for the test sections, and efforts are under way to perform more in-depth traffic data collection using site-specific WIM and AVC equipment. Thus for this project, traffic effects are indirectly incorporated by considering age (time) effects. A summary of the key data elements for each of the 23 test sections is presented in Table 2.

Ride Quality and Serviceability

The ride quality of the CRC pavement test sections as denoted by the international roughness index (IRI) ranged from a low of

TABLE 2 Key Data Elements

Test Section ID	Average Crack Spacing, meter	Average IRI, m/km	Average Max. Deflection, mm			Edge Deflection as % of Basin Defl. (afternoon)	Measured E, MPa	Average Split Ten. Strength, MPa	Basin Test l Average, mm	Afternoon Edge Crack l Average, mm	Edge Crack l as % of Basin l (afternoon)	Basin Test k Average, kPa/mm	Basin Test D Average, kN-m	Afternoon Edge Crack k Average, kPa/mm	Afternoon Edge Crack D Average, kN-m	Edge Crack k as % of Basin k (afternoon)	Edge Crack D as % of Basin D (afternoon)
			Basin Testing	Morning Edge Crack Testing	Afternoon Edge Crack Testing												
IL-1	1.6	1.47	0.056	0.132	0.097	53	37,206	3.38	1,016	813	24	78	832,389	74	323,189	95	39
IL-2	1.3	2.01	0.109	0.305	0.277	77	39,273	3.98	940	635	21	54	423,186	45	73,209	83	17
IL-3	1.1	2.40	0.124	0.254	0.236	58	33,761	4.15	965	991	31	44	383,721	21	198,502	47	52
IL-4	0.6	2.48	0.099	0.201	0.175	54	29,627	3.25	1,067	991	28	45	579,662	28	269,023	62	46
IL-5	0.9	2.23	0.112	0.236	0.168	46	33,761	3.33	965	991	31	49	421,387	29	282,082	60	67
IA-1	1.8	1.14	0.104	0.175	0.135	39	30,316	3.33	1,016	838	25	49	526,024	49	243,681	100	46
IA-2	0.9	1.30	0.127	0.340	0.244	59	28,249	3.51	1,041	1,016	30	37	440,259	18	196,536	49	45
IA-3	0.9	1.86	0.107	0.196	0.231	66	35,828	3.86	940	889	29	53	414,722	26	162,644	49	39
OK-1	2.6	0.84	0.069	0.127	0.135	60	39,962	3.29	889	610	21	98	614,997	91	125,483	92	20
OK-2	1.4	na	0.069	0.104	0.094	42	45,474	3.95	1,016	762	23	77	820,828	92	310,012	119	38
OK-3	1.4	1.17	0.074	0.132	0.117	48	35,828	3.42	1,041	889	26	67	791,190	56	347,312	83	44
OK-4	1.9	na	0.076	0.236	0.196	78	44,096	3.27	838	635	23	115	569,035	66	108,049	58	19
OK-5	1.9	0.79	0.076	0.127	0.109	44	22,737	3.32	864	686	24	98	546,158	86	190,199	88	35
OR-1	1.2	na	0.069	0.104	na	na	24,804	3.64	965	na	na	80	692,111	na	na	na	na
OR-2	1.7	na	0.048	0.124	0.089	56	29,627	3.33	965	787	25	113	981,667	83	319,052	73	33
OR-3	1.4	na	0.119	0.183	na	na	32,383	3.09	889	na	na	62	389,667	na	na	na	na
PA-1	1.5	1.19	0.056	0.112	na	na	28,938	3.33	635	na	na	219	356,341	na	na	na	na
PA-2	1.3	1.19	0.135	0.163	0.147	33	33,761	3.76	1,067	660	19	44	565,610	78	148,071	178	26
WI-1	0.9	1.77	0.071	0.155	0.112	48	38,584	4.57	660	660	31	164	311,103	106	200,695	65	65
WI-2	0.9	1.53	0.071	0.178	0.137	59	31,005	3.36	864	762	27	99	550,684	65	220,392	66	40
WI-3	1.1	1.28	0.069	0.188	0.112	50	26,871	3.08	762	711	28	126	423,409	89	228,308	71	54
WI-4	1.4	1.99	0.081	0.406	0.130	49	35,139	4.36	965	686	22	72	623,841	88	193,799	122	31
WI-5	1.0	1.47	0.137	0.216	0.163	36	36,517	3.56	889	762	26	49	303,263	54	181,069	111	60
Average	1.3	1.56	0.089	0.191	0.155	53	33,641	3.57	924	789	26	82	546,141	62	216,065	84	41
Std Dev	0.4	0.51	0.027	0.078	0.055	12	5,737	0.40	117	134	4	44	180,531	27	75,149	32	14
Maximum	2.6	2.48	0.137	0.406	0.277	78	45,474	4.57	1,067	1,016	31	219	981,667	106	347,312	178	67
Minimum	0.6	0.79	0.048	0.104	0.089	33	22,737	3.08	635	610	19	37	303,263	18	73,209	47	17

Notes:

1. l = radius of relative stiffness (RRS); k = modulus of subgrade reaction; D = concrete slab rigidity
2. Values of concrete modulus of elasticity and average splitting tensile strength were measured using cores obtained during field testing.
3. Deflection data are for 40 kN FWD load

0.84 m/km to a high of 2.48 m/km. This represents good to very good ride quality considering that the test section ages ranged from 0.3 to 22 years at the time of testing. Thus, CRC pavements tend to provide a good riding surface even when a high amount of medium to high severity cracking is present. Also, there was a slight increase in IRI (rougher ride) with age.

Deflections Under Load

Average Sensor 1 deflections (maximum deflection under the load plate) ranged from a low of 0.048 mm to a high of 0.137 mm under the 40-kN FWD load for the basin (interior) testing. The deflection values are, of course, affected by slab thickness and base and subgrade support. The deflections and the subsequent backcalculated pavement stiffness characteristics therefore represent the conditions at the time of testing only.

The deflections measured at the transverse crack along the midslab location were generally comparable to the basin deflections, generally measured between crack locations. However, edge deflections measured at transverse crack locations tended to be almost twice as much as the basin (or midslab crack location) deflections for the morning testing (upward slab curl along the edges). The edge deflections tended to be less for the afternoon testing but still considerably more than basin test deflections. The afternoon edge deflections were reduced by about 10 to 30 percent from the morning edge deflections. Figure 1 shows a comparison of edge and midslab deflections at crack locations with basin test deflections. The tied-concrete shoulders appear not to have contributed much to reducing edge deflections.

Also, the relative change in edge deflection between morning and afternoon testing appears not to have been affected much by slab support condition—firm support such as LCB, ATB, or CTB versus softer support provided by granular or permeable bases.

Loss of Support Analysis

Loss of support analysis was performed using the data from deflection testing along the edge locations. At each test location, FWD loads of about 40, 53, and 67 kN were used. The maximum deflections at each of the three load levels were used to extrapolate loss of support conditions along the edge. Most of the sections exhibited some loss of support during the morning and the afternoon testing. The loss of support for the afternoon testing tended to be slightly lower. There appeared to be no significant influence of shoulder type or base type on the magnitudes of the loss of support. However, it should be noted that the data are confounded by actual temperature conditions and pavement thicknesses at each site.

Overall Pavement Stiffness

For concrete pavements, the overall pavement stiffness can be described very effectively using the radius of relative stiffness (RRS), *l*, value. The *l*-value is an important structural parameter of concrete pavements and has a direct influence on pavement behavior (structural response). The RRS was estimated for each section using the theoretical formula and using the actual slab thickness (average core thickness), laboratory measured modulus of elasticity value, and best estimate of the modulus of subgrade reaction. The RRS values were also backcalculated from the deflection testing using Program ILLIBACK. These RRS values are presented in Table 2. The following is a summary of the comparison of the RRS values.

- For basin testing, the backcalculated RRS values were independent of load levels, which ranged from 40 to 70 kN. Thus, a single load level of 40 kN is considered adequate for CRC pavement basin testing. However, multiple load levels should be used for testing along the pavement edge if loss of support determination is desired.

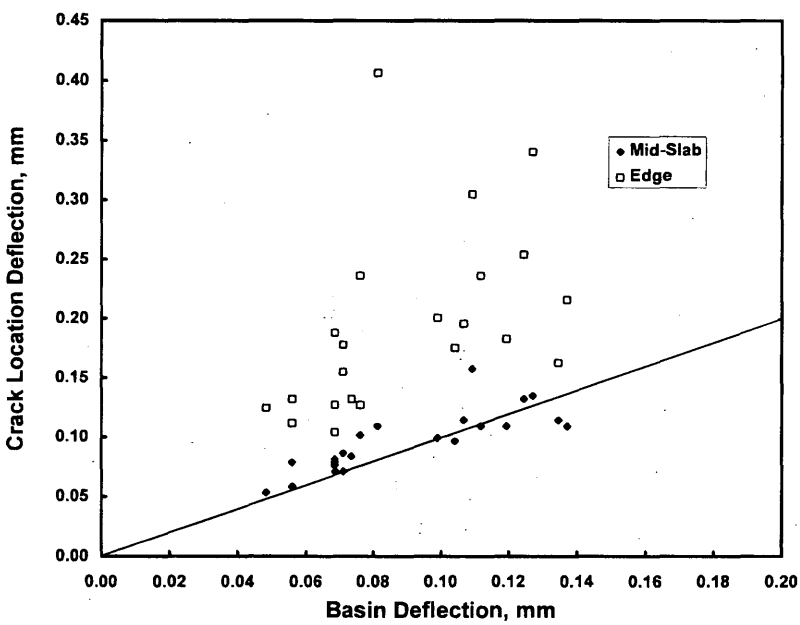

FIGURE 1 Comparison of basin and crack location deflections.

TABLE 3 Average Values for Various Parameters for 23 Test Sections

	Average Values		
	ℓ, mm	k, kPa/mm	D, kN-m
Basin Testing	914	81	546,000
Mid-Slab Crack Testing			
Morning Testing	762	103	341,000
Afternoon Testing	838	92	391,000
Edge Crack Testing			
Morning Testing	762	54	171,000
Afternoon Testing	787	62	216,000

- RRS values for testing at crack locations were generally lower than those along basin (noncrack) locations.
- RRS values for midslab crack location increased some from morning to afternoon testing. However, there was very little increase in the edge crack location RRS values from morning to afternoon testing even though actual deflection values were lower.
- The crack location RRS values for edge testing were only slightly lower than for the midslab testing.
- Based on the review of the RRS and *D*-values, it appears that concrete shoulders may not be very effective in all cases for structural strengthening of the mainline CRC pavements. The use of concrete shoulder may still be strongly desired for other reasons, such as maintenance-free shoulder, effective joint sealing, and so forth.

The deflection test data were further analyzed to backcalculate the modulus of subgrade reaction *k* and the slab rigidity *D*. Although the RRS term describes the overall stiffness of the total pavement system, the *D*-term describes the rigidity of the concrete slab only. Table 3 illustrates the average values for the various parameters for all 23 test sections.

Thus, the effective *k*-values along the edges are about 60 to 70 percent of the values for the midslab locations, and the *D*-values along the edge are about 30 to 60 percent of the values for the midslab locations. The basin testing (uncracked locations) resulted in the highest *D*-values. These trends in *k*- and *D*-values are what one would expect and appear to be more descriptive of the actual physical condition (edge) of the pavement system. It is also likely that the backcalculated *D*-value would be much lower at those edge locations that exhibit the beginning of a punchout or exhibit wide cracks. Thus, it is recommended that the *D*- and *k*-values be used in interpreting the results of edge testing, in addition to using RRS.

Crack Spacing Analysis

The average crack spacings for each site are shown in Figure 2. During the study, it was realized that a good method for characterizing the cracking pattern for CRC pavements did not exist. In the past, use has been made of the cumulative frequency distributions for representing the total number of cracks that have spacings equal to or less than the designated crack spacing. This is certainly a good method, providing a clear visual description of the cracking pattern. The cumulative frequency plots for each of the test sections are given in Figure 3. These plots can be used to identify the number of

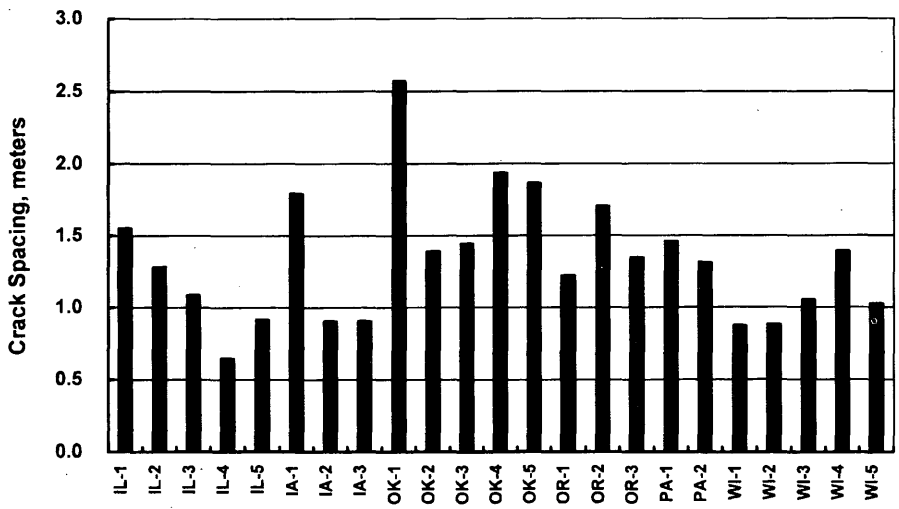

FIGURE 2 Crack spacing summary.

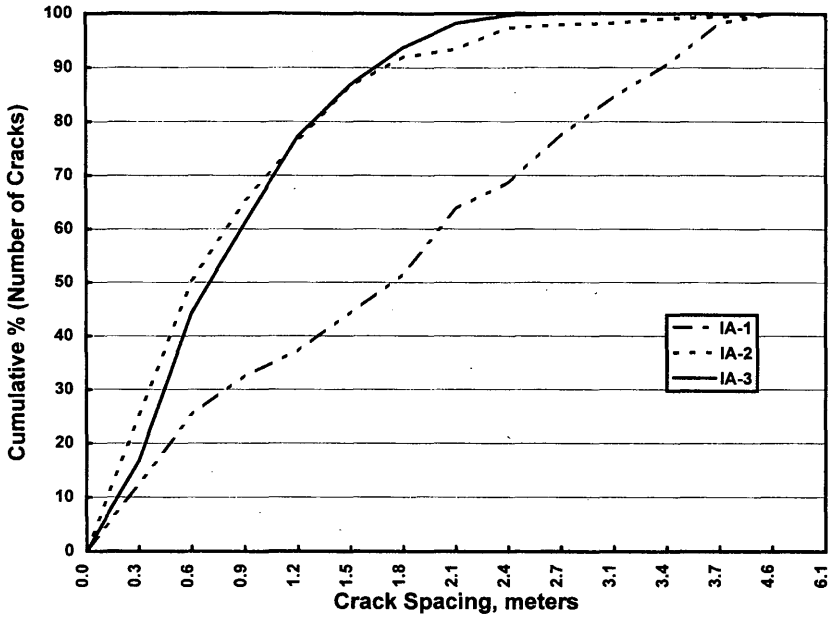

FIGURE 3 Crack spacing distribution (by number of cracks).

cracks (by percentage) that are greater or less than the designated crack spacing.

The cumulative frequency plots of the type presented in Figure 3 do not, however, represent the true picture of the cracking pattern as the focus of these plots is the number of cracks. A more representative characterization is the cumulative frequency based on the length of paving exhibiting a designated crack spacing. Thus, as an example, if 40 percent of the cracks (by number) have crack spacing equal to or less than 0.9 m, the length of paving exhibiting crack spacing equal to or less than 0.9 m may be only 20 percent or less. Similarly, if 10 percent of the cracks (by number) have crack spacing greater than 3.1 m, the length of paving exhibiting crack spacing greater than 3.1 m may exceed 20 percent. It is the length of paving that exhibits a certain cracking pattern that is as equally important as the number of cracks that exhibit a certain cracking pattern. The cumulative frequency plots based on length of paving are given in Figure 4.

Table 4 shows a comparison of the crack spacing characterization using the frequency distributions based on the number of cracks and the length of paving involved. The length of paving definition appears to be more descriptive. For cluster cracking, it indicates the potential for cluster cracking–related problems, in the presence of poor support conditions, based on the amount (by length) of cracking that is less than 0.9 m. It also clearly indicates the length of

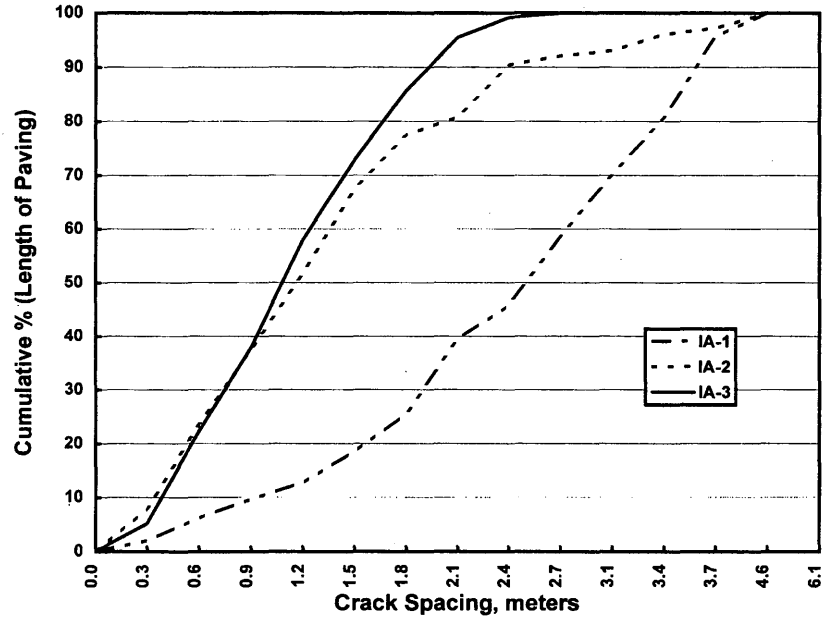

FIGURE 4 Crack spacing distribution (by length of paving).

TABLE 4 Crack Spacing Distributions

Test Section ID	Age as of Fall 1991 Testing, years	Long. Steel Amount, %	Total No. of Cracks (305 m)	% of Cracks = or < 0.92 Spacing (by no.)	% Length with Cracks or < 0.92 Spacing	% of Cracks > 1.84 m Spacing (by no.)	% Length with Cracks > 1.84 m Spacing	% of Cracks > 3.05 m Spacing (by no.)	% Length with Cracks > 3.05 m Spacing
IL-1	0	0.70	195	37	16	33	60	9	25
IL-2	15	0.59	237	45	22	23	43	3	7
IL-3	20	0.60	279	51	30	10	21	1	1
IL-4	20	0.60	470	86	79	1	2	0	0
IL-5	5	0.70	329	67	44	10	25	0	0
IA-1	20	0.65	169	33	10	49	73	15	27
IA-2	22	0.65	336	65	40	8	23	2	8
IA-3	15	0.65	334	61	41	6	10	0	0
OK-1	4	0.50	118	28	5	58	88	43	73
OK-2	5	0.50	217	40	18	25	50	8	21
OK-3	3	0.50	210	36	16	29	52	7	17
OK-4	7	0.50	156	15	5	51	72	13	25
OK-5	2	0.61	164	24	9	45	67	13	26
OR-1	7	0.60	248	36	18	12	23	1	1
OR-2	4	0.60	179	25	10	34	53	8	20
OR-3	20	0.54	227	41	21	23	43	3	9
PA-1	15	0.45	208	33	15	28	47	3	7
PA-2	22	0.55	231	39	20	20	38	2	6
WI-1	18	0.65	347	69	38	9	25	1	2
WI-2	6	0.67	345	68	52	2	6	0	0
WI-3	7	0.67	288	48	32	5	10	0	0
WI-4	7	0.67	218	34	17	25	41	0	0
WI-5	16	0.61	295	54	34	7	14	0	0
Average	11	0.60	252	45	26	22	39	6	12
Std Dev	7	0.07	82	18	18	17	24	9	17
Maximum	22	0.70	470	86	79	58	88	43	73
Minimum	0	0.45	118	15	5	1	2	0	0

paving that incorporates undesirable longer crack spacing, in excess of 3.1 m. A concern with longer spaced cracks is the development of crack spalls, steel rupture, and punchout at companion closely spaced cracks. These problems are also better characterized by the number of crack locations where these problems may develop in the future. Thus, for problem cluster cracking, the length of paving involved is more significant than the number of cracks. For longer spaced cracks, it is the number of cracks that is more significant than the length of paving involved.

To relate the crack spacing to the structural response of the pavements, the concept of the average of several of the closest crack spacings was developed. Individual crack spacing is very difficult to relate to the structural response that is provided by the effective length (or area) of the CRC pavement. The effective length is generally considered to be about one and a half to two times the RRS value on each side of the applied load—about 1.2 to 1.8 m on each side of the load. Thus, it was necessary to develop a different approach to represent the crack spacing pattern that would better incorporate the effective length of the pavement. The concept that was developed was to use the average spacing of the closest five cracks (ASCFC).

The plot of the ASCFC with distance is also useful in identifying locations of cluster cracking (groups of cracks with average spacing of less than about 0.6 m). Similarly, cracking patterns with large crack spacings can also be easily identified. The ASCFC trends provide a more visual definition of crack spacing pattern than use of the standard deviation or the coefficient of variation parameters. The ASCFC plot (with distance) can also be used to identify the extent of a pavement section that exhibits "acceptable" cracking pattern. For example, if acceptable values of ASCFC are assumed to be between 0.9 and 1.8 m, then as shown in Figure 5 the length of the pavement section outside the acceptable limits can be easily identified. It is possible that this length can be used as a performance indicator and compared with the extent of other manifested distresses, such as punchout and patching, ride quality, and so forth.

The RRS values were compared with crack spacing for each test section. The plot of basin test RRS values along side ASCFC indicates that pavement stiffness is not dependent on crack spacing as long as there is high load transfer efficiency at the transverse cracks. The load transfer effectiveness was generally greater than 90 percent for most of the test sections. However, there appears to be some interaction between cluster cracking (average crack spacing of less than 0.6 m) and RRS.

Overall, the variability in the RRS values along the test section appears to be more influenced by the apparent variability in the support condition. The extent of variability does not appear to be influenced by the base type (stabilized versus granular) or by the subgrade type (fine grained versus coarse grained).

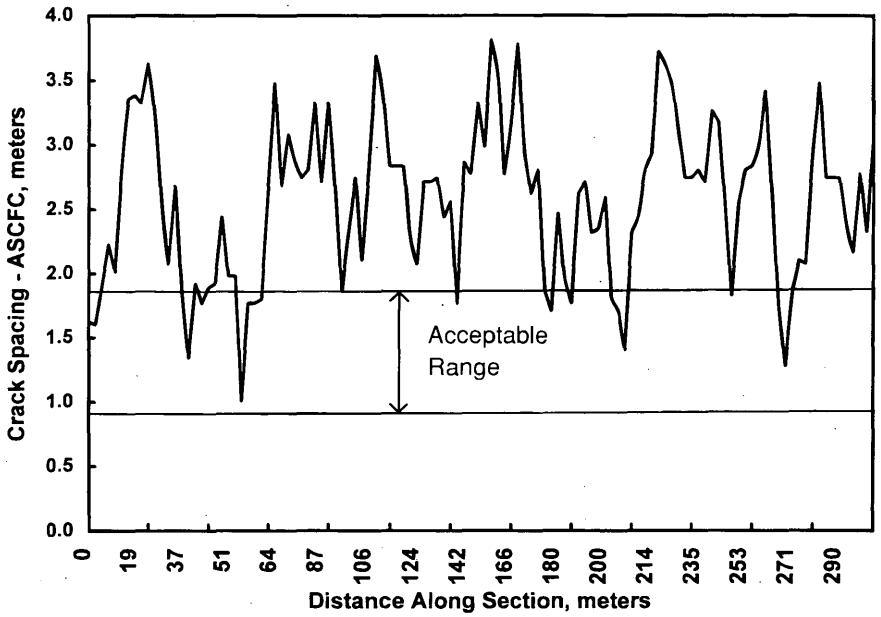

FIGURE 5 Illustration of procedure to identify extent of marginal cracking pattern.

Effect of Design Features on Crack Spacing Development

Thickness Effects No clear trends were apparent. The data were also confounded by age, percentage of steel, and climatic region.

Tied-Concrete Shoulder Effects No definitive trends were apparent between AC and PCC shoulder. The data were also confounded by age, percentage of steel, and climatic region.

Permeable Base Effects The two sections with permeable base exhibited slightly higher average crack spacings. However, both of these sections were young—IL-1 was only a few months old and OK-5 was only 2 years old. To further study the effect of permeable CTB, data from an additional CRC section constructed on a permeable CTB were obtained. This section was located along I-295 in Virginia (just south of the Exit 9B sign, near Milepost 8) and was constructed during the summer and fall of 1991. The section details are as follows:

- Slab thickness = 228 mm,
- Permeable CTB thickness = 101 mm,
- CTB thickness = 152 mm,
- Percentage of steel = 0.65,
- No tubes or chairs used—concrete placed in two lifts with the steel placed at the surface of the bottom lift,
- Permeable CTB cement content = 130 kg/m^3,
- Permeable CTB aggregate = ASTM No. 57, and
- Shoulder type = jointed plain concrete.

A 305-m length of the section was surveyed on May 17, 1994. The section exhibited the following cracking pattern:

- Total number of cracks per 305 m = 322,
- Average crack spacing = 0.95 m, and
- Standard deviation of crack spacing = 0.54 m.

The foregoing data indicate that 3 years after construction, the crack spacing along the permeable base section exhibits acceptable cracking pattern. Most of the cracks either exhibited no distress or were of low severity. Thus, the concern that CRC pavements constructed over permeable CTB may not exhibit acceptable cracking pattern (because of interlocking or bonding with the permeable base) may not be justifiable. However, it should be stressed that an adequate amount of steel ($\geq$0.65 percent) should be used to minimize any potential problems related to use of the permeable CTB.

Epoxy-Coated Bar Effects The three sections with epoxy-coated bars exhibited slightly lower average crack spacing. Although the sample size is small, it appears that the use of epoxy-coated reinforcement may not result in undesirable cracking pattern. [The current FHWA Technical Advisory T 5080.14 (dated June 5, 1990) recommends that the bond area be increased 15 percent to increase the bond strength between the concrete and reinforcement if epoxy-coated steel reinforcement is used.] This implies that 15 percent more steel bars should be used if epoxy-coated bars are used. The sections with epoxy-coated bars had the following steel amounts: OK-3 = 0.5 percent; WI-2 and WI-3 = 0.67 percent.

Thus, on the basis of limited data, it appears that use of 15 percent more steel bars may not be warranted provided the steel content is properly estimated.

Effect of Age on Crack Spacing There appears to be a trend toward a decrease in crack spacing with age with crack spacing stabilizing after about 8 to 10 years. Crack spacing appears to have an effect on ride quality and estimated present serviceability index (PSI). Shorter crack spacing results in higher IRI (and lower PSI) values, indicating that cluster cracking may result in poorer riding surface.

Load Transfer Efficiencies at Cracks and Crack Width Analysis

Load transfer efficiencies were determined using the data from the morning and afternoon testing at crack locations. All sections,

except the Oklahoma sections and WI-1 exhibited high load transfer efficiencies (greater than 90 percent) at crack locations. The Oklahoma sections have the widest crack spacings due to a smaller steel amount. This may be contributing to the development of the poor load transfer at crack locations.

Crack widths at the test section ranged from 0.2 to about 0.84 mm (ignoring the apparent high values noted at the two Pennsylvania sites) during the mornings. The morning slab middepth temperatures during crack width measurements ranged from 5°C to about 18°C. The cracks did close a little during the afternoon when midslab temperatures increased from about −15°C to −9°C. For each section, the crack widths were normalized to middepth slab temperatures of 5°C and −18°C to allow comparisons between sites. The normalization was performed by using the laboratory measured coefficient of thermal expansion for the 30.5-m subsection used for crack width measurements.

The normalized crack width (at 5°C) ranged from 0.24 mm at IL-1 to 1.01 mm at OK-1 and WI-1. The average normalized crack width at 5°C was 0.59 mm. Limiting crack width criteria for CRC pavements are presented in the AASHTO Guide based on studies performed in Texas. A maximum crack width of 1.07 mm is recommended to avoid spalling. For the wet-freeze region test sections, using the crack width data normalized to −18°C, the IA-1, WI-1, and WI-4 were marginal for the AASHTO crack width criteria. It should be noted that WI-1 also had lower load transfer efficiency at the crack locations.

Effect of Steel Amount

The longitudinal reinforcement has a significant influence on the performance of CRC pavements. Higher amounts of reinforcement result in smaller crack spacing for a given set of conditions (concrete quality, climatic conditions). Figure 6 shows the effect of steel amount on crack spacing. Considering that the data points incorporate a broad range of pavement age, concrete quality, and climatic conditions, there is a strong overriding linkage between the percentage of steel and crack spacing. With a steel amount of about 0.8 percent, average crack spacing may approach about 0.6 m, which borders on undesirable crack spacing in the presence of poor support conditions and results in a high incidence of cluster cracking and a high potential for future punchouts when the support condition is marginal. A steel amount in the range of 0.6 to 0.7 percent appears to provide average long-term crack spacing ranging from 0.9 to 1.5 m. It should also be pointed out that some of the European experience indicates that close crack spacing (e.g., average crack spacing of 0.6 m) from using a steel amount of 0.85 percent can still provide excellent performance under heavy truck traffic provided that a good support condition is constructed (*4*).

It should be noted that during the design process, the amount of steel determined to obtain acceptable crack spacing, crack width, and steel stresses is based on the assumption that the design concrete strength will be obtained. However, for a given (design) steel content, if a higher concrete strength is actually obtained, crack spacings may be larger than anticipated. Similarly, if lower concrete strength is actually obtained during construction, a much closer crack spacing may result. This is very important to establish, especially when using a marginal amount of steel—less than 0.6 percent. The larger crack spacing may result in higher steel stress and wider cracks resulting in premature failures. Therefore, if the possibility exists that higher-than-specified concrete strengths may be obtained on any given project, the prudent course would be to specify a slightly higher steel content to accommodate the expected higher concrete strength.

Based on the data obtained as part of this study, use of steel in an amount less than 0.6 percent is not recommended because the cracking pattern that develops is marginal. The larger crack spacings that develop as a result of a low steel amount create potential locations for steel ruptures and punchouts at closely spaced cracking adjacent to widely spaced (greater than 3.7 m) cracks.

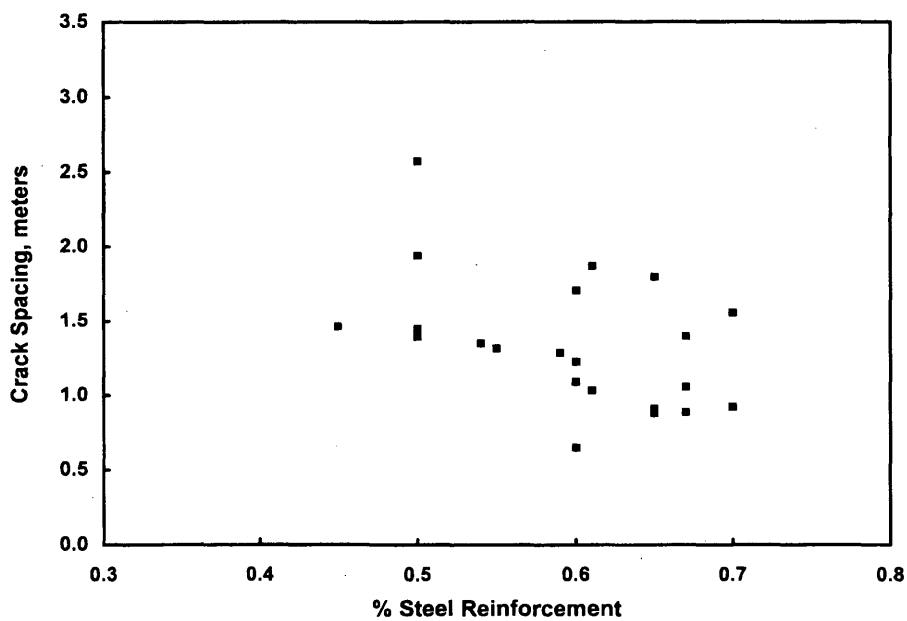

FIGURE 6 Average crack spacing as function of percentage of steel reinforcement.

Summary of Distresses

Pavements 15 years old and older generally exhibited moderate severity of spalling at transverse cracks. The older pavements also exhibited various amounts of patching. Sections WI-1 and WI-5 had the most patches (partial and full depth) within the 305-m sections tested. Only two sections (OK-4 and PA-2) exhibited punchouts that had not been patched. There appeared to be no correlation between patching amount and ride quality, indicating that the patches, if constructed properly, are not detrimental to ride quality. Steel corrosion based on core examination was found at most of the sections in the wet-freeze regions with the exception of sections where epoxy-coated reinforcement was used.

SUMMARY AND RECOMMENDATIONS

The study has highlighted many new methods for evaluating CRC pavement performance incorporating the results of distress surveys (cracking pattern), crack width measurements, deflection testing along the edge and crack locations, and ride quality evaluation. An attempt was made to determine why certain CRC pavement sections behaved (in terms of cracking pattern) significantly differently from other sections with many factors being similar for these sections. The different cracking patterns at IA-1, OK-1, and OR-2 (compared with other in-state sections) could not be explained directly. It is quite possible that the ambient temperature conditions and curing conditions at these sections may have contributed to the development of the cracking pattern.

There is a strong interaction among percentage of steel, concrete strength, and crack spacing. For conventionally used concrete strengths (splitting tensile strength at 28 days of about 3,000 kPa), steel in the amount of 0.6 to 0.7 percent appears to provide desirable long-term average crack spacing in the range of 0.9 to 1.5 m. The reader is cautioned about the use of steel content less than 0.6 percent; it is clear from the Oklahoma test sections and a recent Maryland project along U.S. 50 (not reported here) that use of 0.5 percent steel will result in longer crack spacings and possible premature development of punchouts at closely spaced cracks adjacent to longer spaced cracks. The use of 0.65 percent as the minimum steel content is strongly recommended with the conventional concrete strengths typically used in the United States. If a higher steel content is to be used, appropriately higher strength concrete should be specified to maintain desirable average crack spacing in the range of 0.9 to 1.5 m or a stabilized base must be specified.

The effect of tied-concrete shoulder could not be classified as positive with respect to improving the structural response of the CRC pavements (as indicated by deflection testing along the edges). Use of tied-concrete shoulders may have other advantages and as such may be used in conjunction with CRC pavements. The use of widened lanes for CRC pavement appears to be promising and should be seriously considered as a design option. Based on the good performance of the three Oregon sections (each incorporating a 4-m-wide outside lane), using widened lanes should not cause concern because of the longer aspect ratio for each cracked portion of the pavement.

The effect of base type on CRC performance was not pronounced. The concern about using a hard support (e.g., LCB) could not be clearly addressed. The two sections with permeable bases exhibited higher crack spacing. However, both sections were young and one of the sections was constructed with a smaller amount of steel. Also, a separate evaluation of a 3-year-old Virginia CRC pavement constructed with a permeable CTB indicated that adequate crack spacing can develop in CRC pavements incorporating permeable CTB.

The use of epoxy-coated reinforcement resulted in no undesirable cracking pattern. The FHWA Technical Advisory T5080.14 (dated June 5, 1990) recommends that the bond area be increased 15 percent to increase the bond strength between the concrete and reinforcement if epoxy-coated steel reinforcement is used. This implies that 15 percent more steel should be used if epoxy-coated bars are used. Based on the limited field data, it appears that the use of 15 percent more steel may not be warranted provided the steel content is properly estimated. However, additional field data need to be compiled to verify this observation.

Based on the deflection testing, the following summary is presented.

- Load transfer efficiencies at transverse cracks of CRC pavements, even after many years of service, remain high—generally greater than 90 percent, provided that an adequate steel amount is used.
- The radius of relative stiffness, l, did not characterize well the effective pavement stiffness along the edge. The better parameter to describe the edge structural stiffness is the slab rigidity, D. The D-values were found to be considerably lower along the edge than at the interior. The backcalculated D-value may be a better indicator of potential punchout locations.
- Deflection data did not correlate well with the cracking pattern, indicating that the pavement stiffness is not dependent on crack spacing as long as there is high load transfer efficiency at the transverse cracks. Overall, the variability in the backcalculated pavement stiffness values appears to be influenced more by the apparent variability in the support condition.

Further research and development for CRC pavement should focus on improving the cracking pattern of the pavement through improved construction and design technology. For many years, the design of CRC pavement has focused on the percentage of steel reinforcement and the expected drop in pavement temperature over the course of a year. However, it is clear that the crack pattern of CRC pavement cannot be controlled by the steel design alone and that other considerations should be included in the design process, such as the type of aggregate, method of curing, concrete shrinkage potential, depth of steel cover, and rate of strength gain in the first 3 days, among others. Also, the design process for a CRC pavement should continue through construction and not end as soon as the plans and specifications are prepared. A more active interaction between the design process and actual ambient conditions during construction needs to be developed to achieve CRC pavements with acceptable cracking patterns. This may require imposing of guidelines on acceptable ambient conditions for placement of CRC pavements.

ACKNOWLEDGMENTS

The authors acknowledge the fine support provided by the many state highway agencies during the various phases of the data collection process, specifically, the many highway agency personnel from Illinois, Iowa, Oklahoma, Oregon, Pennsylvania, and Wisconsin that supplied site-specific pavement-related data and provided access and traffic control during the testing. Special thanks also go to the Oregon Department of Transportation for providing

more extensive field testing support (FWD testing and coring). The support of the State Technical Advisory Committee and various FHWA staff (particularly Jim Sherwood and Roger Larson) is gratefully acknowledged.

REFERENCES

1. Tayabji, S. D., P. J. Stephanos, J. S. Gagnon, and D. G. Zollinger. *Performance of CRC Pavements: Volume 2—Field Investigation of CRC Pavements.* Report prepared for the Office of Research and Development, FHWA, U.S. Department of Transportation, June 1994.
2. Tayabji, S. D., D. G. Zollinger, J. R. Vederey, and J. S. Gagnon. *Performance of CRC Pavements: Volume 3—Analysis and Evaluation of Field Test Data.* Report prepared for the Office of Research and Development, FHWA, U.S. Department of Transportation, June 1994.
3. Ioannides, A. M. *Program ILLI-BACK—A Closed-Form Backcalculation Procedure for Rigid Pavements.* Savoy, Ill., 1988.
4. Verhoeven, K. Cracking and Corrosion in Continuously Reinforced Concrete Pavement. *Proc., 5th International Conference on Concrete Pavement Design and Rehabilitation,* Purdue University, West Lafayette, Ind., 1993.

Publication of this paper sponsored by Committee on Rigid Pavement Design.

Estimating Load Transfer From Measured Joint Efficiency in Concrete Pavements

YU T. CHOU

Relationships between joint efficiency and load transfer for jointed plain concrete pavements have been established using the finite-element method ILLISLAB program. Efforts were made to show that the relationship depends not only on *a/l* but also on *L/l*, where *L* is the size of the square concrete slabs, *a* is the radius of the single-wheel load, and *l* is the radius of relative stiffness of the concrete slab. It is proposed that the relationship between joint efficiency and load transfer be developed based on *L/l* values. Four sets of curves were developed using *L/l* and for each set, the curves were separated for different ratios of *a/l*. The procedure of equivalent single-wheel radius for multiple-wheel gear loads is discussed and recommended.

The load transfer of jointed plain concrete pavements has been estimated on the basis of measured deflections across the joints (joint efficiency) using falling weight deflectometer (FWD) tests. The procedure is expedient and reliable. Review of the procedure indicated that the methodology can be improved, and this paper documents the proposed improvement.

Finite-element methods have been used to estimate load transfer from measured deflections of FWD tests. The results of an analysis conducted using the finite-element program WESLIQID in which a range of thicknesses, moduli of subgrade reaction, and joint stiffness parameters on 6.1-m (20-ft) square slabs were used to determine joint efficiency and load transfer for a variety of conditions were reported (*1*). These data were used (*2*) to determine a quadratic regression equation relating joint efficiency and load transfer. A relationship between load transfer and joint efficiency that closely parallels the Rollings regression equation by using the finite-element program ILLISLAB was developed (*3*).

LOAD TRANSFER ALONG JOINTS

Joints are placed in rigid pavements to control cracking and provide enough space and freedom for movement. Load is transferred across a joint principally by shear forces and in some cases by moment transfer. Shear force is provided by either dowel bars, keyed joint, or aggregate interlock. Moment transfer, on the other hand, is provided by the strength of the concrete slab or in-place thrust, or both, that is produced by heating the slab. When a joint has a visible opening, the transfer of moment across the joint becomes negligible. It is therefore justified to assume that there is no moment transfer across a joint (except in cases such as a tied joint where some moment transfer may be expected if the joint remains tightly closed).

Pavement Systems Division, Geotechnical Laboratory, U.S. Army Engineer Waterways Experiment Station, Vicksburg, Miss. 39180-6199.

If moment transfer across a joint is neglected, the amount of load transfer at a joint is governed by the difference in deflection between the two slabs along the joint. At the U.S. Army Corps of Engineers, the load transfer is defined as the ratio of the strain on the unloaded side of the joint to that of the total strain (the sum of the strains on both unloaded and loaded sides) expressed as a percentage. The load transfer is 50 percent if deflections of both slabs are equal. The measured joint efficiency is defined as the ratio of deflections of the unloaded to the loaded slabs. Field measurements with strain gauges conducted by the Corps of Engineers in many military airfields (*4*) indicated that the dowel bars were not effective; their average load transfer across a joint was only about 25 percent.

ESTIMATE OF LOAD TRANSFER FROM FALLING WEIGHT DEFLECTOMETER

Finite-Element Analysis

The ILLISLAB program was used (*5*) to show that load transfer is a function of both the joint efficiency and the ratio of the radius of loaded area *a* to the radius of relative stiffness *l*, or an *a/l* ratio. The *a/l* ratio accounts for differences in the way the load is applied to the joint by considering *a*, and for the relative stiffness between the slab and foundation subgrade soil *l*, which accommodates the variables of slab thickness *h*, modulus of elasticity *E*, Poisson's ratio ν, and modulus of subgrade reaction *k*, as shown in Equation 1.

$$l = \{Eh^3/[12\,(1 - \nu^2)]k\}^{0.25} \quad (1)$$

By varying only the radius of loaded area *a*, and with the following conditions:

- Slab thickness h = 25.4 cm (10 in.), ν = 0.15;
- Slab length L = 4.58 m (15 ft), l = 91.8 cm (36.135 in.);
- Slab width W = 3.57 m (11.7 ft), E = 27,560,000 kPa (4,000,000 psi); and
- Modulus of subgrade reaction k = 3,204 kg/m^3 (200 pci).

A number of finite-element runs were conducted with varying joint stiffness (spring constant) for each of four *a/l* ratios—0.047, 0.156, 0.312, and 0.584. The slab thickness and slab size were kept constant at 25.4 cm (10 in.) and 4.58 m (15 ft) in length and 3.57 m (11.7 ft) in width, respectively, in the computation. The results are plotted in Figure 1.

Although the curves developed by Korovesis (*5*) and extended by Pittman (*6*) (Figure 1) account for differences in the way the load is applied to the slab by considering the ratio *a/l*, a constant slab size

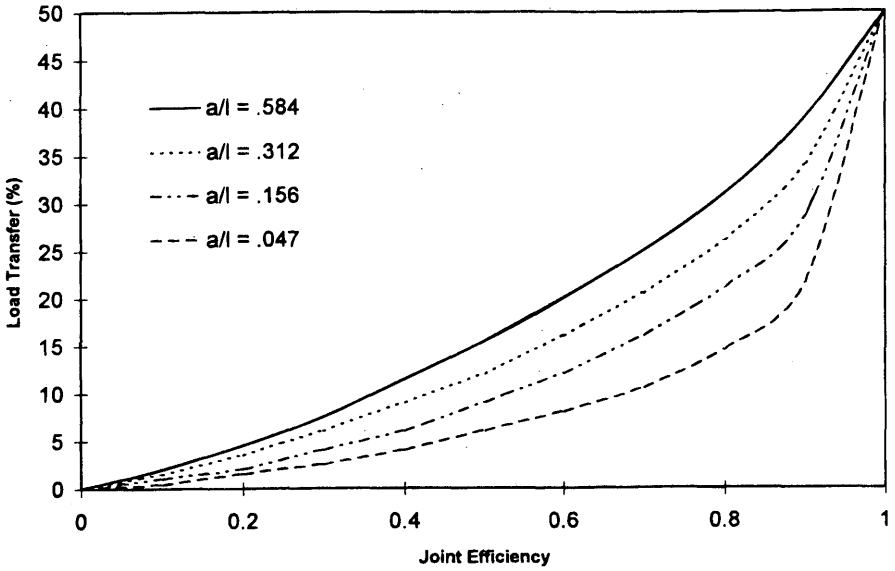

FIGURE 1 Relationship between joint efficiency and load transfer.

4.58 m (15 ft) long, 3.57 m (11.7 ft) wide, and 25.4 cm (10 in.) thick was used throughout that work developing the relationship between joint efficiency and load transfer. However, slab size is critical in problems involving deflections, which are discussed in the following paragraphs.

Westergaard's solution has been used for computing maximum edge stresses in concrete slabs. The slab is assumed to be infinite in length in the two directions. Field results indicated that computed stresses using Westergaard's solution were close to the measured values. By using the finite-element method ILLISLAB, it was found that slab size has much less effect on computed stress than on computed deflection. The computed results for single square slabs are presented in Table 1, which shows that as the slab size increases, deflection decreases and stress increases, but the rate of change is more significant in deflection than in stress.

Concrete pavement thickness design is based on the critical tensile stress, and when the finite-element method is used, it is generally believed that slab size is not critical as long as the slab is of rea-

TABLE 1 Computed Stresses and Deflections [E = 27,560,000 kPa (4,000,000 psi), k = 689 kPa (100 pci), ν = 0.15]

Slab Size L, m	L/l	Deflection mm	Stress kPa	Percent Change Deflection	Percent Change Stress
3.05	2.44	1.90	3,272.1	0	0
4.58	3.65	1.26	3,688.2	-33.8	12.7
6.10	4.87	1.13	3,801.2	-40.7	16.2
7.63	6.09	1.08	3,810.2	-43.3	16.4
9.15	7.31	1.05	3,809.5	-44.6	16.4

Notes:

The change in percentage is based on values computed for L=3.05m (10 ft). The single-wheel load is placed at the center of the slab edge. 1 m = 3.279 ft, 1 cm = 0.3937 in., 1 kPa = 0.1451 psi.

sonable size. For instance, a 4.58-m^2 (15- by 15-ft) slab is believed large enough for stress analysis under a single-wheel load on a 30.5-cm (12-in.) diameter area. This is correct in pavement thickness design in which the magnitude of critical tensile stress controls. It is particularly true for highway pavements where the slab thickness is relatively thin compared with airfield pavements. Based on the results of the analysis of this study, it was found that in the relationship between load transfer and joint efficiency in which deflections are involved, the slab size should vary depending on the following variables: slab thickness, subgrade strength, concrete modulus, and loaded area. A dimensionless factor L/l was introduced in which L is the size of the square slab and l is the radius of relative stiffness defined in Equation 1. Equation 1 shows that a larger slab is needed for thicker pavements, greater concrete moduli, or weaker subgrades. In other words, when a comparison is made involving deflection for two different slabs, the L/l values should be compatible. This may be demonstrated using the ILLISLAB program.

The analysis was made on a two-slab system under a single-wheel load placed at the slab edge at the center of the joint. Several values of joint stiffness, represented by spring constants, were used in the computation, and the E, K, and ν values were the same as shown for Table 1. Figure 2 shows the relationship between the joint efficiency and load transfer for two sets of L/l curves. For each L/l value, the slab thickness h and l are constants and the loaded area a varies, which results in varying a/l ratios. It needs to be pointed out that the slab size L in the two cases being nearly the same—4.64 and 4.61 m (15.2 and 15.1 ft)—is purely coincidental.

Figure 1 demonstrated that in the relationship between joint efficiency and load transfer, the curves with varying a/l ratios are plotted in descending order, with larger a/l at the upper position. The load transfer capability can be determined from the measured joint efficiency for a given a/l ratio. Figure 2 shows both Curves 3 and 5 having the same a/l ratio of 0.082, but the curves do not yield the same result, (i.e., for a given joint efficiency, different load transfer is obtained for different L/l value). Also, Curve 4 (L/l = 2.5), which has an a/l ratio of 0.415, is plotted below Curves 2 and 3 (L/l = 5), which have a/l ratios smaller than 0.415. Figure 2 demonstrated that when curves with different L/l values are plotted together, the curves will not be placed in order following the a/l ratios, which defeats the purpose of the relationship between the joint efficiency and load transfer. It is suggested that the curves be plotted separately based on the L/l value. Explaining it in a different manner, when conducting an FWD test, if the slab size L is 3.05 m (10 ft) and the slab thickness is 50.8 cm (20 in.), resulting in a L/l value of 1.7 [183.6 cm (l = 72.3 in.)], the load transfer should not be determined from the results of ILLISLAB analysis on a 6.1-m (L = 20-ft) slab (L/l = 3.4 and l = 72.3 in.) because a different load transfer will be obtained for the same a/l value.

The maximum stress and deflection in Westergaard's closed form solutions for a circular load at the slab edge are functions of a/l. However, it is of paramount importance to point out that this is true only for maximum stress and defection (i.e., at locations directly under the load).

Proposed Method

Figures 3 to 6 present the relationship between measured joint efficiency and load transfer for four different values of L/l. For each L/l, curves with varying a/l ratios are plotted. L/l ratios are determined

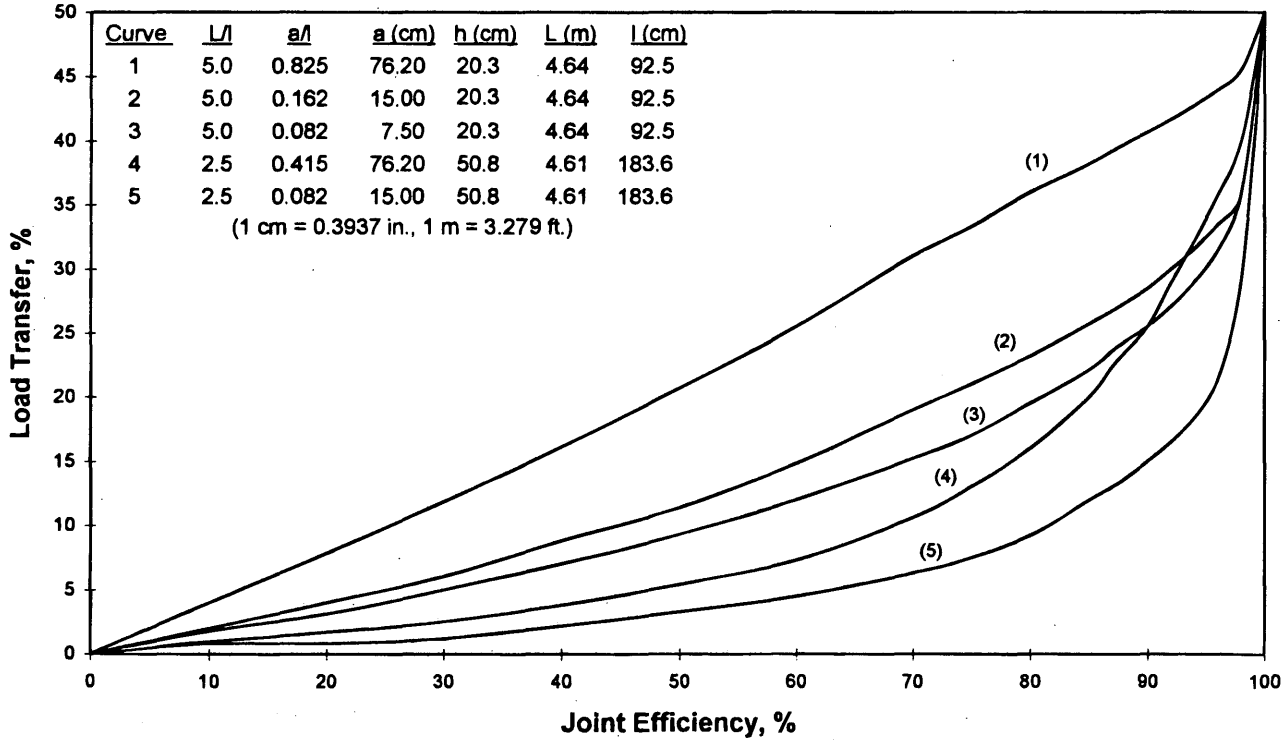

FIGURE 2 Relationship between joint efficiency and load transfer, L/l = 5.0 and L/l = 2.5.

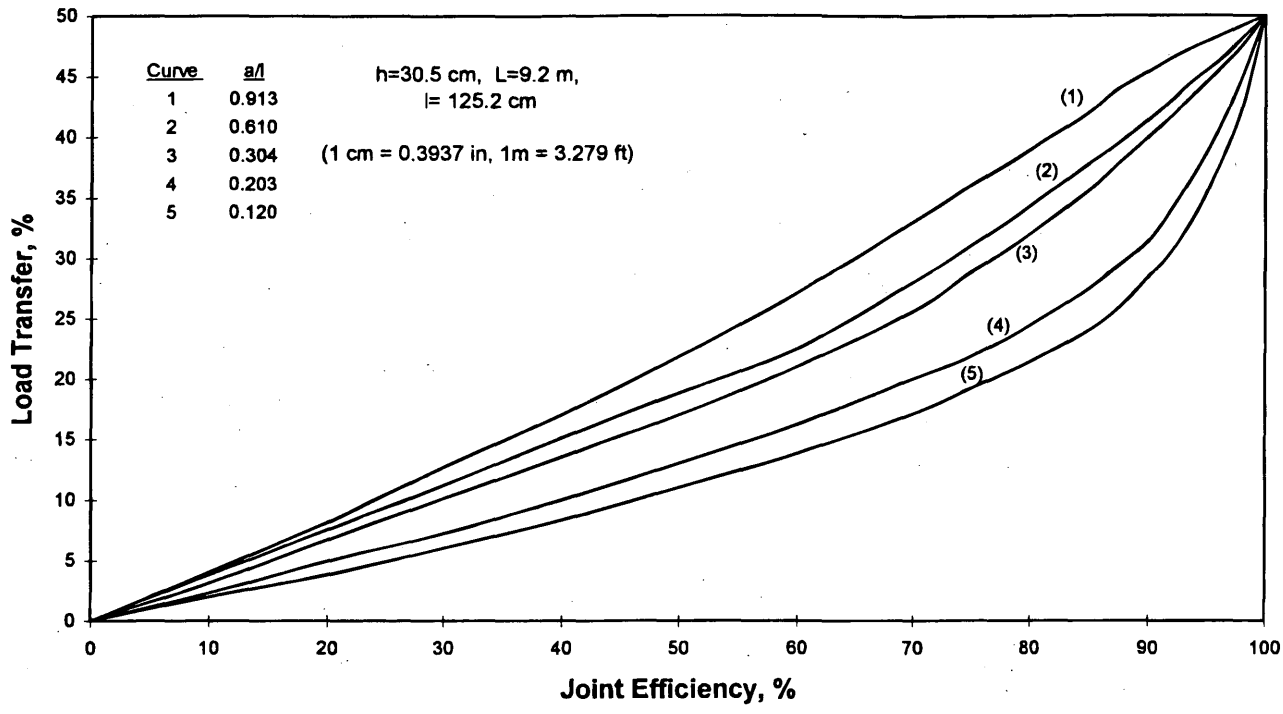

FIGURE 3 Relationship between joint efficiency and load transfer, L/l = 7.5.

with different slab size L and concrete slab thickness h. The E, k, and ν values are constants. Table 1 results in constant l for each L/l value. Figures 3 to 6 show that for L/l values less than 5, the difference between joint efficiency and load transfer is significant, but the difference becomes smaller in curves $L/l = 5$ (Figure 4) and 7.5 (Figure 3).

In using the ILLISLAB program, the following guidelines were used.

- Circular wheel loads were converted to square loads of the same area and same magnitude.
- The foundation was represented by the Winkler energy consistent uniform subgrade, not the springs subgrade used in the Westergaard's solution.
- Maximum tensile stress and deflection were selected in determining the joint efficiency and load transfer.

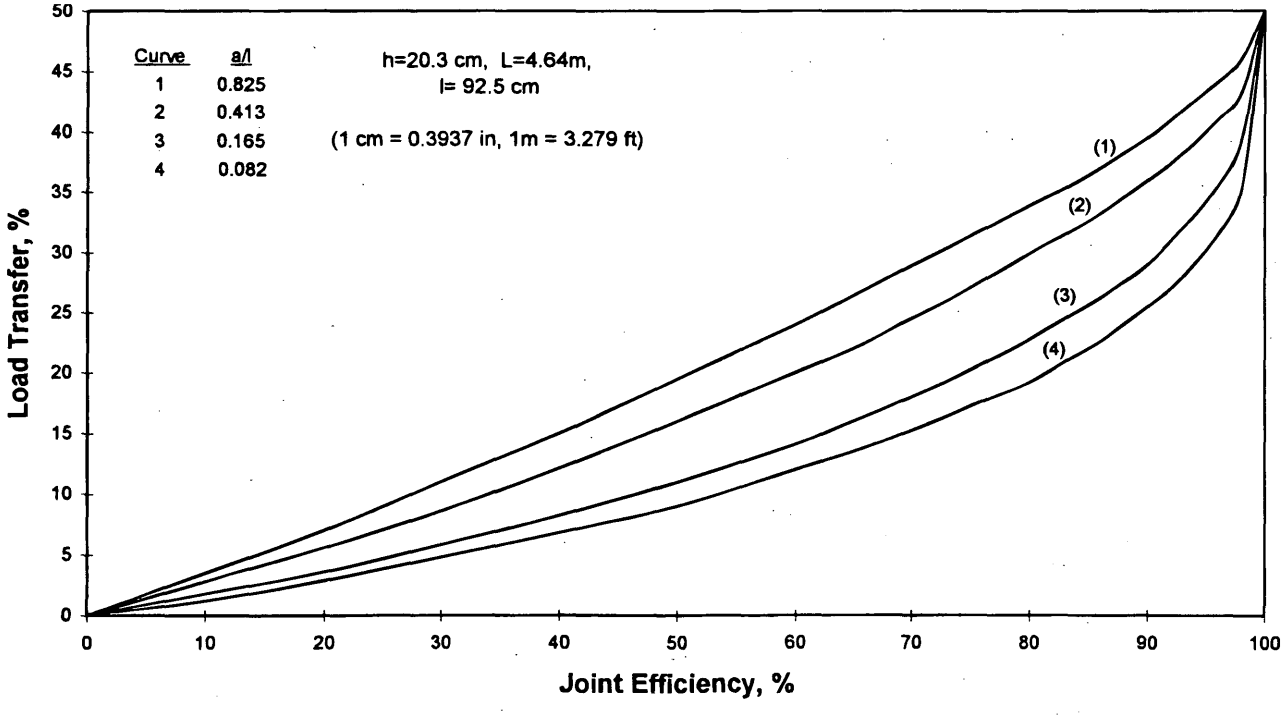

FIGURE 4 Relationship between joint efficiency and load transfer, L/l = 5.0.

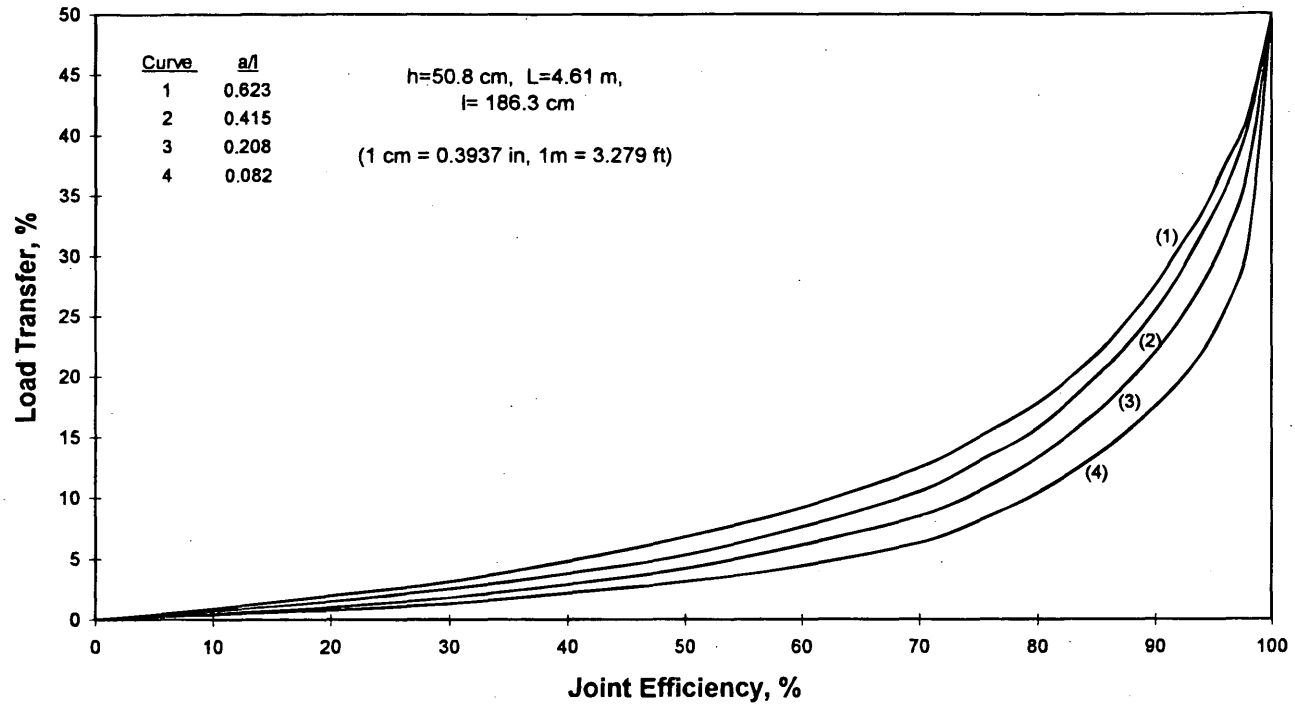

FIGURE 5 Relationship between joint efficiency and load transfer, L/*l* = 2.5.

• The total number of elements depends on the size of the slab *L*. A 25.4-cm (10- by 10-in.) grid is generally used in both directions of the slab, resulting in an element aspect ratio of unity. For smaller loaded areas, grid sizes smaller than 10 in. were used at and near the load, but the aspect ratio for elements near slab edges and locations away from the load were kept less than two. For thinner slabs [h = 20.3 cm (8 in.)], element sizes smaller than 25.4 cm (10 in.) were used.

To verify the correctness of the curves presented in the figures, additional computations were made and the results are presented in Figure 7. Curve 1 in Figure 4 ($L/l = 5$ and $a/l = 0.082$) is reproduced

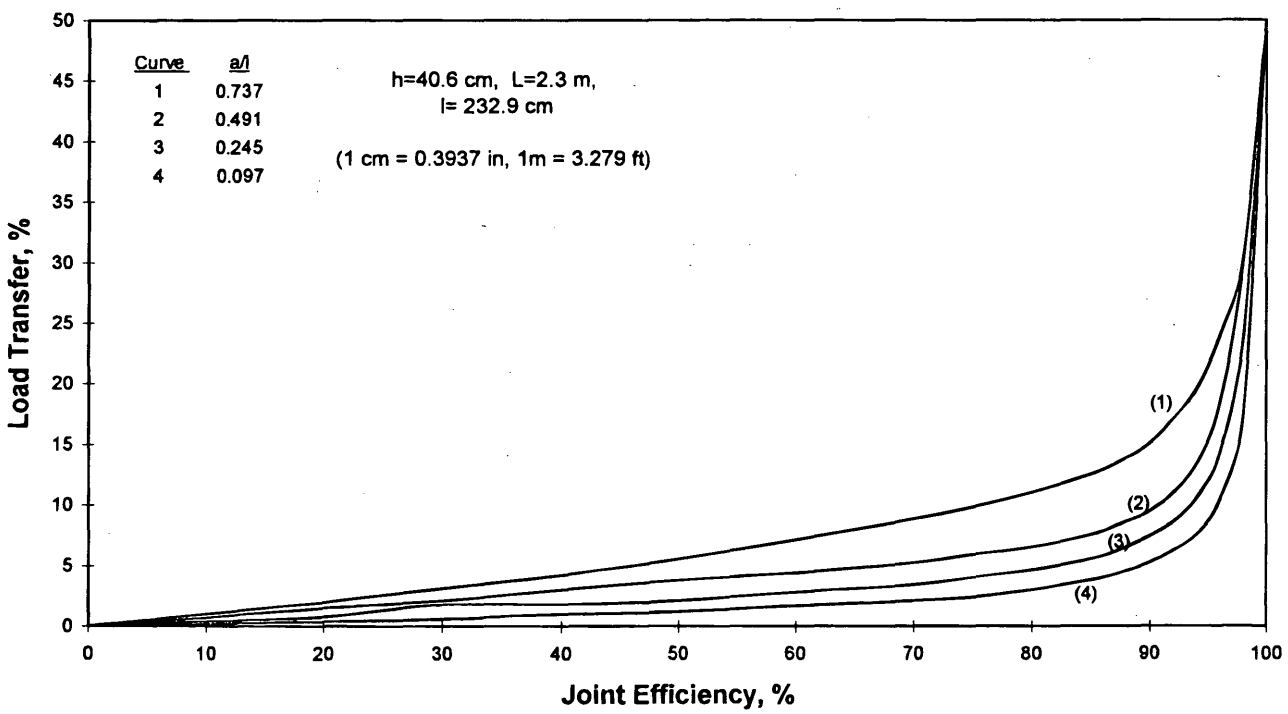

FIGURE 6 Relationship between joint efficiency and load transfer, L/*l* = 1.5.

in the figure in which the points on the curve were computed for the condition a = 7.54 cm (2.97 in.), h = 20.3 cm (8 in.), and L = 4.64 m (15.2 ft). For a completely different condition with slab size L = 30 ft, slab thickness h = 50.8 cm (20 in.), and loaded radius a = 15 cm (5.9 in.), that result in L/l = 5 and a/l = 0.082 satisfying the condition for using Curve 1, the joint efficiency and load transfer were computed and represented as the "crosses," which plot very close to Curve 1. It means that for an FWD test with a 30-cm (11.8-in.) diameter loading plate (a = 5.9 in.) and for a test pavement 50.8 cm (20 in.) thick and a slab size of 9.15 m (30 ft) (i.e., L/l = 5 and a/l = 0.082), the load transfer can be determined from the measured joint efficiency using Curve 1, which has L/l = 5 and a/l = 0.082.

Similarly, Curve 2 in Figure 5 (L/l = 2.5 and a/l = 0.415) is reproduced in the figure. The points on the curve were computed based on the condition a = 76.2 cm (30 in.), h = 50.8 cm (20 in.), and L = 4.61 m (15.1 ft). Similarly, assuming a condition L = 3.14 m (10.3 ft), h = 30.5 cm (12 in.), and a = 51.94 cm (20.45 in.), which resulted in L/l = 2.5 and a/l = 0.415 satisfying the condition for using Curve 2, the computed values of joint efficiency and load transfer are represented as the "dots," which also plot close to Curve 2. In other words, for a single-wheel load with a 152.4-cm (60-in.) diameter loaded area [a = 76.2 cm (30 in.)], a test pavement with a thickness of 30.5 cm (12 in.), and a slab size of 3.14 m (10.3 by 10.3 ft) (i.e., L/l = 2.5 and a/l = 0.415), the load transfer can be determined from the measured joint efficiency using Curve 2, which has L/l = 2.5 and a/l = 0.415.

The reason that the parameter L/l influences the relationship between joint efficiency and load transfer lies in deflections being involved in the relationship. When slab size is increased, deflections are reduced and stresses are increased, and the combination of the changes together with the possible interaction of loaded area can separate the curves having the same a/l ratio but having a different L/l value.

Computations were all made for the condition E = 27,560,000 kPa (4,000,000 psi), ν = 0.15, and k = 1,602 kg/m^3 (100 pci). Attempts were made to vary E, h, and k to determine whether the change would affect the computed results. Curve 1 in Figure 7 was chosen for comparison. The following five sets of h, k, and E values were selected:

- h = 20.3 cm, k = 801 kg/m^3, E = 13,583,483 kPa,
- h = 20.3 cm, k = 3,204 kg/m^3, E = 54,333,933 kPa,
- h = 20.3 cm, k = 8,010 kg/m^3, E = 135,834,834 kPa,
- h = 25.5 cm, k = 3,204 kg/m^3, E = 27,560,000 kPa,
- h = 34.6 cm, k = 8,010 kg/m^3, E = 27,560,000 kPa,
- (1 m = 3.279 ft, 1 kg/m^3 = 0.0624 pci, 1 kPa = 0.1451 psi)

which result in the same radius of relative stiffness of the slab l [92 cm (36.22 in.)] and a/l = 0.082. The computed results are plotted along Curve 1 as squares marked with numbers. The squares are plotted on the curve, indicating the correctness of the method.

MULTIPLE-WHEEL GEAR LOADS

The procedure of equivalent single-wheel radius (ESWR) was proposed (*7*) to determine the load transfer in jointed plain concrete pavements. An ESWR is defined as the radius of a single tire that will cause an equal magnitude of edge stress in the pavement to that resulting from a multiple-wheel load. It was proven that the ESWR so determined can produce the same load transfer as the multiple-wheel load. The ESWR can then be used on curves similar to those shown in Figures 3 to 6 to determine the load transfer of the slabs under the multiple-wheel load based on the measured joint efficiency.

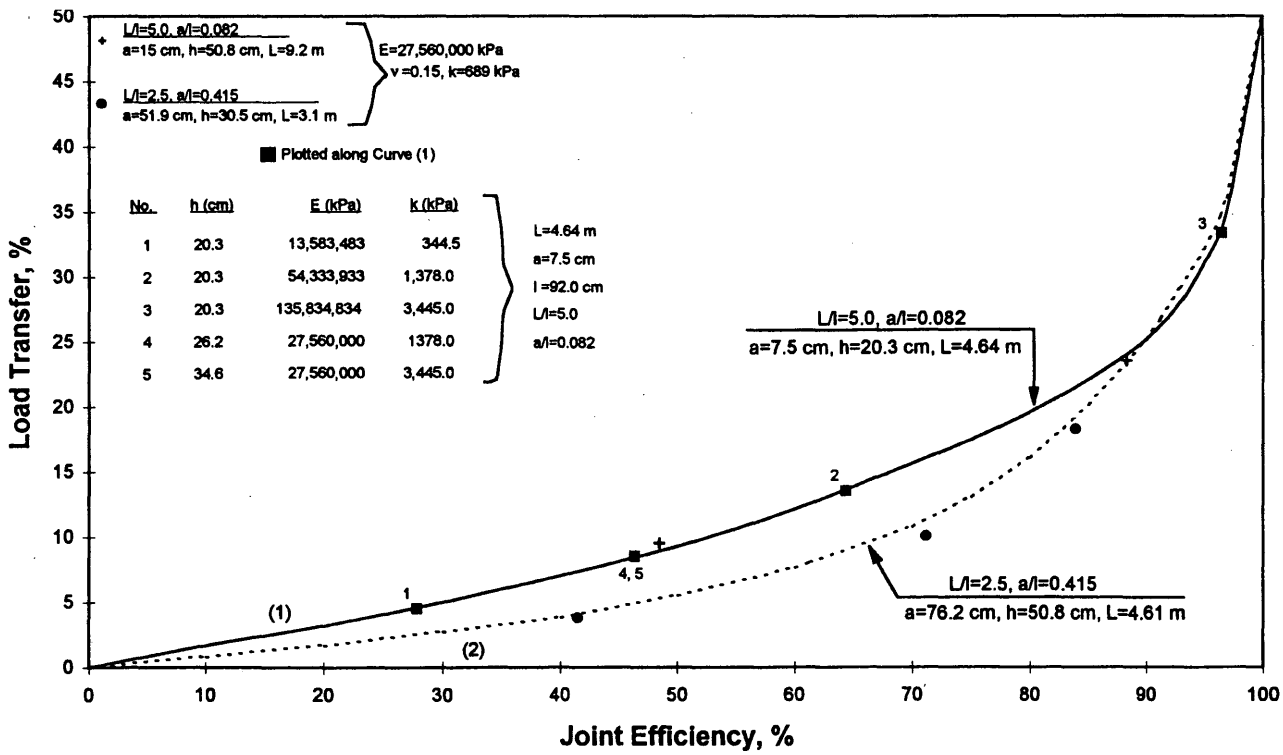

FIGURE 7 Verification of the proposed procedure.

TABLE 2 Computed Stresses and Deflections [E = 27,560,000 kPa (4,000,000 psi), k = 689 kPa (100 pci), ν = 0.15]

Radius of a Circular Loaded Area, cm 2.54 cm (1 in.)	Joint Efficiency, percent
7.5	59.9
15.0	65.0
38.1	62.5
76.2	64.5

Notes:

L = 4.58 m (15 ft), E = 27,560,000 kPa (4,000,000 psi)

k = 1,602 kg/cu m (100 pci), l = 93.35 cm (36.75 in.)

h = 20.32 cm (8 in.), L/l = 5.0

Joint spring constant = 55,120 kPa (8,000 psi)

It was assumed that the joint efficiency is independent of the loaded area during the measurement, that is, for the same slab the measured joint efficiency of the 30-cm (11.8-in.) loading plate FWD test (or other field measurements) is the same as the joint efficiency of the ESWR load. This assumption was verified with the computed results using ILLISLAB as shown in Table 2. The computed joint efficiency in jointed slabs is nearly the same under circular loaded area of different radius.

CONCLUSIONS

The relationships between measured joint efficiency and load transfer for jointed plain concrete pavements presented in Figures 3 to 6, as derived by the ILLISLAB program, may be used to determine the load transfer of concrete pavements based on the measured joint efficiency using FWD tests. The relationships depend not only on a/l but also on L/l, where L is the size of the square concrete slabs, a is the radius of the single-wheel load, and l is the radius of relative stiffness of the concrete slab. It is proposed that the relationship between joint efficiency and load transfer be developed based on L/l and a/l values. The ESWR proposed by Seiler's procedure (*6*) can be used to determine the load transfer of multiple-wheel gear loads.

REFERENCES

1. Chou, Y. T. *Investigation of the FAA Overlay Design Procedure for Rigid Pavements.* DOT/FAA/PM-83/22. Federal Aviation Administration, U.S. Department of Transportation, 1983.
2. Rollings, R. S. *Design of Overlays for Rigid Airport Pavements.* DOT/FAA/PM-87/19. Federal Aviation Administration, U.S. Department of Transportation, 1988.
3. Sawan, J. S., and M. I. Darter. *Structural Design of PCC Shoulders.* In Transportation Research Record 725, TRB, National Research Council, Washington, D.C., 1979.
4. *Field Tests of Doweled Joint Performance.* Ohio River Division Laboratories. Final Report. U.S. Army Engineer Division, Ohio River, Cincinnati, 1959.
5. Korovesis, G. T. *Analysis of Slab-on-Grade Systems Subjected to Wheel and Temperature Loadings.* Ph.D. dissertation. University of Illinois, Urbana, 1990.
6. Pittman, D. *Development of a Design Procedure for Roller-Compacted Concrete (RCC) Pavements,* Ph.D. dissertation, University of Texas, 1993.
7. Seiler, W. J. Expedient Stress Analysis of Jointed Concrete Pavement Loaded by Aircraft With Multiwheel Gear, In *Transportation Research Record* 1370, TRB, National Research Council, Washington, D.C., 1992.

Publication of this paper sponsored by Committee on Rigid Pavement Design.

Three-Dimensional Finite-Element Analysis of Jointed Concrete Pavement with Discontinuities

WAHEED UDDIN, ROBERT M. HACKETT, AJITH JOSEPH, ZHOU PAN, AND ALFRED B. CRAWLEY

A research study was conducted using the finite-element code ABAQUS to investigate the effects of pavement discontinuities on the surface deflection response of a jointed plain concrete pavement-subgrade model subjected to a standard falling weight deflectometer load. A significant improvement over the multilayered linear static analysis that does not allow for any discontinuity is shown. A three-dimensional pavement-subgrade finite-element model with appropriate boundary conditions has been developed. Transverse joints with dowel bars are modeled using gap and beam elements for an uncracked section, a section with cracked concrete layer, and a section with cracked concrete and cracked cement-treated base layers.

Structural analysis of a pavement-subgrade system subjected to a falling weight deflectometer (FWD) or moving wheel load based on layered linear elastic theory provides reasonable results if the pavement-subgrade system behaves as a linearly elastic system (*1*). However, for a deteriorated pavement-subgrade system with cracking and other pavement distresses (Figure 1), and where nonlinear behavior is expected from unbound granular pavement layers and subgrade, predicted linearly elastic response may differ significantly from measured response.

This paper presents some results of finite-element analyses of a jointed plain concrete pavement having discontinuities that is subjected to dynamic loading. Specifically, moduli for uncracked pavement and for pavement having cracks in both the concrete and base layers are backcalculated by matching finite-element simulation results to field measurements.

MULTILAYERED STATIC ANALYSIS OF A PAVEMENT-SUBGRADE SYSTEM

Pavement deflection response is usually analyzed using a multilayered linear elastic model under static load (*1*) to calculate the in situ Young's modulus for each layer in the pavement-subgrade system. In the multilayered linear elastic model of a pavement, each layer is characterized by its Young's modulus and its Poisson's ratio. Assuming a semi-infinite subgrade and infinite lateral boundaries, unique values of surface deflections at specified distances from the load can be theoretically predicted. Pavement nondestructive evaluation is performed through the measurement of surface deflections under a known dynamic load. The backcalculation procedure involves an iterative application of the multilayered elastic theory to calculate the in situ Young's modulus of the pavement layers. Surface deflections are predicted using assumed values of the Young's modulus and the Poisson's ratio of the pavement layers. Calculated surface deflections are matched with measured deflections until the percentage of error is reduced to an acceptably low value (*1,2*). The test load is simulated by an equivalent static load.

With the foregoing assumptions, the linearly elastic response of a pavement-subgrade model is reasonable, in the absence of pavement discontinuities and nonlinearities. However, these assumptions are clearly violated when the pavement is deteriorated or when the granular layers and subgrade exhibit nonlinear behavior, or both. Moreover, the assumption of static loading conditions is inconsistent with dynamic load application that occurs in operational situations.

THREE-DIMENSIONAL FINITE-ELEMENT ANALYSIS

Traditional pavement-subgrade analysis based on static load and multilayered linear elastic formulation with infinite dimensions in the horizontal plane and with a semi-infinite subgrade does not allow for dynamic behavior and pavement discontinuities. On the other hand, the finite-element method allows for the dynamic analysis of pavements and the consideration of finite or infinite dimensions of the physical pavement structure. Concrete pavement joints and voids beneath the pavement have in the past been modeled by the SLAB49 discrete element program (*3*). More recently, finite-element programs have been developed exclusively for pavement analysis, for example, ILLIPAVE for flexible and ILLISLAB for rigid pavements (*4,5*). These programs are capable of performing only static analyses.

The finite-element code ABAQUS is available for comprehensive structural pavement response analysis procedures, such as static and dynamic analysis (impulsive, steady-state vibratory forces, and moving wheel loads), a variety of material models (linear elastic as well as nonlinear elastic and viscoelastic material constitutive models), and problems involving crack modeling and body-to-body contact (*6,7*). The ABAQUS code for dynamic analysis, but of uncracked pavements, has been used successfully (*8*).

The finite-element method enables the evaluation of the state of stress and strain in a continuum by transforming the continuum into an assemblage of finite elements. The elements are interconnected

W. Uddin, R. M. Hackett, A. Joseph, and Z. Pan, Department of Civil Engineering, University of Mississippi, University, Miss. 38677. A. B. Crawley, Mississippi Department of Transportation, P.O. Box 1850, Jackson, Miss. 39215.

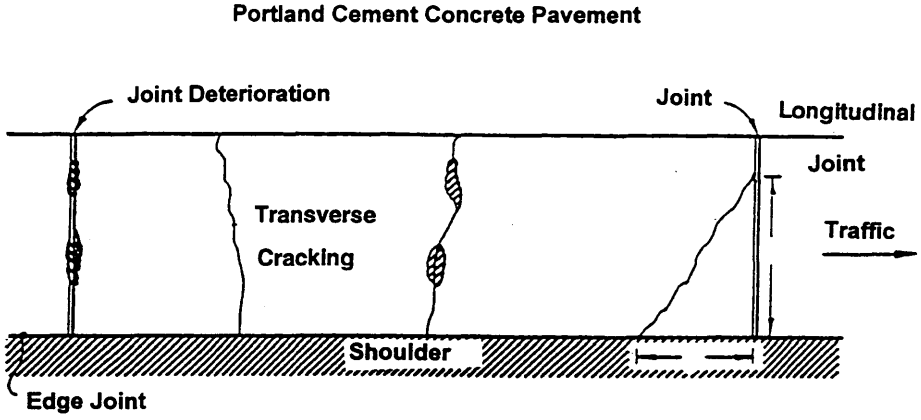

FIGURE 1 Typical concrete pavement discontinuities.

at their common nodes. Dynamic finite-element analysis involves the solution of the differential equation of motion:

$$M\ddot{U} + C\dot{U} + KU = F$$

where

M = mass matrix,
C = damping matrix,
K = stiffness matrix,
$\ddot{U}, \dot{U}, U$ = vectors of acceleration, velocity, and displacement, respectively, and
F = vector of nodal forces.

Integration of this equation yields displacements at the nodal points, for any given instant in time. The stresses and strains are computed through backsubstitution, using the kinematic and constitutive relationships.

THREE-DIMENSIONAL FINITE-ELEMENT MODELING

Finite-element modeling using any software package involves three stages: (a) preprocessing, where the finite element mesh is generated, loads and boundary conditions are assigned, and material properties are defined; (b) analysis, where displacements, stresses, and strains are computed; and (c) postprocessing, where the results are graphically presented. In the current study, the CAD/FEM program PATRAN is used as the pre- and postprocessor, and ABAQUS is used for the analysis. A brief description of these programs follows.

ABAQUS AND PATRAN SOFTWARE

The ABAQUS software (*6,7*) is a comprehensive finite-element code developed to solve two- and three-dimensional problems with static, harmonic, and transient dynamic loading and thermal gradient conditions. Material can be modeled as linear elastic, nonlinear elastic, viscoelastic, plastic, and modified elastic. Effects from cracks, voids, and material degradation can be analyzed. Computer simulation of the actual behavior can lead to a better understanding of pavement performance and to a reliable estimated prediction of loss of support over the pavement life.

PATRAN, a finite-element modeling computer program, supports powerful graphics capabilities for interactive mesh generation and output visualization (*9*). A finite-element model generated through the use of PATRAN is translated into ABAQUS input data, using a forward translation program. Subsequent to the analysis, the results from ABAQUS are translated back into PATRAN for graphical visualization and the plotting of results.

PAVEMENT-SUBGRADE MODEL PARAMETERS

The following dimensions and boundary conditions for a three-dimensional finite-element pavement model were investigated in a previous study (*10*):

- Rollers on the lateral sides of the model.
- Subgrade width of 13.3 m (43.65 ft) for the quarter-symmetric model.
- Pavement length of 9.14 m (30 ft). This is equal to one and one-half times the length of a typical concrete slab on U.S. Highway 78 in Marshall County, Mississippi.
- Discontinuous shoulders along the pavement edges, modeled using gap elements. The outside shoulder is 3.04 m (10 ft) wide.

FINITE-ELEMENT MODEL FOR PAVEMENT WITH NO DISTRESS

Mesh Configuration and Material Properties

The pavement is modeled as a three-layered linear elastic system that consists of a portland cement concrete layer, a cement-treated base (CTB) layer, and a subgrade. The thicknesses and material properties for a jointed plain concrete pavement structure of U.S. Highway 78 are shown on Table 1. FWD deflection data were collected from nine test sections on US-78 in May 1994.

FWD loading was used in the study. The center of the load was located 1.5 m (5 ft) from the edge of the outside shoulder and 3 m (10 ft) from the transverse joint.

Mesh size and configuration are an important part of finite-element modeling; precise mesh refinement is necessary in regions of high stress intensity. A refined mesh was developed for the vicinity of the loaded area and the transverse joint. The finite-element model was generated using PATRAN. The model has a subgrade depth of

TABLE 1 U.S. Highway 78 Pavement Structure and Moduli Backcalculated from Static Analyses

Layer	Thickness mm (inches)	Backcalculated Modulus, Mpa (ksi) 1994 FWD Deflection Data	
Concrete	254 (10.0)	36,855	(5,349)
Cement Treated Base (CTB)	152 (6.0)	4,272	(620)
Subgrade	Semi-infinite	176	(25.6)

12 m (40 ft) and has 7,546 finite elements. A three-dimensional view of the model is shown in Figure 2. The central processing unit time for running the model was approximately 200 sec on a Cray Y-MP supercomputer. This model was used for all of the simulations.

The overall dimensions of the model and the boundary conditions applied on the edges are based on the actual dimensions of the U.S. Highway 78 jointed plain concrete pavement under study and on the results of previous studies (*11*). During the current study, a detailed investigation of the U.S. Highway 78 pavement in Marshall County was conducted; it involved

- Detailed visual distress survey and mapping based on Strategic Highway Research Program procedures to identify good and deteriorated pavement sections,
- Ground-penetrating radar survey to establish pavement thickness nondestructively and to identify possible weak areas,
- Noncontact thermographic survey to establish locations having possible voids or moisture damage, or both,
- Coring to verify pavement layer thickness and to identify areas with loss of support, and
- Nondestructive deflection testing with FWD on transverse joints and midslab locations, and side-by-side Dynaflect testing on selected locations.

Transverse Joint Modeling

In Figure 3, the details of a typical transverse joint with dowel bars are shown. The dowel bars are modeled using beam elements.

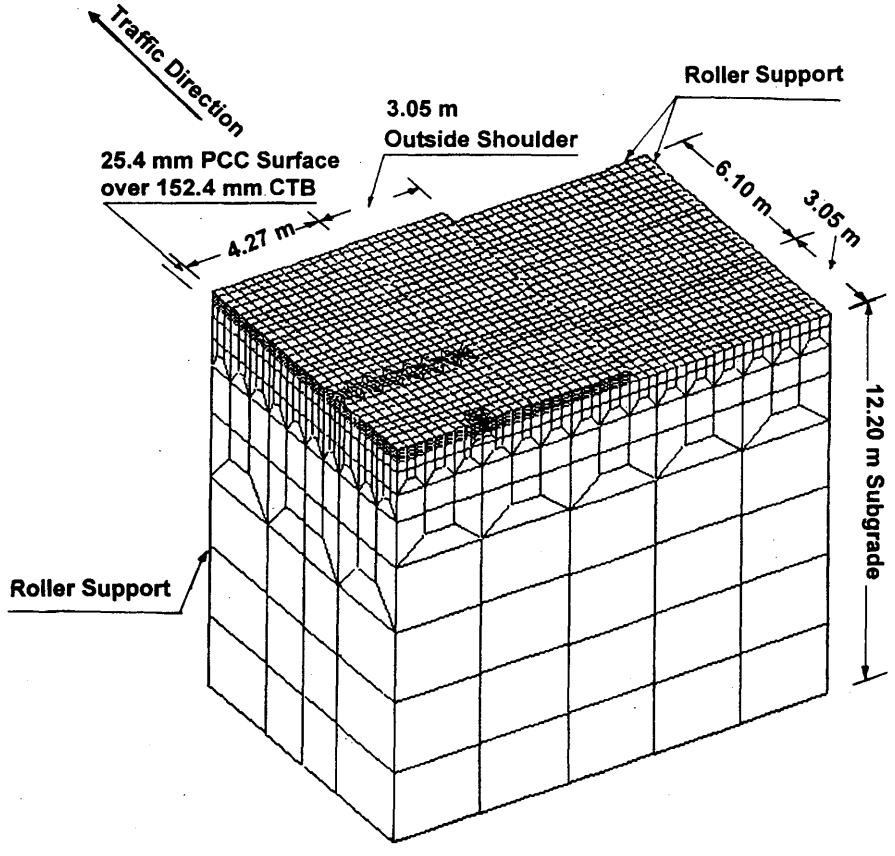

FIGURE 2 Three-dimensional view of the finite-element model.

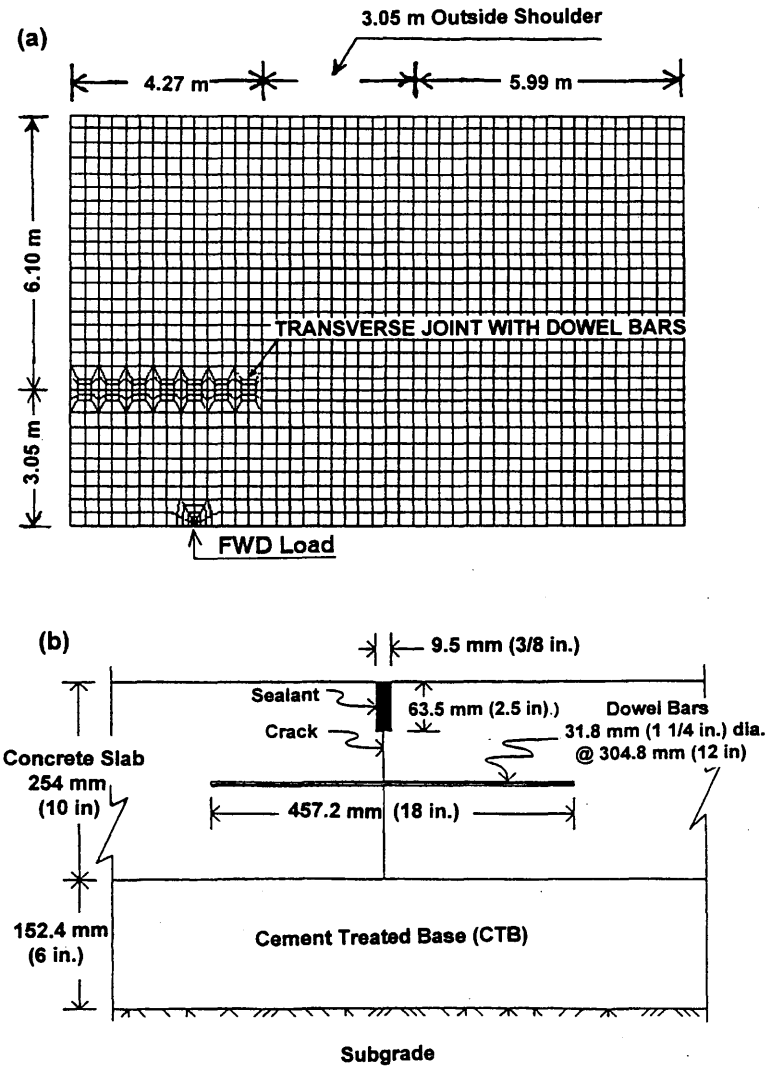

FIGURE 3 (a) Plan view of finite-element mesh and (b) cross section of transverse joint.

While one end of the dowel is fixed into one concrete slab, the other end is free to move back and forth in the adjacent concrete slab, depending on the thermal expansion or contraction of the slabs. Thus, the interaction between the dowel bar and the concrete involves body-to-body contact. Gap elements in ABAQUS are used in this regard. These elements are used to specify the interaction between the dowel and the surrounding concrete medium. The steel dowel bars are 457 mm (18 in.) long, with a circular cross section having a diameter of 31.75 mm (1.25 in.). The dowel bars are placed in the middle of the slab at 305-mm (12-in.) spacing. A Young's modulus of 206,700 MPa (30,000 ksi) and a Poisson's ratio of 0.3 are used to characterize the dowel bars. Also, a crack through the thickness of the concrete slab develops at the transverse joint immediately after construction. Gap elements are used to model the contact between the two faces of the crack. The use of these elements for modeling the crack is explained in detail in a later section.

Static Analysis Results

The FWD deflection data were analyzed using the static layered elastic analysis incorporated in the PEDD1 backcalculation software. The average backcalculated modulus values for uncracked pavement sections are presented in Table 1. These backcalculated modulus values provide an initial estimate of layer material properties for dynamic backcalculation using a simulated FWD load.

Pavement Modulus Backcalculation Using Dynamic Analysis Results

Dynamic analysis was performed using the ABAQUS implicit approach. This is different from the explicit procedure (*7*) in that the implicit method computes the deflections at any time t by knowing the deflections at time $t - 1$ by solving a set of nonlinear equations, whereas the explicit method computes the deflections at any time t by adding the deflection increments between time t and time $t - 1$, computed by double integration of the acceleration obtained from the dynamic equations at that degree of freedom, to the deflection at time $t - 1$. The FWD load time history based on a typical FWD pulse of 33-msec duration, measured on the test pavement, is used to simulate the FWD impact load. The ABAQUS dynamic deflections were compared with the FWD measured deflections, and modulus

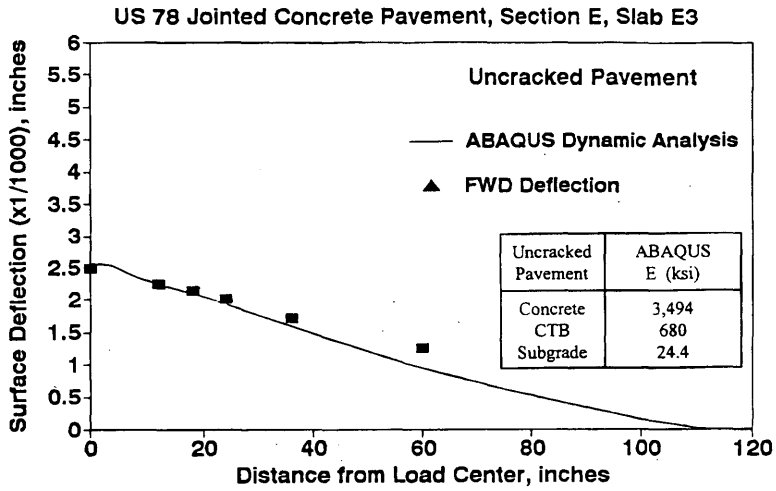

FIGURE 4 Matching of ABAQUS-computed surface deflections with measured FWD deflections for uncracked pavement.

values were adjusted until a close agreement was achieved between computed and measured dynamic deflections. The computed and measured deflections for the uncracked test Slab E3 are shown in Figure 4. The backcalculated modulus values for the uncracked concrete, the uncracked base, and the subgrade are listed in Table 2.

PAVEMENT CRACKING SIMULATION

Longitudinal and transverse cracks, joints, and voids beneath the concrete surface layer are the most critical discontinuities in concrete pavements, as illustrated in Figure 1. The structural response of a deteriorated pavement can differ significantly from that of an uncracked pavement having no distress. ABAQUS dynamic analyses were made to investigate the effect of cracks on the pavement properties.

The effect of cracks in the pavement can be modeled using special-purpose elements. A crack is modeled by having two independent nodes on two free faces of the crack linked by special-purpose unidirectional gap elements. The elements allow two continuous surfaces to be in contact, or not in contact, through contact pressure and friction between the contacting surfaces. ABAQUS monitors the relative displacement of the two nodes of the element in the given direction. This arrangement results in two contact surfaces that are separated by an initial selected gap width at the top. The gap element controls the interaction between the contact surfaces in such a way that these surfaces do not penetrate each other under any contact pressure. An appropriate value of the friction coefficient parameter between the contact surfaces should be assumed in the analysis to simulate aggregate interlock effects across the crack. A zero-friction coefficient means that no shear forces will develop and the contact surfaces will be free to slide. A very large friction coefficient implies that the surfaces will lock and no sliding will occur.

A sensitivity analysis of friction coefficient and gap width was conducted by varying the crack gap width from 5.1 mm (0.2 in.) to 0.25 mm (0.01 in.). It was concluded that the critical gap width was 0.25 mm (0.01 in.) at which the effect of friction coefficient on surface deflection is significant (*10*). This is expected for a low to

TABLE 2 Comparison of Pavement Moduli Values Backcalculated from ABAQUS Dynamic Analyses for Uncracked and Cracked Pavement Sections

Layer	Backcalculated Moduli, MPa (ksi)*		
	Uncracked Pavement	Cracked Concrete, Uncracked CTB	Cracked Concrete, Cracked CTB
Concrete	24,074 (3,494)	12,746 (1,850)	12,746 (1,850)
Cement Treated Base (CTB)	4,685 (680)	4,685 (680)	2,067 (300)
Subgrade	168 (24.4)	168 (24.4)	168 (24.4)
Test Section Location	E slab E3	F slab F3	G slab G1

* (Based on FWD deflection data measured in 1994 on US Highway 78 in Marshall County, Mississippi)

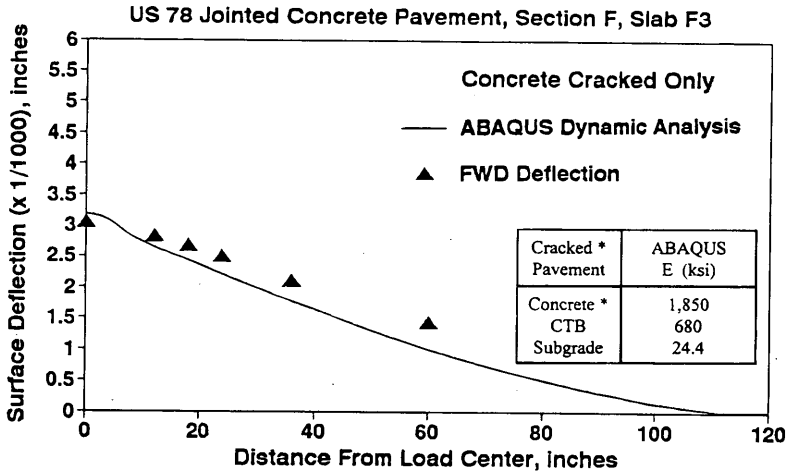

FIGURE 5 Matching of ABAQUS-computed surface deflections with measured FWD deflections for pavement with crack in concrete layer.

medium severity crack in the pavement concrete layer. Therefore, a gap width of 0.25 mm (0.01 in.) and a friction coefficient of 0.5 were used in this study.

Longitudinal, diagonal, and transverse cracks were observed at some pavement sections of U.S. Highway 78. A crack of low severity observed on one of the test section slabs (Slab F3) initiates from the transverse joint at a distance of 1.5 m (5 ft) from the pavement edge. A core extracted from this test section indicates cracking in the concrete layer only. This distress was simulated in the finite-element model and the calculated ABAQUS dynamic deflections were substantially higher than the corresponding deflection calculated for the uncracked pavement. The effective concrete modulus for this cracked pavement slab is naturally expected to be smaller in magnitude than that for the uncracked pavement layer. After a few iterations, a lower concrete modulus value yielded ABAQUS dynamic deflections that agree reasonably well with the FWD deflections measured at this cracked pavement site, as shown in Figure 5. The backcalculated modulus values for the cracked concrete, the uncracked base, and the subgrade are listed in Table 2.

Using the FWD data, distress data, and core data collected in this study, Slab Gl, in test Section G, was selected as representative of cracking in concrete and cement-treated base layers. By applying a similar iterative approach, the modulus values were backcalculated to the point where the computed dynamic deflections agreed reasonably well with the measured deflections, as shown in Figure 6. The backcalculated modulus values for the cracked concrete, the cracked base, and the subgrade are listed in Table 2. These results are indicative of the importance of using dynamic analysis to backcalculate appropriate values of pavement modulus.

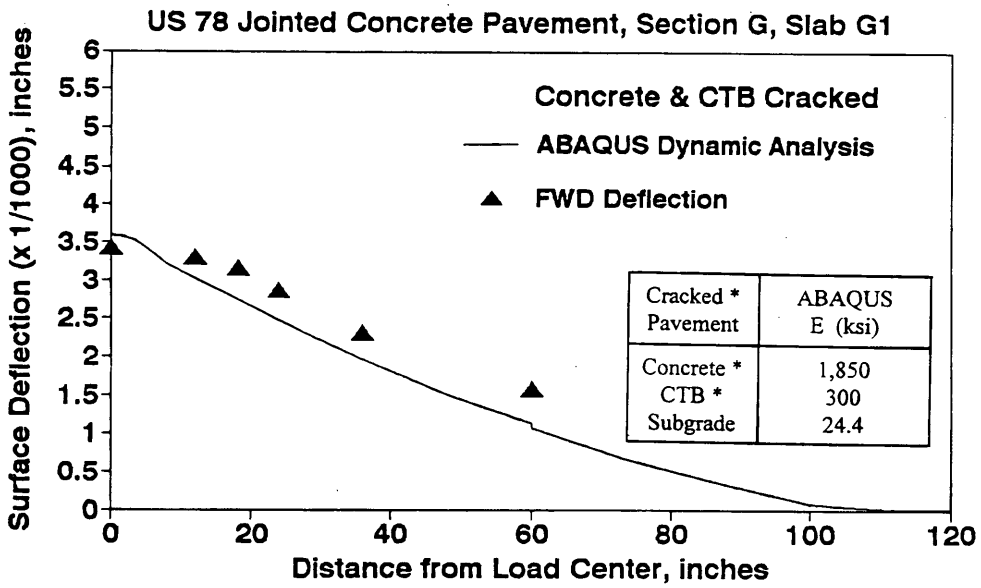

FIGURE 6 Matching of ABAQUS-computed surface deflections with measured FWD deflections for pavement with crack in concrete and cement treated base layers.

SUMMARY AND CONCLUSIONS

The effects of pavement cracking and FWD dynamic loading on the structural response of jointed plain concrete pavement-subgrade systems have been studied using the ABAQUS finite-element code. General observations and specific conclusions follow.

Advances in high-speed, high-capacity computational simulation have provided a capability of modeling with extreme accuracy the response of physical systems that are distinguished by discontinuities and highly nonlinear behavior. Jointed concrete pavements certainly fall within this category of physical systems that require sophisticated analyses to achieve efficient and economical design and construction. It is important to recognize the applicability of advanced modeling procedures to these types of systems and to use them to gain much greater understanding of their behavior than could be gained from the use of simplified approximate methods that fail, in many cases, to accurately portray the actual system response.

Lower backcalculated modulus values are to be expected for cracked pavements, compared with those backcalculated for uncracked pavements. In this study, procedures for quantifying this knowledge are demonstrated. This study also demonstrates the extensive usefulness of three-dimensional finite-element simulation of the effect of cracks and dynamic loading for accurately calculating values of deflection and stresses and strains, as well as the values of reduced moduli, associated with deteriorated pavement systems, and resulting from the presence of cracks and voids. It is impossible to carry out these types of studies with traditional multilayered linear elastic analyses as well as other finite-element programs that do not allow crack modeling and dynamic analysis.

Further three-dimensional finite-element modeling is under way to investigate the effects of voids beneath the surface concrete layer and the effects of thermal gradients on jointed concrete pavement response, using the ABAQUS concrete material model.

ACKNOWLEDGMENTS

The work was conducted as part of a research study supported by the Mississippi Department of Transportation and FHWA. The finite-element simulations were conducted on the Cray Y-MP supercomputer at the University of Mississippi with the support of the Mississippi Center for Supercomputing Research staff.

REFERENCES

1. Uddin, W., A. H. Meyer, W. R. Hudson, and K. H. Stokoe II. Project-Level Structural Evaluation of Pavements Based on Dynamic Deflections. In *Transportation Research Record 1007*, TRB, National Research Council, Washington, D.C., 1985, pp. 37–45.
2. Uddin, W., A. H. Meyer, and W. R. Hudson. Rigid Bottom Considerations for Nondestructive Evaluation of Pavements. In *Transportation Research Record 1070*, TRB, National Research Council, Washington, D.C., 1986, pp. 21–29.
3. Hudson, W. R., and H. Matlock. Analysis of Discontinuous Orthotropic Pavement Slabs Subjected to Combined Loads. In *Highway Research Record 131*, HRB, National Research Council, Washington, D.C., 1966.
4. Elliott, R. P., and M. R. Thompson. *Mechanistic Design Concepts for Conventional Flexible Pavements*. Transportation Engineering Series 42. University of Illinois, Urbana, 1985.
5. Tabatabie, A. M., and E. J. Barenberg. Finite Element Analysis of Jointed or Cracked Concrete Pavements. In *Transportation Research Record 671*, TRB, National Research Council, Washington, D.C., 1978.
6. *ABAQUS, Theory Manual Version 5.3*. Hibbitt, Karlsson, & Sorenson, Inc., Pawtucket, R.I., 1993.
7. *ABAQUS, User's Manual*. Hibbitt, Karlsson, & Sorenson, Inc., Pawtucket, R.I., 1993.
8. Zaghloul, S., and T. White. Use of a Three-Dimensional, Dynamic Finite Element Program for Analysis of Flexible Pavement. In *Transportation Research Record 1388*, TRB, National Research Council, Washington, D.C., 1993, pp. 60–69.
9. *PATRAN User's Manual*. PDA Engineering, PATRAN Division, Costa Mesa, Calif., 1993.
10. Uddin, W., D. Zhang, and F. Fernandez. Finite Element Simulation of Pavement Discontinuities and Dynamic Load Response. In *Transportation Research Record 1448*, TRB, National Research Council, Washington, D.C., 1994, pp. 100–106.
11. *U. S. Highway 78, Marshall County Project Documents*. Mississippi Department of Transportation, 1990, 1991.

Publication of this paper sponsored by Committee on Rigid Pavement Design.

Pavement–Falling Weight Deflectometer Interaction Using Dynamic Finite-Element Analysis

S. NAZARIAN AND K. M. BODDAPATI

In almost all linear elastostatic programs used in backcalculation procedures, a uniform pressure distribution is assumed for the applied load. As such, the loading system of any falling weight deflectometer (FWD) should be designed so that the load transferred to the pavement is uniform. This is difficult because the pressure distribution under the FWD is also affected by the pavement profile being tested. The other aspect of the FWD testing that is typically ignored is the dynamic nature of the load. The dynamic effects are related to the pulse width as well as the variation in the stiffness of the subgrade. A finite-element study has been carried out to investigate the significance of these parameters on the determination of the remaining lives of pavements. Cases where the imparted load would or would not yield a uniform pressure distribution under the FWD plate are identified. An investigation of the effects of the plate-pavement interaction on the static interpretation of the dynamic deflections is presented. The results indicate that the dynamic nature of the load may more significantly affect the deflections measured away from the load, whereas the plate-pavement interaction may affect the deflection of the first sensor. The errors in the estimation of the layer moduli that would be obtained from the standard backcalculation procedures are also determined. The results of this study confirm that the plate-pavement interaction and the dynamic effects are important for the FWD test on flexible pavements.

In almost all falling weight deflectometer (FWD) backcalculation procedures, a uniform pressure distribution is assumed for the applied load. If the assumption of uniform stress distribution is deviated, the deflections of the sensors near the affected loading may be in error (*1*). As such, the backcalculated moduli, critical stresses and strains, and, naturally, the prediction of the pavement life may be in error.

The pavement deflections under a static load may differ from those under an impulse load because of effects such as inertia, damping, and resonance. Previous studies indicate that static analysis of FWD deflection data may, in general, lead to inaccurate estimates of pavement moduli (*2–5*).

The major objective of the study summarized here was to assess the significance of a nonuniform pressure distribution under dynamic loading on the measured and backcalculated parameters. The pressure distribution under the loading plate and the effects of the components of the plate on the results obtained from the FWD were quantified in a previous work by Boddapati and Nazarian (*6*) and will not be repeated here.

Two models were used. In one model, the typical composite FWD loading plate on top of the pavement system was discretized in a finite element mesh; in the other, a uniform load distribution was assumed on top of the pavement. Through sensitivity analyses, the effects of stiffness and thickness of different pavement layers on the response of the pavement were studied. The variations in the measured deflection basin and the critical stresses and strains were discussed and quantified.

Soil properties usually vary with depth, and the soil is underlain at some depth by significantly stiffer material. The presence of bedrock or stiff layers at a finite depth may result in the dynamic amplification of the response (*7*). However, the duration of an FWD impulse is also an important parameter. Considering all the aforementioned problems, an analysis is performed on the dynamic effects of the FWD loading on critical stresses and strains within the pavement.

The goal of this paper is neither to address the analytical and numerical complications of the analysis nor to propose a new algorithm to address these problems. It is, instead, to obtain the numerical results from a complicated and involved process and present them as a guide for those involved in the FWD testing. Although the results are not substantiated by fieldwork, they qualitatively demonstrate the reasons for some of the persistent problems encountered in matching deflection basins. The results are presented to initiate a dialogue, and, it is hoped, to lead to future research to verify the results and to further development to resolve them.

BACKGROUND

Deflection basins from dynamic loading differ in several respects from the deflection basins from static analysis. A rigorous elastodynamic analysis of the FWD indicates that the inertia of the pavement is instrumental in the displacement response of the pavement. Mamlouk and Davis (*2*) and Shao et al. (*4*) incorporated inertial effects into a rigorous elastodynamic analysis of pavement response and have indicated that these effects are significant.

Kang (*8*) developed a mathematical model that could take into account not only the dynamic nature of the loads, but also the variation of material properties in the soil-pavement system.

Little attention has been focused on the distribution of load under the FWD plate. Uzan and Lytton (*1*) conducted an analytical study that indicated the consequences of a nonuniform pressure distribution under the FWD load. However, they made no attempt to quantify the distribution of the stress.

Shahin et al. (*9*), using stress-sensitive film, demonstrated that the stress distribution is in some instances nonuniform. However, they did not quantify the effects that the stress distribution may have on the response of the pavement.

Boddapati and Nazarian (*6*) numerically demonstrated that the stress distribution under the FWD plate is reasonably uniform for

The Center for Geotechnical and Highway Materials Research, University of Texas at El Paso, El Paso, Texas 79968.

rigid pavements; for flexible pavements, the stress distribution is influenced by the plate-pavement interaction. The thickness of the polyvinyl chloride (PVC) and steel plates and the rubber pad used in the construction of the FWD affect the deflection basin. The most significant parameter was found to be the stiffness of the rubber pad.

OVERALL APPROACH

Deflection basins from three sets of numerical cases were compared. The first set, the control case, corresponded to the elastostatic case with a uniform load applied to the pavement surface. For simplicity, these results will be referred to as STATUNFRM, which stands for static condition with uniform load distribution. This represents the algorithm normally used in the backcalculation procedure. The second set, DYNUNFRM, corresponded to the case where the dynamic nature of the load was considered but the FWD-pavement interaction was ignored (a uniform load was assumed). For the last set, DYNFWDINT, both the FWD-pavement interaction and the dynamic nature of the load were considered. In this manner, the dynamic effects can be determined by comparing the results from STATUNFRM and DYNUNFRM. The influences of the FWD-pavement interaction can be similarly delineated by comparing the DYNUNFRM case with the DYNFWDINT case.

Sensitivity analyses were also performed. In these analyses, the stiffness and thickness of each pavement layer were varied several times to determine the influence each had on the FWD-pavement interaction. In the following sections, the pertinent details and results are presented.

Physical Model

The composite loading plate of FWD was assumed to consist of a steel plate having an elastic stiffness of 70 GPa and a Poisson's ratio of 0.3 over a PVC plate having an elastic stiffness of 7 GPa and a Poisson's ratio of 0.3. The diameter of the FWD loading plate was assumed to be 300 mm, with a 25-mm-diameter hole at the center. The steel and PVC plates rest over a rubber pad having an elastic stiffness of 35 MPa and a Poisson's ratio of 0.49. Steel and PVC plates were assumed to be 25 mm thick, and the rubber pad, 6 mm thick.

The sensitivity analyses were conducted using a standard pavement section as the control pavement section. The standard pavement section was assumed to have three layers: an asphalt concrete (AC) layer over a granular base over a subgrade. The thickness of the AC and base layers were assumed to be 75 mm and 300 mm, respectively. The moduli of the AC, base, and subgrade were assumed to be 3 500 MPa, 350 MPa, and 70 MPa, respectively. The Poisson's ratio of the AC and base layers was assumed to be 0.35. A Poisson's ratio of 0.45 was assigned to the subgrade.

For dynamic analyses, a half-sinusoidal load was assumed to affect the composite loading plate of an FWD. The duration of the simulated impulse loading was 40 msec, with the peak load at 20 msec. The response of the pavement was observed for 250 msec. The peak stress was assumed to be 930 kPa.

Finite-Element Model

The program ABAQUS, developed by Habbit, Karlsson and Sorensen, Inc., was used throughout this study. The problem was assumed to be axisymmetric in nature. The characteristics of the finite-element mesh were carefully selected to ensure accurate results. The lateral boundaries were placed about 12 m from the center of the load. To determine the stress distribution under the plate, a well-refined mesh along the interface of the plate and pavement surface was necessary. As a result, a minimum of about 7,500 elements were used in this study. With such a mesh, the maximum difference between the results from the finite-element program and known cases was less than 1 percent (*10*). In addition, for dynamic executions, appropriate absorbing boundaries were incorporated to minimize any reflection of energy into the model region.

All materials were considered to be linear-elastic, homogeneous, and isotropic. Some of these assumptions may be invalid in some actual field cases. However, because the results presented in the following section are comparative, the deviation from these assumptions may only slightly affect the generality of the conclusions.

RESULTS

The deflection basins resulting from the control condition (STATUNFRM), dynamic condition (DYNUNFRM), and dynamic-with-interaction case (DYNFWDINT), using the standard pavement profile previously described, are compared in Table 1. Except under the loaded area, deflection basins calculated using both dynamic algorithms are similar. These similarities in deflections confirm that the FWD-pavement interaction has little effect on the deflections of sensors that are away from the loading plate.

On the other hand, large variations between the deflections from the static and dynamic algorithms are observed. The variation is small for a sensor located about 30 cm from the load (about 3 percent); it increases to about 50 percent for a sensor located about 180 cm from the load. These differences emphasize the importance of considering the dynamic nature of the FWD loads.

Under the load, on the other hand, the static and dynamic conditions having a uniform loading yield similar deflections. However, as soon as the FWD-pavement interaction is considered, the central deflection differs by about 5 percent. This exhibits the importance of the FWD-pavement interaction. Even though the difference is small, it will significantly affect the backcalculated moduli (see next section). Based on this discussion and for the sake of brevity, only the deflections from DYNFWDINT are compared with those of the STATUNFRM.

In the next sections, these types of comparisons will be carried out to demonstrate and delineate the dynamic effects as well as the FWD-pavement interaction.

Sensitivity Study

Asphalt Layer

To compare the results from the static and dynamic analyses, two cases are presented. In one, the stiffness of the asphalt layer was varied from 1.75 GPa to 7 GPa. In the other, the thickness of the AC layer was varied from 25 mm to 125 mm.

Asphalt Modulus The differences in the deflection basins calculated from DYNFWDINT and STATUNFRM algorithms as a function of the modulus of the AC layer are presented in Table 2. As indicated in Table 1, for the standard pavement section (modulus of 3.5 GPa), the differences in deflections vary from 3 to about

TABLE 1 Dynamic and Static Deflections Calculated From Different Analyses for Control Pavement Section

Radial Distance (cm)	Deflections Calculated by				
	STATUNFRM (microns)	DYNUNFRM (microns)	Variation*1 percent	DYNFWDINT (microns)	Variation*2 percent
(1)	(2)	(3)	(4)	(5)	(6)
0	884	889	-0.6	836	5.3
30	550	568	-3.3	568	-3.2
60	349	375	-7.4	375	-7.4
90	238	269	-13	269	-13
120	167	202	-21.3	202	-21.3
150	120	160	-33.3	160	-33.3
180	88	133	-51.0	133	-51.0

*1 Variation = [(Column2 - Column3) / Column2] * 100
*2 Variation = [(Column2 - Column5) / Column2] * 100
STATUNFRM = Static condition with a uniformly distributed load
DYNUNFRM = Dynamic condition with a uniformly distributed load
DYNFWDINT = Dynamic condition when FWD/pavement interaction is considered

51 percent. For the other two AC stiffnesses, the differences in the deflections are similar to the standard one. Therefore, it can be concluded that the modulus of the asphalt layer has minor influences on the variation in deflection basins under the static and dynamic loads.

Inspecting the differences between the central deflections obtained from the two approaches, one can conclude that the FWD-pavement interaction is affected somewhat by the modulus of the AC. As the modulus of the AC increases from 1.75 to 7 GPa, the difference between the two dynamic deflections decreases from 8 to 3 percent. Therefore, the stiffer the AC layer is, the less significant the FWD-pavement interaction will be.

Thickness The differences in the deflection basins calculated by STATUNFRM and DYNFWDINT constantly decrease as the thickness of the AC layer increases (see Table 2). As the thickness of the AC increases from 25 to 125 mm, the difference between the central deflections from the STATUNFRM and DYNFWDINT decreases from 11 to 2 percent.

Base Layer

To find the influence of the base layer on the dynamic response of a pavement system, its thickness and stiffness were perturbed. The stiffness of the base layer was varied from 88 to 1400 MPa, and the thickness was varied from 150 to 450 mm.

Modulus The differences in the deflection basins calculated by DYNFWDINT and STATUNFRM are largely influenced by the base stiffness (see Table 3). The higher the stiffness of the base layer is, the smaller the differences in deflections calculated by DYNFWDINT and STATUNFRM will be.

The differences between the central deflections calculated by DYNFWDINT and STATUNFRM decreased from 8 to 3 percent as the stiffness of the base layer increased from 88 to 1 400 MPa.

The differences between the static and dynamic deflection basins become less significant. For example, the differences in the deflections for the sensor located 180 cm from the load decrease to 32 percent from about 70 percent as the modulus increases from 88 to 1 400 MPa.

Thickness The thickness of the base layer has a limited influence on the differences in the central deflections (see Table 3). Therefore, the FWD-pavement interaction is not sensitive to the thickness of the base.

On the other hand, it appears that the dynamic effects are influenced by the thickness of the base. The differences in deflections obtained by the dynamic and static approaches decreased from 69 to 37 percent as the thickness of the base increased from 150 to 450 mm.

Subgrade

The stiffness of the subgrade was varied from 17.5 to 280 MPa. The variation in the deflection, as a function of radial distance for different stiffnesses of the subgrade, is shown in Table 4. The differences between the two approaches (DYNFWDINT and STATUNFRM) are largely influenced by the stiffness of the subgrade. For a

TABLE 2 Influence of Asphalt Layer on Deflection Basins

Layer Modulus

AC Modulus (MPa)	Method of Calculation	Deflection Measured at (cm)						
		0	30	60	90	120	150	180
(1)	(2)	(3)	(4)	(5)	(6)	(7)	(8)	(9)
1250	STAT-UNFRM	950	555	350	238	165	118	85
	DYN-FWDINT*	878 (8)	575 (-4)	378 (-8)	270 (-14)	200 (-23)	158 (-35)	133 (-54)
7000	STAT-UNFRM	790	530	340	233	165	118	88
	DYN-FWDINT*	765 (3)	543 (-3)	363 (-7)	263 (-12)	198 (-20)	158 (-32)	130 (-49)

Layer Thickness

AC Thickness (mm)	Method of Calculation	Deflection Measured at (cm)						
		0	30	60	90	120	150	180
(1)	(2)	(3)	(4)	(5)	(6)	(7)	(8)	(9)
25	STAT-UNFRM	1130	588	363	238	163	115	83
	DYN FWDINT*	1008 (11)	613 (-4)	393 (-8)	273 (-15)	200 (-25)	160 (-39)	133 (-59)
125	STAT-UNFRM	688	488	330	230	165	120	90
	DYN-FWDINT*	670 (2)	500 (-3)	350 (-6)	258 (-11)	198 (-19)	158 (-29)	130 (-45)

Numbers in Parentheses Denote Percent Difference from Results Obtained using STATUNFRM and DYNFWDINT

* Difference = [(STATUNFRM - DYNFWDINT) / STATUNFRM] * 100

All deflections are in microns

subgrade with a very low stiffness (17.5 MPa), the deflections calculated by STATUNFRM were always higher. The differences decreased from 20 to 5 percent as the radial distance from the load increased from 0 to 180 cm. As the subgrade stiffness increased to 280 MPa, the variation in the deflection calculated at 180 cm increased to 56 percent.

Stiff AC and base layers over a 17.5 MPa subgrade can be modeled as a foundation on a weak base. This increases the difference between the fundamental frequency of the pavement and that of the impulsive force, which in turn decreases the peak deflections, compared with those of STATUNFRM. Therefore, the difference between the deflections obtained by the STATUNFRM and DYNFWDINT is positive and decreases from 19.6 to 4 percent. As the subgrade stiffness increased to 280 MPa, the differences varied between 5 and −56 percent (negative sign indicates higher dynamic deflections).

Depth to Rigid Base

Two main parameters that influence dynamic deflections are the natural frequency of the pavement system and the frequency content of the FWD impulse. The natural frequency of the pavement system is directly related to the stiffness of the paving layers and depth to a rigid base (if present). The stiffer the pavement system or the closer the rigid layer to the surface is, the higher the natural frequency will be. The frequency content of the impulse is directly related to the duration of the impulse. The longer the impulse width is, the more energy will concentrate toward lower frequencies. The interaction of these two parameters is studied here.

Data file DYNFWDINT was executed for depths to the rigid base varying from 1.9 to 7.5 m. A 50 percent decrease in depth to the rigid base (from 7.5 to 3.8 m) only slightly influenced the peak amplitude under the load. A further decrease in the depth to the rigid base (to 1.9 m) resulted in a much more significant decrease in the deflection.

When a depth to bedrock of 3.8 m was used, the differences in static (rigid base at 7.5 m) and dynamic deflections increased from 6 to 14 percent.

A further decrease in the subgrade thickness influenced the deflection basins for two reasons. First, the decrease in the subgrade thickness increases the fundamental frequency of the pavement, and thus the energy associated with the impulsive force input. Second, the

TABLE 3 Influence of Base Layer on Deflection Basins

Layer Modulus

Base Modulus (MPa)	Method of Calculation	Deflection Measured at (cm)						
		0	30	60	90	120	150	180
(1)	(2)	(3)	(4)	(5)	(6)	(7)	(8)	(9)
88	STAT-UNFRM	1490	825	388	225	150	108	80.0
	DYN-FWDINT*	1375 (8)	855 (-4)	430 (-11)	273 (-21)	200 (-34)	160 (-50)	135 (-70)
1400	STAT-UNFRM	510	380	293	223	170	128	95
	DYN-FWDINT*	500 (3)	388 (-2)	305 (-4)	240 (-8)	190 (-11)	155 (-21)	128 (-32)

Layer Thickness

Base Thickness (mm)	Method of Calculation	Deflection Measured at (cm)						
		0	30	60	90	120	150	180
(1)	(2)	(3)	(4)	(5)	(6)	(7)	(8)	(9)
150	STAT-UNFRM	1110	693	388	235	155	108	80
	DYN-FWDINT*	1060 (5)	720 (-4)	425 (-9)	278 (-18)	200 (-30)	160 (-48)	135 (-69)
450	STAT-UNFRM	748	448	298	218	160	120	93
	DYN-FWDINT*	695 (7)	455 (-2)	313 (-6)	238 (-10)	188 (-16)	150 (-25)	125 (-37)

Numbers in Parentheses Denote Percent Difference from Results Obtained using STATUNFRM and DYNFWDINT

* Difference = [(STATUNFRM - DYNFWDINT) / STATUNFRM] * 100

All deflections are in microns

decrease in the depth to bedrock results in less material that can be strained. In Table 5, the deflections by STATUNFRM with a rigid base fixed at 7.5 m are also compared with those by STATUNFRM with varying depths to the rigid base. In this manner, the contribution of the dynamic nature of a load to the variation in deflections can be better appreciated. In Table 5, the standard STATUNFRM refers to the standard practice in backcalculation when the depth to bedrock is fixed at an arbitrary depth (7.5 m here).

With the rigid base fixed at 3.8 m, the differences in deflections varied from 6 to 47 percent as the radial distance increased from 0 to 180 cm. A further decrease in the subgrade thickness to 1.9 m increased the difference from 17 to 102 percent.

In general, as reflected in Table 5, the contribution of the dynamic nature of the load to differences in deflections is mixed. In some cases (for depth to bedrock of 3.8 m), the dynamic effects are constructive; that is, the deflections obtained when considering the dynamic effects are closer to those obtained when a static condition and deep depth to bedrock are assumed. In other cases, the dynamic nature of the load adds to the differences between the standard static solutions. This indicates that the derivation of a simple relationship for correcting for depth to bedrock may not be easy.

Pulse Duration

To study the influence of the frequency content of impact, the pulse duration was changed from 20 to about 80 msec. The exercise was repeated for several depths to the rigid base. Typical results are shown in Figure 1.

For a subgrade thickness of 7.5 m, the central deflection calculated by DYNFWDINT with a pulse of 20 msec resulted in a value lower than those calculated for 40 and 80 msec. The trend is illustrated in Table 6 and Figure 1.

A decrease in the subgrade thickness to 3.8 m results in a behavior that differs somewhat from that for a subgrade thickness of 7.5 m (see Table 6). The peak deflection at the center increased as the pulse duration increased from 20 to 80 msec. However, in this case, the deflections from impulses of 20 and 40 msec have changed only slightly, whereas those from the 80 msec are significantly smaller.

As reflected in Table 6, a further decrease in the rigid base thicknesses to 1.9 m resulted in smaller peak deflections. At 180 cm away, the peak deflections decreased with the increase in pulse duration (with the decrease in frequency of impulse). The negative

TABLE 4 Influence of Subgrade Stiffness on Deflection Basins

Subgrade Modulus (MPa)	Method of Calculation	Deflection Measured at (cm)						
		0	30	60	90	120	150	180
(1)	(2)	(3)	(4)	(5)	(6)	(7)	(8)	(9)
18	STAT-UNFRM	1740	1360	1060	833	650	505	390
	DYN-FWDINT*	1400 (20)	380 (17)	880 (17)	693 (17)	553 (15)	445 (12)	373 (5)
280	STAT-UNFRM	493	208	93	55	38	28	20
	DYN-FWDINT*	455 (8)	220 (-6)	105 (-13)	68 (-21)	50 (-31)	38 (-42)	30 (-56)

Numbers in Parentheses Denote Percent Difference from Results Obtained Using STATUNFRM and DYNFWDINT
* Difference = [(STATUNFRM - DYNFWDINT) / STATUNFRM] * 100
All deflections are in microns

deflections were caused by the heave in the soil at the outermost deflection station.

The deflection bowls resulting from the three pulse widths of 20, 40, and 80 msec for subgrade thicknesses of 7.5, 3.8, 1.9 m, respectively, are compared with those from STATUNFRM for a 7.5-m-thick subgrade. This is done to define the differences between the pavement analysis done ignoring the existence of the bedrock and dynamic effects.

For the case of depth to bedrock at 7.5 m, the differences between the two approaches (STATUNFRM and DYNFWDINT) for pulse widths of 40 and 80 msec varied from 1 to about 52 percent when the radial distance increased from 0 to 180 cm. The pulse width of 20 msec, which contains energy at higher frequencies, caused differences from 15 to about 26 percent as the radial distance increased from 0 to 180 cm. One interesting point is that some of the deflections are overestimated and others are underestimated.

TABLE 5 Influence of Rigid Base Depth on Deflections Measured

Rigid Base Depth, m	Method of Calculation	Deflection Measured at (cm)						
		0	30	60	90	120	150	180
Standard STATUNFRM		870	543	345	235	165	118	88
7.5	DYN-FWDINT	823 (5)*1	560 (-3)	370 (-7)	265 (-13)	200 (-21)	158 (-33)	130 (-51)
	STAT-UNFRM	870 (0)*2	543 (0)	345 (0)	235 (0)	165 (0)	118 (0)	88 (0)
3.8	DYN-FWDINT	815 (6)	553 (-2)	358 (-4)	248 (-6)	178 (-9)	133 (-12)	100 (-14)
	STAT-UNFRM	820 (6)	493 (9)	295 (14)	188 (20)	118 (28)	75 (37)	45 (47)
1.9	DYN-FWDINT	730 (16)	458 (15)	260 (25)	148 (37)	80 (52)	38 (69)	13 (86)
	STAT-UNFRM	725 (17)	398 (27)	208 (40)	108 (55)	48 (71)	15 (87)	-3 (102)

Numbers in Parentheses Denote the Percent Difference from Results Obtained with STATUNFRM Assuming Depth to Rigid Base of 7.5 m (Standard STATUNFRM)
*1 Difference = [(Std. STATUNFRM - DYNFWDINT) / STATUNFRM] * 100
*2 Difference = [(Std. STATUNFRM - STATUNFRM) / STATUNFRM] * 100
All deflections are in microns

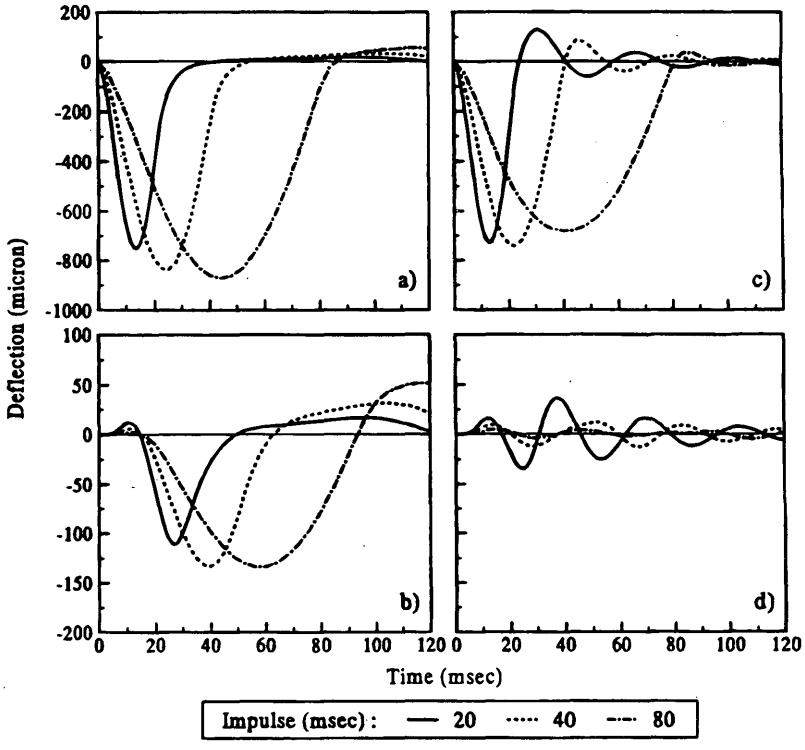

FIGURE 1 Influence of pulse duration on deflection. (*a*) Central deflection for depth to rigid base of 7.5 m, (*b*) deflection at 180 cm for depth to rigid base of 7.5 m, (*c*) central deflection for depth to rigid base of 1.9 m, and (*d*) deflection at 180 cm for depth to rigid base of 1.9 m.

For a pulse width of 20 msec with a subgrade thickness of 3.8 m, a better agreement between the static and dynamic analyses is obtained. The differences are within plus or minus 15 percent. However, in some cases, the deflections are overestimated and in others underestimated. A significant difference exists between this case (depth to bedrock of 3.8 m) and the previous case (depth to bedrock of 7.5 m). When the bedrock was at the depth of 7.5 m, the deflections from the 20-msec impulse were always smaller than those of the 40- and 80-msec impulses. For the shallower bedrock, deflections from the 80-msec impulse are smaller past a radial distance of 120 cm.

Further decreases in subgrade thickness to 1.9 m in DYNFWDINT naturally resulted in smaller deflections compared with those deflections obtained from STATUNFRM with a subgrade of 7.5 m.

When the rigid base was located at 1.9 m, the difference constantly increased from 18, 16, and 23 percent to about 142, 86, and 106 percent with the radial distance increasing from 0 to 180 cm for the pulses of 20, 40, and 80 msec, respectively. In this case, the 80 and 20 msec pulses consistently produce the lowest deflections, clearly demonstrating the importance of the pulse width–bedrock interaction.

For a 3.8-m depth of bedrock, the dynamic loads are, in most cases, constructive. In other words, for this case, the dynamic nature of the load reduces some of the effects of misassuming depth to bedrock. This pattern is true for a depth of bedrock of 1.9 m, except for a long-duration impulse (80 msec when the differences due to dynamic loads and static loads are small).

In summary, in all cases, depths to bedrock and impulse width interact to produce significant difference between the static and dynamic analysis. In some instances, the dynamic nature of the load neutralizes some of the effects associated with ignoring the presence of bedrock. However, in many cases, the errors may still be too large to ignore the dynamic nature of the load and depth to bedrock. Finally, when bedrock is present, the deflections measured by different FWD devices manufactured by different companies may be different.

Influence on Pavement Evaluation

The elastostatic program BISAR was used in this study. A subroutine based on rutting and fatigue failure criteria was developed to calculate the pavement life using the Asphalt Institute procedure. The backcalculated pavement layer stiffnesses, critical stresses, critical strains, and remaining lives of pavement structures are discussed in the following sections.

As indicated before, the dynamic effects were more pronounced at outer sensors. Static interpretation of these results may largely influence the backcalculated base and subgrade stiffnesses.

The backcalculated pavement layer stiffnesses and critical parameters are shown in Table 7. Typically, the backcalculation could not be performed with small basin-fitting errors (the reasons are described later). The mismatches averaged 8 percent, which is large. Based on the experience of the authors, such level of mismatch is not uncommon for flexible pavements. Practically speaking, the

TABLE 6 Influence of Pulse Width on Deflection Basins

Depth to Rigid Base of 7.5 m

Impulse msec	Method of Calculation	Deflection Measured at (cm)						
		0	30	60	90	120	150	180
Standard STATUNFRM		870	543	345	235	165	118	88
20	DYNFWDINT	740 (15)[2]	488 (10)	313 (9)	218 (7)	165 (0)	130 (-10)	110 (-26)
40	DYNFWDINT	823 (5)	560 (-3)	370 (-7)	265 (-13)	200 (-21)	158 (-33)	130 (-51)
80	DYNFWDINT	858 (1)	585 (-8)	390 (-14)	280 (-19)	210 (-28)	163 (-39)	133 (-52)

Depth to Rigid Base of 3.8 m

Impulse msec	Method of Calculation	Deflection Measured at (cm)						
		0	30	60	90	120	150	180
STATUNFRM		820 (6)[1]	493 (9)	295 (14)	188 (20)	118 (28)	75 (37)	45 (47)
20	DYNFWDINT	740 (15)[2]	488 (10)	310 (10)	218 (7)	160 (3)	123 (-5)	98 (-13)
40	DYNFWDINT	815 (6)	553 (-2)	358 (-4)	248 (-6)	178 (-9)	133 (-12)	100 (-14)
80	DYNFWDINT	815 (6)	543 (0)	343 (0)	233 (1)	160 (3)	110 (6)	75 (11)

Depth to Rigid Base of 1.9 m

Impulse msec	Method of Calculation	Deflection Measured at (cm)						
		0	30	60	90	120	150	180
STATUNFRM		725 (17)[1]	398 (27)	208 (40)	108 (55)	48 (71)	15 (87)	-3 (102)
20	DYNFWDINT	718 (18)[2]	460 (15)	270 (22)	163 (31)	95 (42)	55 (54)	-38 (142)
40	DYNFWDINT	730 (16)	458 (15)	260 (25)	148 (37)	80 (52)	38 (69)	13 (86)
80	DYNFWDINT	670 (23)	398 (27)	205 (40)	108 (54)	53 (68)	23 (82)	-5 (106)

Numbers in Parentheses Denote Difference from Results Obtained with Assuming Depth to Rigid Base of 7.5 m (Standard STATUNFRM reported in Table 6a)

[1] Difference = [(Std. STATUNFRM - STATUNFRM) / Std. STATUNFRM] * 100

[2] Difference = [(Std. STATUNFRM - DYNFWDINT) / Std. STATUNFRM] * 100

designer has to face a dilemma: Should the FWD data be discarded or should the results be used in the design? If the data are discarded, substantial effort and funds are wasted. On the other hand, if the data are used, the consequences (at least theoretically) are as follows.

As reflected in Table 7, except in isolated cases, the backcalculated moduli of the AC layer are equal to 28 GPa (upper limit for AC layer modulus assigned to BISDEF), regardless of the asphalt layer stiffness.

For the base layer, the backcalculated moduli are closer to the actual values. Typically, as the pavement structure becomes stiffer, the base modulus is more accurately predicted. The base modulus (except in a few cases) is underestimated, possibly

TABLE 7 Influence of Different Pavement Profiles on Backcalculated Parameters and Remaining Lives

Parameter	Moduli (MPa)			Thickness (mm)		Backcalculated Moduli (MPa)			Avg. Basin Fitting Mismatch (percent)	Remaining Life (million ESAL)	
	AC	Base	Sub grade	AC	Base	AC	Base	Sub grade		Rutting	Fatigue
Standard Pavement	3500	350	70	75	300	6664 (-90)*	329 (6)	72.1 (-3)	0.7	2.4 (-200)	2.4 (-24)
AC Modulus	1750	350	70	75	300	28000 (-1500)	245 (30)	54.6 (22)	9.5	2.4 (-200)	2.4 (-54)
	3500					28000 (-700)	280 (20)	55.3 (21)	8.7	2.9 (-165)	2.8 (-118)
	7000					28000 (-300)	343 (2)	56.0 (20)	7.4	3.7 (-130)	3.5 (-141)
AC Thickness	3500	350	70	25	300	28000 (-700)	490 (-40)	56.0 (19)	8.0	0.7 (-101)	2.5 (88)
				75		28000 (-700)	280 (20)	55.3 (21)	8.7	2.9 (-165)	2.8 (-118)
				125		9430 (-169)	287 (18)	56.7 (19)	7.1	6.7 (-63)	4.3 (-52)
Base Modulus	3500	87.5	70	75	300	28000 (-700)	71 (19)	52.5 (25)	8.7	1.8 (-722)	1.0 (-910)
		350				28000 (-700)	280 (20)	55.3 (21)	4.5	2.9 (-165)	2.8 (-118)
		1400				28000 (-700)	1099 (22)	57.4 (18)	3.3	32.7 (-24)	21.2 (87)
Base Thickness	3500	350	70	75	150	28000 (-700)	183 (48)	55.3 (21)	11.6	0.8 (-610)	1.4 (-95)
					300	28000 (-700)	280 (20)	55.3 (21)	8.7	2.9 (-165)	2.8 (-118)
					450	10374 (-196)	399 (-14)	57.4 (18)	4.0	12.2 (-54)	2.8 (-86)
Subgrade Modulus	3500	350	17.5	75	300	28000 (-700)	322 (8)	18.9 (-8)	4.6	0.5 (-416)	2.4 (-87)
			70			28000 (-700)	280 (20)	55.3 (21)	8.7	2.9 (-165)	2.8 (-118)
			280			22650 (-547)	333 (5)	224 (20)	1.1	88.8 (-100)	4.2 (-204)

Numbers in parantheses corresponding to percent differences between actual and backcalculated values
* Difference = [(Actual Value - Backcalculated Value) / Actual Value] * 100

to compensate for the overestimation of the modulus of the AC layer.

In all cases, the subgrade moduli are underpredicted by about 10 to 20 percent, indicating that the modulus of the subgrade is accurately predicted. This phenomenon is counter-intuitive given the large differences between the dynamic and static deflections for the outer sensors (see Tables 2, 3, and 4). From a careful inspection of the deflections from any case presented in Tables 3 through 5, one will notice that the differences between the dynamic and static deflections become increasingly larger as the distance from the load increases. Deflections from Sensors 3 (radial distance of 60 cm) through 7 (radial distance of 180 cm) contribute significantly to the backcalculation of the modulus of the subgrade. The differences between the dynamic and static deflections of Sensor 3 are typically not more than 10 percent. Therefore, on the average, the differences in the dynamic and static deflections of the sensors contributing significantly to the modulus of the subgrade can be considered to be about 20 percent and as such a subgrade modulus with an accuracy of about 20 percent.

One important lesson to be learned is that estimating the modulus of the subgrade from the last sensors, where the dynamic and static deflections are deviating the most, may not be appropriate. From this discussion, one can observe why the deflection-basin-fitting mismatch is large for most cases reported in Table 7. It is practically impossible to simultaneously achieve close fits for the deflections from the middle sensors (60 and 90 cm) and far sensors (150 and 180 cm). The remaining lives of the pavement are typically overestimated by 2 to 10 times (Table 7). This indicates the importance of considering the FWD-pavement interaction and the dynamic nature of imparted load in the FWD tests.

Pulse Duration

Table 8 presents the effects of the pulse duration on the remaining life. The basin-fitting mismatches were on the average about 8 percent. The backcalculated moduli of the AC layer are constant and equal to 28 GPa, regardless of the pulse duration. The backcalculated base layer moduli are within 20 percent of actual value. For small pulse durations, the subgrade moduli are closely estimated. The differences in backcalculated subgrade moduli and the actual values are increased with the increase in pulse duration. In all cases, the remaining lives by rutting and fatigue are overestimated.

Depth to Rigid Base

For a depth to the rigid base of 3.8 m, the backcalculated modulus of the AC layer is overestimated by a factor of 1.6, whereas the moduli of base and subgrade layers are closely estimated (Table 8). The average basin-fitting mismatch for this case is small. Because of the small variations in the backcalculated moduli of base and subgrade layers to the actual values, the remaining lives by rutting and fatigue are also closely calculated.

A further decrease of depth to the rigid base to 1.9 m resulted in an overestimation of the AC layer modulus by a factor of 8. On the contrary, the modulus of the base layer is underestimated by a factor as high as 10. The backcalculated subgrade modulus is almost four times the actual value. By combining the effects of overestimated and underestimated moduli of AC and base layers, the remaining life by fatigue matches the actual values. High backcalculated moduli of subgrade resulted in a rut life that is almost 24 times higher than the actual value.

TABLE 8 Influence of Relevant Dynamic Characteristics on Backcalculated Moduli and Remaining Lives

Pulse Duration

Pulse Duration (msec)	Backcalculated Moduli (MPa)			Avg.Basin Fitting Mismatch (percent)	Remaining Life (million ESAL)	
	AC	Base	Subgrade		Rutting	Fatigue
(1)	(2)	(3)	(4)	(5)	(6)	(7)
20	28000 (-700)*	294 (16)	67.2 (4)	9.5	4.5 (-315)	3.2 (-142)
40	28000 (-700)	280 (20)	55.3 (21)	8.7	2.9 (-165)	2.8 (-118)
80	28000 (-700)	343 (20)	53.2 (24)	7.4	2.7 (-146)	2.8 (-115)

Depth to Rigid Base

Rigid Base Depth (m)	Backcalculated Moduli (MPa)			Avg.Basin Fitting Mismatch (percent)	Remaining Life (million ESAL)	
	AC	Base	Subgrade		Rutting	Fatigue
(1)	(2)	(3)	(4)	(5)	(6)	(7)
7.5	28000 (-700)	280 (20)	55.39 (21)	8.7	2.9 (-165)	2.8 (-118)
3.8	5720 (-63)	371 (-6)	65.8 (6)	0.8	1.4 (-29)	1.6 (-19)
1.9	28000 (-700)	35 (90)	266 (-280)	14.5	245 (-22172)	1.1 (-15)

Numbers in Parentheses Represent Percentage Difference between Actual and Backcalculated Pavement Parameters.

* Difference = [(Actual Value - Backcalculated Value) / Actual Value] * 100

SUMMARY AND CONCLUSIONS

The influence of the plate-pavement interaction considering the dynamic nature of the FWD load is studied here. An investigation was conducted to assess the significance of these parameters on the measured and backcalculated parameters. Through a sensitivity study, the effects of the stiffness and thickness of different pavement layers on dynamic plate-pavement interaction were studied.

The dynamic nature of the FWD load is also considered, and the calculated deflection basins as a function of pavement strength parameters are compared with those calculated by elastostatic analysis. Under dynamic loads, the deflections at a given point are influenced by several parameters. Two of these parameters consist of the natural frequency of the pavement system and the frequency content of the FWD impulse. The natural frequency of the pavement system is directly related to the stiffness of the paving layers and depth to the rigid base (if present). The frequency content of the impulse is directly related to the duration of the impulse. The interaction of these parameters are also studied here.

On the basis of the results presented, the following conclusions can be drawn.

- Deflections measured on flexible pavements can be significantly influenced by the FWD-pavement interaction.
- Stiffer pavements are less influenced by the plate-pavement interaction.
- The dynamic nature of the load significantly affects the deflections measured away from the load.
- For typical pavements, base layer stiffness and thickness (to a lesser extent), as well as subgrade stiffness, influence the pavement response to dynamic loads.
- Depth to bedrock and the duration of impulse interact to produce significantly different static and dynamic deflections. Both factors should be considered.
- When the bedrock is present, the deflections measured by different FWD devices with different pulse durations may be different.
- If the dynamic FWD-pavement interaction is not considered, the remaining lives will be significantly overestimated.

ACKNOWLEDGMENT

This work was supported by the Center for High Performance Computing (CHPC) of the University of Texas System. The financial support and technical advice obtained from CHPC are appreciated.

REFERENCES

1. Uzan, J., and R. L. Lytton. Analysis of Pressure Dissertation Under Falling Weight Deflectometer Loading. *Journal of Transportation Engineering*, Vol. 116, No. 2, 1990.
2. Mamlouk, M. S., and T. G. Davis. Elasto-Dynamic Analysis of Pavement Deflections. *Journal of Transportation Engineering*, Vol. 110, No. 6, 1994.
3. Sebaaly, B., T. G. Davis, and M. S. Mamlouk. Dynamics of Falling Weight Deflectometer. In *Transportation Research Record 1022*, TRB, National Research Council, Washington, D.C., 1985.
4. Shao, K. Y., J. M. Roesset, and K. H. Stokoe II. *Dynamic Interpretation of Dynaflect and Falling Weight Deflectometer Tests on Pavement Systems*. Research Report 437-1. Center for Transportation Research, University of Texas at Austin, 1986.
5. Chang, D.-W., Y.V. Kang, J.M. Roesset, and K. Stokoe II. Effect of Depth to Bedrock on Deflection Basins Obtained with Dynaflect and Falling Weight Deflectometer Tests. In *Transportation Research Record 1355*, TRB, National Research Council, Washington, D.C., 1992.
6. Boddapati, K. M., and S. Nazarian. *Stress Distribution Due to Pavement–Falling Weight Deflectometer Interaction*. ASTM STP 1198. American Society of Testing and Materials, Philadelphia, Pa., 1994.
7. Seng, C. R., K. H. Stokoe II, and J. M. Roesset. *Effect of Depth of Bedrock on the Accuracy of Backcalculated Moduli Obtained with Dynaflect and FWD Tests*. Research Report 1175-5. Center for Transportation Research, University of Texas at Austin, 1993.
8. Kang, Y. V. *The Effect of Finite Width on Dynamic Deflections of Pavements*. Ph.D. dissertation. University of Texas at Austin, 1990.
9. Shahin, M. Y., J. A. Crovetti, and B. E. Touma. The Effect of Various Load Distributions on the Backcalculated Moduli Values in Flexible Pavements. In *Transportation Research Record 1336*, TRB, National Research Council, Washington, D.C., 1991.
10. Boddapati, K. M. *Effects of Pavement–Falling Weight Deflectometer Interaction on Measured Pavement Response*. M.S. thesis. University of Texas at El Paso, 1992.

Publication of this paper sponsored by Committee on Flexible Pavement Design.

Viscoelastic Analysis of Hot Mix Asphalt Pavement Structures

G. M. ROWE, S. F. BROWN, M. J. SHARROCK, AND M. G. BOULDIN

A new method of analysis for mechanistic pavement design has been developed based on improved material characteristics, which more accurately reflects fatigue cracking and permanent deformation performance. The key components of the method involve the (a) dissipated energy *fatigue criterion* in which the cumulative energy dissipated in asphaltic materials is directly proportional to fatigue damage, (b) viscoelastic materials characterization, and (c) pavement analysis using the finite-element method for determining response to repeated wheel loading. The changing properties of asphaltic materials with temperature are a key feature of the procedure with temperature conditions being provided by using a heat flow model. Output of the program includes predictions of percentage fatigue damage and rut depth at various numbers of load applications.

An improved method of pavement analysis has been developed that more accurately reflects field performance than many procedures used in the past. It uses a viscoelastic characterization of the asphaltic material along with input about traffic, geometry, and climate. The need for the development of a new procedure is evident from the lack of prediction capability with existing procedures, particularly when new or unfamiliar materials are used. For example, polymer modified asphalts have different characteristics from conventional asphalts, particularly with regard to their ability to exhibit elastic recovery at elevated temperatures. This can be considered by using a simple rheological model such as the Burgers model (Figure 1), which contains elastic, viscous, and viscoelastic elements. The combination of elastic and viscous elements in series is a Maxwell element, whereas arranging the viscous and elastic elements in parallel is a Kelvin element. The strain associated with the viscoelastic element is completely recovered at infinite time. The introduction of polymers into asphalt materials increases the proportion of strain that is recoverable after loading and reduces that associated with the viscous element. Current programs used for pavement design generally rely on elastic analysis, for example, of layered systems in the *Shell Pavement Design Manual* (*1*). Design to limit permanent deformation is often related to vertical elastic strain at the formation level, which is conceptually invalid and, hence, a semiempirical procedure. It is based on backanalysis of pavements with known performance. It has been shown (*2*) that the measured strain response in pavement experiments is not well predicted by linear elastic theory. Thus, the use of elastic analysis methods alone has limitations and can result in incorrect characterization of pavement performance.

G. M. Rowe, SWK Pavement Engineering, Inc., P.O. Box 211, Millington, N.J. S. F. Brown, University of Nottingham, University Park, Nottingham, England. M. J. Sharrock, SWK Pavement Engineering, Inc., 22 Andover Road North, Winchester, England. M. G. Bouldin, Applied Technology, 1339 Allston, Houston, Tex.

A finite-element (FE) program known as PACE has been developed to perform the computations using viscoelastic material characteristics defined by testing mix specimens with a repeated load creep test or conducting a frequency sweep test. Strain hardening is considered by describing the material properties obtained from the repeated load creep test as a function of temperature and shear strain expressed in terms of the second deviatoric strain invariant. Temperature depth profiles for any location are incorporated by using on FE heat flow model known as HiRoad.

This paper describes the computational functions of the program, the material models, traffic data, temperature predictions, and computation procedures.

FINITE-ELEMENT MODEL

The software consists of a core FE program that interacts with other programs and subroutines that provide information on material properties, pavement temperatures, and traffic conditions (Figure 2). The greater part of the existing finite-element code, initially drawn upon for program development, is based on work described by Owen and Hinton (*3*). A brief description of the main features of the code follows.

The displacement method was adopted, so the unknowns are *translational displacements* at each node in the x and y global directions. Eight-node *isoparametric elements* are used, so the same shape functions are used for the geometry of the element as for the variation of the unknowns. Three independent stress components are allowed at each integration point to cater for *plane strain* conditions.

Linear isotropic elasticity is assumed for modeling elastic behavior with *Young's modulus* and *Poisson's ratio* part of the input. Viscoelastic materials are treated as a special case of viscoelastic-plastic behavior, in which the *yield stress* in the plastic slider element, for the onset of viscoplasticity is reduced to zero (see Figure 3). Elastic material behavior is also obtained as a special case, by specifying a very large yield stress for the plastic element so that viscoplastic flow cannot occur.

Wheel loading is applied in increments. At each increment, an initial solution is obtained with the current *out-of-balance forces* and a set of *pseudoforces* generated to drive the viscous flow during a subsequent time-stepping process. Each increment of load therefore makes up an initial solution followed by further equation solutions at a number of time steps. The size of time step employed is related to the material properties.

The method by which the basic one-dimensional *rheological model* is used for analysis with the finite-element method is briefly outlined in the following. Where viscoplastic components are referred to, these would also relate to purely viscous components, since the yield stress for plasticity F_o can be zero, in view of the rheological model employed (as illustrated in Figure 3).

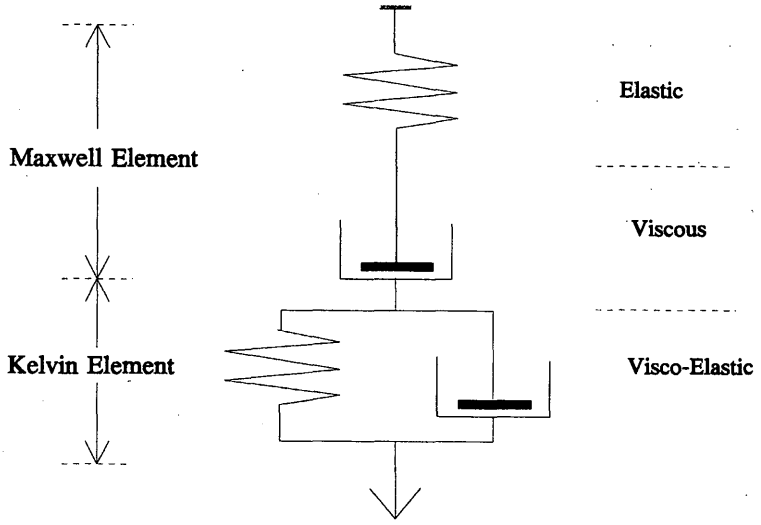

FIGURE 1 Burgers model.

The total strain is assumed to be separable into elastic and viscoplastic components and, hence, in terms of strain rates:

$$\dot{\epsilon} = \dot{\epsilon}_e + \dot{\epsilon}_{vp} \tag{1}$$

The elastic component is assumed to experience the total stress acting, and therefore the total stress rate depends on the elastic strain rate by way of the elasticity matrix D:

$$\dot{\sigma} = D\dot{\epsilon}_e \tag{2}$$

Viscoplastic flow is assumed to occur when a scaler function of the stress (which is common to the elastic component and the viscoplastic component) and/or of the viscoplastic strain exceeds the scaler yield condition determined by the yield criterion. The yield condition may also be a function of a strain hardening parameter K. For flow to occur,

$$F(\sigma,\epsilon_{vp}) > \sigma_y(K) \tag{3}$$

The viscoplastic strain rate is determined from the current *state of stress* by the relationship:

$$\dot{\epsilon}_{vp} = \gamma < \mathcal{F}(F) > \frac{\partial F}{\partial \sigma} \tag{4}$$

In Equation 4, $\partial F/\partial\sigma$ represents a *plastic potential* and γ is a fluidity (reciprocal of viscosity). The yield function F is that of Von Mises and the function $F(F)$ chosen is given by

$$\mathcal{F}(F) = \frac{F - \sigma_y}{\sigma_y} \tag{5}$$

For the case of purely viscous flow, with zero yield stress for plasticity,

$$\mathcal{F}(F) = F \tag{6}$$

The resulting viscous strain increment is assumed to be entirely (shear) deviatoric (no volume change) and proportional to the current deviator stresses. The mixture viscosity is, consequentially, a shear viscosity in these circumstances. This is considered to lead to a reasonable approximation of viscous flow with viscous or visco-elastic material behavior. The time stepping is implemented by dividing the time into n intervals with the strain increment in a time interval of $\Delta t^n = t^{n+1} - t^n$, being written in the general form

$$\Delta\epsilon^n_{vp} = \Delta t^n [(1 - \theta)\,\dot{\epsilon}^n_{vp} + \theta\dot{\epsilon}^{n+1}_{vp}] \tag{7}$$

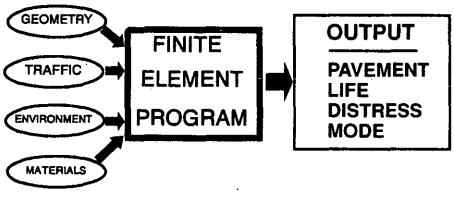

FIGURE 2 Finite-element program.

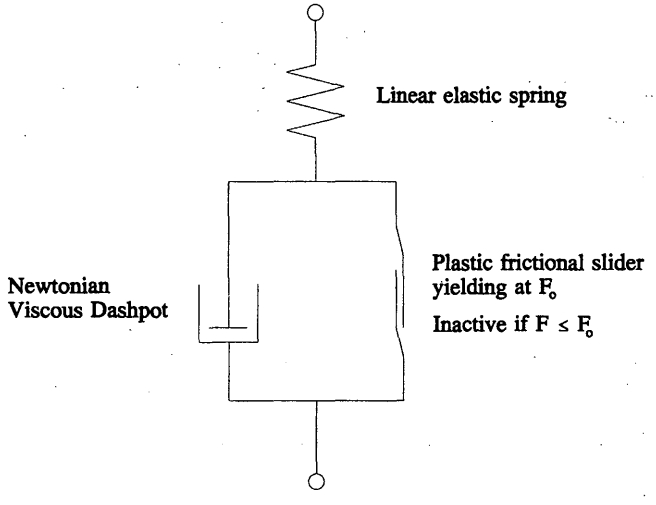

FIGURE 3 Rheological representation of model used.

The significance of this expression is that when $\theta = 0$, the iteration scheme is the fully "explicit" (forward difference) time integration. The strain increment is completely determined from the conditions at the start of the time interval. When $\theta = 1$, the iteration scheme is fully "implicit" (backward difference) time integration. If $\theta = 0.5$, then the scheme becomes "implicit trapezoidal" and uses information from both ends of the time interval. The program currently uses the explicit scheme of iteration for the integration ($\theta = 0$).

Equation 4 can be expressed as a linearized series as

$$\dot{\epsilon}_{vp}^{n+1} \simeq \dot{\epsilon}_{vp}^{n} + H^n \, \Delta\sigma^n \tag{8}$$

where

$$H^n = \left(\frac{\partial \epsilon_{vp}}{\partial \sigma}\right)^n \equiv H^n(\sigma^n) \tag{9}$$

The general expression, Equation 7, for the strain increment results in

$$\Delta \epsilon_{vp}^{n} = \dot{\epsilon}_{vp}^{n} \, \Delta t^n + C^n \, \Delta\sigma^n \tag{10}$$

where

$$C^n = \theta \Delta t^n H^n \tag{11}$$

Equation 2 can be expressed in incremental form as

$$\Delta\sigma^n = D\Delta\epsilon_e^n = D(\Delta\epsilon^n - \Delta\epsilon_{vp}^n) \tag{12}$$

where

$$\Delta\epsilon^n = B^n \Delta d^n \tag{13}$$

The total strain increment is expressed in terms of the displacement increment as shown in Equation 13 and by substituting for $\Delta\varepsilon_{vp}^n$ from Equation 10, the stress increment becomes

$$\Delta\sigma^n = \hat{D}^n(B^n \Delta d^n - \dot{\epsilon}_{vp}^n \, \Delta t^n) \tag{14}$$

where

$$\hat{D}^n = (D^{-1} + C^n)^{-1} \tag{15}$$

To obtain a set of global equations in these circumstances, the conditions of equilibrium are next considered. Using Equations 10 and 14, the displacement increment during a time step is obtained from the following:

$$\Delta d^n = [K_T^n]^{-1} \Delta V^n \tag{16}$$

where

$$\Delta V^n = \int_\Omega [B^n]^T \hat{D}^n \, \dot{\epsilon}_{vp}^n \, \Delta t^n d\Omega + \Delta f^n \tag{17}$$

where Δf^n represents the increment of loading, assumed nonzero only at the start of time stepping during a load increment.

The parameter K_T^n is a tangential stiffness matrix defined by

$$K_T^n = \int_\Omega [B^n]^T \hat{D}^n B^n d\Omega \tag{18}$$

The algorithm shown in Equation 18 gives a linearized approximation to the incremental equilibrium, Equation 17, and, therefore, the total stresses accumulated from stress increments will not, in general, be quite correct. The technique adopted to reduce this error and to avoid using an iterative process in the solution, is as follows: a set of residual or out-of-balance forces ψ^{n+1} are determined for time $n + 1$ from the relation in Equation 19. These residual forces are then added to the applied force increment at the next time step:

$$\psi^{n+1} = \int_\Omega [B^{n+1}]^T \sigma^{n+1} \, d\Omega + f^{n+1} \tag{19}$$

After each load pulse is applied and values of deviatoric shear strain obtained, a loop in the program is made to the material file where, for the design temperatures, all the material properties are updated to be consistent with the second deviatoric strain invariant and the temperature. Thus, the model is considered to introduce nonlinear viscoelasticity into the material behavior (strain hardening) with successive load applications.

Experience has shown that real materials cannot be characterized by simple models as shown in Figure 3 but, in fact, require more complex models to explain their behavior. A method of obtaining more realistic material response, in the context of FE modeling, is to build up a composite action by using a number of different "overlays" of simpler materials, each with different characteristics. The material to be analyzed is assumed to be composed of several layers, each of which undergoes the same deformation (*strain compatibility*). The total stress field in the material is then obtained by a summation to which each part of the overlay contributes in proportion to the fractional weighting allocated in the total material. In a two-dimensional situation, the total thickness is taken to be unity and the weighting for each material simply equals its thickness in the overlay (*4–6*). This concept is illustrated in Figure 4.

This technique has been implemented to obtain a model that will allow input of parameters associated with a *generalized Maxwell model* (Figure 5). The initial version of the software uses properties associated with a *two-element Maxwell model with strain hardening* for permanent deformation calculations and a *four-element Maxwell model* for fatigue life calculations. With two elements, a reasonable description of the material is obtained but if 4 to 10 elements are used, an excellent fit results over a wider time range (*7*).

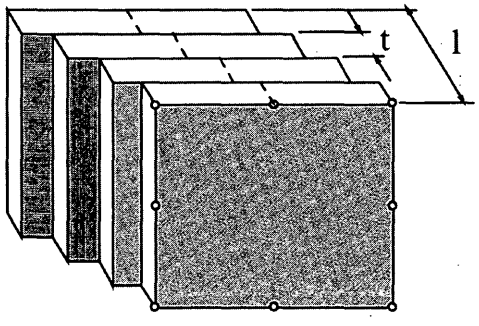

Unit thickness overlay composed of 4 materials, 2-D situation

FIGURE 4 Overlay model.

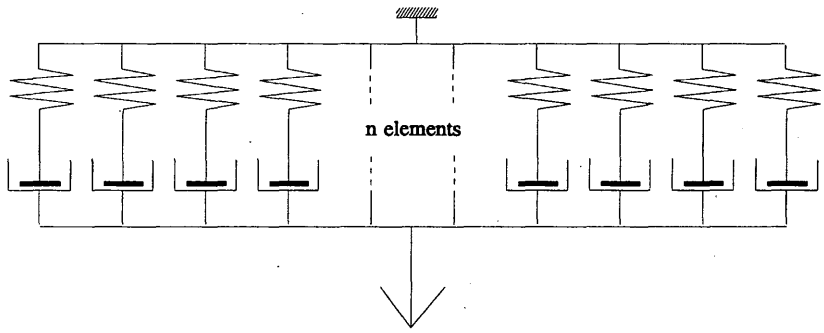

FIGURE 5 Generalized Maxwell model.

CLIMATE

Climatic factors play a dominating role in asphalt pavement design procedures since they affect both permanent deformation and fatigue cracking, as well as other modes of pavement distress. To enable a rigorous analysis of climatic effects to be introduced, an FE heat flow model HiRoad was used to generate 24 temperature-depth profiles, one for each hour of the day. The calculations are repeated for 12 periods corresponding to each of the 12 months of the year. The model uses an energy balance calculation with boundary conditions that consist of a heat transfer coefficient used in conjunction with air temperature, together with a radiation flux, at the upper surface and a fixed temperature at a 1-m depth, equal to the average monthly air temperature. The computation is started at dawn, assuming a constant temperature with depth for simplicity. The heat flow equations are integrated by an explicit time-stepping procedure, while simultaneously, the heat transfer conditions at the surface are varied with time according to the predetermined patterns of air temperature together with direct and diffuse radiation. After 24 hr, dawn is again reached. The temperature-depth variation found at this time is treated as a new estimate of the starting conditions, and the time-stepping process is repeated for another 24 hr. In this way, successive approximations of the initial boundary conditions are obtained. When the initial and final states of the 24-hr period match closely, the desired solution for the period has been determined. The radiation at the surface is obtained as follows:

- Day—a mean value of solar constant of 1,362 W/m^2 is assumed, that is, the radiation intensity normal to the sun's direction above the earth's atmosphere. This is taken to vary seasonally by ±3.5 percent due to the varying radius of the earth's orbit. Generally accepted published information on the proportion of the radiation reaching the ground is assumed, dependent on the elevation of the sun, the height above sea level, and cloud cover. An absorptivity of 0.9 is taken for the asphaltic materials.
- Night—A constant reradiation of 120 W/m^2 to space is assumed. This is developed and terminated linearly during the first hour and last hour of darkness, to give a pattern continuous with the daytime radiation input.

An approximate daily variation of air temperature for each month is constructed from average daily maximum and minimum temperatures, with an allowance of plus and minus a number of standard deviations to cover the required proportion of the extremes, varying linearly with maximum and minimum temperature over the year. Together with the computed surface temperature, this defines the remaining surface heat transfer, using a heat transfer coefficient of 23 W/m^2/°C.

The heat flow calculation is done iteratively, employing the previously mentioned FE method. Typical thermal properties are assumed for the asphaltic mixture as follows: conductivity (K_c) 1.5 W/m°K, mass density (ρ) 2 400 kg/m^3, specific heat (Cp) 960 J/kg°K.

Those properties are used to obtain diffusivity:

$$\kappa = \frac{K_c}{(\rho \times Cp)} \tag{20}$$

Thus, the default value used in the FE heat flow calculations for diffusivity is 6.51e−7 m^2/s. Typical examples for computed temperature depth profiles are given in Figure 6. These are then used to determine temperature and damage weighted material properties for design. The weighting methods are discussed with the performance models.

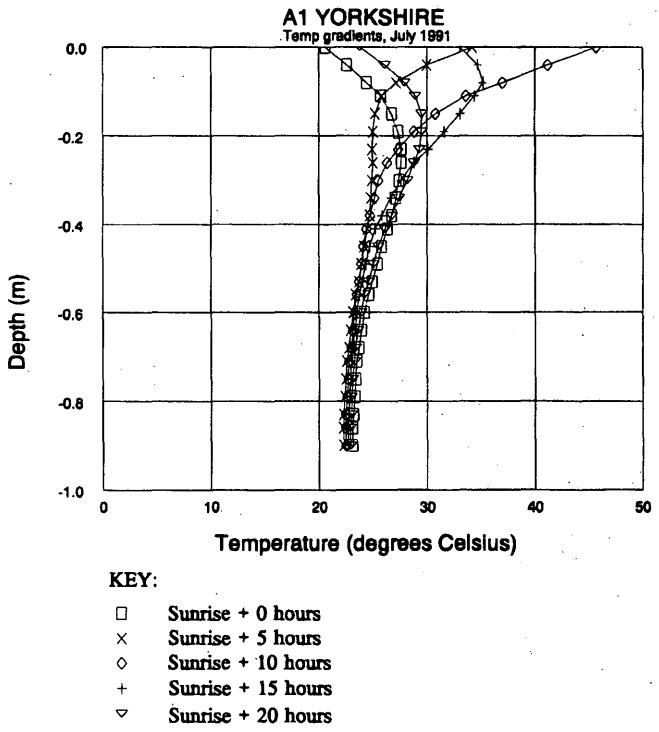

FIGURE 6 Typical calculated temperature depth relationship.

TRAFFIC AND PAVEMENT GEOMETRY

Traffic Loading

Estimation of the number of cumulative equivalent single-axle loads (ESALs) is often required for design purposes. If known ESALs are used as input, however, the definition of an ESAL is a function of the analysis method, and although traditionally a fourth power law has been assumed, it is often not valid for the calculations. Consequently, the software allows the user to consider the effect of other axle loads or wheel configurations to obtain a conversion to ESALs. The latter is of particular interest because it allows the user to investigate the effect of different wheel load configurations with respect to the anticipated pavement damage (*8–10*).

Pavement Geometry

In most situations, a computer program for pavement design must have the capability to consider several bound and unbound layers. The program enables use of up to six asphalt bound layers (typically construction layers) and a further eight lower layers that could be either bound existing pavement layers, unbound granular layers (typically foundation layers), or soils. Generally, they consist of one granular base layer and up to seven foundation layers. The material model for the lower layers would consider the material to be elastic, whereas viscoelastic behavior is used for the upper asphalt bound layers. Nonlinear resilient response of the foundation is typically considered by increasing the foundation stiffness with depth. The user could use an elastic lower layer to describe an existing bound asphalt layer that is to be overlaid with a new asphalt layer and only model the upper layers (or layer) as viscoelastic layers.

PERFORMANCE MODELS

Two separate calculation procedures are performed, the first for fatigue cracking and the second for the permanent deformation. This approach is similar to existing procedures (*1*), and no interaction of the mechanisms of failure is currently considered.

Fatigue Cracking

Fatigue performance is predicted by considering the energy dissipated (work done) in asphaltic materials under loading, with the damage being proportional to the cumulative dissipated energy. This approach is similar to that used in the *Shell Pavement Design Manual* (*1*), with some additional features made possible by recent research, including a direct calculation of dissipated energy from the FE analysis and incorporation of an improved model for determining pavement life from consideration of dissipated energy. The calculation for fatigue life consists of the following steps:

1. Calculate dissipated energy contours in the pavement structure over a range of temperatures that cover the highest to lowest expected.
2. Calculate the fatigue life, from the relationships proposed in a work by Rowe (*11*), at each value of temperature considered in the program.
3. Calculate the damage under a single-axle load at a temperature, T, assuming Miners' linear damage rule to be valid:

$$D_T = \frac{1}{N} \tag{21}$$

4. For each month, using the relationship between damage and temperature, calculate the mean damage for the month. This is done by considering the traffic and temperature in 24 one-hr increments, that is,

$$D_m = \frac{\int_1^{24} \check{N}(t) D_T dt}{\int_1^{24} \check{N}(t) dt} \tag{22}$$

where

$$\check{N}(t) = \frac{N(t)}{\int_1^{24} N(t) dt} \tag{23}$$

5. Assuming a uniform flow of traffic over the year, calculate the yearly traffic weighted mean damage from the following:

$$\bar{D} = \frac{1}{12} \int_1^{12} D_m dm \tag{24}$$

6. Using the relationship established earlier between temperature and damage under a standard axle load, it would be possible to equate the yearly traffic weighted mean damage to temperature and material properties. However, this is not necessary since life can be computed from

$$N = \frac{1}{\bar{D}} \tag{25}$$

To account for the effect of rest periods, lateral wander by traffic, and crack growth, the figures from Equation 25 are multiplied by factors of 10 or 14 for either 10 or 45 percent cracking, respectively (*12*). A typical contour plot of damage calculated by the FE analysis is shown in Figure 7, while Figure 8 indicates the prediction of cracking percentage against the number of axle loads.

Permanent Deformation

The permanent deformation performance calculated from the model uses developments of procedures in the *Shell Pavement Design Manual* (*1*) and those developed by Nunn (*8*). The major assumptions are

- Dilation is not allowed, so the effective Poisson's ratio associated with the permanent strain is less than 0.5;
- Uniaxial or shear properties are used to define a triaxial stress state; and
- A yield condition is not currently implemented.

In addition to the foregoing assumptions, it is assumed that material properties change as the material undergoes permanent deformation and the viscoelastic properties are changed as a function of the permanent deviatoric strain. This introduces nonlinear

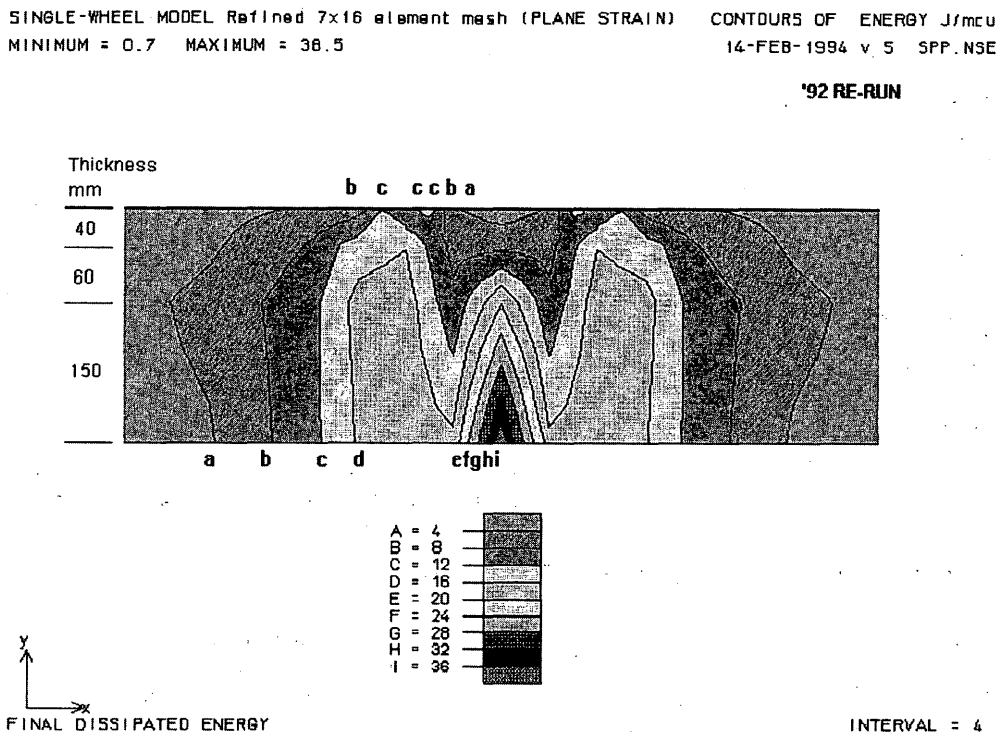

FIGURE 7 Fatigue damage contour.

(*incrementally linear*) properties and also a variation of properties within different elements of the pavement structure at a similar time increment. This aspect is different from the assumptions made in many design procedures (*1,8*) that use cumulative loading time to describe the nonlinear change in material properties. Temperature weighting is considered a function of the "inverse loss compliance," $1/D''$, using the model presented in a work by Bouldin et al. (*7*).

Thus, the steps used to compute permanent deformation are as follows:

1. Calculate the traffic weighted pavement temperature using $1/D''$.
2. For traffic Increment 1, calculate the permanent deformation for one axle and the permanent deviatoric strain.
3. Apply deformation for number of load passes considered in increment.
4. Obtain new material properties as a function of deviatoric shear strain.
5. Calculate permanent deformation for one axle pass in an increment.
6. Repeat Steps 3 to 5 until the design life or until a critical rut depth is obtained.

Typical examples of a rut development plot and deformed pavement shape are given in Figures 9 and 10, respectively.

CONCLUSIONS

A new method of pavement analysis based upon realistic material properties has been developed. Viscoelastic characterization of the material is used with appropriate criteria for fatigue damage and

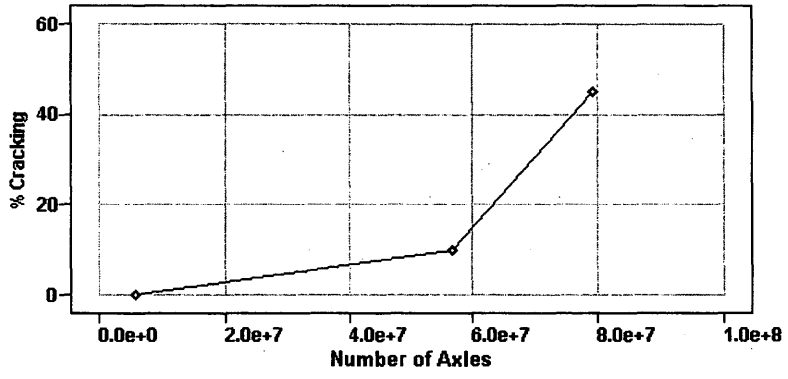

FIGURE 8 Percentage cracking versus life, damage development from fatigue calculation: crack initiation, 5.66*e*6 axles; 10 percent cracking, 5.66*e*7 axles; 45 percent cracking, 7.92*e*7 axles.

Axles	Rut(mm)
1.00E0	0.0000
3.00E0	0.0599
7.00E0	0.1022
1.50E1	0.1625
3.10E1	0.2440
6.30E1	0.3503
1.27E2	0.4837
2.55E2	0.6471
5.11E2	0.8463
1.02E3	1.0883
2.05E3	1.3911
4.10E3	1.7865
8.19E3	2.3102
1.64E4	3.0093
3.28E4	3.9497
6.55E4	5.2239

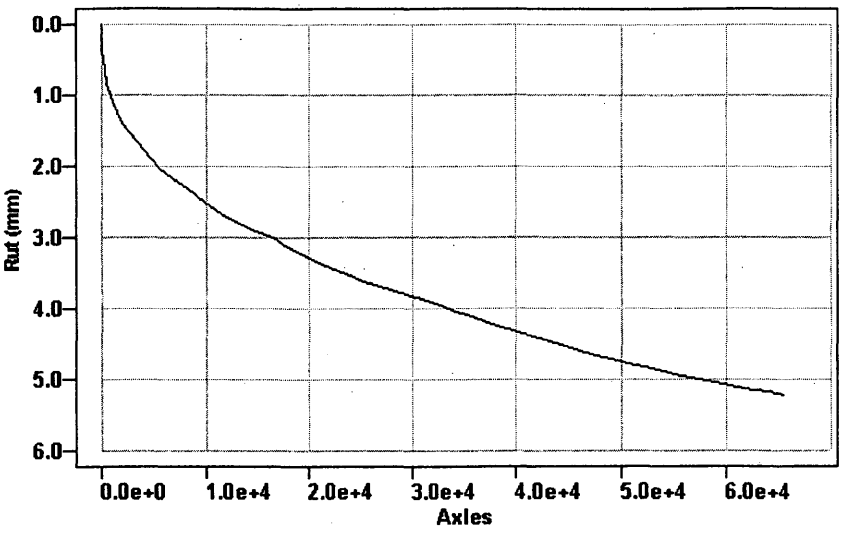

FIGURE 9 Computed rut development to 65535 wheel passes.

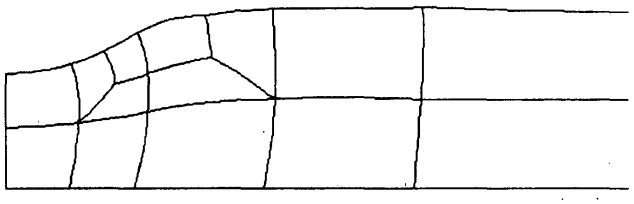

FIGURE 10 Deformed pavement shape (half of section), computed rut profile at 65536 wheel passes, deformations multiplied by factor 7.

permanent deformation. The key components of the method involve the following:

1. Dissipated energy fatigue criterion. This considers the energy dissipated (work) in asphaltic materials with the damage being directly proportional to the cumulative dissipated energy. This criterion replaces the "strain criterion" currently considered for fatigue damage.
2. Viscoelastic materials characterization. Repeated load creep testing allows the viscoelastic properties of an asphaltic material to be obtained. These parameters are directly related to rutting and enable predictions of deformation in the field and comparisons to be made between different materials.
3. Pavement modeling. A computerized method for determining stresses and strains associated with viscoelastic pavement materials has been developed. The computer program PACE uses a finite-element method and considers various inputs, such as pavement geometry, material properties, traffic, and environment. This method allows computation of pavement deformation and dissipated energy (as related to fatigue damage) to be performed.

NOTATION

English Symbols

B^n = Strain matrix at time station t^n (constant, when infinitesimal strain assumed)
C_P = Specific heat
C^n = Matrix proportional to H^n
d = Displacement vector
D = Elasticity matrix
D'' = Extensional loss compliance
D_m = Monthly traffic weighted mean damage
D_T = Fatigue damage at a temperature T
$\bar{D}$ = Yearly traffic weighted mean damage
$\hat{D}$ = Elastic-viscoplastic matrix
e = Elastic
E = Elastic modulus
f^n = Force vector (applied forces acting at time station n)
$F(\sigma,\epsilon_{vp})$ = Scaler yield function
FE = Finite element
H^n = Matrix dependent on yield criterion adopted, at time station n
J'' = Shear loss compliance
K = Tangential stiffness matrix
K_c = Conductivity
n = Time station
N = Number of axles
$\check{N}$ = Normalized traffic distribution
Pi = Proportion of traffic in increment i
s = Specific heat
T = Transpose of vector or matrix
T = Temperature
vp = Viscoplastic
V = Viscosity
V^n = Force vector of pseudoloads for time steps at time station n

Greek Symbols

γ = Fluidity, reciprocal of viscosity (scaler)
Δ = A small change in any quantity
Δt^n = Time interval between t^n and t^{n+1}
$\Delta\sigma^n$ = Stress change occurring in time interval Δt^n (vector)
ε = Strain vector
$\dot{\varepsilon}$ = Strain rate

θ = Time stepping algorithm parameter (scaler)
κ = Diffusivity
ρ = Density
σ = Stress vector
$\dot{\sigma}$ = Stress rate
σ_y = Uniaxial yield stress (scaler)
$\Phi(F)$ = Scaler function of stress
Ψ = Out-of-balance force, or residual vector
Ω = Domain of problem

Other Symbols

$\langle\rangle$ = Macaulay brackets
$\partial F/\partial\sigma$ = "Plastic" potential for associated plasticity; enables strain rate to be defined as a function of stress gradient
$\mathcal{F}$ = Function
$\dot{}$ = Derivative with respect to time
t^n, t^{n+1} = Two successive time stations

REFERENCES

1. *Shell Pavement Design Manual*, Shell International Petroleum Company, London, England, 1978.
2. Huhtala, M., R. Alkio, J. Pihljamaki, M. Pienmaki, and P. Halonan. Behavior of Bituminous Materials Under Moving Wheel Loads. *Journal of the Association of Asphalt Paving Technologists*, Vol. 59, 1990, pp. 422–442.
3. Owen, D. R. J., and E. Hinton. *Finite Elements in Plasticity: Theory and Practice*. Pineridge Press, Swansea, Wales, 1980.
4. Zienkiewicz, O. C., G. C. Nayak, and D. R. J. Owen. *Composite and Overlay Models in Numerical Analysis of Elasto-Plastic Continua*. Presented at International Symposium on Foundations of Plasticity, Warsaw, Poland, 1972.
5. Owen, D. R. J., A. Prakash, and O. C. Zienkiewicz. Finite Element Analysis of Non-Linear Composite Materials by Use of Overlay Systems. *Computers and Structures*, Vol. 4, 1974, pp. 1251–1267.
6. Pande, G. N., D. R. J. Owen, and O. C. Zienkiewicz. Overlay Models in Time Dependent Nonlinear Material Analysis. *Computers and Structures*, Vol. 7, 1977, pp. 435–443.
7. Bouldin, M. G., G. M. Rowe, J. B. Sousa, and M. J. Sharrock. Repetitive Creep as a Tool to Determine the Mix Rheology of Hot Mix Asphalt. *Journal of the Association of Asphalt Paving Technologists*, Vol. 63, 1994, pp. 182–223.
8. Nunn, M. E. *Prediction of Permanent Deformation in Bituminous Pavement Layers*. Research Report RR26. Transport and Road Research Laboratory, Crowthorne, England, 1986.
9. Huhtala, M. The Effect of Different Trucks on Road Pavements. *Proc., International Symposium on Heavy Vehicle Weights and Dimensions*, Canada, 1986.
10. Bell, C. A. and S. Randhawa. Truck Tire Issues: Evaluation of Impacts of High Pressure Tires and Single-Tired Axles in Oregon. Oregon State University, 1992.
11. Rowe, G. M. Performance of Asphalt Mixtures in the Trapezoidal Fatigue Test. *Journal of the Association of Asphalt Paving Technologists*, Vol. 62, 1993, pp. 344–384.
12. Deacon. J. A., A. A. Tayebali, J. S. Coplantz, F. N. Finn, and C. L. Monismith. *Fatigue Response of Asphalt—Aggregate Mixes: Part III Mix Design and Analysis*. SHRP Project A-003A. Asphalt Research Program, Institute of Transportation Studies, University of California, Berkeley, 1992.

Publication of this paper sponsored by Committee on Flexible Pavement Design.

DIPLOMAT: Analysis Program for Bituminous and Concrete Pavements

LEV KHAZANOVICH AND ANASTASIOS M. IOANNIDES

Burmister's layered elastic theory is extended to accommodate an interior loading of a multilayered pavement system incorporating an arbitrary sequence of elastic plates and spring beds, in addition to isotropic layers. The formulation is coded into a new computer program, called DIPLOMAT, thereby allowing for the first time direct comparisons between the distinct analytical approaches conventionally used for so-called rigid and flexible pavements. The new program is as user friendly and computationally efficient as the widely used layered elastic analysis program BISAR. In addition to permitting multiple-wheel loads, DIPLOMAT may be used to investigate the effects of a variety of interface and boundary conditions, including that of a rigid base. When considering a plate on grade, DIPLOMAT reproduces the closed-form solutions by Westergaard (dense liquid foundation) and by Losberg (elastic solid foundation). On the other hand, for a pavement section consisting of up to five isotropic layers, the new program reproduces the BISAR solutions for bonded or unbonded layers. A number of applications of the program are presented, including an assessment of the structural contribution of compressible (granular or bituminous) bases under a concrete pavement slab, and determination of the interface spring stiffness that accounts for constructed layer compressibility. Some implications of program results to pavement design are also discussed.

In determining the structural response of highway and airport pavements, one of two fundamentally different hypotheses has been traditionally used to idealize the properties of the subgrade. For portland cement concrete (PCC) pavement systems, the simplest of these theories is used: the supporting soil medium is considered a bed of closely spaced, independent, linear springs. Each spring deforms in response to the stress applied directly to it, and neighboring springs remain unaffected. The spring stiffness, k, is called the modulus of subgrade reaction and is assumed to be spatially independent. This idealization is commonly called a "dense liquid" and is almost universally ascribed to Winkler (*1*).

For asphalt concrete (AC) pavements, on the other hand, a second support characterization theory is conventionally used, in which the soil is regarded as a linearly elastic, isotropic, homogeneous solid, of semi-infinite extent. The terms "elastic solid," "elastic continuum," or "Boussinesq's half-space" are often applied to this idealization (*2*). It is regarded as a more realistic representation of actual subgrade behavior than the dense liquid model, inasmuch as it takes into account the effect of shear interaction between adjacent subgrade support elements.

In a parallel fashion, two distinct theoretical models have been traditionally used in idealizing the constructed layers in the pavement system. For PCC pavements, medium-thick plate theory is conventionally used (*3*). This approach is again the simpler of the two and proceeds from the assumption that the constructed layer, typically a PCC slab, resists the applied loads by bending alone, experiencing no compression through its thickness in the process. A more realistic representation of in situ behavior of constructed pavement layers may be obtained by assuming that they behave as linearly elastic, homogeneous, and isotropic materials not subject to the restrictive assumptions of plate theory. In view of the relatively higher compressibility of asphalt concrete, the layered elastic approach has been adopted in current analysis procedures for AC pavements (*4,5*).

These conventional choices may lead to the impression that the elastic solid foundation is inextricably associated with layered elastic analysis. It has been recently demonstrated not only that is this not the case but also that a formulation based on the isotropic layer–dense liquid subgrade combination might in fact have numerical advantages over conventional applications of layered elastic analysis (*6*). A literature survey conducted recently (*7*) revealed that similar ideas had also been promulgated in the former Soviet Union (*8*).

This paper describes the development of a new structural analysis program, code-named DIPLOMAT, which can be used for both PCC and AC pavement systems. Much like conventional layered elastic analysis programs, DIPLOMAT can accommodate multilayered pavement sections, loaded by multiple-wheel loads. In addition, however, it allows the user the option to specify that the last layer in the pavement system be a bed of springs and that one or more of the constructed layers be treated as plates. Such a structural model is interesting from theoretical as well as practical perspectives. For the first time, it allows analyses of both PCC and AC pavement systems based on the same assumptions and can facilitate comparisons between the behavior and performance of these two heretofore distinct pavement types. In this respect, the formulation in DIPLOMAT constitutes an extension and generalization of Burmister's layered elastic theory.

FORMULATION OF BOUNDARY VALUE PROBLEM

The formulation of the boundary value problem (BVP) posed by a multilayered pavement system involves four major components: the equilibrium equations, the strain-displacement relationships, the constitutive law, and the boundary and initial conditions. Complete details of this formulation are provided in a work by Khazanovich (*9*). Only the highlights are presented herein, with emphasis placed on the boundary (or interface) conditions used.

The equilibrium equations, constitutive laws, and strain-displacement relationships for a uniform, isotropic (Burmister) layer have been presented elsewhere (*10*). For an axisymmetric problem, it is convenient to use the cylindrical coordinate system

L. Khazanovich, ERES Consultants, Inc., 505 W. University Ave., Champaign, Ill. A. M. Ioannides, Department of Civil Engineering, University of Illinois, 205 N. Mathews Ave., #2230C, Urbana, Ill. 61801.

(r, Φ, z). In this coordinate system, some components of the displacement vector and stress tensor are identically equal to zero due to axisymmetry. The remaining stress and displacement components can be rewritten in terms of the biharmonic stress function, Φ (*11*). The fact that function Φ is biharmonic, that is,

$$\nabla^4 \Phi = 0 \tag{1}$$

provides satisfaction of the equilibrium condition in this case. Following Burmister (*4,5*), the biharmonic function Φ for isotropic layer i is expressed in the following form:

$$\Phi_i = \int_0^\infty [A_i(m)e^{m z} - B_i(m)e^{-m z} + C_i(m)ze^{m z} - D_i(m)ze^{m z}]J_0(m\,r)\,dm \tag{2}$$

where

J_n = Bessel function of nth order,
z = local vertical coordinate, which in contrast to Burmister's convention is measured here down from top surface of each layer i, and
$A_i(m)$, $B_i(m)$, $C_i(m)$, and $D_i(m)$ = unknown functions that do not depend on coordinates.

These constants are evaluated by satisfying the boundary conditions.

The governing equilibrium equations, strain-displacement relationships, and constitutive law for a uniform Kirchhoff plate are given elsewhere (*12*). Accordingly, the plate deflection profile is given by

$$\nabla^4 w = \frac{q^*}{D} \tag{3}$$

where q^* is the net (total) pressure applied to top and bottom surfaces of plate, and D is plate flexural stiffness, defined as

$$D = \frac{E\,h^3}{12(1 - \mu^2)} \tag{4}$$

Here h, E, and μ denote the plate thickness, modulus of elasticity, and Poisson's ratio, respectively. Note that for a general multilayered system, the applied pressure, q^*, is unknown and is determined from the boundary conditions for the adjacent layers, above and below the plate. The deflection profile for a plate, w^i, can be presented in a form similar to that used by Losberg (*13*):

$$w^i = \int_0^\infty \frac{W_i(m)}{E_i} J_0(m\,r)\,m\,dm \tag{5}$$

where function $W_i(m)/E_i$ is the zero-order Hankel transform of the deflection profile and is the only function to be determined for a plate.

The governing equilibrium equations, strain-displacement relationships, and constitutive law for a bed of springs can be derived from the corresponding equations for the isotropic layer, if the horizontal displacements u and v are set to zero, along with the two transverse shear strains and the layer's Poisson's ratio, μ (*14*). Thus, the following equation can be written for the spring bed:

$$\sigma_z = -k(w_t - w_b) \tag{6}$$

where

σ_z = vertical stress in springs,
w_t and w_b = vertical displacements of top and bottom ends of springs, and
k = spring stiffness.

It should be noted that the presence of spring beds does not introduce additional unknown functions. The response of these springs can be expressed in terms of the responses of the adjacent layers, above and below the springs.

To complete the formulation of the BVP for a multilayered system, it is necessary to specify boundary conditions between the layers. The presence of different layer options makes formation of the BVP in this case more difficult than for the original Burmister (*4*) problem. Here, the boundary conditions for each layer depend on the kind of model adopted for its adjacent layers (above and below it). To reduce the number of possible combinations, the following restrictions have been accepted: (a) a plate cannot have a common border with another plate, and (b) a spring bed cannot have a common border with another spring bed.

These restrictions impose no reduction in the generality of the proposed approach. Two plates resting on one another can be replaced by an equivalent plate with parameters as defined by Ioannides et al. (*15*). At the same time, n spring beds in series can also be replaced by one equivalent spring bed with effective spring stiffness, k_{eff}

$$k_{eff} = \frac{1}{\sum_{i=1}^{n} \frac{1}{k_i}} \tag{7}$$

where k_i is stiffness of each individual spring bed. Stresses in every spring bed are equal to the corresponding stress in the equivalent bed.

In what follows, the boundary conditions for the BVP will be formulated for different combinations of isotropic layers, plates, and spring beds. It is assumed that all layers are numbered sequentially from top to bottom as 1 to n, with the nth layer being an elastic solid half-space, or a finite isotropic layer or spring bed resting on a rigid base. The case of the pavement surface layer being a spring bed is trivial and is not considered below.

Boundary Conditions at Interface Between Two Isotropic Layers

Following Burmister (*4,5*), two kinds of boundary conditions at the interface between two isotropic layers are usually considered: a rough interface or a smooth interface. Both kinds of conditions assume continuity of vertical displacements and of vertical stresses across the interface, whose normal is in the z direction. Thus, the following continuity conditions are always satisfied:

$$\sigma_z^{i,b} = \sigma_z^{i+1,t} \tag{8}$$

$$w^{i,b} = w^{i+1,t} \tag{9}$$

where $\sigma_z^{i,b}$ *and* $\sigma_z^{i+1,t}$ are vertical stresses at the bottom surface of the upper layer and at the top surface of the lower layer, respectively; $w^{i,b}$ *and* $w^{i+1,t}$ are vertical displacements at the bottom surface of the upper layer and at the top surface of the lower layer, respectively.

The rough interface condition also assumes continuity of horizontal displacements and of shear stresses across the interface. This assumption can be written in the following form:

$$\tau_{rz}^{i,b} = \tau_{rz}^{i+1,t} \tag{10}$$

$$u^{i,b} = u^{i+1,t} \tag{11}$$

where $\tau_{rz}^{i,b}$ *and* $\tau_{rz}^{i+1,t}$ are shear stresses at the bottom surface of the upper layer and at the top surface of the lower layer, respectively; $u^{i,b}$ and $u^{i+1,t}$ are radial displacements at the bottom surface of the upper layer and at the top surface of the lower layer, respectively.

The smooth interface condition does not require continuity of horizontal displacements or of shear stresses across the interface, but allows free slip of one layer with respect to the other in the horizontal direction. Therefore, this kind of interface leads to the following conditions:

$$\tau_{rz}^{i,b} = 0 \tag{12}$$

$$\tau_{rz}^{i+1,t} = 0 \tag{13}$$

One can note that either Equation 12 or Equation 13 can be replaced by Equation 10.

Boundary Conditions at Interface Between Isotropic Layer and Rigid Base

The interface between an isotropic layer and a rigid base can also be rough or smooth. Both types of interface conditions require zero vertical displacement at the bottom of the isotropic layer, n, above the rigid base:

$$w^{n,b} = 0 \tag{14}$$

The rough interface condition requires that radial displacements also vanish at the bottom surface of the isotropic layer:

$$u^{n,b} = 0 \tag{15}$$

The smooth interface does not resist horizontal displacements along the bottom of the isotropic layer and leads to the condition of vanishing shear forces at this interface:

$$\tau_{rz}^{n,b} = 0 \tag{16}$$

Boundary Conditions for Elastic Solid Half-Space

In this case, displacements should vanish as depth tends to infinity, that is,

$$w = u = 0 \qquad \text{as } z \to \infty \tag{17}$$

It may be verified that satisfaction of these conditions also leads to vanishing stresses at infinite depth.

Boundary Conditions at Interface Between Isotropic Layer and Plate or Spring Bed

If an isotropic layer, i, has a common boundary with a plate or a spring bed, this interface is always smooth and free of shear stresses

$$\tau_{rz}^{i,s} = 0 \tag{18}$$

where superscript s denotes t or b (top or bottom surface, respectively), depending on which surface of the layer is considered.

If the adjacent layer is a plate, then its vertical deflections are equal to the corresponding layer vertical deflections at the interface:

$$w^{i,s} = w^{P} \tag{19}$$

where w^P is the adjacent plate deflection.

If the adjacent layer is a spring bed, then normal stresses in the isotropic layer at the interface are equal to the vertical stresses in the spring bed, σ_z^S

$$\sigma_z^{i,s} = \sigma_z^S \tag{20}$$

Boundary Conditions for Plate

As mentioned earlier, to specify boundary conditions for a plate means to specify equations for the applied net (total) pressure, q^*, in Equation 3. If plate i is not the surface layer of the multilayered pavement system, then this pressure is the difference between the vertical stress at the top surface of the layer right below the plate and the vertical stress at the bottom surface of the layer right above the plate, as follows:

$$q^* = -\sigma_z^{i-1,b} + \sigma_z^{i+1,t} \tag{21}$$

If either adjacent layer is a spring bed, then the normal stress in the springs can be written in terms of the plate deflection and of the deflection of the other end of the spring bed, in a manner similar to Equation 6.

Boundary Conditions for Uppermost Surface of Multilayered System

It is assumed in this study that the applied loading is normal to the uppermost surface of the multilayered system. Therefore, if the first layer is an isotropic layer, then two boundary conditions should be satisfied at this surface: equality of normal stress to the applied pressure, p, and presence of no shear stresses. These conditions can be presented as follows:

$$\sigma_z^{1,t} = p \tag{22}$$

$$\tau_{rz}^{1,t} = 0 \tag{23}$$

If the first layer is a plate, then the following equation should be satisfied:

$$\nabla^4 w^1 = p + \sigma_z^{2,t} \tag{24}$$

where $\sigma_z^{2,t}$ is the vertical stress at the top surface of the second layer.

Equations 8 through 24 allow the formation of a complete system of equations for a BVP for any combination of isotropic layers, plates, and spring beds. In solving these equations, the Hankel transforms of the boundary conditions are first obtained, and then these transforms are rewritten in terms of the unknown functions A_i, B_i, C_i, D_i, and W_i. If the multilayered system consists only of N_L

isotropic layers, then the stress and deflection distributions are described by four N_L unknown functions. N_L layers have $N_L - 1$ shared interfaces, which give rise to four $(N_L - 1)$ equations. The boundary conditions for the uppermost surface of the multilayered system gives two more equations. The final two equations necessary are obtained from the boundary conditions at the bottom surface of the last member of the multilayered system. If this member rests on a rigid base, the pertinent conditions are zero vertical displacements, and either zero horizontal displacements or zero shear stresses, depending on the nature of the interface (rough or smooth). If the last member of the multilayered system is a semi-infinite half-space, the pertinent conditions are vanishing displacements, u and w. Thus, the complete system consists of four N_L equations with four N_L unknown functions.

It should be noted that every time an additional plate is inserted into a multilayered system consisting of N_L isotropic layers, the total number of equations increases by one. It should also be noted that introduction of a spring bed at any existing interface does not change the total number but only the form of the equations. Therefore, the total number of equations in the system is equal to $(4N_L) + N_P$, which is also the number of unknown functions. Solution of the linear system of equations with N_T unknown functions leads to the determination of the responses for the multilayered pavement system.

VERIFICATION OF PROGRAM DIPLOMAT

The formulation presented has been coded in FORTRAN into program DIPLOMAT (*9*). The program is capable of analyzing up to five layers over a rigid base or up to four layers over an elastic solid half-space. To accommodate multiwheel loading, superposition is used, and Cartesian coordinates (x, y) are adopted, instead of polar coordinates (r, ϕ). To verify the program, several series of runs were performed. Some of the results obtained will be presented below where they will be compared with solutions obtained from other programs when appropriate.

Comparison With BISAR

If all layers in the multilayered system are isotropic, such a system may be analyzed using any of the conventional computer programs for layered elastic systems. In this study, results obtained using programs DIPLOMAT and BISAR (*16*) were compared. The following multilayered system, representing a typical AC pavement system, was analyzed:

Layer 1—127-mm-thick (5-in.) AC layer with modulus of elasticity E_1 = 5 517 MPa (800,000 psi), Poisson's ratio μ_1 = 0.25;
Layer 2—152-mm-thick (6-in.) base layer with modulus of elasticity E_2 = 207 MPa (30,000 psi), Poisson's ratio μ_2 = 0.3;
Layer 3—508-mm-thick (20-in.) subbase layer with modulus of elasticity E_3 = 103 MPa (15,000 psi), Poisson's ratio μ_3 = 0.45; and
Layer 4—Subgrade with modulus of elasticity E_s = 34.5 MPa (5,000 psi), Poisson's ratio μ_s = 0.45.

All layers were assumed to be unbonded. The radius of the applied load was set at 150 mm (5.9 in.) (falling weight deflectometer load), and the applied pressure at 689 kPa (100 psi). Calculations were performed for the following locations:

Point A—AC layer, top surface, under the center of applied load.
Point B—AC layer, top surface, 305 mm (12 in.) from the center of applied load.
Point C—AC layer, top surface, 610 mm (24 in.) from the center of applied load.
Point D—AC layer, top surface, 914 mm (36 in.) from the center of applied load.
Point E—AC layer, bottom surface, under the center of applied load.
Point F—Base layer, top surface, under the center of applied load.
Point G—Base layer, bottom surface, under the center of applied load.
Point H—Subbase layer, top surface, under the center of applied load.
Point I—Subbase layer, bottom surface, under the center of applied load.
Point J—Subgrade layer, top surface, under the center of applied load.

The results of these calculations are presented in Table 1. It can be observed that BISAR and DIPLOMAT produce identical results for this system. Equally satisfactory coincidence between BISAR and DIPLOMAT has been obtained for sections with bonded layers as well.

Plate Over Isotropic Elastic Solid Half Space

A series of runs was performed involving a plate resting on an isotropic elastic solid half-space, to compare the maximum plate bending stresses obtained by DIPLOMAT with the closed-form solution presented by Losberg (*13*). The modulus of elasticity and Poisson's ratio for the plate were set equal at 27.6 GPa (4 Mpsi) and 0.15, respectively. The modulus of elasticity, E_s, and Poisson's ratio, μ_s, for the elastic solid half-space were set equal to 276 MPa (40,000 psi) and 0.45, respectively. The plate thickness varied from 102 mm (4 in.) to 406 mm (16 in.). The total applied load was 178 kN (40,000 lb) and the applied pressure was 2 759 kPa (400 psi). Table 2 presents the maximum plate bending stresses obtained by using DIPLOMAT and Losberg's closed-form solution

$$\sigma = \frac{-6P(1+\mu)}{h^2}\left[0.1833\,\mathrm{Log}_{10}\left(\frac{a}{\ell_e}\right) - 0.049 - 0.012\left(\frac{a}{\ell_e}\right)^2 + 3.537\,10^{-3}\left(\frac{a}{\ell_e}\right)^3 - 5.012\,10^{-4}\left(\frac{a}{\ell_e}\right)^4\right] \quad (25)$$

where ℓ_e is the radius of the relative stiffness of the plate-on-elastic solid system, defined as follows:

$$\ell_e = \sqrt[3]{\frac{2D(1-\mu_s^2)}{E_s}} \quad (26)$$

Again, excellent agreement is observed between results obtained using DIPLOMAT and Losberg's closed-form solution. Near-perfect agreement has also been obtained between DIPLOMAT and Westergaard's closed-form solution.

Isotropic Layer Over Spring Bed

This problem was analyzed by Glazyrin (*8*) and by van Cauwelaert (*6*). In this study, a series of runs for an isotropic layer with modu-

TABLE 1 Stresses and Displacements in Four-Layered AC Pavement System

(a) Using *BISAR*

Point	w mm	u mm	σ_y MPa	σ_x MPa	σ_z MPa
A	1.097	0.000	-2.522	-2.522	-0.689
B	0.899	-0.050	-0.978	2.990	0.000
C	0.660	-0.042	-0.346	0.137	0.000
D	0.485	-0.030	-0.004	0.160	0.000
E	1.087	0.000	2.411	2.411	-0.115
F	1.087	0.000	-0.118	-0.118	-0.115
G	1.021	0.000	0.076	0.076	-0.085
H	1.021	0.000	-0.105	-0.105	-0.085
I	0.815	0.000	0.051	0.051	-0.026
J	0.815	0.000	-0.025	-0.025	-0.026

(b) Using *DIPLOMAT*

Point	w mm	u mm	σ_y MPa	σ_x MPa	σ_z MPa
A	1.0965	0.0000	-2.5238	-2.5238	-0.6890
B	0.8987	-0.0500	-0.9784	-2.9882	0.0000
C	0.6612	-0.0422	-0.3462	0.1371	0.0000
D	0.4844	-0.0302	-0.1417	0.1600	0.0000
E	1.0876	0.0000	2.4115	2.4115	-0.1151
F	1.0876	0.0000	-0.1178	-0.1178	-0.1151
G	1.0206	0.0000	0.0760	0.0760	-0.0854
H	1.0206	0.0000	-0.1050	-0.1050	-0.0854
I	0.8164	0.0000	0.0511	0.0511	-0.0265
J	0.8164	0.0000	-0.0252	-0.0252	-0.0265

Notes: E_1 = 5517 MPa (800,000 psi); μ_1 = 0.25; h_1 = 127 mm (5 in.); E_2 = 207 MPa (30,000 psi); μ_2 = 0.30; h_2 = 152 mm (6 in.); E_3 = 103 MPa (15,000 psi); μ_3 = 0.45; h_3 = 508 mm (20 in.); E_4 = 34.5 MPa (5,000 psi); μ_4 = 0.45.
Load = 44.5 kN (10,000 lbs); pressure = 689 kPa (100 psi);
Unbonded interfaces. Tension is positive.
(w, u): Displacements in z and x directions, respectively.
(σ_y, σ_x, σ_z): Stresses in y, x, and z, directions, respectively.

lus of elasticity equal to 27.6 GPa (4 Mpsi) and Poisson's ratio equal to 0.15, resting over a spring bed with stiffness, k, of 54.3 kPa/mm (200 psi/in.) was performed. The isotropic layer thickness varied from 102 mm (4 in.) to 408 mm (16 in.). The total applied load was 44.5 kN (10,000 lb) and the applied pressure was equal to 689 kPa (100 psi). The solution obtained using DIPLOMAT was compared with van Cauwelaert's solution evaluated using the commercial software MATHEMATICA (*17*). The results of calculations are presented in Table 3. Excellent agreement is observed in the results obtained using these two different numerical solutions.

APPLICATIONS OF PROGRAM DIPLOMAT

Using DIPLOMAT To Obtain Interlayer Spring Stiffnesses

In a previous paper (*18*), the authors presented a finite-element formulation that accommodates through-the-thickness compressibility and separation of the constructed layers in a multilayered PCC pavement system. Accordingly, a bed of springs is inserted between consecutive plates, as proposed by Totsky (*19*). The interface spring stiffness, k_I, is an important parameter to be determined. DIPLOMAT is a good tool for this purpose. Determination of k_I using DIPLOMAT involves the following steps:

TABLE 2 Maximum Bending Stresses in Plate on Elastic Solid Foundation Under Interior Loading

h mm	Bending Stress, MPa: Losberg (13)	Bending Stress, MPa: *DIPLOMAT*
102	7.655	7.655
203	4.901	4.902
254	3.392	3.394
305	1.919	1.918
356	1.526	1.525
406	1.246	1.246

Notes: E_1 = 276 GPa (4 Mpsi); μ_1 = 0.15; E_s = 207 MPa (30,000 psi); μ_s = 0.45;
Load = 178 kN (40,000 lbs); pressure = 689 kN (100 psi).

1. Consider a multilayered system consisting of isotropic layers resting on a dense liquid foundation. The elastic parameters of the isotropic layers and their thicknesses are equal to the corresponding elastic parameters and thicknesses of the constructed layers in the field. The stiffness of the dense liquid foundation is equal to the field modulus of subgrade reaction. Using computer program DIPLOMAT, find the maximum bending stress in each of the layers in this system under interior loading.
2. Consider another multilayered system consisting of alternating plate and spring beds. The elastic parameters of the plates and their thicknesses are equal to the corresponding elastic parameters and thicknesses of the constructed layers in the field. Using a trial-and-error approach and computer program DIPLOMAT, find the values of the spring interlayer stiffnesses, which lead to maximum bending stresses in the plates close to the corresponding maximum bending stresses in the isotropic layers, obtained in Step 1.

To establish the validity of this suggestion, predictions for the maximum bending stresses at the bottom of the constructed layers in multilayered pavement systems obtained using different models have been compared. The following models were used in analyzing two unbonded constructed layers resting on a dense liquid foundation: (a) isotropic layers, (b) plates separated by a Totsky spring interlayer, and (c) plates resting on one another. All three of these models can be accommodated in DIPLOMAT. For Model b, the interlayer spring stiffness, k_I, may be calculated using the aforementioned DIPLOMAT-based iterative procedure, or using one of two equation-based approaches. The first of these, involves the following equation originally presented by Totsky (*19*):

$$k_I = K\left(\frac{E_j E_{j+1}}{h_j E_{j+1} + h_{j+1} E_j}\right) \tag{27}$$

where subscripts j and $j + 1$ denote the plates just above and just below the springs, respectively. The constant K is set at 2.461, per Totsky's own recommendation. An alternative simple mathematical expression, which results in a good first estimate of k_I, has been derived by the authors (*18*):

TABLE 3 Maximum Tensile Bending Stresses in Isotropic Layer on Dense Liquid Foundation Under Interior Loading

h	Bending Stress, MPa	
mm	van Cauwelaert (6)	*DIPLOMAT*
102	4.588	4.587
152	2.383	2.383
203	1.469	1.469
254	0.994	0.994
305	0.713	0.713
356	0.535	0.535
406	0.415	0.415

Notes: E_1 = 276 GPa (4 Mpsi); μ_1 = 0.15;
k = 54.3 kPa/mm (200 psi/in.)
Load = 44.5 kN (10,000 lbs); pressure = 689 kPa (100 psi).
Tension is positive.

$$k_l = \frac{1}{\frac{1}{k_1} + \frac{1}{k_2}} \tag{28}$$

where

$$k_1 = \frac{2E_1(1 - \mu_1)}{h_1(1 - \mu_1 - 2\mu_1^2)} \tag{29}$$

and

$$k_2 = \frac{2E_2(1 - \mu_2)}{h_2(1 - \mu_2 - 2\mu_2^2)} \tag{30}$$

with subscripts 1 and 2 denoting the upper and lower plates, respectively. Model c can be considered a special case of Model b, in which k_l becomes extremely large. In this study, the plate theory closed-form approach presented by Ioannides et al. (*15*) was used for Model c.

Eight pavement sections were considered. Three of these represent a concrete slab resting on an unbonded stabilized base of variable thickness. Four others model an unbonded concrete overlay over an existing concrete slab of variable thickness. The final section represents a thick unbonded AC overlay on an existing concrete slab.

Table 4 indicates that the maximum bending stresses obtained using the plate theory closed-form approach can differ from those obtained by employing the more realistic model of two unbonded isotropic layers resting on a dense liquid foundation, especially for relatively thin unbonded concrete overlays. At the same time, for all cases considered, the iterative DIPLOMAT-based approach results in estimates of the stiffness parameter for the spring interlayer in the Totsky model that achieve closer maximum bending stresses in the corresponding plates and isotropic layers than either of the two equation-based approaches.

Spring interlayer stiffnesses from the two equation-based approaches produce similar results for all cases considered. For the slab-on-stabilized–base cases, these solutions are close to the corresponding isotropic-layers-on-dense-liquid solutions. For the unbonded concrete overlay cases, the equation-based approaches produce solutions that overestimate the upper layer stresses, yet are in better agreement with the isotropic-layers-on-dense-liquid solutions than the predictions of the plate theory closed-form approach. Therefore, they may serve in obtaining a first approximation of the interlayer stiffness. Moreover, in the actual pavement, the PCC overlay is often separated from the existing concrete slab by a bond-breaker layer. This layer is neglected in this analysis but can increase overlay stresses (E. J. Barenberg, personal communication, 1992). Therefore, using Equation 28 may be more appropriate.

Consider, for example, a typical airport pavement section consisting of a 203-mm (8-in.) unbonded PCC overlay over an existing 406-mm (16-in.) PCC slab, resting on a dense liquid foundation [k = 27.1 kPa/mm (100 psi/in.)]. The radius of the applied interior load is 150 mm (5.9 in.), and the applied pressure is 689 MPa (100 psi). Both constructed layers have Young's modulus values of 27.6 GPa (4 Mpsi) and Poisson's ratios of 0.15. Assume that the overlay and the existing slab are separated by a bituminous interlayer with a thickness (h_b) of 51 mm (2 in.), a modulus of elasticity (E_b) of 5517 MPa (800 ksi), and a Poisson's ratio (μ_b) of 0.35. For this case, the three isotropic-layers-on-dense-liquid model predicts that the maximum tensile stresses in the overlay and existing slab are 510 kPa (74 psi) and 347 kPa (50.4 psi), respectively. These values are close to those predicted by the Totsky model with k_l defined by Equation 28, which ignores the bituminous interlayer. If the bituminous interlayer modulus of elasticity were only 2 759 MPa (400,000 psi), the isotropic-layers-on-dense-liquid maximum tensile stresses in the overlay and existing slab would be 568 kPa (82.4 psi) and 341 kPa (49.5 psi), respectively. In this case, it is preferable to use the following equation for the spring interlayer stiffness:

$$k_l = \frac{1}{\frac{1}{k_1} + \frac{1}{k_2} + \frac{1}{k_b}} \tag{31}$$

with k_1 and k_2 as given by Equations 29 and 30 and

$$k_b = \frac{2E_b(1 - \mu_b)}{h_b(1 - \mu_b - 2\mu_b^2)} \tag{32}$$

Equation 31 leads to a k_l value equal to 54.3 MPa/mm (200,000 psi/in.) in this case. For this interlayer stiffness, the Totsky model predicts maximum tensile stresses in the overlay and the existing slab equal to 568 kPa (82.4 psi) and 341 kPa (49.5 psi), respectively, that is, the same values as predicted by the isotropic-layers-on-dense-liquid solution.

Estimation of Base Layer Contribution to Stress Reduction

In a previous paper (*15*), the authors presented a method for assessing the structural contribution of base layers in PCC pavement systems in a manner that accounted for the through-the-thickness compressibility of both constructed layers. This entailed adjusting the value of the maximum bending stress in the upper layer obtained on the basis of plate theory, by calculating a correction increment. An equation for the latter was derived using layered elastic analysis results, which used the elastic solid idealization. Application of the same correction increment to dense liquid cases was cautiously recommended at that time, pending the development of more appropriate numerical analysis tools. DIPLOMAT provides an opportunity to assess the validity of the correction increment, while

TABLE 4 Comparison Between Totsky Model and Isotropic Layers on Dense Liquid Models for Three-Layered System (*a*) Model Parameters, (*b*) Maximum Bending Stresses in Layers 1 and 2

(a)

	E_1	μ_1	h_1	E_2	μ_2	h_2	Interlayer Spring Stiffness, k_I, from		
							Eq. (27)	Eq. (28)	*DIPLOMAT*
	GPa		mm	GPa		mm	MPa/mm	MPa/mm	MPa/mm
CASE 1	276	0.15	203	13.8	0.45	152	20.3	55.3	135.6
CASE 2	276	0.15	203	13.8	0.45	203	15.5	43.4	27.1
CASE 3	276	0.15	203	13.8	0.45	254	12.5	35.8	135.6
CASE 4	276	0.15	203	276	0.15	203	162.8	143.2	271.3
CASE 5	276	0.15	203	276	0.15	254	144.6	127.2	257.7
CASE 6	276	0.15	203	276	0.15	305	130.2	114.5	244.1
CASE 7	276	0.15	203	276	0.15	406	108.5	95.5	230.6
CASE 8	55.2	0.30	152	276	0.15	203	38.2	41.5	263.1

(b)

MODEL	Isotropic Layers		Plate Theory		Totsky Model with k_I from Eq. (27)		Eq. (28)		*DIPLOMAT*	
LAYER	1	2	1	2	1	2	1	2	1	2
CASE 1	1.571	0.089	1.536	0.090	1.543	0.082	1.543	0.086	1.543	0.088
CASE 2	1.530	0.103	1.495	0.116	1.509	0.099	1.502	0.106	1.502	0.103
CASE 3	1.481	0.112	1.426	0.138	1.461	0.110	1.447	0.120	1.454	0.111
CASE 4	0.889	0.772	0.841	0.841	0.944	0.744	0.951	0.737	0.923	0.765
CASE 5	0.696	0.653	0.593	0.744	0.751	0.637	0.765	0.631	0.717	0.662
CASE 6	0.563	0.537	0.414	0.621	0.625	0.528	0.636	0.523	0.573	0.551
CASE 7	0.415	0.362	0.214	0.429	0.490	0.360	0.504	0.356	0.417	0.378
CASE 8	0.171	1.447	0.138	1.516	0.358	1.406	0.347	1.412	0.172	1.495

Notes: No curling; interior loading; radius of applied load = 150 mm (5.9 in.); pressure = 689 kPa (100 psi); k = 27.1 kPa/mm (100 psi/in.).

retaining the conventional dense liquid subgrade idealization. For each of the two conditions for the interface between the two constructed layers (unbonded or bonded), eight runs were conducted, selected to correspond to a wide variety of practical cases. The results are shown in Table 5. It is observed that for the unbonded interface condition, retaining the elastic solid-based correction increment equation yields results that are in very reasonable agreement with DIPLOMAT. On the other hand, DIPLOMAT indicates that the corrected plate theory solution for bonded layers may result in bending stress overestimation by about 25 percent.

DESIGN IMPLICATIONS

With the increasing popularity of multilayered concrete pavement systems in recent years, DIPLOMAT can contribute toward bridging an apparent gap in the pavement engineering tool chest. The new program provides the ability to analyze a concrete pavement system as a truly multilayered one. Individual layers in the system may be assumed to be incompressible through their thickness (e.g., PCC slab or stabilized base) or compressible (e.g., AC overlay or granular base). This new capability will be particularly useful in the area of maintenance and rehabilitation of concrete pavements. Although at the first design stage it is feasible—and even desirable—to treat base and subbase layers as nonstructural layers, placed only for construction expediency and drainage purposes, their structural function cannot be ignored in forensic studies aimed at realistic characterization of in situ pavement properties and the concomitant design of overlays. DIPLOMAT provides the opportunity to establish more conclusively the structural contribution of base and subbase layers, without the need to resort to questionable empirical concepts, such as "bumping-the-*k*-value" or establishing correlations between k and the soil Young's modulus, E_s (*15*). In addition, the algorithm developed may be easily incorporated in a unified multilayered pavement moduli backcalculation scheme, whose absence is a severe inhibitor to current rehabilitation efforts. The development of a unified backcalculation procedure is particularly called for following the FAA's adoption of a unified design procedure based on layered elastic analysis (*20*).

Another potential benefit from the development of DIPLOMAT is that for the first time it can provide a two-dimensional comprehensive approach that retains, as an option, all assumptions conventionally made in the analysis of both concrete and bituminous pavements. It is a well-documented axiom that the parameter used to characterize the dense-liquid foundation, the modulus of subgrade reaction k, cannot be reliably correlated to the elastic modulus E_s, used with the elastic solid subgrade characterization (*21*). If the last isotropic layer in DIPLOMAT is extended so that its thickness tends to infinity (or is simply made large enough), the model adopted would correspond to the conventional layered elastic analysis. If on the other hand the thickness of the last isotropic layer tends

TABLE 5 Verification of Corrected Plate Theory Solution Using DIPLOMAT

E_1 GPa	h_1 mm	E_2 GPa	h_2 mm	k kPa/mm	S.R.	LS.R.	Max. Bend. Stress in Upper Layer Using *DIPLOMAT* MPa	Max. Bend. Stress in Upper Layer Using Corrected Pl.Theory MPa
UNBONDED LAYERS								
27.6	254	2.76	320	17.1	1.2	0.1	0.950	0.993
20.7	237	2.07	406	13.6	1.5	0.1	0.964	1.001
34.5	203	2.41	493	18.3	2.0	0.1	1.191	1.207
41.3	152	4.82	394	14.1	3.0	0.1	1.591	1.556
13.8	176	0.69	279	45.6	1.2	0.2	1.590	1.610
13.8	178	1.89	274	58.9	1.5	0.2	1.315	1.336
16.5	127	2.07	254	34.5	2.0	0.2	2.121	2.126
15.2	152	4.13	297	81.6	3.0	0.2	1.152	1.040
BONDED LAYERS								
15.2	381	1.36	152	32.3	1.2	0.1	0.362	0.445
27.6	406	2.41	287	90.9	1.5	0.1	0.268	0.359
27.6	254	2.76	254	32.0	2.0	0.1	0.574	0.714
20.7	257	2.07	406	46.1	3.0	0.1	0.446	0.590
13.6	229	0.69	127	99.8	1.2	0.2	0.865	0.959
41.3	152	4.12	102	115.3	1.5	0.2	1.513	1.718
34.5	126	3.44	127	77.3	2.0	0.2	1.659	1.954
10.3	127	1.38	190	48.8	3.0	0.2	0.997	1.310

Notes: $\mu_1=\mu_2=0.15$; Load=44.5 kN (10,000 lbs) @ 861 kPa (125 psi) (radius, a= 128 mm (5.05 in.).

$$S.R. = \text{Stiffness Ratio} = \left(\frac{h_{eU}}{h_1}\right)^3 \text{ for unbonded} = \left(\frac{h_{eB}}{h_{1F}}\right)^3 \text{ for bonded}$$

$$LS.R. = \text{Load Size Ratio} = \left(\frac{a}{\ell_m}\right)$$

$$h_{eU} = \sqrt[3]{\left(h_1^3 + \frac{E_2}{E_1} h_2^3\right)}$$

$$h_{eB} = \sqrt[3]{\left(h_{1F}^3 + \frac{E_2}{E_1} h_{2F}^3\right)}$$

$$h_{1F} = \sqrt[3]{\left(h_1^3 + 12\,\beta^2 h_1\right)}$$

$$\beta = \left(x - \frac{h_1}{2}\right) = \left(\frac{h_1 + h_2}{2}\right) - \alpha$$

$$x = \frac{E_1 h_1 \frac{h_1}{2} + E_2 h_2 \left(h_1 + \frac{h_2}{2}\right)}{E_1 h_1 + E_2 h_2}$$

$$h_{2F} = \sqrt[3]{\left(h_2^3 + 12\,\alpha^2 h_2\right)}$$

$$\alpha = \left(h_1 + \frac{h_2}{2} - x\right)$$

$$\ell_m = \sqrt[4]{\frac{E\,h_m^3}{12\,(1-\mu^2)\,k}}$$

$$h_m = h_{eU} \text{ or } h_{eB}$$

to zero and the constructed layers are assumed to behave as plates resting on a bed of springs, this would correspond to the conventional Westergaard problem.

A number of follow-up possibilities and enhancements to DIPLOMAT are possible. Prominent among these is the capability to account for the dynamic effects on pavements of moving wheel loads. Findings and conclusions from recent work conducted by a number of investigators (*22,23*) could easily be incorporated into DIPLOMAT, in view of the retention in the latter of both layered elastic and plate theory assumptions.

To address the issue of edge loading within the context of a comprehensive pavement analysis and design procedure, an interesting

formulation proposed by researchers in the former Soviet Union could be adapted and enhanced for use in DIPLOMAT. Called the Method of Compensative Loads, this approach can lead to an analytical (closed-form) solution for the edge-loading problem, using any chosen subgrade idealization (*7*). Edge loading is solved by superposition of the corresponding interior loading solution plus a solution for a set of comprehensive loads that restore the boundary conditions along the location of the edge. Such a solution would be much easier to implement in a design algorithm than current finite-element techniques.

CONCLUSIONS

In this study, Burmister's layered elastic theory has been extended to accommodate a multilayered pavement system incorporating an arbitrary sequence of plates and spring beds, in addition to isotropic layers. The formulation has been coded into a new computer program, called DIPLOMAT, thereby allowing for the first time direct comparisons between the distinct analytical approaches conventionally employed for so-called rigid and flexible pavements. The new program is as user friendly and computationally efficient as the widely used layered elastic analysis program BISAR. In addition to permitting multiple-wheel loads, DIPLOMAT may be used to investigate the effects of a variety of interface and boundary conditions, including that of a rigid base. When considering a plate on grade, DIPLOMAT reproduces the closed-form solutions by Westergaard (dense liquid foundation) and by Losberg (elastic solid foundation). On the other hand, for a pavement section consisting of up to five isotropic layers, the new program reproduces the BISAR solutions for bonded or unbonded layers. A number of applications of the program are presented, including an assessment of the structural contribution of compressible (granular or bituminous) bases under a concrete pavement slab, and the determination of the interface spring stiffness that accounts for constructed layer compressibility. It is illustrated with several examples that using a DIPLOMAT-based iterative procedure it is possible to find a set of values for the spring interlayer stiffnesses in a given pavement system, which produce an adequate match of maximum bending stresses obtained using the plate and the isotropic layer models for the constructed layers in the pavement system. Some implications of program results to pavement design are also discussed.

ACKNOWLEDGMENTS

Funding for this study was provided by the University of Illinois Campus Research Board. This support is gratefully acknowledged. Also acknowledged are the useful comments and suggestions of Arthur R. Robinson.

REFERENCES

1. Winkler, E. *Die Lehre von der Elastizitat und Festigkeit (The Theory of Elasticity and Stiffness)*. H. Dominicus, Prague, Czechoslovakia, 1867.
2. Boussinesq, M. J. *Application of Potential to the Study of the Equilibrium and Movement of Elastic Solids, Particularly the Calculation of Deformations and Stresses Produced Within Such Solids, by Some Load Applied Upon a Small Portion of Their Surface or Their Interior: Continuous Paper from Extensive Notes on Diverse Points of Physical Mathematics and Analysis*. (in French) Gauthier-Villars, Paris, France, 1885.
3. Westergaard, H. M. New Formulas for Stresses in Concrete Pavements of Airfields. *Transactions*, Vol. 113, 1948, pp. 425–439.
4. Burmister, D. M. The Theory of Stresses and Displacements in Layered Systems and Application to the Design of Airport Runways. *HRB Proc.*, Vol. 23, 1943, pp. 126–144.
5. Burmister, D. M. The General Theory of Stresses and Displacements in Layered Systems. *Journal of Applied Physics*, Vol. 16, No. 2, 1945, pp. 89–96; No. 3, pp. 126–127; No. 5, pp. 296–302.
6. van Cauwelaert, F. Westergaard's Equations for Thick Elastic Plates. *Proc., 2nd International Workshop on the Theoretical Design of Concrete Pavements*, Sigüenza, Spain, 1990, pp. 165–175.
7. Khazanovich, L., and A. M. Ioannides. *Glasnost* and Concrete Pavement Engineering: Insights Concerning Slabs-on-Grade From the Former Soviet Union. *Proc., 5th International Conference on Concrete Pavement Design and Rehabilitation*, Purdue University, West Lafayette, Ind., Vol. 1, 1993, pp. 3–18.
8. Glazyrin, V. C. On Problem of Analysis of Plates Resting on Elastic Foundation. (in Russian) *Stroitel'naya Mekhanica i Raschet Sooruzhenii*, No. 1, Moscow, Russia, 1965, pp. 14–19.
9. Khazanovich, L. *Structural Analysis of Multi-Layered Concrete Pavement Systems*. Ph.D. dissertation, University of Illinois, Urbana, 1994.
10. Timoshenko, S. P., and J. N. Goodier. *Theory of Elasticity*, 3rd ed. McGraw-Hill Co., New York, 1970.
11. Love, A. E. H. *Mathematical Theory of Elasticity*, 4th ed. Cambridge University Press, Cambridge, England, 1927.
12. Timoshenko, S., and S. Woinowsky-Krieger. *Theory of Plates and Shells*, 2nd ed. McGraw-Hill Co., New York, 1959.
13. Losberg, A. *Structurally Reinforced Concrete Pavements*. Doktorsavhandlingar Vid Chalmers Tekniska Högskola, Göteborg, Sweden, 1960.
14. Kerr, A. D. On the Determination of Foundation Model Parameters. *Journal of Geotechnical Engineering*, Vol. 111, No. 11, 1985, pp. 1334–1340.
15. Ioannides, A. M., L. Khazanovich, and J. L. Becque. Structural Evaluation of Base Layers in Concrete Pavement Systems. In *Transportation Research Record 1370*, TRB, National Research Council, Washington, D.C., 1992, pp. 20–28.
16. Peutz, M. G. F., H. P. M. Van Kempen, and A. Jones. Layered Systems Under Normal Surface Loads. In *Highway Research Record 228*, HRB, National Research Council, Washington, D.C., 1968, pp. 34–45.
17. Wolfram, S. Mathematica: A System for Doing Mathematics by Computer. Addison-Wesley Publishing Company, Inc., Redwood City, Calif., 1988.
18. Khazanovich, L., and A. M. Ioannides. Structural Analysis of Unbonded Concrete Overlays Under Wheel and Environmental Loads. Presented at 73rd Annual Meeting of the Transportation Research Board, Washington, D.C., 1994.
19. Totsky, O. N. Behavior of Multi-Layered Plates and Beams on Winkler Foundation. (in Russian) *Stroitel'naya Mekhanika i Raschet Sooruzhenii*, No. 6, Moscow, Russia, 1981, pp. 54–58.
20. Barker, W. R., and C. R. Gonzalez. Pavement Design by Elastic Layer Theory. *Proc. Specialty Conference Aircraft/Pavement Interaction—An Integrated System*, ASCE/ATD/APC, Kansas City, Mo., 1991, pp. 21–43.
21. Ioannides, A. M. Subgrade Characterization for Portland Cement Concrete Pavements. *Proc., International Conference on Geotechnical Engineering for Coastal Development—Theory and Practice*, Port and Harbour Institute, Ministry of Transport, Yokohama, Japan, 1991, pp. 809–814.
22. Tabatabaie, A. M. Dynamic Analysis of Pavement Systems: Model Evaluations. Presented at 70th Annual Meeting of the Transportation Research Board, Washington, D.C., 1991.
23. Chatti, K., J. Lysmer, and C. L. Monismith. Dynamic Finite-Element Analysis of Jointed Concrete Pavements. Presented at 72nd Annual Meeting of the Transportation Research Board, Washington, D.C., 1993.

Publication of this paper sponsored by Committee on Flexible Pavement Design.

Analytical Procedures in Nondestructive Testing Pavement Evaluation

PER ULLIDTZ AND N. F. COETZEE

An overview of typical procedures currently used for pavement evaluation using nondestructive testing deflection data is provided, focusing primarily on backcalculation. Some of the more typical problems encountered in these approaches are briefly discussed. Critical issues related to fundamental theoretical assumptions of static loading, as well as material continuity, homogeneity, and elastic behavior, are addressed, particularly in the context of validation of backcalculation results.

Structural evaluation of pavement deflection response using nondestructive test (NDT) data has been growing since the introduction of the Benkelman beam at the WASHO Road Test in the early 1950s. Developments in analytical techniques, coupled with improved deflection measurement capabilities, have resulted in the current so-called backcalculation techniques widely used in pavement evaluation. This paper provides an overview of existing techniques used for structural analysis of pavement NDT deflection data, discusses some of the issues and shortcomings of these procedures, and provides some conjecture on expected and possible future developments in the field.

DEFLECTION USES

Early use of deflection data typically involved consideration of maximum deflection directly under the load, relative to empirical standards. Usually some statistical measure of deflections on a pavement section is compared with a "tolerable" deflection level for that section under the expected traffic. If the measured value exceeds the tolerable deflection, an empirical procedure determines the corrective measure required—usually an overlay—to reduce the measured deflections to the tolerable level. Examples of this approach include the Asphalt Institute's MS-17 (*1*) and CalTrans's Test Method 356 (*2*). In some states, maximum deflections are monitored during spring thaw, and load restrictions are placed when the thawing pavement's deflection reaches a certain level. Empirical use of deflection basin data usually involves one of the basin parameters that combine some or all of the measured basin deflections into a single number.

With a trend toward mechanistic pavement analysis and design, which are based on fundamental engineering principles, the use of deflection data has become more sophisticated. Complete deflection basins are used, in a procedure known as backcalculation, to estimate in situ elastic moduli for each pavement layer. Knowledge of the existing layer thicknesses is typically necessary for this procedure. The backcalculated moduli themselves provide an indication of layer condition. They are also used in an elastic layer or finite-element program to calculate stresses and strains resulting from applied loads. These stresses and strains are used with fatigue or distress relationships to evaluate damage accumulation under traffic and predict pavement failure. They can also be used to evaluate corrective measures, such as overlays, rehabilitation, or reconstruction. It is these mechanistic analyses of pavement deflection that this paper is intended to address. Briefly, the backcalculation procedure involves calculation of theoretical deflections under the applied load using assumed pavement layer moduli. These theoretical deflections are compared with measured deflections and the assumed moduli are then adjusted in an iterative procedure until theoretical and measured deflection basins reach an acceptable match. The moduli derived in this way are considered representative of the pavement response to load and can be used to calculate stresses or strains in the pavement structure for analysis purposes.

Currently, calculation of theoretical deflections, and the subsequent stress or strain calculations, typically involve linear elastic theory. Elastic theory may be applied through the use of the following:

- Traditional layered elastic programs based on numerical integration procedures, such as ELSYM5, CHEVRON (various versions), BISAR, and WESLEA;
- The Odemark-Boussinesq transformed section approach instead of numerical integration;
- Finite-element programs, either those that have been specifically oriented toward pavement analysis, such as ILLI-PAVE or MICHPAVE, or general structural analysis programs such as SAP (various versions), ANSYS, ABACUS, ADINA, and so forth;
- Plate theory, such as the Westergaard solutions for portland cement concrete (PCC) pavements; and
- Neural networks trained to reproduce results that emulate one of the foregoing applications (*3,4*).

BACKCALCULATION

An in-depth summary of the historical developments of NDT, backcalculation, and theoretical considerations, as well as associated technology were provided in a state-of-the-art presentation in 1988 (*5*). Some of the concerns regarding the differences between backcalculated results using different backcalculation programs on the same deflection data were illustrated. These are typically technical problems but they are exacerbated by the continuing development of similar backcalculation programs. In many cases, new programs have little to differentiate them from existing software other than a name. In a description of the Strategic Highway Research Program (SHRP) backcalculation procedure software selection a table listing

P. Ullidtz, Technical University of Denmark, Bldg. 115 IVTB, DK-2800 Lyngby, Denmark. N. F. Coetzee, Dynatest Consulting, Inc., P.O. Box 71, Ojai, Calif. 93024-0071.

the most common backcalculation procedures in use at that time was originally included (*6*). This table, somewhat modified, is included here as Table 1 to illustrate similarities and differences between programs. In reviewing Table 1, one should keep in mind that the CHEVRON and ELSYM5 numerical integration routines are identical and, until recently, produced erroneous results under certain circumstances due to an error in the integration procedure. This error was corrected in 1992 by Irwin and verified by comparison with the BISAR program (L. H. Irwin, personal communication, 1993).

The programs included in Table 1 are by no means a comprehensive listing of backcalculation routines. Other programs in use today include COMDEF, 15BCONPAS, PROBE, ILLIBACK, LMBS, DEFMET, RPEDDI, PHONIX, PEACH, FALMAN, CLEVERCALC, EPLOPT, OAF, SEARCH, EFROMD, and more. Most of the programs rely on linear elastic layered theory, or a variation thereof, for the basic structural model. In comparing results from these programs, the primary criterion used for evaluating accuracy is based on the goodness of fit of computed deflections to measured deflections. As computing power has increased, so has the ability to improve the goodness of fit. In many cases, improving the goodness of fit does not necessarily mean that the theoretical model better represents actual pavement response. If an existing pavement structure is in such a condition that it clearly violates some of the fundamental assumptions of elastic theory, then a good fit between measured and calculated deflections should not be expected, and goodness-of-fit should not be the determining factor for deciding if a solution is realistic or not. This point is also made by Lytton (*5*), who discusses the need for experience in analysis, with materials and with deflections to ensure that the backcalculation process yields the most acceptable set of moduli for a given deflection basin. It should be noted that essentially all pavements violate the fundamental assumptions of linear elastic theory, albeit to differing degrees.

Also important, and related to the issue discussed previously, is the provision of a modulus value through backcalculation that is a layer parameter and not necessarily the layer material modulus, which can be measured using laboratory tests on a sample of the layer material. This is due to the geometry of typical deflection basin measurements that is on the order of a 1.8-m (6-ft) length so that the effect of horizontal layer and material variability over that dimension is included in the backcalculated moduli. This variability includes damage such as cracking, both on the macro- and microstructural level. Simply stated, the problem lies with the in situ modulus being unknown, so that backcalculated values cannot be validated directly.

PROBLEMS ENCOUNTERED IN BACKCALCULATION

Some of the more common problems encountered in backcalculation are briefly described in the following paragraphs. More detailed discussions are available elsewhere (*7*). In many cases, pavement deflection measurements include irregularities that are generally related to differences between measured pavement response and the theoretical models used to predict that response. These irregularities may result from a number of reasons, including pavement distress, variations in layer thickness, nonlinear material response, presence of bedrock or other stiff layers, moisture and temperature effects, and so forth. Anomalies within the pavement structure, such as culverts and utility ducts are not discussed here since they can be observed and are considered atypical. It should be pointed out that as backcalculation techniques mature, some of the problems are being addressed by software modification.

Input Data Effects

Input data effects include seed moduli, modulus limits, and layer thicknesses, as well as program controls, such as number of iterations and convergence criteria. Because of the nonuniqueness of the solution, it is possible to obtain different backcalculated moduli for a given deflection basin by using different seed moduli or limits. Many of these problems are being addressed by software development, such as using the measured deflection data to aid in selection of relevant input values.

Compensating Layer and Nonlinearity Effects

Compensating layer and nonlinearity effects essentially result from incorrect modeling of the pavement material response and the sequential nature of the backcalculation iterative procedure, as well as the geometry of a deflection basin test. A typical result may show, as an example, subgrade modulus that is significantly higher than expected for the material type, while the base layer modulus is far too low and the surfacing modulus is too high. This probably occurs most commonly for a significantly stress softening subgrade, where the subgrade stress level for the outer sensors in a falling weight deflectometer (FWD) test is very much lower than the subgrade stress level directly beneath the load plate. The apparent subgrade modulus for the outer sensor location is therefore higher than the apparent subgrade modulus directly beneath the load plate. If the subgrade is modeled as a linear elastic material, then—since most backcalculation routines first calculate subgrade modulus from the outer sensors—the higher modulus value is calculated and assumed to be constant throughout. At the next iteration, when the base modulus is being calculated, the too high subgrade modulus is compensated for by calculating a modulus that is too low for the base, to match the deflections measured in this region. In other words, alternating layers exhibit a high or low compensating effect. Ideally, correctly modeling nonlinear material response will avoid this type of error, and this is becoming more and more common (e.g., ELMOD, MODCOMP3, EVERCALC, and BOUSDEF can all use nonlinear material models). If an elastic subgrade is used, the inclusion of a stiff layer, or the use of a layered subgrade, can help alleviate the problem. This is at least partially the reason why some backcalculation routines include a stiff layer by default at some depth [usually approximately 6 m (20 ft)]. It is also worth noting that the effect of too rapidly decreasing deflections with distance is often due to the dynamic nature of the impulse load.

Subgrade Stiff Layer

For the purpose of a general definition, a "stiff" layer is one below which there is little or no apparent contribution to the measured surface deflections. Stiff layers can be real or apparent and are possibly the most common problem encountered during the evaluation of deflection basins.

TABLE 1 Partial List of Layer Moduli Backcalculation Programs (*6*)

Program Name	Developed By	Forward Calculation Method	Forward Calculation Subroutine	Back-calculation Method	Non-Linear Analysis	Rigid Layer Analysis	Layer Interface Analysis	Maximum Number of Layers	Seed Moduli	Range of Acceptable Modulus	Ability to Fix Modulus	Convergence Routine	Error Convergence Function
BISDEF	USACE-WES	Multi-Layer Elastic Theory	BISAR (Proprietary)	Iterative	No	Yes	Variable	Cannot Exceed No. of Deflec., Works Best For 3 Unknowns	Required	Required	Yes	Sum of Squares of Absolute Error	Yes
BOUSDEF	ZHOU, et.al. OREGON STATE UNIV.	Odemark-Boussinesq	Odemark-Boussinesq	Iterative	Yes	Yes	Fixed (Rough)	5, Works Best for 3 Unknowns	Required	Required	Yes	Sum of Percent Errors	Yes
CHEVDEF	USACE-WES	Multi-Layer Elastic Theory	CHEVRON	Iterative	No	Yes	Fixed (Rough)	Cannot Exceed No. of Deflec., Works Best For 3 Unknowns	Required	Required	Yes	Sum of Squares of Absolute Error	Yes
ELMOD/ ELCON	P. ULLIDTZ DYNATEST	Odemark-Boussinesq	Odemark-Boussinesq	Iterative	Yes (Sub-grade Only)	Yes (variable)	Fixed (Rough)	Up to 4, Exclusive of Rigid Layer	None	No	Yes	Relative Error on 5 Sensors	No
ELSDEF	TEXAS A&M UNIV., USACE-WES	Multi-Layer Elastic Theory	ELSYM5	Iterative	No	Yes	Fixed (Rough)	Cannot Exceed No. of Deflec., Works Best For 3 Unknowns	Required	Required	Yes	Sum of Squares of Absolute Error	Yes
EMOD	PCS/LAW	Multi-Layer Elastic Theory	CHEVRON	Iterative	Yes (Sub-grade Only)	No	Fixed (Rough)	3	Required	Required	Yes	Sum of Relative Squared Error	No
EVERCALC	J. MAHONEY, et.al.	Multi-Layer Elastic Theory	CHEVRON	Iterative	Yes	Yes	Fixed (Rough)	3 Exclusive of Rigid Layer	Required	Required	Yes	Sum of Absolute Error	No
FPEDDI	W. UDDIN	Multi-Layer Elastic Theory	BASINPT	Iterative	Yes	Yes (Variable)	Fixed (Rough)	Unknown	Program Gener-ated	Unknown	Unknown	Unknown	No
ISSEM4	R. STUBSTAD	Multi-Layer Elastic Theory	ELSYM5	Iterative	Yes (Finite Cylinder Concept)	No	Fixed (Rough)	4	Required	Required	Yes	Relative Deflec. Error	No
MODCOMP 3	L. IRWIN, SZEBENYI	Multi-Layer Elastic Theory	CHEVRON	Iterative	Yes	Yes	Fixed (Rough)	2 to 15 layers, Max 5 Unknown Layers	Required	Required	Yes	Relative Deflec. Error at Sensors	No
MODULUS	TEXAS TRANS. INSTITUTE	Multi-Layer Elastic Theory	WESLEA	Data Base	No	Yes (Variable)	Fixed?	Up to 4 Unknown plus Stiff Layer	Required	Required	Yes	Sum of Relative Squared Error	Yes
PADAL	S.F. BROWN, et. al.	Multi-Layer Elastic Theory	UNKNOWN	Iterative	Yes (Sub-grade Only)	Unknown	Fixed?	Unknown	Required	Unknown	Unknown	Sum of Relative Squared Error	Unknown
WESDEF	USACE-WES	Multi-Layer Elastic Theory	WESLEA	Iterative	No	Yes	Variable	Up to 5 Layers	Required	Required	Yes	Sum of Squares of Absolute Error	Yes
MICHBAK	MICHIGAN STATE	Multi-Layer Elastic Theory	CHEVRON	Iterative	No	Yes	Fixed	Up to 4 Unknown plus Stiff Layer	Required	Optional	Yes	Sum of Relative Squared Error	Yes

The stiff layer may, in fact, consist of rock or other stiff materials. However, the effect has also been observed where a water table is encountered near the surface. Possibly the most common phenomenon is due to the previously described subgrade nonlinearity effects resulting in an apparent stiff layer effect with backcalculated moduli exhibiting the compensating effect. For the case where an actual rigid layer exists, computer backcalculation programs such as MODULUS, BISDEF, and WESDEF have a rigid layer subroutine built in. Bedrock information can be obtained from geologic maps, by coring, or by penetration resistance measurement. Depth to the stiff layer can also be estimated from the deflection data as done in ELMOD and MODULUS. The best approach is to model the actual situation as closely as possible.

One approach for the "apparent" stiff layer problem—if a layered elastic backcalculation program is used—is to divide the subgrade into two or more layers, allowing the backcalculation program to assign modular ratios that achieve the best fit.

Pavement Layer Thickness Effects

As a result of limitations in the backcalculation software and the limited time available to perform backcalculation activities in a production environment, pavement layer thicknesses are generally assumed to be constant over the pavement section under test. This is seldom the case. Pavement layer thickness variations result from various construction and maintenance details, even under specially controlled conditions.

On Texas SHRP sections, it has been found that asphalt concrete thicknesses may vary up to 2 in. within 500 ft. Pavement layer thickness variations will produce variations in the deflections from point to point that are indistinguishable from layer moduli variations. The net result is that this variation manifests itself in the backcalculated moduli for the various layers. In some cases, these moduli variations are not significant. However it is desirable to use correct layer thicknesses, and various techniques, such as GPR, are improving the ability to obtain thickness data.

It should be noted that surface layer thicknesses of less than 75 mm (3 in.) cannot be reliably characterized with FWD data, primarily due to the geometry of the loading and measuring system. Moduli of thin layers are generally difficult to determine from FWD data.

Relative Layer Stiffness Effects

Backcalculaton can describe a pavement layer's stiffness only to the degree to which that layer affects the deflections. Thin layers contribute only a small portion to the overall deflection and as a result, the accuracy of their backcalculated values is reduced.

To some extent, the layer thickness discussion covers relative layer stiffness effects. However, the intent of this section is to emphasize that the layer stiffness (i.e., combination of thickness and modulus) needs to be relatively significant (compared with other pavement components) for it to influence the surface deflections. If this is not the case, then backcalculation approaches will not be successful in identifying the effect of the layer. As an example, consider a 200-mm-thick (8-in.) natural gravel base course. If this layer is placed on an average subgrade and surfaced with a chip seal, it is relatively stiff, and backcalculation will easily evaluate the difference in modulus between the base and subgrade. On the other hand, if this base material occurs beneath a 400-mm (16-in.) PCC slab, it is not relatively stiff and it is unlikely that the backcalculation process will be able to reliably separate the contribution of this layer from the subgrade effect.

Similar problems occur for many unbound base and subbase combinations. These materials often differ only in terms of gradation and indicator specifications, and their moduli are relatively similar, so that their contributions to the deflection response are difficult to separate. Similarly, if the surfacing consists of more than one asphalt concrete (AC) layer, they should be considered as a single layer. There is generally not enough difference between the response of an AC surfacing layer and an asphalt-treated base to evaluate these layers separately.

CRITICAL ISSUES IN BACKCALCULATION

When evaluating backcalculation procedures, it is important to be aware of the simplifications made in modeling the pavement structure. Most of the current procedures are based on the following assumptions:

- The loading is static,
- The materials are continuous and homogeneous, and
- The relationship between strain and stress follows Hooke's law, that is, linear elastic.

The Royal Dutch/Shell Laboratory in Amsterdam began studying pavement dynamics using a road vibration machine in 1951. Both dynamic deflections and wave propagation were used to determine the stiffness of different pavement layers (*8,9*). The work of Lamb (*10*) was used by the Laboratoire Central des Ponts et Chaussées in France (*11*) and more recently the work of Kausel and Peek (*12*) has been used by several researchers (*13,14*). Finite-element methods have also been used for dynamic analysis of road structures (*15,16*).

In spite of all the effort put into dynamic analysis, it is not widely used. One reason is the computational capacity required. Dynamic finite-element analysis, for example, requires a mainframe computer. More important, however, are the additional parameters needed to characterize the materials. In a dynamic analysis, the viscous and viscoelastic properties of the material should be considered; Poisson's ratio becomes more critical when using wave propagation; and the density of the different materials must also be known.

This leads to the second assumption: the materials are continuous or compatible. All of the above-mentioned methods are based on continuum mechanics, but few pavement materials are continuous. Most pavement materials are particulate in nature, and even in asphalt at normal temperature, the deformations from elastic compression of the grains are negligible compared with the deformations from sliding of the grains.

In well-compacted granular materials, volume expansion (dilation) often occurs under loading. In a paper on plasticity in soils, it was concluded,

> There has been a good deal of debate about unstable behavior that develops in association with volume expansions. Loading of such a soil is accompanied by local inhomogenities in the form of slip lines, shear bands, or "bifurcations," as they are now commonly called. . . . It occurs in real soils in nature very frequently, is the source of many soil engineering problems, and so far is not represented by a single soil

model. At present, it is also difficult to see how a suitable model could be implemented in a finite element code, since each individual element must have the opportunity of developing shear bands as the loading progresses. Their position cannot be predicted in advance (*17*).

Since then, more widespread use has been made of the distinct-element method or micromechanical modeling based on the work of Cundall (*18*) and Strack and Cundall (*19*). This, however, puts an even larger strain on computing capacity and also requires knowledge of the grain-to-grain contact characteristics and on the influence of water or bitumen. Even though the distinct-element method cannot be used for backcalculation in the foreseeable future, it may still be used to study the distribution of stresses and strains in granular materials, and possibly to modify methods based on continuum mechanics.

From the foregoing, it is already clear that the use of Hooke's law for pavement materials is very much a simplification of reality, and even that the development of other constitutive equations considering viscosity, nonlinearity, or anisotropy may not be of much help.

In addition, it may be recalled that pavement response also depends on the distance from the pavement edge (or a joint) and on the degree of cohesion or friction between pavement layers. The material characteristics and layer thicknesses also vary along the length and width of the pavement and with the depth in the subgrade, as well as with the climatic conditions (temperature, temperature gradient, moisture content and distribution, frost, etc.).

Even with all these shortcomings, it is still necessary to use backcalculation procedures. The deterioration of pavements depends on the stresses and strains in the layers; to determine the critical stresses or strains, the stiffnesses of the layers must be known. Laboratory testing may be used for some materials, but are often expensive and not very reliable. A validation (and modification) of existing backcalculation procedures is needed. Some validation can be done by comparing moduli derived from backcalculation with moduli determined by laboratory testing, but only for a few bitumen or cement bound materials. A thorough validation must be based on a comparison of stresses and strains derived from backcalculation with stresses and strains measured in the pavement layers.

Validation through comparison of measured and calculated stresses and strains (or deflections at multiple depths) is not a simple matter. It has been attempted over a number of years at a number of locations, using a variety of instruments for measuring the in situ stresses and strains. In some cases, such as that reported in a work by Lenngren (*20*), very good correlation has been found. A very interesting international experiment on measuring strain in bituminous layers was conducted at Nardo, Italy, under the sponsorship of Organization for Economic Cooperation and Development (*21*). With the renewed interest in full-scale testing of instrumented pavements, similar international experiments could prove very useful.

SUMMARY AND CONCLUSION

- The use of backcalculated moduli is essential to the application of mechanistic principles to pavement evaluation. Backcalculation techniques and software have advanced greatly over the past decade. In spite of that advancement, many routine problems are still encountered that are handled in a variety of more or less satisfactory ways. However, the critical issues remain since they are the fundamental assumptions of the theoretical models typically used. Possibly the most "correct" approach in the future will involve use of stochastic, nonlinear, dynamic finite-element analysis applied at the particulate level, which would require the routine availability of massive computing power. Application of neural networks to backcalculation shows some promise.
- Backcalculation programs cannot be verified through theoretical means. Even the most sophisticated theoretical models like dynamic, three-dimensional viscoelastoplastic finite-element programs are based on simplifications, such as not considering the particulate nature of most pavement materials. No theoretical model constitutes the "truth"; they are all simplified models of reality.
- Most pavement materials do not have a modulus. The example of a handful of sand makes that obvious. The apparent modulus depends on the stress condition, which is influenced by moisture or bitumen content, temperature, loading time, and so forth. Trying to verify backcalculation procedures by comparing the moduli derived from the procedure with moduli determined by other means is, therefore, extremely difficult for most pavement materials.
- The most promising method for verification of backcalculation procedures appears to be through comparison of stresses and strains predicted by the procedure to values measured in actual pavements. The measurement of stresses and strains in pavements is very difficult, because the presence of a measuring instrument changes the stress or strain condition. Nevertheless, this appears to be the only solution, and instrumentation of pavements is taking place in many parts of the world.
- It is important to verify the models used for calculating pavement response if pavement engineering is to move away from being a craft to being a science. It should be kept in mind, however, that pavement response is seldom the final answer, but only an intermediate result used to predict the pavement performance. It is equally important that the relationships between response and performance be verified through the use of accelerated full-scale testing (preferably on instrumented pavements) and through long-term pavement performance studies.

REFERENCES

1. *Asphalt Overlays for Highway and Street Rehabilitation.* Manual Series No. 17 (MS-17). Asphalt Institute, 1983.
2. *Asphalt Concrete Overlay Design Manual.* California Department of Transportation, 1979.
3. Meier, R. W., and G. J. Rix. Backcalculation of Flexible Pavement Moduli Using Artificial Neural Networks. Presented at 73rd Annual Meeting of the Transportation Research Board, Washington, D.C., 1994.
4. Meier, R. W., and G. J. Rix. Backcalculation of Flexible Pavement Moduli From Dynamic Deflection Basins Using Artificial Neural Networks. Submitted for presentation at the 74th Annual Meeting of the Transportation Research Board, Washington, D.C., 1995.
5. Lytton, R. L. *Backcalculation of Pavement Layer Properties.* ASTM STP 1026, ASTM, 1988.
6. *SHRP's Layer Moduli Backcalculation Procedure: Software Selection.* Contract No. SHRP-90-P-001B. Prepared by PCS/Law Engineering for SHRP, 1991.
7. Pavement Deflection Analysis—Participant Workbook. Prepared by Dynatest Consulting, Inc. and Soils and Materials, Inc., for FHWA National Highway Institute, 1993.
8. Nijboer, L. W., and C. van der Poel. A Study of Vibration Phenomena in Asphaltic Road Constructions. *AAPT,* Vol. 22, 1953.
9. Nijboer, L. W. Dynamic Investigation of Road Constructions. Shell Bitumen Nomograph No. 2. 1955.
10. Lamb, H. On Waves in an Elastic Plate. *Proc.*, Royal Society, London, England, 1916.

11. Guillemin, R., and J. C. Gramsammer. *Auscultation dynamique des chaussées à l'aide du vibreur léger.* Note d'information technique. Laboratoire Central des Ponts et Chaussées, France, November 1971.
12. Kausel, E., and R. Peek. Dynamic Loads in the Interior of a Layered Stratum: An Explicit Solution. *Bulletin of the Seismological Society of America*, Vol. 72, No. 5, 1982.
13. Sebaaly, B. E., M. S. Mamlouk, and T. G. Davies. Dynamic Analysis of Falling Weight Deflectometer Data. In *Transportation Research Record 1070,* TRB, National Research Council, Washington, D.C., 1986.
14. Nazarian, S., and K. H. Stokoe II. *In Situ Determination of Elastic Moduli of Pavement Systems by Spectral-Analysis-of-Surface-Waves Method (Theoretical Aspects).* Research Report 437-2. Center for Transportation Research, University of Texas, Austin, 1987.
15. Zaghloul, S., and T. White. Use of a Three-Dimensional Dynamic Finite Element Program for Analysis of Flexible Pavements. In *Transportation Research Record 1388*, TRB, National Research Council, Washington, D.C., 1993.
16. Mallela, J., and K. P. George. Three-Dimensional Dynamic Response Model for Rigid Pavements. Presented at 73rd Annual Meeting of the Transportation Research Board, Washington, D.C., 1994.
17. Scott, R. F. Plasticity and Constitutive Relations in Soil Mechanics. *Journal of Geotechnical Engineering*, Vol. 111, No. 5, 1985.
18. Cundall, P. A. *BALL—A Program to Model Granular Media Using the Distinct Element Method.* Technical Note No. TN-LN-13. Dames & Moore Advanced Technology Group, London, England, 1978.
19. Strack, O. D. L., and P. A. Cundall. *The Distinct Element Method as a Tool for Research in Granular Media.* University of Minnesota, 1978.
20. Lenngren, C. A. *Relating Bearing Capacity to Pavement Condition.* Ph.D. dissertation. Royal Institute of Technology, Stockholm, Sweden, 1990.
21. *Strain Measurements in Bituminous Layers.* Organization for Economic Cooperation and Development Road Transport Research, 1985.

Publication of this paper sponsored by Committee on Flexible Pavement Design.

General Axle Load Equivalency Factors

JERRY J. HAJEK

The cumulative pavement damage effects of all highway vehicles are usually quantified using axle load equivalency factors. The existing axle load equivalency factors depend on, among other variables, pavement type and thickness. This means that the axle factors and consequently the number of equivalent axle loads change along a highway corridor as the construction of the pavement changes, even when the traffic loads do not change. General axle load equivalency factors that are independent of pavement-related variables and axle configurations and have a magnitude similar to the AASHTO axle factors are proposed. The general axle factors can simplify the management of pavement traffic load data and are suitable for routine pavement design purposes. Analysis of errors in prediction of cumulative equivalent axle load applications also suggests that the largest uncertainty is due not to the errors associated with axle load equivalency factors but to other variables, such as traffic volume estimates and axle weights.

The effect of heavy loads on pavement damage, such as fatigue cracking and rutting of asphaltic concrete pavements, has traditionally been expressed using the concept of axle load equivalency factors. Other terms used are wheel load equivalency factors, pavement load equivalency factors, pavement damage factors, and truck factors (*1*). For simplicity, the axle load equivalency factors are herein called axle factors (AFs).

AFs attempt to capture the combined influence of the entire traffic mix on pavement damage by converting the pavement damage caused by different axle loads and axle groups to that caused by a standard axle load. For convenience, AFs have been related to a standard axle load of 80 kN (18,000 lb) carried by a single axle with dual tires called the equivalent single-axle load (ESAL). A summation of all AFs for a given truck is called a truck factor (TF). Thus, a TF is equal to the number of ESALs per truck. In this way, all loads of a highway traffic mix can be converted, using AFs and TFs, into a total number of ESALs that is used for pavement management and pavement design purposes. The AFs provide the basic information needed.

Many different AFs have been proposed in the past. The most recognized AFs are those developed by AASHTO (*2*). AASHTO AFs, and other similar axle factors, have been developed for specific pavement types, pavement distresses, axle configurations, and other variables. Consequently, these AFs are not directly transferable or are not general in the way, for example, traffic volumes are. AFs, and consequently the number of equivalent single-axle loads, can change along a transportation corridor several times even when traffic loads and volumes do not change. To obtain a universal summary measure of traffic loads, the use of general axle load equivalency factors, which are independent of pavement-related variables and axle configurations, is proposed. In this paper, the general axle load equivalency factors are called general axle factors and are abbreviated GAFs.

Ontario Ministry of Transportation, 1201 Wilson Avenue, Downsview, Ontario, Canada, M3M 1J8.

The objectives of this paper are to

- Explore the need for the development and use of GAFs and to work to obtain a consensus on their usefulness and eventual definition. The GAFs proposed herein represent only one possible version for their definition.
- Stimulate discussion about calculation and use of AFs.
- Provide a better understanding of concepts used for summarizing the damaging effect of pavement traffic loads and, in particular, AFs.

A proposal of GAFs is intended to simplify the management of traffic load data for pavement design and maintenance.

DETERMINATION OF AFs

AFs can be obtained in two basic ways: field experiments or evaluation of pavement responses to individual axle loads.

AF From Field Experiments

A number of axle loads, N, of a given magnitude and type, required to cause a certain level of pavement deterioration, is determined in the field and is compared to the number of standard axle loads, N_{ESAL}, required to cause the same amount of pavement deterioration on an identical pavement structure. The resulting AF depends on the type and strength of the pavement structure used in the experiment and on the definition of pavement damage and its level.

$$AF = \frac{N_{ESAL}}{N} \tag{1}$$

The best known example of the full-scale pavement experiment is the AASHO Road Test of the early 1960s (*2*). The AASHTO AFs were related mainly to pavement roughness and were defined for two pavement types (flexible and rigid), two axle configurations (single and tandem), and different levels of pavement serviceability (i.e., initial serviceability and terminal serviceability). They are based on relationships derived from the AASHO Road Test data and not on direct observations of load equivalency ratios as suggested by Equation 1. AFs for triple axles were developed later using analytical procedures.

AF From Evaluation of Pavement Responses to Individual Loads

Measured or calculated pavement responses to traffic loads are used to calculate AF by assuming the following general relationship:

$$AF_{r,i} = \left(\frac{R_{r,i}}{R_r}\right)^n \quad (2)$$

where

$AF_{r,i}$ = axle factor based on pavement response r for axle type i,
$R_{r,i}$ = amount of pavement response r to the axle load of defined magnitude and type designated as i,
R_r = amount of pavement response r to the standard 80-kN single-axle load, and
n = exponent that ensures similarity between Equations 1 and 2, usually set to about 4.

Again, as with AFs obtained by field experiments, AFs obtained by this method depend on pavement type and strength and on the pavement response type. The pavement response type serves as a surrogate for the pavement distress type. Of course, this method is easier to use than the previous method, which relies on extensive field experiments.

There are two significant complications facing the user. First, this method assumes that the changes in pavement responses (such as strains or stresses) can be related to the severity and type of pavement distresses and, consequently, to pavement damage. Second, according to Equation 2, it is assumed that the pavement response to an axle group load can be characterized and summarized by one quantity, or by one number, $R_{r,i}$. However, pavement response to an axle group loading is complex. For example, the surface deflection of a flexible pavement caused by a triple axle exhibits three distinct and different deflection bowls (from the individual axles) superimposed on a total deflection bowl.

Need for General Axle Load Equivalency Factors

The foregoing discussion indicates that the current definition of axle load equivalency factors is too specific. In general, AFs vary depending on the following factors:

- Pavement type,
- Pavement thickness (for a given pavement type),
- Pavement distress mode (e.g., roughness, rutting, fatigue cracking),
- Severity or level of distress, and
- Axle configuration.

Consequently, traffic loads summarized using existing AFs (e.g., total number of ESALs per year) can change when the pavement is rehabilitated, although the actual traffic loads may not. Also, the AASHTO AFs are available for two pavement types only (asphaltic concrete pavements and rigid pavements). There are other pavement types for which AFs are not available:

- Surface-treated pavements,
- Gravel roads,
- Semi-rigid pavements [portland cement concrete (PCC) pavements with thick asphalt concrete (AC) overlays, or asphalt concrete pavements with thick PCC-treated bases].

This means that either the damaging effect of traffic loads on these pavements cannot be summarized or the wrong factors are being used to do it.

There is a need for a traffic load statistic (such as an ESAL) that is independent of pavement variables in the same way annual average daily traffic (AADT) volumes are. Such a statistic would be useful for pavement management purposes, for example, for evaluating and comparing pavement loading trends on a network consisting of a variety of pavement types. The proposed general axle load equivalency factors can be used to obtain such statistics in the form of general ESALs.

DEFINITION OF GENERAL AXLE LOAD EQUIVALENCY FACTORS

The general axle load equivalency factors, GAFs, proposed here have a similar meaning and roughly the same magnitude as the AASHTO axle load equivalency factors. In fact, the GAFs, defined by Equation 3, are identical to AASHTO AFs for single-axle loads on flexible pavements with the structural number (a number related to the pavement strength) equal to 5, and the terminal serviceability index equal to 2.5.

$$\text{GAF} = (0.01169\,L + 0.064)\left(4 + \frac{8.9}{L}\right) \quad (3a)$$

where L is the axle load (of any type or spacing) in kN.
In kips, Equation 3(a) becomes

$$\text{GAF} = (0.052\,L + 0.064)\left(4 + \frac{2}{L}\right) \quad (3b)$$

where L is the axle load (of any type or spacing) in 1,000 lb.

Equation 3 was originally proposed elsewhere (*3*), and its functional form was obtained by curve fitting to resemble typical AASHTO AF. It should be noted that the GAFs are not only independent of pavement-related variables, they are also independent of axle configuration and spacing—a significant simplification from the AASHTO approach. Any changes in the GAFs can be directly attributed to changes in traffic loads.

GAFs defined by Equations 3a and 3b provide one possible formulation. The present objective is not to establish definitive GAFs but to demonstrate need for their existence.

COMPARISON OF GENERAL AXLE LOAD EQUIVALENCY FACTORS WITH OTHER FACTORS

Figure 1 compares GAFs with those developed by AASHTO (*2*) and works by Monismith (*4*), Painter (*5*), and Claessen (*6*) for single and tandem axles, respectively. The AASHTO AFs in Figure 1 are for SN = 5 and p_t = 2.5 psi. The GAFs are for all pavement types; the other factors used in Figure 1 are for asphalt concrete pavements only. Overall, the figures suggest that, for a typical range of axle loads, the proposed GAFs are similar to those calculated by the other four methods, including the AASHTO method. AASHTO AFs have been compared with AFs that have been derived in 10 other studies over the past 12 years (*7*).

It should be noted that analyses of the AASHO Road Test data do not produce unique values for AFs; AFs depend not only upon pavement distress types and levels but also upon the regression models and methods that are used to quantify them (*7*).

The following sections describe consequences of simplifying assumptions involved in the formulation of the GAF and the influence of major variables on the accuracy of traffic load estimates. The purpose of the discussion is to quantify, at least in relative terms, the influence of major factors on AF and on the ESAL calculations. Although many of the variables involved interact, for clarity the discussion addresses variables one by one under three main headings.

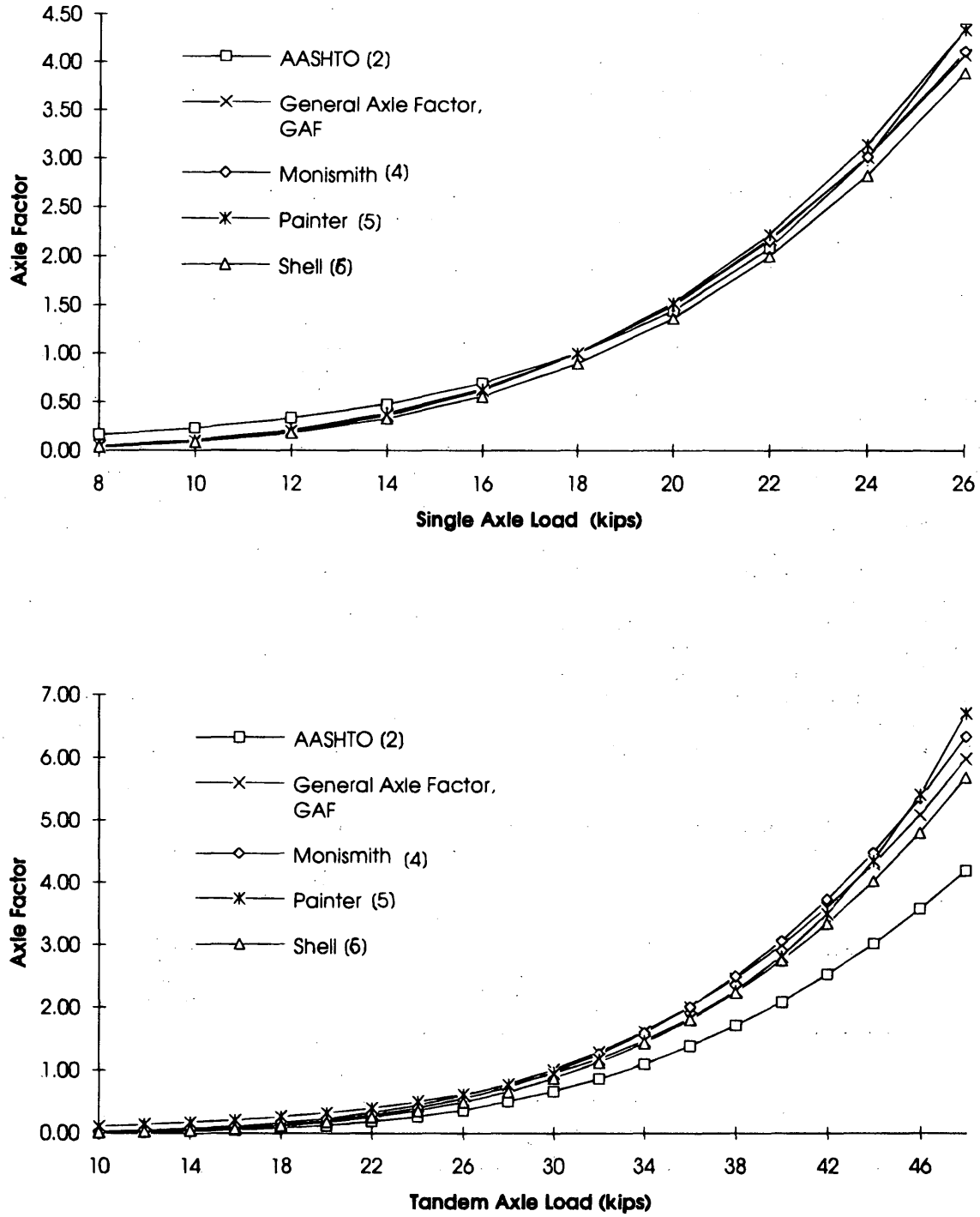

FIGURE 1 Comparison of axle factor values for single axles (*top*) and tandem axles (*bottom*).

- Variables affecting AASHTO axle factors,
- Other variables affecting axle factors, and
- Variables affecting overall traffic load estimates.

VARIABLES AFFECTING AASHTO AXLE FACTORS

Because the AASHTO AFs are widely used, all variables included in the determination of the AASHTO factors are described. The discussion is centered on the comparison of GAFs with the AASHTO factors.

Pavement Structure

AASHTO AFs are significantly influenced by the two pavement types, flexible and rigid, considered by the AASHTO Pavement Design Guide. However, the influence of pavement type is only significant for tandem and triple axles. For example, according to Table 1, the AF for a 160-kN (36,000-lb) tandem axle is 1.36 for a flexible pavement but 2.48 for a rigid pavement—an 82 percent increase. In comparison, a single axle of 80 kN (18,000 lb) has an AF of 1 for either pavement type. A single axle of 107 kN

(24,000 lb) has an AF of 3.03 for a flexible pavement and 3.36 for a rigid pavement—an increase of only about 11 percent.

A possible explanation of the differences in AF for the two pavement types is illustrated in Figure 2 (*top*) using the example of a tandem axle. For AC pavements, the tensile strain on the bottom of the asphalt concrete layer is considered one of the critical design parameters. The response curves for this strain in Figure 2 (*top*) show that the strain on the bottom of the asphalt concrete layer changes—from tensile to compressive—with the distance from the center of the load. The tensile strain is denoted in Figure 2 (*top*) by a negative sign (−), and the compressive strain by a positive sign (+). For closely spaced individual axles, some of the compressive strain from one axle may reduce the critical tensile strain from the other axle, and vice versa. The contributions of individual axles (of the tandem axle) to the peak tensile strain are to some degree counterproductive. This may help to explain why the AF for a tandem axle consisting of two standard axles is 1.38 on a flexible pavement, much less than the 2 that would result if the two standard axles were far apart and could be considered to be two single axles (see Table 1).

For rigid pavements, one of the critical design parameters is the slab deflection at transverse joints. According to Figure 2 (*middle*), the two individual axles of the tandem axle are in synergy: both contribute positively to the total critical deflection at the transverse joint. This may explain why the AASHTO AF for a tandem axle consisting of two standard axles is 2.4, more than 2, which would result if the two axles were far apart (single), and much more than 1.38 as was the case for a flexible pavement (see Table 1).

A similar case can also be advanced for triple axles. However, it should be noted that triple axles were not evaluated by the Road Test. The AASHTO AFs for triple axles were developed by analytical means.

The significant influence of pavement type on the AASHTO AFs is attenuated by the following considerations:

- The tensile strain on the bottom of the AC layer, the parameter related to the AASHTO AF, is a good predictor of fatigue cracking. However, fatigue cracking is not a predominant failure mode of AC pavements, which are part of structurally adequate, mature pavement networks. Systematic analyses of pavement distresses in Ontario showed that the predominant failure modes of AC pavements are deteriorating transverse cracks and wheel track rutting (*8*). These two failure modes, unlike fatigue cracking, are virtually independent of axle configurations and thus also of pavement type.
- Over the years, the slab lengths of jointed PCC pavements have become considerably shorter, and the axle group spacing (of tandem, triple, and quadruple axles) has increased. For example, joint spacing on newly constructed PCC pavements in Ontario is about 4 m. The trailing axles of multiple axle groups on short slabs may no longer synergistically (or significantly) contribute to the total slab deflection at the joint (as in Figure 2 (*middle*)) but, on the other hand, may mitigate it [as in Figure 2 (*bottom*) where a trailing axle is at a midslab when a leading axle is at the joint].
- The Road Test distinction between flexible and rigid pavements is often blurred by the existence of semirigid pavements and full-depth (AC) pavements.

Those considerations indicate that the influence of pavement type may not be as significant as the AASHTO AFs suggest. However, it should be stressed that the purpose of the GAF is not to question

TABLE 1 AASHO Axle Load Equivalency Factors for 80 kN (18000 lb) Loads (*2*)

Pavement Type	Axle Type	Axle Spacing		
		Zero Spacing (single axle only)	Typical Spacing[3]	Large Spacing[3] (independent axles)
Flexible[1]	Tandem (2 x 80 kN)	13.9	1.38	2.00
	Triple (3 x 80 kN)	above 50	1.66	3.00
Rigid[2]	Tandem (2 x 80 kN)	18.3	2.48	2.00
	Triple (3 x 80 kN)	above 50	4.16	3.00

Notes

1) SN = 5
2) D = 10
3) Spacing (typical or large) is not defined by AASHTO.

- $P_t = 2.5$
- The load on each individual axle is always 80 kN (18,000 lb). A tandem axle consists of two axles each carrying 80 kN, and a triple axle consists of three axles each carrying 80 kN.

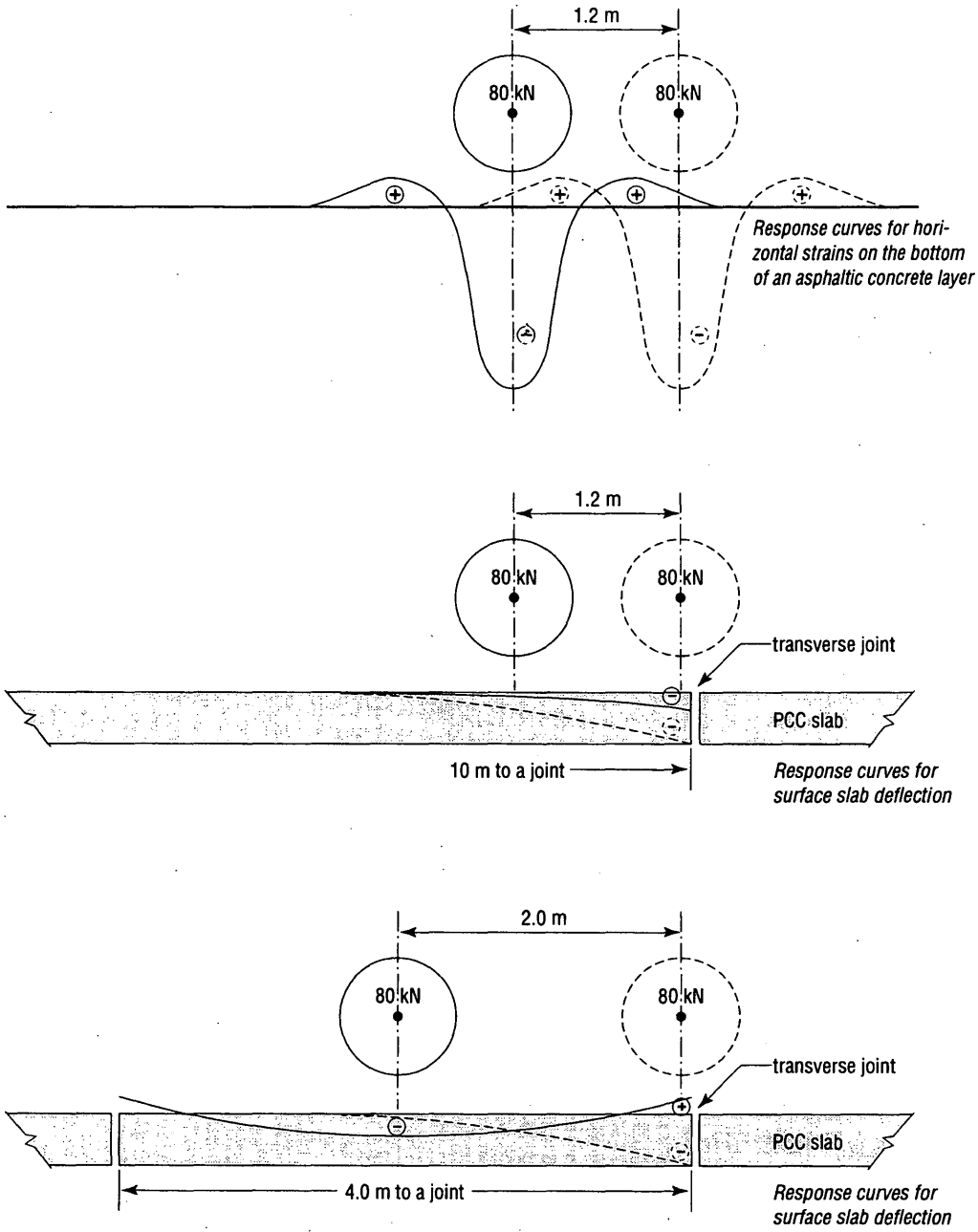

FIGURE 2 Response of asphaltic concrete pavement: short axle spacing (*top*); response of rigid pavement: short axle spacing, long slab length (*middle*) and large axle spacing, short slab length (*bottom*).

the accuracy of AASHTO's AFs or to improve the accuracy of AFs for specific pavement structures, but to provide a simple general set of axle factors for all pavement types.

Axle Spacing

The influence of axle spacing on the AASHTO AF is illustrated in Figure 3 for tandem and triple axles, respectively. As in Table 1, both tandem and triple axles in Figure 3 are carrying 80-kN (18,000-lb) loads on each individual axle. For a rigid pavement, such a tandem axle has the AASHTO AF of 2.48 regardless of the actual spacing between the two axles. If the spacing between the two axles exceeds an unspecified distance so that the two axles can be considered to be independent, the corresponding AASHTO AF is 2. Similarly, for a flexible pavement, two 80-kN axles far apart have AFs of 2; if they are close, their AF is 1.38; and if the spacing is zero, AF equals 13.9 (see Table 1). This suggests a reversal of curvature of the function relating AF to axle spacing.

Figure 3 (*bottom*) shows an equally significant influence of the axle spacing on the AASHTO AF for triple axles. Again, when the axle spacing between three consecutive axles exceeds an unspecified distance, the AF changes significantly.

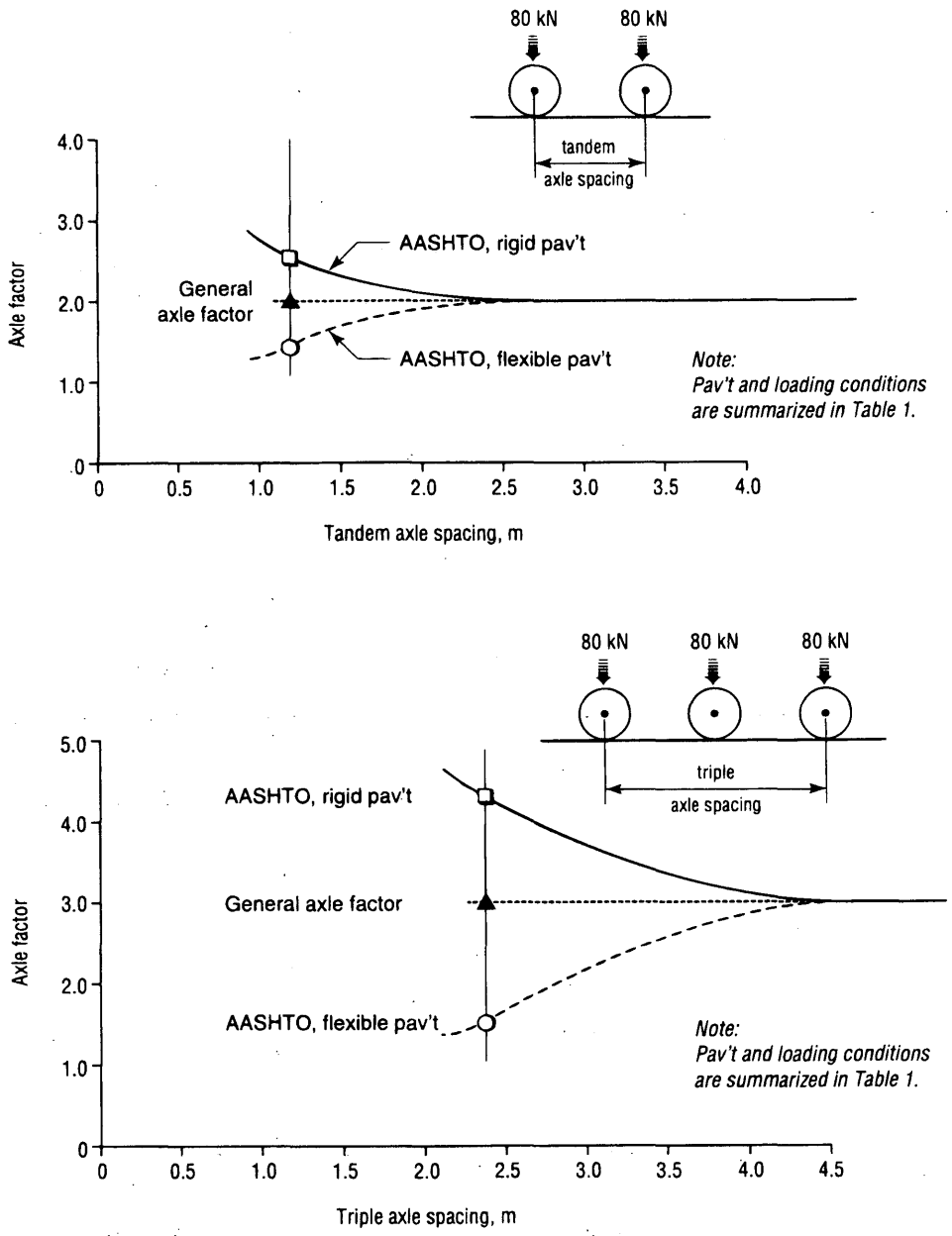

FIGURE 3 Influence of tandem axle spacing on axle factors (*top*) and influence of triple axle spacing on axle factors (*bottom*).

During the time of the Road Test (early 1960s), the tandem axle spacing was uniform (1.22 m) and triple axles (and quadruple axles) were not used. The trucks used in the Road Test reflected the truck fleet on the road. All tandem axles had 1.22-m (48-in.) spacing (and no triple axles were used). The exception was one truck type, used to carry extra heavy loads, which had tandem axle spacing on the tractor of 1.37 m (and again 1.22-m tandem spacing on the trailer) (*9*).

Truck design has changed considerably since the Road Test. The current axle group spacing in many jurisdictions, including Ontario, varies notably and is considerably larger, particularly on trucks with six axles or more, than the spacing 30 years ago. An example of truck axle spacing encountered in Ontario is presented in Figure 4. The figure is based on a 1988 random survey of 2,089 trucks conducted at 16 locations and shows separately axle spacing distribution for trucks with four axles and trucks with seven and more axles. The axle spacing is shown regardless of axle group type.

According to Figure 4, the frequency distribution of axle spacing in the range of 1 to 4 m appears to be bimodal with the dividing line at about 2 to 2.5 m. The bimodal distribution is the result of truck operators using the vehicle weight regulations (*10*) to maximize the payload. Axle spacings up to 1.9 m include most tandem and triple axles. A single axle can always carry a larger load than any axle that is part of an axle group. To qualify as a single axle, the axle spacing from any other axles must exceed 2.4 to 3 m, depending upon jurisdiction. Thus, given a choice, truck designers place additional axles, such as liftable axles, at least 2.4 m from all other axles. This spacing is based on the load-carrying capacity of the bridge components

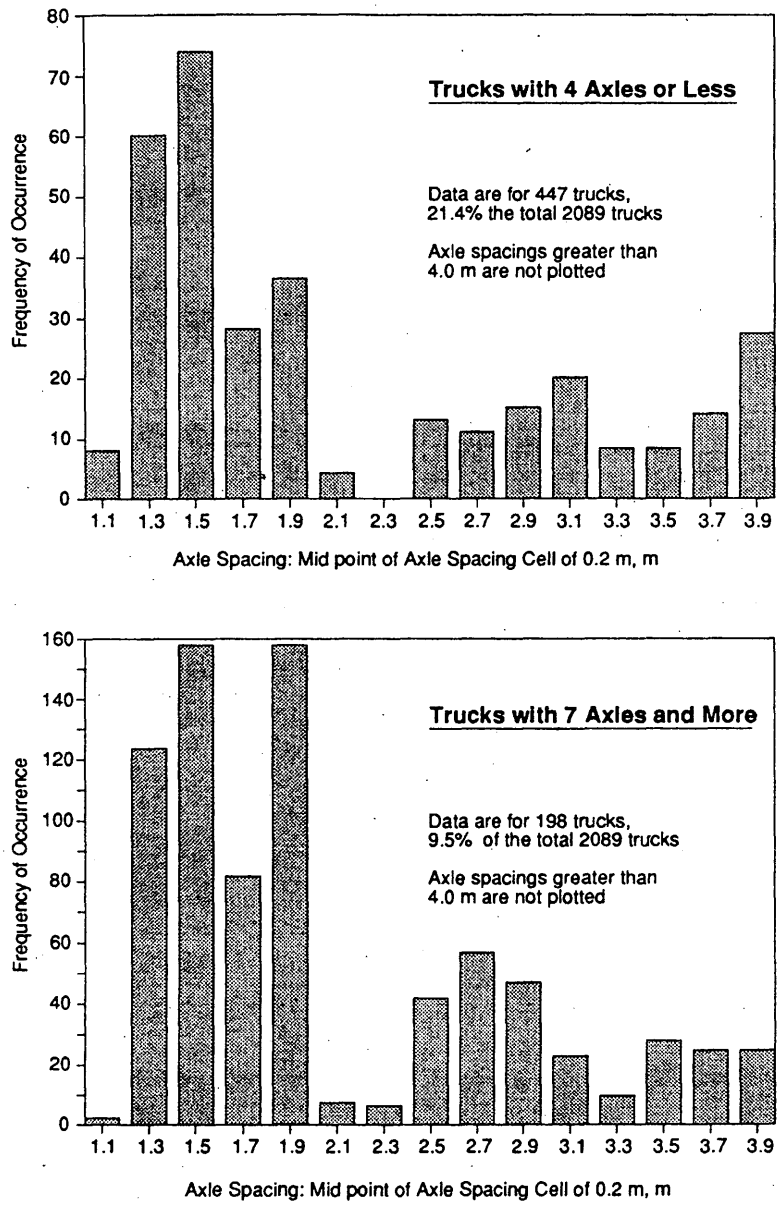

FIGURE 4 Frequency distribution of axle spacing for two truck types.

and not on pavement considerations. There is nothing special about the 2.4-m axle spacing to warrant the drastic change in AF.

GAFs are not influenced by axle configuration or spacing. Referring to Figure 3, the GAF for tandem and triple axles (comprising 80-kN single axles) are 2 and 3, respectively, basically in the midrange of AASHTO AFs for flexible and rigid pavements. This eliminates the need to define how AFs should change with axle spacing; for example, at which distance two single axles become a tandem axle (or two-axle group). Because GAFs are independent of axle spacing, they can also be used for summarizing the loads on quadruple axles.

Pavement Distress Type

By definition, AFs are defined for a specific type of pavement distress and its level (Equations 1 and 2). The AASHTO AFs were developed for the present serviceability index (psi). The psi is dominated by pavement roughness. Cracking, patching, and rutting contribute only about 5 percent to the value of the psi. In general, AFs used by an agency should be based on the pavement distress or distresses that trigger the local need for pavement rehabilitation.

All AFs developed since the time of the Road Test have been based either on independent analyses of the Road Test data, with their often-stated limitations (e.g., accelerated test, only one subgrade, old pavement and truck technology) or on analytical methods. Analytical methods now predominate; AASHO Road Test data have become obsolete [although they are frequently reanalyzed (*7,11*)], while the technology used to measure or calculate pavement responses to loads has improved.

The following pavement responses, linked previously to the formation of pavement distress, have been used for the development of AFs for AC pavements:

- *Pavement surface deflection.* The deflection has been linked to pavement deterioration, measured mainly in terms of roughness. Several pavement distresses, such as cracking, distortion, and rutting, can contribute to pavement roughness.
- *Interfacial strain.* Strain at the bottom of the asphalt concrete layer has been related to fatigue (alligator) cracking.
- *Vertical strain on top of subgrade.* This response has been related both to rutting in the pavement structure and to pavement deterioration.
- *Vertical strain in AC layer.* Vertical strain in the AC layer, about 50 to 75 mm from the pavement surface, has been linked to rutting in the AC layer only (so-called mix instability rutting).

The AFs based on analytical methods depend not only on the selection of pavement responses but also on analytical methods used. For illustration, the dependence of AFs on pavement responses and analytical methods is quantified by the following example.

The example assumes a triple axle and other conditions summarized at the bottom of Table 2. Typical pavement response curves for the first three pavement responses listed are shown in Figure 5. To obtain AF, it is necessary to modify Equation 2 to sum the responses of the individual axles within the triple axle using a summation method.

$$AF_{r,m} = \frac{\sum_{i=1}^{P} (R_i)^n}{R^n} \quad (4)$$

where

$AF_{r,m}$ = axle factor for pavement response r and summation method m.

R_i = amount of discrete pavement response for load cycle i identified by method m.

n = See Equation 2. There is no general or standard exponent. In this example, the exponent used was 3.8 (*12*).

P = number of load cycles (axles).

R = amount of pavement response r to the standard load (80-kN single-axle load).

In the absence of a universally accepted procedure, a number of methods have been proposed to sum pavement responses to individual axle loads. (The pavement responses are shown as D_1, D_2, D_3 and S_1, S_2, S_3 in Figure 5.) In this example, three summation methods have been used: the Roads and Transportation Association of Canada (RTAC) method (*12*), the University of Waterloo method (*13*), and the Peak method (*14*).

The three summation methods differ by the way in which the pavement responses (D_i, S_i) are defined. The reasons for different definitions are summarized elsewhere (*14*). For example, proponents of the Peak method argue that although the surface deflections between two subsequent axles do not reach a rest position (zero deflection), the asphaltic concrete layer at this location reverses its curvature (tensile strain changes to comprehensive strain, Figure 5). Consequently, they believe that the use of the total deflection best models the overall pavement response.

The results of the example are summarized in Table 2 and provide the basis for the following observations:

- Pavement response types (and consequently pavement distress types) influence AF significantly. This also applies when the same summation method is used.

TABLE 2 Influence of Pavement Response Type on Axle Load Equivalency Factors for Triple Axles

Pavement Response Type	Method of Response Summation		
	RTAC	Waterloo	Peak
Surface Deflection	2.2	3.5	8.2
Tensile strain on the bottom of the AC layer	2.8	3.0	N/A
Vertical strain on the subgrade	1.1	3.1	N/A

Conditions
- The triple axle has individual axle spacing of 1.25 m.
- Each axle has an 80 kN (18,000 lb) load, the total triple axle load is 240 kN.
- Flexible pavement with SN = 5.7 and asphaltic concrete thickness of 130 mm.
- Pavement responses were calculated using ELSYM5 [15].
- Exponent n (Equation 4) equals to 3.8
- According to Reference [14].

Note: The corresponding general equivalency factor is 3.

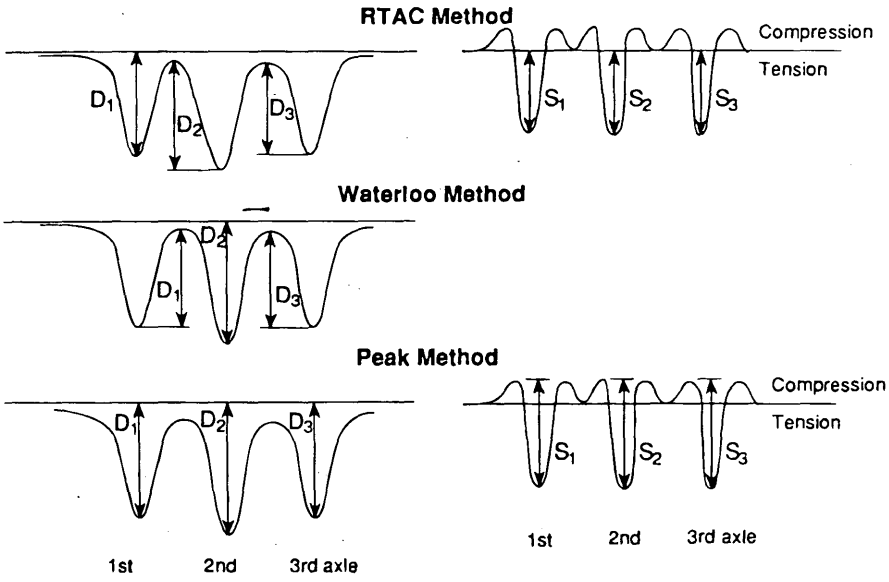

Pavement response curves for
- Surface deflections, or
- Vertical strain on the top of the subgrade

Pavement response curves for
- Tensile strain at the bottom of asphaltic concrete layer

FIGURE 5 Pavement response curves for triple axles.

- AFs, for a given pavement response, are significantly influenced by the summation method used—while there is no standard summation method available.
- It is difficult to obtain definitive AFs using analytical methods; there are too many assumptions involved, which significantly influence the results. The range of AFs given in Table 2 is from 1.1 to 8.2, making the use of analytical methods speculative. This certainly creates a role for the GAFs, which are not linked to any specific pavement distresses. However, by their link to the AASHTO AFs, the GAFs are still linked to the psi.

Pavement Thickness

The influence of the pavement thickness (SN number for flexible pavements and slab thickness, D for PCC pavements) on the AASHTO AFs was evaluated elsewhere (*1*). It was concluded that, for typical pavement structures, the change in AASHTO AFs is limited to about 5 to 10 percent. The influence of pavement thickness on AFs is probably even smaller when considering the total pavement structure including subgrade. (Subgrade is not included in SN and D.) A very good subgrade may considerably reduce the need for a large SN and result in a thin pavement that, nevertheless, has a high overall strength. In other words, the total pavement strength does not vary as much as SN or D vary. Consequently, the influence of pavement thickness on the AF is reduced. At any rate, the influence of pavement thickness is relatively small and is not included in the GAF.

Level of Pavement Distress

For the AASHTO AFs, the influence of the level of pavement distress is accounted for by the initial and terminal serviceability index (p_o and p_t, respectively). The influence of p_o and p_t has also been evaluated (*1*). It was concluded that the change in the AASHTO AFs because of changes in p_o is about ±4 percent and because of changes in p_t about 4 to 20 percent. The influence of serviceability on AF is relatively small and is often disregarded (particularly the influence of p_o), even for AASHTO AFs. It is also disregarded by the GAF.

OTHER VARIABLES AFFECTING AFS

In addition to variables that have been included in the calculation of the AASHTO AFs, and in some other routinely used axle factors, there are other variables that are not included in the calculation or determination of AFs but, nevertheless, influence the value of these factors.

Truck Suspension Type

Pavement response or damage is affected more by dynamic loads than by static loads. The dynamic loads depend, to a large extent, on a truck suspension type and condition. It is beyond the scope of this paper to discuss the influence of different truck suspension systems on pavement damage. However, it is generally recognized that an air suspension provides a better load equalization between axles, and about 10 percent lower dynamic loads than a leaf spring suspension (on moderately rough roads at highway speeds) (*16,17*). Air suspensions, which were not used in the Road Test, appear now on over 50 percent of all new tractors and on 20 percent of all new trailers. According to Equations 1 to 3, a 10 percent change in static load results in about a 45 percent change in AF.

Tire Type and Pressure

The influence of truck tire type and tire pressure on dynamic axle loads is small, if tire pressures are not unusual and the number of tires remains the same (*16*). However, tire truck types (wide-base tires or single tires on steering axles) and tire pressures can significantly influence wheel track rutting and other distresses on AC pavements.

Number of Tires

For the same load, single axles with single tires can be twice as damaging as single axles with *double tires* (*12,18*).

Speed

Truck speed is a secondary variable that interacts with truck suspension systems and pavement roughness. Although axle loads applied at lower speeds can cause higher pavement damage than loads applied at higher speeds, particularly on AC pavements, higher speeds produce higher dynamic loads.

In summary, neither analyses of the AASHTO Road Test data nor analyses of pavement response parameters to loads produce unique or definitive values for AFs. In addition to physical characteristics, such as pavement type or truck suspension type, the resulting AFs also depend on analytical methods that are used to calculate them.

VARIABLES AFFECTING OVERALL TRAFFIC LOAD ESTIMATES

The AFs are only one of the several variables necessary for estimating accumulated pavement traffic loads. For pavement design and management purposes, traffic loads are usually summarized using ESAL. A generic formula for the calculation of a total number of ESALs (ΣESAL), for one lane in one direction of a multilane highway, is

$$\sum \text{ESAL} = \sum_{i=1}^{n} (\text{AADT} \cdot DF \cdot T_i \cdot \text{LDF} \cdot \text{TF}_i \cdot \text{days} \cdot \text{years} \cdot \text{growth}) \quad (5)$$

where

$\sum$ESAL = total number of ESALs during the design period,
i = truck class (type),
n = number of truck classes,
AADT = average annual daily traffic (current),
DF = directional factor (directional split),
T_i = proportion of AADT volume that belongs to truck class i (if $n = 1$, T_i = truck proportion),
LDF = lane distribution factor for trucks,
TF_i = truck factor for truck class i [TF_i = sum of AF for all axles (and axle groups) of truck type i],
days = days per year for truck traffic,
years = design period in years, and
growth = traffic growth rate (for traffic loads).

Virtually all variables in Equation 5 are subject to approximations, assumptions, and errors. The errors associated with the individual variables used in Equation 5 are compounded and are reflected in the overall error associated with ΣESAL estimates. Typical estimated differences between the actual and estimated values for the variables used in Equation 5 are summarized in Table 3. Considering the estimated error ranges given in Table 3, it appears that the errors associated with methods used to establish AFs are overshadowed by errors associated with other variables. A similar conclusion was reached in a work by Witczak (*1*), who found that the largest uncertainty associated with computing the total number of ESALs is due to errors not related to the method used for determinating axle factors. The use of GAFs will not significantly change this situation.

ROLE OF GAFS IN PAVEMENT DESIGN AND MANAGEMENT

The sum of GAFs for all axles of a truck equals a general truck factor (GTF). The use of GTF for the calculation of ESALs (using, for example, Equation 4) will yield general ESALs (GESALs). Like GAFs and GTFs, the GESALs are independent of pavement type and thickness, level of pavement damage, and axle configuration.

Pavement design thickness is not overly sensitive to changes in traffic loads. A doubling of traffic loads (e.g., ESAL) typically results in a 25-mm (1-in.) increase in the thickness of the asphaltic concrete layer or the PCC slab. This does not mean that traffic loads are unimportant and that approximate GAFs are sufficient. The objective of the GAF is to provide a simpler and easier way to handle pavement traffic loads that should lead to their better management and use in pavement design.

GAFs are not intended to replace all other AFs. It is suggested, however, that the GAFs and the associated GESALs are suitable and appropriate for summarizing the damaging effect of traffic loads for pavement management purposes and for routine pavement design work. It should be noted that the GAFs have (or can have) magnitudes similar to several other axle factors, including AASHTO factors. The use of GAFs, or similarly conceived factors, greatly simplifies the management of pavement traffic loads. Specialized axle factors may still be required for quantifying pavement damage for unusual traffic loads, specific pavement distresses, and research purposes.

SUMMARY AND CONCLUSIONS

1. The AASHTO definition of axle load equivalency factors is too specific for pavement management purposes. Traffic loads summarized using existing axle load equivalency factors change with pavement type and pavement thickness even when traffic loads remain constant.
2. Considering the variety of pavement structures and truck configurations, there is a need for a summary universal pavement traffic load statistic that is independent of pavement-related variables and axle configurations.
3. The uncertainty associated with computing the accumulated number of ESALs is due primarily to errors in parameters other than those related to the determination of axle factors. These include, for example, traffic volume estimates and axle weights.

TABLE 3 Estimated Errors Associated with Variables Used for ESAL Predictions

Variable[1]	Estimated Error Range[2], %	Comments
T_i (truck class)	± 10 to ± 100	± 10 for Automatic Vehicle Classifiers ± 100 if truck percentage is estimated
AADT	± 10 to ± 100	AADT estimates for highways built on a new alignment are often unreliable
LDF	± 10 to ± 40	The distribution of heavy trucks on multilane facilities is different from that of passenger cars (which is often used instead)
Days	± 20	Usually 300 days are assumed in Ontario
Growth	± 10 to ± 100	Difficult to predict for new facilities where historical data are missing
TF_i[3]		
Load measurements	± 10 to ± 100+	±10 for weigh-in-motion scales ±100 where loads are estimated
Truck suspension type	± 40	Air suspension compared to walking beam
Level of pavement distress	± 2 to ± 10	± 2 for initial serviceability ± 10 for terminal serviceability
Pavement thickness	± 5	for SN or D

1) Defined for Equation 5.

2) Typical range between the actual and estimated values, expressed as the percentage of the actual value.

3) Only a few contributing variables are listed.

4. The summation of pavement traffic loads can be greatly simplified using general axle factors. The general axle factors would be particularly useful for pavement management purposes, for example, for evaluating and comparing pavement loading trends on a network consisting of a variety of pavement types.

5. The proposed general axle factors are independent of pavement-related variables and axle configurations. Furthermore, the general axle factors can have similar magnitudes as the existing AASHTO axle load equivalency factors.

6. The proposed general axle factors and the associated general ESALs would be suitable and appropriate for pavement management and routine pavement design purposes.

ACKNOWLEDGMENTS

I express my appreciation to John Billing, Ontario Ministry of Transportation, for his helpful and valuable comments and review of the manuscript.

REFERENCES

1. Witczak, M. W. *Equivalent Wheel Load Factors.* Report prepared for Association of American Railroads. University of Maryland, Feb. 1981.
2. *AASHTO Guide for Design of Pavement Structures 1993.* American Association of State Highway and Transportation Officials, Washington, D.C. 1993.
3. Maghsoudi, A. *A Method for Estimating the Number of Equivalent Standard Axle Loads From Visual Classification Counts.* Internal Report PAV-78-02. Ontario Ministry of Transportation, Downsview, Ontario, Canada, 1978.
4. Monismith, C. L. *An Introduction to the Analytical Design of Asphalt Concrete Pavements,* University of California, Berkeley, 1981.
5. Painter, L. J. Analysis of AASHO Road Test Data by the Asphalt Institute. *Proc., International Conference on the Structural Design of Asphalt Pavements,* University of Michigan, Ann Arbor 1962.
6. Claessen, A. I. M. *Asphalt Pavement Design: The Shell Method, Manual on Asphalt Pavements and Overlays for Road Traffic.* Shell International Petroleum Company Ltd., London, England, 1978.
7. Irick, P. E., S. B. Seeds, and M. A. Diaz. *Characteristics of Load Equivalence Relationships Associated With Pavement Distress and Performance, Phase II Study.* Trucking Research Institute, Alexandria, Va., 1991.

8. Hajek, J. J., and W. A. Phang. Moving From Subjective to Objective Evaluation of Pavement Performance. *Proc. 1986 RTAC Conference,* Toronto, Ontario, Canada, 1986.
9. Special Report 61E: *The AASHO Road Test: Report 5—Pavement Research.* HRB, National Research Council, Washington, D.C., 1962.
10. *Vehicle Dimensions and Weight Limits in Ontario.* Compliance Branch, Ministry of Transportation, Downsview, Ontario, Canada, 1986.
11. Small, K. A., C. Winston, and C. A. Evans. *Road Work.* The Brookings Institution, Washington, D.C., 1989.
12. Christison, J. T. *Vehicle Weights and Dimension Study, Vol. 9: Pavement Response to Heavy Vehicle Test Program, Part 2—Load Equivalency Factors.* Roads and Transportation Association of Canada, Ottawa, Ontario, 1986.
13. Hutchison, B. G., R. C. G. Haas, P. Meyer, K. Hadipour, and T. Papagiannakis. Equivalencies of Different Axle Load Groups. *Proc. 2nd North American Conference on Managing Pavements,* Toronto, Ontario, Canada, 1987.
14. Hajek, J. J., and A. C. Agarwal. Influence of Axle Group Spacing on Pavement Damage. In *Transportation Research Record 1216,* TRB, National Research Council, Washington, D.C., 1989, pp. 58–66.
15. *ELSYM5.* Report FHWA-RD-85. FHWA, U.S. Department of Transportation, 1985.
16. Mamlouk, M. S. A Rational Look at Truck Axle Weight. Presented at Annual Transportation Research Board Meeting, Washington, D.C., 1991.
17. Davidson, E. Dynamic Load Distribution of Axle Suspension Systems on Truck Tractors and Semi-Trailers. Report FHWA/CA/RO/83-19. California Department of Transportation, Sacramento, 1983.
18. Hallin, J. P., J. Sharma, and J. P. Mahoney. Development of Rigid and Flexible Pavement Load Equivalency Factors for Various Widths of Single Tires. In *Transportation Research Record 949,* TRB, National Research Council, Washington, D.C., 1983, pp. 4–13.

Publication of this paper sponsored by Committee on Flexible Pavement Design.

Accelerated Dynamic Loading of Flexible Pavements at the Canterbury Accelerated Pavement Testing Indoor Facility

BRYAN D. PIDWERBESKY

New Zealand pavement design and construction practices are significantly indigenous, having evolved to suit the local conditions. Asphalt-bound aggregate systems are used for some urban streets and interurban motorways, and some rigid pavements were constructed 50 years ago, but virtually all highway traffic is carried by thin-surfaced unbound granular pavements. The need to ensure that designs and materials are adequate for modern vehicles provided the impetus for developing an accelerated pavement testing facility that reproduces vehicle dynamics. First, the development of the Canterbury Accelerated Pavement Testing Indoor Facility (CAPTIF) is described. The main feature of CAPTIF is the Simulated Loading and Vehicle Emulator, which can apply a myriad of loading conditions via an array of tire and load configurations at high rates of accelerated loading. Second, research projects conducted since 1986 are discussed and the significant results are presented. The research conducted at CAPTIF has contributed to the understanding of the behavior and performance of thin-surfaced, unbound granular pavements and the effect of vehicle dynamics on pavement wear.

The New Zealand road network totals nearly 100 000 km in length, of which 55 000 km have all-weather surfaces, and serves a population of 3.3 million over an area of 268 675 km^2. The typical pavement consists of a sprayed chip seal over unbound granular base and subbase layers. The pavement engineering design and construction practices used in New Zealand are described elsewhere (*1–3*).

The thickness design procedure for thin-surfaced, unbound granular flexible pavements is based on multilayer linear elastic theory. The procedure assumes that surface thicknesses of less than 35 mm do not contribute to the structural capacity of the pavement and that the stresses are dissipated through the depth of the granular cover layers above the subgrade. The design theory presupposes that the primary mode of structural failure is permanent deformation in the subgrade, so the main criterion is to limit the vertical compressive strain in the subgrade to acceptable magnitudes (*3*). The New Zealand subgrade criteria are derived from the *Shell Pavement Design Manual* (*4*).

At present, the maximum gross vehicle weight permitted on national highways is limited to 430 kN, and the maximum loads permitted for single-, tandem-, and triple-axle groups are 80, 145, and 175 kN, respectively. The New Zealand term for equivalent single-axle load is equivalent design axle (EDA); one EDA is defined as an 80-kN axle load on dual tires inflated to 550 kPa. Typically, the maximum design life would be on the order of 10^6 EDA.

Because of New Zealand's unique situation with respect to both the road user charges incurred by heavy vehicles and the dependence on thin-surfaced flexible pavements, research has been undertaken to isolate the influence of various components of the vehicle-pavement interaction system, such as the static and dynamic components of vehicle loading, and the relative effects of vehicles, the environment, and the pavement materials. Laboratory testing and computer analysis alone are inappropriate. Thus, trials using full-scale equipment and pavements are necessary, either in the field or in a test track under controlled conditions. Therefore, the first New Zealand accelerated loading facility was constructed in 1969 (*5*).

The first machine was used for a number of pavement research projects and finally became unserviceable in 1983. An assessment of the need for a new, improved accelerated pavement loading facility identified four primary research priorities:

- Evaluation of the performance of aggregates, such as marginal materials;
- Modified designs for surfacings, especially chip seals;
- Evaluation of pavement design assumptions by collecting data describing the long-term performance of pavements; and
- Investigation of the relationship between vehicle loading conditions and the deterioration of pavements for a wide spectrum of pavement and loading characteristics.

Accelerated pavement testers have been constructed in a variety of configurations (*6–8*). The facilities are generally classified as being circular or linear test tracks. A circular test track in which full-scale pavements could be constructed and a loading apparatus capable of imposing realistic dynamic heavy vehicle loading were selected because

- The machines can be operated continuously without being interrupted for direction changes, thereby greatly increasing the rate of load cycling;
- After initial acceleration, the speed of the loading system can be kept constant for long periods of time or varied, depending on the requirements of specific projects;
- Circular tracks can be divided into a number of either annular rings or longitudinal segments, each containing a pavement with some unique characteristics, and all segments can be tested simultaneously under the same or varying loading conditions;
- The configuration of each loading assembly in a multiarmed machine, such as tire types and pressures, axle numbers and weights, suspensions, and loads, can be altered so that the response of the same pavement under various loading conditions can be determined; and
- The interaction of pavements and vehicle dynamics can be examined using a combination of unsprung and sprung masses possessing realistic damping characteristics.

University of Canterbury, Private Bag 4800, Christchurch, New Zealand.

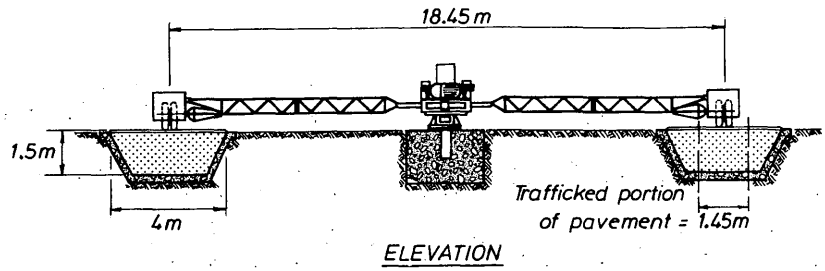

FIGURE 1 Elevation view of SLAVE and cross section of track.

DESCRIPTION OF FACILITY

The Canterbury Accelerated Pavement Testing Indoor Facility (CAPTIF) is housed in a hexagon-shaped building that is 26 m wide and 6 m high. An annular concrete tank, 1.5 m deep and 4 m wide, confines the bottom and sides of the track (Figure 1), enhancing the control of moisture contents in the subsurface systems and drainage. The track has a median diameter and circumference of 18.5 and 58.1 m, respectively. Normal field construction and compaction equipment is used in the facility. The main feature of CAPTIF is the Simulated Loading and Vehicle Emulator (SLAVE).

Simulated Loading and Vehicle Emulator

SLAVE was designed for the accelerated testing and evaluation of subgrades, pavements, and surfacings by replicating the effect on the pavement of actual road traffic conditions. An elevation view of SLAVE is presented in Figure 1. A sliding frame within the central platform is moved horizontally a maximum of 1 m (from stop to stop) by two hydraulic rams; this radial movement produces multiple wheel paths. The base elevation can be altered by up to 150 mm, to maintain the dynamic balance of the machine if the pavement surface level changes due to rutting or an overlay being applied.

Each vehicle consists of the axle, which is driven by a hydraulic motor, a suspension, a frame, instrumentation, and standard wheel hubs and truck tires (Figure 2). SLAVE vehicles can carry single or dual tires; their loads can be adjusted to between 21 and 60 kN (42 to 120 kN axle loads) by adding or removing steel weights. The suspensions can be multileaf steel spring, a parabolic steel leaf spring, or an air spring; each vehicle can carry the same or a different suspension for simultaneous testing. The speed can be any value between 0 and 50 km/hr and can be varied while running. The vehicles can be moved slowly and positioned at any location on the track, using a handheld, infrared remote control.

SLAVE operations are controlled directly by its internal electronics. The external or onshore computer is an IBM-compatible personal computer. Whenever a parameter is to be altered, the new command is sent by the external computer through a communications link under the track and a slip ring within the central pedestal. SLAVE and the computers can safely be left running without supervision.

Testing routines can be programmed in terms of start-stop times, distance or revolutions to be run, traveling speeds, and tracking pattern of wheelpath positions, and so forth. Any combination of these may be included in a programmed testing routine because the SLAVE software will use default values for those items not defined in the shore computer program. Manual control can be imposed when desired to override the current program. In addition to conventional hydraulic pressure, electrical current, and motor overload devices, the SLAVE electronics continually scans the safety monitors, and if a condition occurs that requires human inspection, brakes the vehicles to a stop.

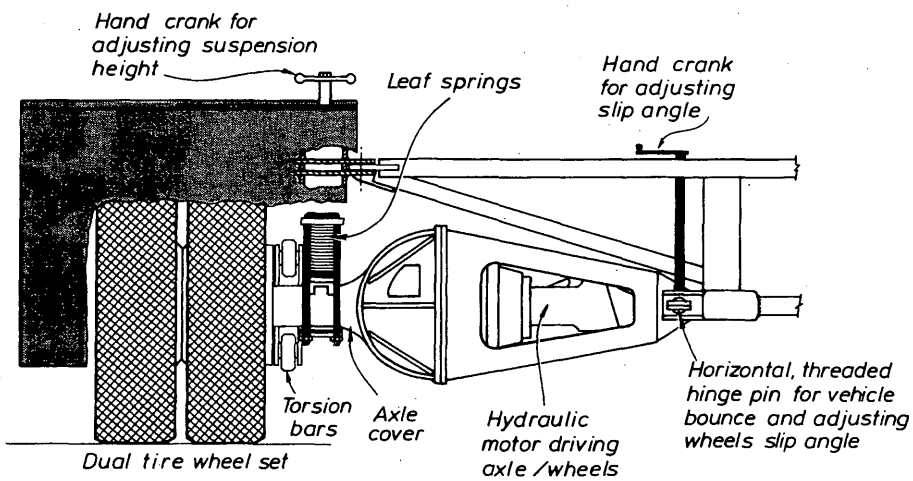

FIGURE 2 Cross section of one SLAVE vehicle.

Instrumentation and Data Acquisition

Since SLAVE was commissioned in 1987, electronic systems have been introduced that measure dynamic and residual strains and displacements, surface profiles, rebounds, and temperatures in the pavement and subgrade. The CAPTIF deflectometer, which is a modified version of the geobeam device developed by Tonkin and Taylor Ltd. of Auckland and resembles a Benkelman beam, measures the surface deflection of a pavement under a wheel load. The deflectometer probe is positioned between the tires of a dual-tired wheel and, as the wheel is moved away, the rebound of the pavement is measured to the nearest 0.01 mm, every 50 mm of horizontal movement. There are no moving parts on the device; an electromagnetic gap-measuring sensor at the end of the beam measures the vertical distance between the sensor and a steel disk placed on the pavement surface. A separate, associated device measures the horizontal movement of the wheel.

The CAPTIF profilometer measures transverse surface profiles using similar electronics. The profilometer consists of a braced aluminum beam, 4.4 m long, supported at each end by adjustable feet. An aluminum carriage is driven along the beam by an electric motor and drive chain. The carriage holds a linear variable displacement transducer with a jockey wheel riding along the pavement surface. Vertical displacement is recorded every 25 mm of horizontal travel of the carriage.

The output signals from the foregoing are digitized by electronics contained within the devices, and the digital data are captured by a Psion handheld computer. A DIPStick profiler is used to measure the longitudinal surface profiles for roughness surveys. The output from temperature probes installed in the pavements are automatically recorded hourly by a Taupo F-10-24K-48A data logger. A Hewlett Packard 3852S microprocessor-based unit and computer capture data signals from accelerometers and displacement transducers mounted on the chassis and axles of each vehicle, for measuring the dynamic loads being applied by the axles, and transmit the data to a trackside computer via radiowaves, while the vehicles are running at speeds of up to 50 km/hr.

The soil strain measuring system determines minute strains (100 μm/m) with good resolution (±50 μm/m) using Bison soil strain sensors. The sensors use the principle of inductance coupling between two free-floating, flat, circular wire-wound induction coils coated in epoxy, with a diameter of 50 mm (*9*). One of the two disks acts as the transmitter coil, creating an electromagnetic field that induces a current in the receiving coil. The magnitude of the induced current is inversely proportional to the spacing between the two coils (Figure 3). The gauge length is the separation distance between each paired coil. The Bison disks are installed during the formation of the subgrade and the overlying layers to minimize the disturbance to the materials.

The CAPTIF strain-measuring system is a modified prototype of the Saskatchewan soil strain displacement-measuring system developed by Saskatchewan (Canada) Highways and Transportation. The CAPTIF system uses a dedicated computer containing a specially built general-purpose input-output board, circuit boards, rectifiers, amplifiers, and assembler code written specifically for this application. Each sensor in an array is scanned simultaneously when triggered, every 30 mm of vehicle travel, so that a continuous bowl shape of strain versus distance traveled is obtained.

PAVEMENT RESEARCH PROGRAM

The research projects conducted at CAPTIF since 1986 are summarized in Table 1. The major findings are discussed in this section. In

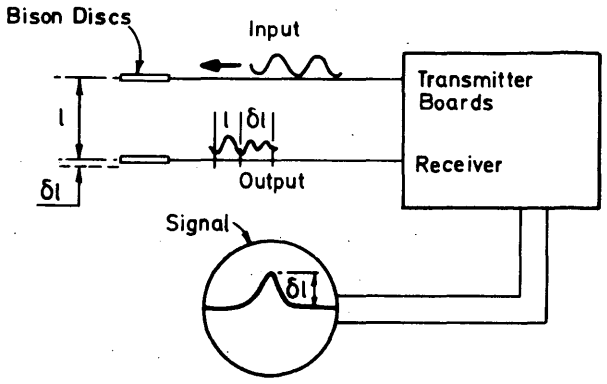

FIGURE 3 Principle of Bison strain sensors.

all the projects, the subgrade and the granular layers were spread by a small bulldozer and compacted by a 40-kN dual-drum roller. The surface of the base course is finished with a pneumatic-tired roller.

Inaugural Project

The purpose of this project was (a) to commission the SLAVE and evaluate its capabilities and (b) to monitor the performances of four granular pavements to provide an initial evaluation of the construction and operation techniques required for the accelerated trafficking facility. The average California bearing ratio (CBR) of the clayey loess subgrade was 30 percent. The pavement thicknesses ranged from 150 to 300 mm, in 50-mm increments; the pavement material for all four was a well-graded aggregate with a maximum particle size of 40 mm, except the uppermost lift had a maximum size of 18 mm. The surfacing was a double seal coat; soon after loading began, the seal began flushing, even though there was no loss of chip and the base course was firm. After flushing became severe, the initial coats were removed and the base course lightly releveled. A single coat of bitumen sprayed at a lower-than-normal rate was coated with a first layer of larger stone chips (A.L.D. of 12 mm) interlocked with smaller chips (A.L.D. of 8 mm).

Each SLAVE vehicle applied a wheel load of 40 kN to represent an equivalent design axle (EDA) SLAVE applied 1.53 million EDA loads to the pavement during the project. There was no significant difference in the performances of the four pavements; even the thinnest unbound granular pavement of compacted, well-graded crushed aggregate can sustain at least 1.5×10^6 80-kN axle load repetitions in the absence of deleterious ground moisture and environmental factors (*10*). The pavement thickness design procedure should be modified to explicitly consider the effect of such factors.

Comparative Rutting of Tire Types

The vertical deformation caused by a single low-profile radial tire (14.00/80 R 20 on Vehicle B) and dual standard radial tires (10.00 R 20 on Vehicle A) was compared. The load applied by each wheel set was 40 kN. The clayey loss subgrade material had an average CBR of 30 percent. The pavement consisted of a 40-mm-thick surfacing of an open-graded bituminous mix, a 150-mm-thick base course of a high-quality crushed aggregate, and a 150-mm-thick subbase of coarse aggregate with a maximum particle size of

TABLE 1 Summary of Projects at CAPTIF

Project and Variables	Load Repetitions (EDA)	Wheel Loads (kN)	
		Veh. A	Veh. B
Inaugural: 4 thicknesses unbound granular pavements under chip seals	1.5×10^6	40	40
Comparative Rutting: duals and wide-base single tires	94,700	40	40
Effect of Particle Shape and Gradation on Basecourse Performance: 9 pavements	54,300	40	40
Lime-stabilised subbases: 3 thicknesses	30,500	21, 40	21, 40
Strain response of subgrades and unbound granular pavements: wheel load, tire pressure and tire type	51,000	40	21-46
Modified Binders in Asphalt Mixes: 6 modified binders	3.2×10^6	40-46	40-46
Life-cycle performance of a thin-surfaced unbound granular pavement	740,000	40	40
Dynamic wheel loads and pavement wear: single unit and multi-leaf spring suspensions	35,000	38	38
DIVINE[a] (Element 1): air bag and multi-leaf suspensions		50	50

[a] Dynamic Interaction of Vehicles and Infrastructure Experiment

65 mm. Further information about the pavement and temperatures are provided in Table 2. After 16,000 loading cycles, the average permanent deformation (as measured by the transverse profilometer) created by the single low profile radial tire was 92 percent greater than that of the dual radial tires, as shown in Figure 4 (*11*).

Effect of Particle Shape and Gradation on Unbound Base Course Performance

The study evaluated the effect of particle shape and gradation on the performance of unbound base course aggregates constructed according to a revised specification (*12*). Aggregates consisting of different combinations of rounded and angular crushed particles were created for three different particle size distributions using Talbot's equation.

$$P_d = 100\left[\frac{d}{D}\right]^n \quad (1)$$

where

P_d = percentage of sample passing sieve size d,
d = sieve size (mm),
D = largest particle size in sample (mm), and
n = gradation exponent.

The values for the gradation exponent (n), 0.4, 0.5, and 0.6, represent the lower limit, midpoint, and upper limit of the gradation envelope for New Zealand primary base course aggregate, respectively (*13*). Nine base course aggregates were created, as shown in Table 3. The base course aggregates were placed in nine sequential segments in the track, with an average depth of 108 mm ± 7 mm; the maximum dry density varied according to the gradation. Segments A, B, C, and I could not be compacted, so they were removed and replaced with a local aggregate; the four segments, which were adjoining, were combined into one segment designated A1. The 48-mm-thick (± 6 mm) surfacing was an open-graded bituminous mix (porous asphalt) with the same properties as described in Table 2.

After 54,000 EDA cumulative loadings, the subgrade deformation under loading was similar for all test segments, and base course deformation differed (Table 3). Particle shape had the greatest effect on the performance of the aggregates, compared with gradation. Aggregates consisting of 30 percent or less angular particles could not be compacted, and the best performance was achieved with aggregates of 70 percent or more angular particles, which is required by the New Zealand base course aggregate specification (*13*).

Behavior of Lime-Modified Subbases

Three pavements were constructed, two with lime-stabilized clay subbases of thicknesses 150 and 250 mm, and the third with an unmodified high-quality, well-graded, crushed aggregate, as shown in Figure 5. The laboratory CBR of the unstabilized and stabilized clay specimens were 5 and 20 percent, respectively. For all three pavements, the surfacing was a 30-mm-thick layer of asphaltic concrete and the base course was a 150-mm-thick layer of high-quality, well-graded crushed aggregate (*13*). The subgrade had a CBR of 3 percent, which represents the worst possible case, and a compacted dry density of 1 700 kg/m^3 ± 4 percent at a moisture content

TABLE 2 Asphalt Properties and Temperatures for Comparative Rutting of Tire Types

Mix Properties		Temperatures (°C)		
Bitumen penetration grade (100 g, 5 sec, 15°C)	80/100		Min.	Max.
Binder content (%)	5.5	Air	10	23
Air voids (%)	23	Tire Tread (A)	11	33
Hydrated lime (%)	2	Tire Tread (B)	11	33
		Pavement	10	22
Aggregate Gradation (% passing by mass)				
13.2 mm (sieve size)	100			
9.5	92			
4.75	25			
2.36	10			
1.18	7			
600 μm	5			
300	4			
150	2			
75	1			

of 20 percent. Laboratory tests showed that the optimum lime content for the subbase material was 4 percent. The maximum dry densities (at optimum moisture contents) of the unstabilized and lime-stabilized subbase material were 1 680 kg/m^3 (at 18 percent) and 1 520 kg/m^3 (at 25 percent), respectively. A geotextile (Typar 3407) was placed on top of the subbase to separate the base course aggregate material and the subbase, therefore enhancing the measurement of the layer profiles without interfering with the stress development and distribution within the pavement. The minimum temperature during curing was +6°C; during loading, the pavement temperature ranged between −3°C and +20°C.

Elastic deflections and permanent deformation of the pavement surface were measured; some results are presented in Table 4. Pavement failure was defined as vertical surface deformation of 25 mm. The pavement containing the 150-mm-thick lime-stabilized layer performed substantially better than the same thickness of unstabilized aggregate. Increasing the stabilized subbase thickness by 100 mm yielded a 15-fold increase in the life of the pavement. The moduli of the lime-stabilized layers were lower than that predicted by laboratory testing and computer analyses, primarily because the pavement could not be fully compacted on such a weak subgrade (*14*).

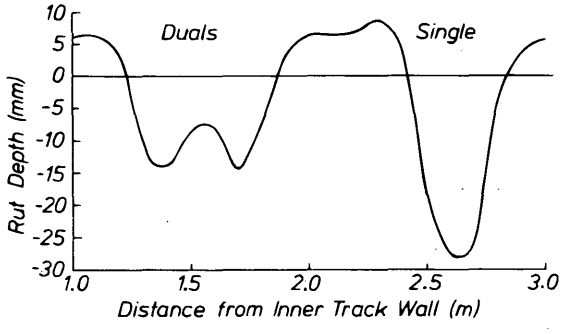

FIGURE 4 Pavement surface deformation under single- and dual-tire wheel loads.

Effect of Binder Modification on Asphalt Pavement Performance

The trial involved constructing six test sections of various asphaltic concrete mixes over 200 mm of unbound granular base course and a silty clay subgrade possessing a CBR of 13 percent. The base course aggregate was a well-graded, crushed gravel, compacted at a moisture content of 4 percent to a maximum dry density of 2 150 kg/m^3. The design life of all test sections was 1 × 10^6 EDA, so the depth of the asphalt concrete varied from 80 to 125 mm, depending on the characteristics of the different mixes. The bitumens used for the test sections were

- Standard paving grade (conforming to a German specification for B80 Grade),
- Binder modified with a plastomeric polymer,
- Binders modified with three types of elastomeric polymer, and
- High-stiffness (pen. grade 21 @ 25°C) binder.

TABLE 3 Properties and Performance Data for Particle Shape and Gradation Experiment

Segment	Angular Particles (%)	n	Maximum Surface Rebound (mm)	Maximum Surface Rut Depth (mm)	Subgrade Dry Density (kg/m^3)	Subgrade Deformation (mm)	Basecourse m/c (%)	Basecourse Dry Density (kg/m^3)
A	0	0.6	--	--	2190	--	--	2060
B	0	0.5	--	--	2160	--	--	2060
C	0	0.4	--	--	2200	--	--	2070
D	100	0.4	1.6	25	2210	10	2.7	1930
E	100	0.5	1.7	36	2250	10	2.7	1990
F	100	0.6	1.6	18	2210	7	2.7	1920
G	50	0.5	1.3	28	2280	7	2.4	2080
H	70	0.5	1.9	14	2220	8	2.9	2040
I	30	0.5	--	--	2240	--	2.2	2090

-- The surfaces of Segments A, B, C and I could not be compacted properly for surfacing

The surface deflection bowls, the vertical strains at various depths in the pavement and subgrade, longitudinal and transverse profiles, and temperatures in the bottom of the asphalt layer and in the base course were measured after specified intervals of loading cycles. A falling weight deflectometer was also used to measure the pavement structural capacity for the first part of the experiment. Data collected at CAPTIF were electronically transmitted daily to British Petroleum International in England. The wheel load was 40 kN for both vehicles for the first 920,000 loading cycles and 46 kN for the remaining 1.2 million loading cycles. The dual radial tires in both vehicles were inflated to 700 kPa, and the vehicle speed was 40 km/hr. Altogether, SLAVE applied 3.2 million EDAs to the test pavements. Details of the project and results are provided elsewhere (*15*). The rut depth was only 4 mm, indicating negligible compaction in the subsurface layers. The project concluded before the predefined failure criterion of a maximum surface rut depth of 25 mm occurred because the pavement design was conservative (pavements designed for 1×10^6 EDA should have exhibited greater deterioration after 3.2×10^6 EDA) and because the project costs exceeded the budgeted funds. The test sections exhibited negligible deterioration in their structural condition and minimal surface distress. It was concluded that the thinner asphalt concrete layers constructed with modified binders and the high-stiffness binder provided performance equivalent to that of the thicker layer containing a conventional binder (*15*).

Dynamic Wheel Forces and Pavement Wear

The objective of the current research program (1992–1997) is to compare the pavement deterioration caused by dynamic loads generated under different types of suspensions: steel parabolic leaf spring and shock absorber, multileaf steel suspension, and air bag suspension with shock absorber. By using the accelerometers and displacement transducers fitted to the SLAVE vehicles, vertical dynamic loads created by the vehicle bounce are related to subsur-

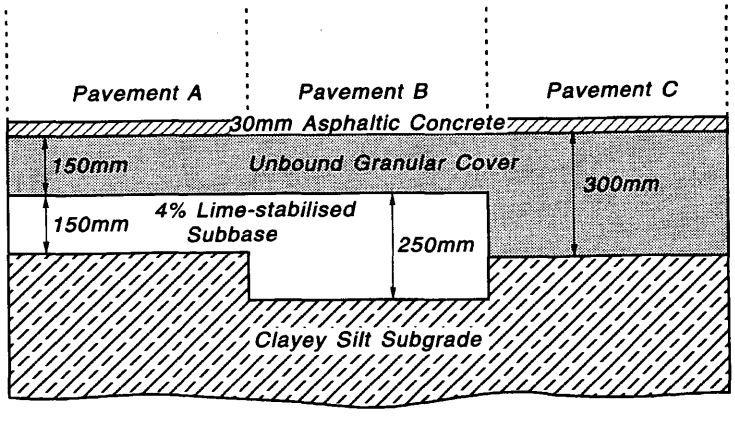

FIGURE 5 Cross section of pavements with lime-stabilized subbases.

TABLE 4 Properties and Performance Data for Lime-Stabilized Subbase Experiment

		Pavement Design		
		A	B	C
Subbase Dry Density (kg/m^3)		1490 ± 5%	1540 ± 4%	--
Moisture Content at Construction (%)		23.5	24.5	--
Basecourse Dry Density (kg/m^3)		2100 ± 2%	2070 ± 2%	2095 ± 2%
Moisture Content at Construction (%)		4	5	5
Surface Deflection[a] before Loading (mm)		4.5	1.4	9.7
Surface Deflection[a] at Failure (mm)		8.5	6.0	9.7
Cycles to Failure (21 kN wheel Load)		4400	30500	30
Asphaltic Concrete Mix				
Asphalt Binder Content (%)	6.5			
Bulk Density (kg/m^3)	2242			
Air Voids (%)	7.0			
Marshal Stability (kN)	15.36			
Marshal Flow (mm)	2.8			

[a] Benkelman Beam deflection test with 21 kN wheel load

face strains and longitudinal surface profiles measured by the DIP-Stick profiler and a laser device mounted on one vehicle. Altogether, five pavements will be constructed and tested sequentially. Sufficient subgrade soil and base course aggregate were procured for five pavements and have been stockpiled to ensure that the material properties of the pavement are the same for each suspension. The base course aggregate of well-graded crushed gravel was produced to stringent specifications (*13*) using a portable aggregate blending plant.

SUMMARY AND CONCLUSIONS

The development and operation of the CAPTIF, including SLAVE and the instrumentation systems, have been described. Research projects conducted since 1986 have been discussed, and the significant results were presented.

The CAPTIF SLAVE was designed to generate realistic dynamic wheel loads instead of attempting to eliminate them. The SLAVE vehicles that apply the loads are fitted with suspensions based on actual heavy vehicle components.

The facility has been beneficial in evaluating the performance of aggregates and pavement design assumptions by collecting data describing the long-term performance of pavements and investigating the relationship between vehicle loading conditions and the deterioration of pavements for a wide spectrum of pavement and loading characteristics.

ACKNOWLEDGMENTS

CAPTIF is owned by Transit New Zealand and operated by the University of Canterbury. The author acknowledges the financial support of Transit New Zealand, British Petroleum International, the New Zealand University Grants Committee, and the University of Canterbury for the research described in this paper. Firestone Tires New Zealand provided the tires. Ian Wood Associates provided the design details for SLAVE. The author is grateful to A. W. Fussell for contributions to the research described.

REFERENCES

1. Dunlop, R. J. Some Aspects of Pavement Design and Performance for Low-Volume Roads in New Zealand. In *Transportation Research Record 702*, TRB, National Research Council, Washington, D.C., 1979, pp. 47–54.
2. Brown, T. J. The Maintenance and Rehabilitation of Sealed Rural Roads. In *Transportation Research Record 1106*, TRB, National Research Council, Washington, D.C., 1987, pp. 175–187.
3. *State Highway Pavement Design and Rehabilitation Manual*, Transit New Zealand, Wellington, 1987.
4. *Shell Pavement Design Manual.* Shell International Petroleum Co. Ltd., London, England, 1978.
5. Williman, A., and W. D. O Paterson. A Track for the Accelerated Testing of Highway Pavements. *New Zealand Engineering*, Vol. 26, No. 3, 1971, pp. 73–77.
6. *Full-Scale Pavement Tests.* Road Transport Research Programme, Organization for Economic Cooperation and Development, Paris, France, 1985.
7. Shackel, B. *The Heavy Vehicle Simulator System in South Africa.* Report RP/3/80. National Institute of Traffic and Road Research, Pretoria, 1980.
8. Sparks, G. H., and J. B. Metcalf. *Full-Scale Pavement Test Facility.* Internal Report 329-1. Australian Road Research Board, Melbourne, 1980.
9. Brown, S. F., and B. V. Brodrick. *Instrumentation for Monitoring the Response of Pavements to Wheel Loading.* Sensors in Highway and Civil Engineering, Institution of Civil Engineers, London, England, 1981, pp. 118–129.

10. Pidwerbesky, B. D. Inaugural Project At New Zealand's Modern Pavement Testing Facility. In *Proc., Australian Road Research Board Conference*, Canberra, Vol. 14, No. 8, 1988, pp. 1–7.
11. Pidwerbesky, B. D., and R. W. Dawe. *Relative Rutting Effect of Different Tire Types.* Civil Engineering Report 90-7. University of Canterbury, Christchurch, New Zealand, 1990.
12. *Construction of Unbound Granular Pavement Courses.* Specification B/2. National Roads Board, Wellington, New Zealand, 1987.
13. *Crushed Basecourse Aggregate.* Specification M/4. National Roads Board, Wellington, New Zealand, 1987.
14. Owiro, A. O., and B. D. Pidwerbesky. *CAPTIF Project Four: Lime Stabilised Sub-Bases.* Civil Engineering Report 90-10. University of Canterbury, Christchurch, New Zealand, 1990.
15. Stock, A. F., L. Planque, and B. Gundersen. Field and Laboratory Evaluation of Specialist High Performance Binders. In *Proc., 7th Intl. Conf. on Asphalt Pavements*, Vol. 2, Nottingham, England, 1992, pp. 323–337.

Publication of this paper sponsored by Committee on Flexible Pavement Design.

Strain Response and Performance of Subgrades and Flexible Pavements Under Various Loading Conditions

BRYAN D. PIDWERBESKY

Specific fundamental loading parameters (load magnitude and number of repetitions, tire inflation pressure, and basic tire type) that influence the behavior of thin-surfaced granular pavements were examined. The pavement response and performance measurements included continuous surface deflection basins, longitudinal and transverse profiles, and vertical strains in the granular layers and subgrade. The first pavement trial considered only the elastic response of a thin-surfaced, unbound granular pavement over a weak subgrade, to varying wheel loads, tire inflation pressures, and two basic tire types (bias and radial ply). The axle load had the greatest effect on pavement response and the tire type had no apparent effect, but increases in the tire pressure resulted in slight decreases in the magnitude of the vertical compressive strain in the subgrade and unbound granular cover. Two subsequent pavements were tested to study the relationship between elastic response at different cumulative loadings and the structural capacity of each pavement. The magnitudes of the resilient strains measured are substantially greater than the levels predicted by the models on which current flexible pavement design procedures are based for the same number of loading repetitions to failure. Subgrade strain models for thin-surfaced unbound granular pavements are evaluated. The pavement construction, loading routine, analysis, and results are discussed.

The New Zealand model used for designing the thicknesses of thin-surfaced, unbound granular flexible pavement layers assumes that surface thicknesses of less than 35 mm do not contribute to the structural capacity of the pavement and that the stresses are dissipated through the depth of the granular cover layers above the subgrade. The subgrade strain criterion for flexible pavements in the *Shell Pavement Design Manual* (*1*),

$$\epsilon_{CVS} = 0.028\ N^{-0.25} \quad (1)$$

where ϵ_{cvs} is the vertical compressive strain in the subgrade, and N is the number of repeated equivalent single axle loads, is the basis of the New Zealand subgrade strain criteria for limiting rutting. The subgrade strain criteria for primary and secondary highways, respectively, in New Zealand are (*2*)

$$\epsilon_{CVS} = 0.021\ N^{-0.23} \quad (2)$$

$$\epsilon_{CVS} = 0.025\ N^{-0.23} \quad (3)$$

In New Zealand, the term for equivalent single-axle load is equivalent design axle (EDA). One EDA is defined as one passage of an 80-kN single-axle load on dual tires inflated to 550 kPa. Other axle loads are related to the reference axle by the fourth-power rule (the exponent is 4).

University of Canterbury, Private Bag 4800, Christchurch, New Zealand.

However, the flexible pavement design model is based on multilayer linear elastic theory and assumes that the pavement material properties can be characterized by linear elastic, homogeneous, and isotropic behavior, whereas, in reality, the behavior of unbound granular materials tends to be nonlinear, elastoplastic, nonhomogeneous, and anisotropic. Because of the unique situation in New Zealand, with respect to the road user charges incurred by the road transport industry and the dependence on thin-surfaced flexible pavements, research was needed to verify the subgrade strain criteria. The research described in this paper involved a series of instrumented pavements constructed in the Canterbury Accelerated Pavement Testing Indoor Facility (CAPTIF) and subjected to a variety of tire pressures, tire types, and loads.

DESCRIPTION OF FACILITY AND INSTRUMENTATION

The main feature of CAPTIF is the Simulated Loading and Vehicle Emulator (SLAVE), illustrated in Figure 1; the primary characteristics are summarized in Table 1. SLAVE "vehicles" are equipped with half-axle assemblies that can carry either single or dual tires. The configuration of each vehicle, with respect to suspensions, wheel loads, tire types, and tire numbers, can be identical or different for simultaneous testing of different load characteristics.

Electronic systems have been acquired or developed to measure subsurface strains and temperatures, transverse and longitudinal surface profiles, and pavement rebound. The CAPTIF deflectometer measures the surface rebound of a pavement under the influence of a wheel load to the nearest 0.01 mm every 50 mm of horizontal movement in much the same way as a Benkelman beam except that the former uses an electromagnetic gap-measuring sensor at the end of the beam to measure the vertical distance between the sensor and a target disk placed on the pavement surface. The CAPTIF profilometer measures the transverse surface profiles to an accuracy of ± 1 mm.

The soil strain measuring systems determine extremely small strains with high resolution using Bison soil strain sensors. The gauge length is the separation distance between each paired coil; strain (ϵ) is the quotient of the change in gauge length (ΔL) divided by the initial gauge length (L). The strain disks are installed during the formation of the subgrade and the overlying pavement layers, resulting in negligible disturbance to the materials. The strain disks have a diameter of 50 mm and are 7 mm thick.

Two data-acquisition systems for the Bison strain coils were used. In the interim system, all the coils in an array were connected

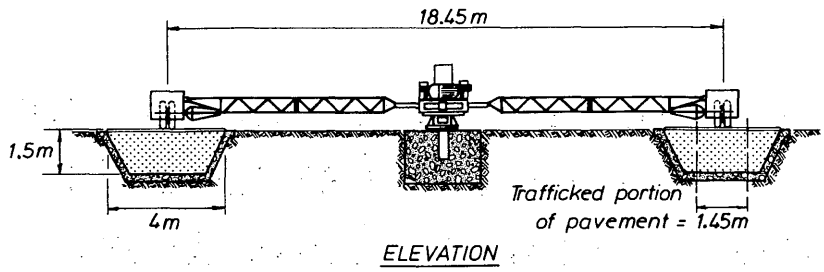

FIGURE 1 SLAVE and cross section of track.

to a manual switching apparatus. Then, the two leads from the switching apparatus were connected to a Bison soil strain gauge, Model 4101A, a single-channel linearizing monitor that supplied the alternating current to the transmitter coil and measured the output from the paired coil. The output voltages from the gauge and pavement temperature probes were recorded through the HP Model 3852S data-acquisition unit using an HP 44711A 24-channel FET multiplexer module. The output from the multiplexer was fed into a 13-bit digital voltmeter (HP 44702A). The data-acquisition unit stored the data in memory before downloading them to an HP PC308 controller board installed in an IBM-compatible AT. The error in the interim strain-measuring system was ±50 μm/m. Before installation, the sensors were calibrated to generate an output voltage versus separation distance relationship for each sensor configuration. During the loading routine, the normal sampling rate was 100 Hz, but the sampling rate increased to at least 10 kHz (depending on the vehicle speed) for a 0.5-sec period whenever triggered by the test vehicle cutting an infrared beam at the start of the instrumented pavement section.

The permanent system is a modified prototype of the more sophisticated Saskatchewan soil strain displacement-measuring (SSSD) system, developed by Saskatchewan (Canada) Highways and Transportation. SSSD is essentially a computer and associated units containing custom-built control, general-purpose input-output, transmitter, and receiver boards. Once triggered by the moving vehicles' cutting a light beam, all the sensors in an array are scanned simultaneously every 30 mm of vehicle travel, and a continuous bowl of strain-displacement versus distance traveled is obtained.

Dynamic wheel forces are dominated by the behavior of sprung mass, so the wheel forces are the sum of the vehicle mass multiplied by the chassis acceleration and the unsprung mass multiplied by the vertical axle acceleration. The dynamic loads were quantified by the vertical acceleration measured by PCB 308B accelerometers mounted on each vehicle. The piezoelectric accelerometers have a linear response from 1 to 3,000 Hz of 100 mV/g. The accelerometers were connected to a PCB 483A 12-channel signal conditioning unit, and the signals were recorded on a Hewlett-Packard 3968A instrumentation recorder. The analog signals were digitized using the HP 3852 data acquisition system sampling at 200 Hz per channel.

FULL-SCALE PAVEMENT INVESTIGATIONS

The experiment involved constructing three sequential test pavements at CAPTIF (Stages 1, 2, and 3). In Stage 1, the pavement response to the primary loading variables (load magnitude, tire inflation pressure, and basic tire type, all on dual-tired wheels) were measured. The final two stages involved testing the life-cycle performance of different pavements and subgrades under selected loading conditions.

Stage 1 Pavement Response to Different Loading Conditions

Initial tasks included selecting and developing instrumentation and data-acquisition systems and preparing the vehicles and track. The silty clay subgrade had a California bearing ratio (CBR) of 5 percent at its natural moisture content. The liquid limit and plasticity index were 43 and 23 percent, respectively. The base course aggre-

TABLE 1 Characteristics of SLAVE

Item	Characteristic
Test Wheels	Dual- or single-tires; standard or wide-base; bias or radial ply; tube or tubeless; maximum overall tire diameter of 1.06 m
Load of Each Vehicle	21 kN to 60 kN, in 2.75 kN increments
Suspension	Air bag; multi-leaf steel spring; single or double parabolic
Power drive to wheel	Controlled variable hydraulic power to axle; bi-directional
Transverse movement of wheels	1.0 m centre-to-centre; programmable for any distribution of wheelpaths
Speed	0-50 km/h, programmable, accurate to 1 km/h
Radius of Travel	9.1 m

SLAVE is designed to be operated continuously without supervision.

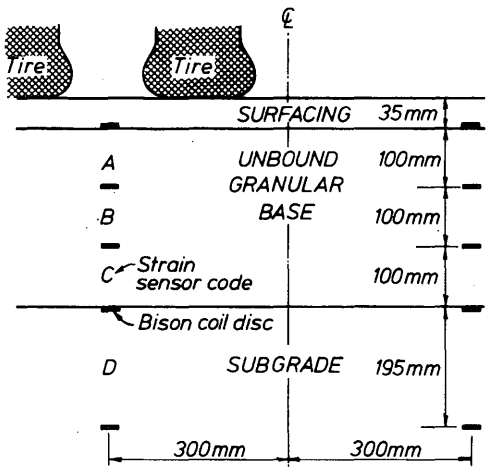

FIGURE 2 Array of strain coil sensors.

gate was a well-graded crushed river gravel (Canterbury greywacke) with a laboratory CBR of 80 percent. The moisture content during compaction was 5 percent. The surfacing was an asphalt concrete consisting of a graded aggregate (maximum particle size 10 mm), 6.4 percent bitumen, and 4.7 percent air voids. The penetration grade of the bitumen was 80/100. The bulk density and bulk specific gravity of the mix were 2 300 kg/m^3 and 2.306, respectively, and the mix temperature was 155°C. The Marshall stability and flow were 18.1 kN and 4.3 mm, respectively.

The bottom layer in the track consisted of a drainage layer of coarse gravel 150 mm thick covered with a nonwoven geotextile. On top of that was an 800-mm-thick layer of well-compacted loess. The bottom coil of each vertical strain sensor array was carefully positioned in the top of the loess. The subgrade layer of silty clay was placed and compacted to a 200-mm depth over the loess. All layers of the subgrade and the granular cover were spread by a small bulldozer and compacted by a Sakai SW41 (40-kN) dual drum roller.

The next set of strain sensors and a set of temperature probes were placed at the interface of the subgrade and granular cover layers. Then, a spunbonded polypropylene geotextile was placed over the subgrade to facilitate the determination of subsurface layer profiles following the testing routine. The granular cover was constructed in three 100-mm lifts, to aid compaction and to allow installation of the paired strain sensors at 100-mm gauge lengths without disturbing the materials. Each array of strain sensors was installed, as shown in Figure 2. Temperature probes were placed at two levels in the granular cover beside the strain coils.

In the uppermost 50 mm of the crushed rock base course, the maximum particle size was only 20 mm to aid workability and compaction. The surface of the base was finished with a pneumatic-tired roller, then a tack coat of emulsified bitumen (60 percent, 180/200 penetration grade) was sprayed. The asphalt concrete was placed, leveled by hand, and compacted. A 3-m straight-edge beam was used to check the roughness, and the maximum deviation was 4 mm. The thickness of the nonstructural surfacing was 35 mm (± 3 mm), which was too thin for inclusion of any instrumentation.

The dynamic characteristics of each vehicle were evaluated to confirm that they were similar. Dynamic wheel forces were measured at a constant speed of 40 km/hr. The vehicles exhibited similar dynamic characteristics, as shown in Table 2.

Vehicle A carried a constant half-axle load of 40 kN (equating to a full axle load of 80 kN) with dual bias ply tires inflated to 550 kPa, so that it was a reference throughout the testing routine. The characteristics of Vehicle B were modified. The maximum cold tire inflation pressures allowed by the tire supplier were 700 and 825 kPa for the bias and radial ply, respectively. All radial and bias ply tires were 10.00R20 and 10.00×20, respectively. The experimental matrix of loading conditions of Vehicle B is shown in Table 3.

The surface deflection bowls, and the vertical strains at various depths in the pavement and subgrade were measured for each of the 20 loading conditions. The strains were measured under the center of the dual tires. Longitudinal and transverse profiles were measured after specified increments of cumulative loading cycles. After the experimental matrix was completed, the maximum surface rut depth was only 7 mm; the deformation within the unbound granular pavement was 2 to 3 mm, which was insufficient to have affected the properties of the pavement.

Deflection basins were measured at three locations on the test section and averaged to determine one basin for each experimental point. The deflection basins were compared on the basis of (a) tire type, (b) tire inflation pressure, and (c) wheel load; neither tire type nor tire inflation pressure had a substantial effect on the deflection basin shape. In general, the peak deflection value was independent of tire type. Also, tire pressure had a negligible effect on the peak deflection. The major influence on peak deflection was the wheel load.

The vertical compressive strains were measured in three layers (upper base course, lower base, and subgrade) for each of the 20 loading conditions. The peak compressive strains are defined as the difference between the nominal average residual strain recorded before the approach of the test vehicle to the sensor and the maximum strain (averaged over five cycles) measured under the test vehicle. Figure 3 (*top*) shows a representative sample of the original data from the subgrade, for one specific loading condition (dual radial tires, inflated to 825 kPa and loaded to 40 kN). The longest

TABLE 2 Dynamic Load Coefficients (dlc)

Vehicle	Wheel Load (kN)	Tire Pressure (kPa)	Tire Type	dlc
A	40	580	Bias ply	0.22-0.24
B	40	580	Radial ply	0.22-0.24
B	46	825	Radial ply	0.16-0.18

$$\text{Dynamic load co-efficient (dlc)} = \frac{\text{Standard Deviation of Wheel Forces}}{\text{Static Load}}$$

TABLE 3 Sequence of Loading Conditions on Vehicle B

Bias ply Tires			Radial ply Tires		
Test No.	Pressure (kPa)	Wheel Load (kN)	Test No.	Pressure (kPa)	Wheel Load (kN)
1	550	40	9	825	46
2	700	40	10	700	46
3	700	21	11	550	46
4	550	21	12	550	31
5	550	31	13	825	31
6	700	31	14	700	31
7	700	46	15	700	21
8	550	46	16	550	21
			17	825	21
			18	825	40
			19	700	40
			20	550	40

spikes represent the passage of a wheel load directly over the sensors, and the lessor spike is the passage of the reference wheel load (dual bias ply type inflated to 550 kPa and loaded to 40 kN) at a transverse distance of 0.6 m. For every loading condition and strain measurement in the subgrade, some vertical compression remained after the passage of each wheel load. Then, when the other wheel load passed over the station, the compression disappeared and the subgrade reverted to the original situation. This phenomenon was repeated for all loading cycles.

If it was simply a case of the paired coil disks becoming misaligned, the effect would have increased with cumulative cycles; but this did not occur. Instead, the subgrade was compressed when one wheel load passed directly over the sensor, then shear forces created by the other wheel load traveling in a wheel path 0.6 m away laterally resulted in extension in the layer, and the sensor returned to its original position. Similarly, in the base course, the residual compression induced by one vehicle passing directly over the sensors was eliminated by extension as the other vehicle passed over a point 0.6 m away transversely, but there was no discernible resilient compression as the second vehicle passed over, as shown in Figure 3 (*bottom*). This cyclic compression and extension contributed little to the permanent deformation of the layers, which is the primary criterion for the model describing the performance of thin-surfaced unbound granular pavements, but could affect the degradation of the materials.

The magnitude of the vertical compressive strain in the subgrade and the base course (Figure 4) decreased slightly as the tire inflation pressure increased, for every wheel load. The vertical compressive strain in the granular layers and the subgrade must be dependent upon the zone of influence of the load as well as the contact area and speed of the vehicle. Thus, when the speed is constant and the contact area is reduced, at higher tire inflation pressures, the zone of influence of the load in the pavement and subgrade is reduced, thereby reducing the strain induced in the subgrade in the same manner as strain magnitude reduces under increasing vehicle speed.

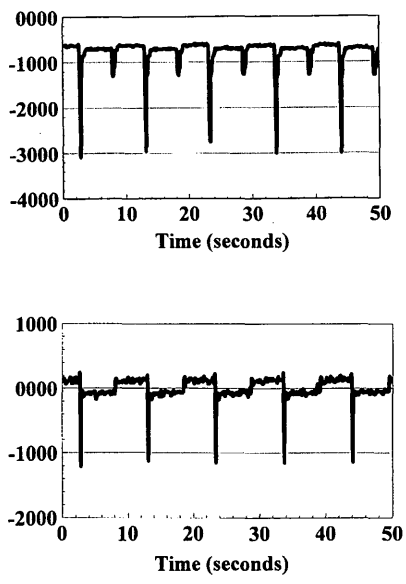

FIGURE 3 Vertical compressive strain (10E = 06) in subgrade (*top*) and base course (*bottom*) under dual radial-ply tires, 825 kPa cold tire pressure, and 40 kN wheel load.

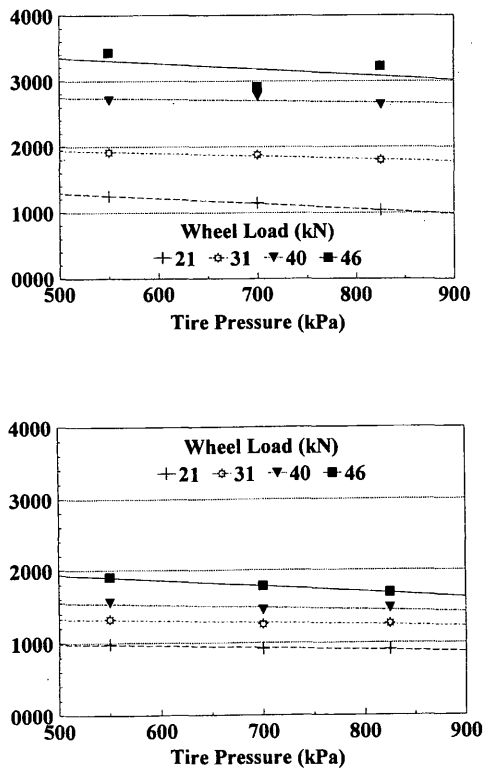

FIGURE 4 Vertical compressive strain (10E = 06) in subgrade (*top*) and base course (*bottom*) under a dual-tired wheel.

Relating Pavement Response to Performance

The objectives of Stages 2 and 3 were to use the system developed in Stage 1 to relate axle loads directly to pavement responses for predicting pavement performance.

Stage 2. Performance of Unbound Granular Base Course Under Thick Asphalt Surface

The Stage 2 pavement had an asphalt concrete surface 85 mm thick (which is thick by New Zealand standards), over a 200-mm unbound granular base course over a clayey subgrade. The in situ CBR of the subgrade for the test section was 13 percent; the subgrade was constructed to achieve a higher bearing capacity (than the Stage 1 subgrade) to achieve a longer pavement life. The base course aggregate was a well-graded crushed river gravel compacted with a moisture content of 4 percent to a maximum dry density of 2 150 kg/m^3. The asphaltic binder was a plastomer-modified bitumen called Practiplast, with a penetration grade of 50 (at 25°C), a softening point of 59.4°C, a viscosity of 2 P (at 169°C), and a shear susceptibility of −0.089 (*3*).

The wheel load was 40 kN for both vehicles for the first 920,000 loading cycles and 46 kN for the remaining 1.2 million loading cycles. The dual radial tires in both vehicles were inflated to 700 kPa. The vehicle speed was 40 km/hr for routine loading and 20 km/hr for the approximately 500 cycles required for completing the strain measurements. The vertical compressive elastic strains in the unbound granular base course and clayey subgrade were measured using arrays of Bison strain coil gauges installed in the subgrade and base course. Altogether, SLAVE applied over 3.2 × 10^6 EDA to the test pavement.

The rut depth at the surface of the test section was only 2 to 4 mm, indicating negligible deformation in the subsurface layers. Surface cracking was insignificant. The project concluded before the predefined failure criterion of a maximum surface rut depth of 25 mm occurred because the maximum allowable overexpenditure on the project was reached (substantial additional research funds were provided) and the next project in the facility had to commence. Stage 2 was conducted simultaneously with another project in the track investigating the effect of different modified binders on the performance of asphalt concrete surface layers, which is reported elsewhere (*3*). It was concluded that the design procedure used was conservative because pavements designed for 1 × 10^6 EDA should have exhibited greater deterioration after 3.2 × 10^6 EDA (*3*). However, according to the New Zealand pavement design procedure (*2*), the pavement had an expected design life of at least 5 × 10^6 EDA.

In the base course, the magnitude of the peak vertical compressive strain decreased slightly during the cumulative loading, from 300 to 220 μm/m. The relationship between the magnitude of the vertical compressive subgrade strain and cumulative loading is shown in Figure 5. The temperatures are the averaged output of the three temperature probes installed directly above the strain sensors in the 85-mm-thick asphalt concrete. Increasing the wheel load from 40 to 46 kN, after 920,000 EDA, resulted in a negligible change in the magnitude of the vertical compressive strain responses in the subgrade (from 1 200 to 1 250 μm/m) and no change in the base course strain. In Stage 1 of this research program, the same increase in wheel load produced a 10 percent increase in the magnitude of the vertical compressive strain in a weak subgrade (CBR of 4 percent under a thin-surfaced, 300-mm unbound granular pavement).

The nominal magnitude of the vertical compressive strain in the subgrade varied between 900 and 1 400 μm/m, and the pavement survived 3.2 × 10^6 EDA without incurring any substantial permanent deformation in the pavement or subgrade. When the temperature of the asphalt concrete decreased thereby increasing the asphalt modulus, the subgrade strain decreased because the stiffer asphalt is more effective in dissipating the stresses from the wheel load.

The AUSTROADS (Australian) subgrade strain criterion (*4*), converted to the same format as Equation 1, is

$$\epsilon_{CVS} = 0.0085\, N^{-0.14} \quad (4)$$

Using Equations 1, 2, and 4, the maximum allowable vertical compressive strain in the subgrade would have been 660, 670, and 1045 μm/m, respectively, for that number of loading cycles, assuming that the pavement would have failed at that point. The Shell and New Zealand subgrade strain criteria (Equations 1 and 2, respectively) are definitely conservative, but the AUSTROADS criterion permits higher strains, which are within the range of the actual strain values measured in this case. Also, the lack of adverse environmental effects would have contributed to extending the life of the pavement.

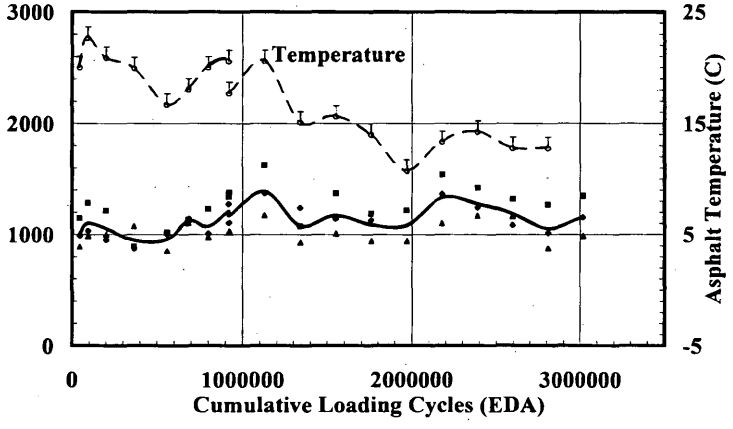

FIGURE 5 Vertical compressive strain (10E = 06) in subgrade under Stage 2 pavement (temperature measured at mid-depth of asphalt layer).

Stage 3. Life-Cycle Performance of Thin-Surfaced Unbound Granular Pavement

The test pavement for this trial consisted of a 25-mm asphalt concrete surfacing layer over 135-mm-thick base course of unbound granular aggregate on a silty clay subgrade of CBR 13 percent; the material properties are the same as those described. The pavement responses and properties were measured as previously described. The pavement was subjected to a constant loading condition (40-kN load and dual radial tires inflated to 825 kPa) until the loading concluded at 740,000 EDA, when the permanent vertical deformation (rut depth) of the surface reached 28 mm (the definition of failure was a maximum rut depth of 25 mm).

The maximum rut depths over the whole pavement were in the range of 15 to 28 mm. In the excavated trenches, the asphalt concrete surfacing and base course of unbound aggregate compacted 8 and 7 mm, respectively, at the centerline under the cumulative loading. The permanent deformation in the subgrade varied between 1 and 13 mm. Most (75 percent) of the permanent deformation occurred in the first 100,000 EDA, then the rutting progressed at a relatively constant rate of 9 μm per loading cycle (one loading cycle equals one EDA). The only significant difference in the longitudinal surface profiles before loading commenced and at the end of the trials was where a localized failure was repaired.

The peak surface deflection was approximately 1.6 mm throughout the life of the pavement, except for a temporary 0.15-mm increase in surface deflection that occurred between 100,000 and 200,000 cumulative EDA. The deflection bowl shapes were the same temporally as well, indicating that the relative moduli of the various layers did not change.

Figure 6 (*top*) illustrates how, after the initial sharp increase in magnitude in the peak vertical compressive strain in the subgrade (ϵ_{cvs}), the strain under cumulative loading varied little, except for the significant decrease at 220,000 EDA. The magnitude of the peak vertical compressive strain in the base course slowly decreased during the first 300,000 loading cycles, from 3 200 to 2 350 μm/m, then remained relatively constant, as shown in Figure 6 (*bottom*).

Until approximately 300,000 EDA, surface deflections and vertical compressive strain levels in the base course and subgrade layers fluctuated. The base course strain levels tended to decrease in magnitude. The magnitude of the subgrade strain tended to increase, until the pavement and subgrade responses achieved a stable condition, with only minor fluctuations in the response to load.

Using Equations 2 and 4, the maximum allowable vertical compressive strains in the subgrade for 740,000 EDA are 940 and 1 280 μm/m, respectively, which are substantially less than the actual strains of approximately 2 800 μm/m. Table 4 shows that the actual strains are two to three times the theoretical maximum strain magnitude allowed by the different criteria, which suggests that the criteria on which the pavement thickness design charts are based could be conservative. However, as before, the strain permitted by the AUSTROAD subgrade criterion (Equation 4) for 740,000 EDA is closer to the measured strains, as shown in Figure 7.

Similar results from a field study involving a privately owned sealed forestry road on the North Island of New Zealand were reported (*5*). In the field study, an instrumented thin-surfaced unbound granular pavement carried logging trucks with axle loads varying from 80 to 160 kN per axle. The strain responses were measured using Bison strain sensors installed in the base course and subgrade. It was found that the strains induced in the subgrade were as much as four times the strains allowed by the subgrade strain criterion, but the pavement performance was acceptable (*5*).

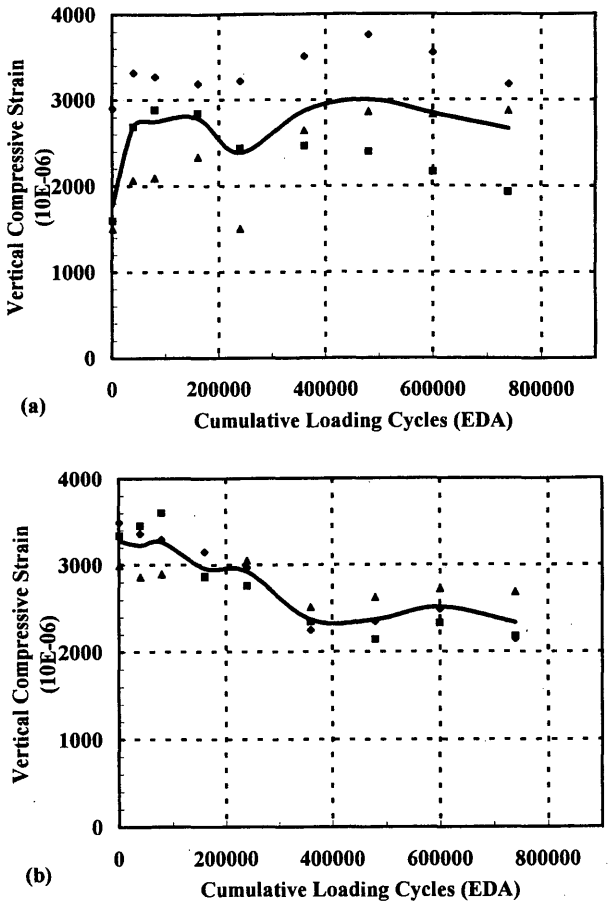

FIGURE 6 Vertical compressive strain (10E = 06) in subgrade (*top*) and base course (*bottom*) under Stage 3 pavement.

CONCLUSION

CAPTIF was used to investigate the fundamental behavior of subgrades and unbound granular pavements under various loading conditions. An electronic-based data-acquisition system for accurately measuring strains in unbound granular layers and subgrades has been developed and used successfully in a number of projects. Instead of relying on simplistic relationships between static axle loads and performance, fundamental pavement responses can be measured for input to pavement performance prediction models. Any procedures for determining load equivalency factors must also consider the type of pavement and the bearing capacity of the subgrade.

With respect to pavement and subgrade response to loading and for the specific conditions of the investigation, the tire type (10.00R20 radial and 10.00×20 bias ply) had an insignificant effect, and the tire inflation pressure (between 550 and 825 kPa) had a minor effect. The vertical compressive strain in the subgrade and unbound granular layers of the pavement decreased slightly as the tire pressure increased.

The magnitude of the vertical compressive strain in the subgrade increased initially, then remained relatively constant. The vertical

TABLE 4 Allowable Vertical Compressive Strain Models Compared with Actual Values

Pavement Number	Number of Load Repetitions (EDA)	Maximum Allowable Vertical Compressive Strain (μm/m) in the Subgrade:				
			New Zealand			Actual (Nominal Value)
		Shell[a]	Primary[b]	Secondary[c]	Australian[d]	
1[e]	3200000	660	670	800	1045	1200
2[f]	740000	955	940	1115	1280	2800

[a] Equation (1)
[b] Equation (2)
[c] Equation (3)
[d] Equation (4)
[e] 85 mm asphalt surface, 200 mm unbound granular basecourse, silty clay subgrade CBR 13%
[f] 25 mm asphalt surface, 135 mm unbound granular basecourse, silty clay subgrade CBR 10%

compressive strain in the unbound base course aggregate tended to decrease slightly in magnitude under cumulative loading; the base course aggregate compacted under repetitive loading and reached a stable condition. The relationship between vertical compressive strains and the cumulative loadings became stable after the pavement was compacted under initial trafficking (in the absence of adverse environmental effects).

The strain magnitudes measured are greater than the levels permitted by the four subgrade strain criteria evaluated; the criteria are intended to govern the allowable vertical compressive strain in the subgrade, to ultimately limit pavement rutting. The subgrade strain criteria are conservative, but the AUSTROADS criteria were the closest to the actual results.

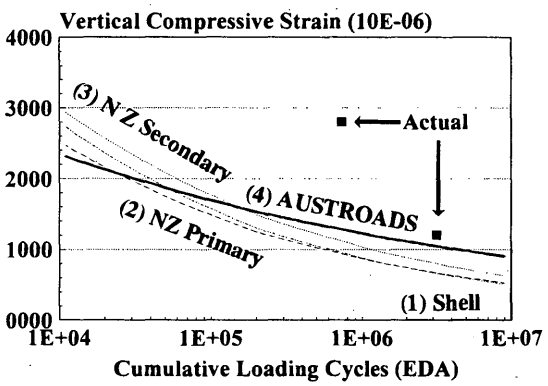

FIGURE 7 Comparison of four subgrade strain criteria governing rutting in flexible pavements.

ACKNOWLEDGMENTS

The author acknowledges the financial support of Transit New Zealand and the University of Canterbury in sponsoring this research project. The author is grateful to A. W. Fussell and G. Crombie for their assistance and to J. de Pont of Industrial Research Limited, Auckland, for analyzing the vertical acceleration data from the SLAVE vehicles. The tires were supplied by Firestone Tires New Zealand Ltd.

REFERENCES

1. *Shell Pavement Design Manual.* Shell International Petroleum, London, England, 1978.
2. *State Highway Pavement Design and Rehabilitation Manual.* National Roads Board, Wellington, New Zealand, 1989.
3. Stock, A. F., L. Planque, and B. Gundersen. Field and Laboratory Evaluation of Specialist High Performance Binders. *Proc., 7th International Conference on Asphalt Pavements,* Vol. 2, Nottingham, England, 1992, pp. 323–337.
4. *Pavement Design—A Guide to the Structural Design of Road Pavements.* AUSTROADS, Sydney, Australia, 1992.
5. Steven, B. D. *The Response of an Unbound Granular Flexible Pavement to Loading by Super-Heavy Vehicles.* Master's thesis. University of Canterbury, Christchurch, New Zealand, 1993.

Publication of this paper sponsored by Committee on Flexible Pavement Design.

Comparison of AASHTO and ROADHOG Flexible Pavement Overlay Design Procedures

KEVIN D. HALL AND QUINTIN B. WATKINS

A comparison of the ROADHOG and AASHTO (1993) overlay design procedures for conventional flexible pavements is presented. Both procedures use a structural deficiency approach to overlay design yet differ in the methods used to estimate the effective structural number of an existing pavement and to estimate the in situ subgrade resilient modulus. Both methods use pavement surface deflections to backcalculate or estimate required design parameters. Specific comparisons include backcalculated subgrade resilient modulus, effective structural number, and recommended overlay thickness for a number of conventional flexible pavement configurations. Pavement surface deflections are generated using the ILLI-PAVE finite-element pavement model and the ELSYM5 elastic layer model. Pavement parameters varied to establish the deflection data base, including asphalt concrete surface thickness and resilient modulus, base course thickness and resilient modulus, and subgrade resilient modulus. The comparisons show that the AASHTO overlay design procedure recommends thicker overlays than does the ROADHOG procedure for pavements overlying relatively stiff subgrade soils. The difference in recommended overlay thickness is linked to differences in the estimates of both SN_f, the structural number required to carry future traffic, and SN_{eff}, the effective structural number of the existing pavement. The two design procedures recommend similar overlay thicknesses for pavements overlying soils with relatively low resilient modulus values. The analyses also show that the backcalculated value of subgrade resilient modulus plays a larger role in determining the overlay thickness for the AASHTO procedure than for the ROADHOG procedure.

The 1986 *AASHTO Guide for Design of Pavement Structures* (*1*) contains a framework for developing a structural overlay design procedure for flexible pavements but does not contain a complete design procedure. Subsequent development of AASHTO overlay design principles (*2*) resulted in the inclusion of a complete flexible pavement overlay design procedure in the 1993 AASHTO guide (*3*). The procedure contained in the 1993 guide is based somewhat on pavement surface deflections measured by a nondestructive testing device, such as the falling weight deflectometer (FWD) and elastic layer theory.

ROADHOG is a deflection-based structural overlay design procedure for flexible pavements developed in 1989 at the University of Arkansas for the Arkansas Highway and Transportation Department (AHTD) (*4*). AHTD designs new pavements using AASHTO procedures. ROADHOG was developed to be compatible with AHTD new-pavement design practices; thus, the structural pavement design concepts in ROADHOG are compatible with AASHTO flexible pavement design. ROADHOG was developed around the framework contained in the 1986 AASHTO guide but differs in its approach to determining the structural number of the existing pavement and the in situ subgrade resilient modulus.

This paper presents some results of a comparison between the flexible pavement overlay design procedures contained in the 1993 AASHTO guide and in ROADHOG. The overlay design parameters compared include the effective structural number of the existing flexible pavement (SN_{eff}), the resilient modulus of the roadbed soil (M_R), and their respective effects on resulting overlay thickness. Surface deflection basins are generated using the ILLI-PAVE finite-element structural model (*5*) and the ELSYM5 elastic layer model (*6*). Deflection basins are generated for conventional flexible pavements [asphalt concrete (AC) surface, granular base, subgrade] with varying AC and granular base layer thicknesses and resilient moduli, and varying subgrade moduli.

FLEXIBLE OVERLAY DESIGN: STRUCTURAL DEFICIENCY APPROACH

Both the AASHTO and ROADHOG procedures use a structural deficiency approach to flexible pavement overlay design. Before looking at comparisons of the two procedures, it is useful to briefly review the structural deficiency concept.

AASHTO pavement design procedures use a structural number (SN) to express the structural capacity of a flexible pavement. The structural number of a pavement layer is determined by multiplying the thickness of the layer (d_i) by a layer coefficient (a_i), which is usually based on some measure of the layer material's strength or stiffness. The structural number of the pavement is determined by summing the individual SNs of the pavement layers, as shown in Equation 1.

$$SN = a_1d_1 + a_2d_2 + \ldots + a_nd_n \quad (1)$$

where

SN = structural number of the pavement,
a_n = layer coefficient of layer n, and
d_n = thickness of layer n.

Within the structural deficiency approach, the structural capacity required of the overlay is equal to the difference between the total structural capacity required to carry future traffic and the structural capacity of the existing pavement. For flexible pavements, this concept is expressed in Equation 2.

$$SN_{ol} = SN_f - SN_{eff} \quad (2)$$

Department of Civil Engineering, 4159 Bell Engineering Center, University of Arkansas, Fayetteville, Ark. 72701.

where

SN_{ol} = structural number required for the overlay,
SN_f = structural number required to carry future traffic, and
SN_{eff} = effective structural number of the existing pavement.

The thickness of the overlay is determined by rearranging the structural number equation (Equation 1) for a single layer.

$$d_{ol} = \frac{SN_{ol}}{a_{ol}} \tag{3}$$

where

d_{ol} = thickness of overlay,
SN_{ol} = structural number of overlay, and
a_{ol} = layer coefficient of overlay material.

The major differences in design procedures fully using the structural deficiency approach can be related to the specific methods used to estimate the effective structural number of the existing pavement (SN_{eff}) and the specific methods used to determine the structural number required to carry future traffic (SN_f). Both the ROADHOG and AASHTO procedures use the AASHTO new-pavement design method to determine SN_f, differing only by the method used to estimate the resilient modulus of the roadbed soil. A comparison of the two procedures, then, focuses on the respective methods of estimating SN_{eff} and M_R.

FLEXIBLE OVERLAY DESIGN: ROADHOG DESIGN PROCEDURE

A complete description of the ROADHOG overlay design procedure is given elsewhere (*7*). The methods used by ROADHOG to estimate SN_{eff} and M_R are briefly described here.

Determination of SN_{eff}

The methodology used in ROADHOG for estimating the effective structural number of a flexible pavement was developed (*8*). The methodology uses two pavement surface deflections: (a) the deflection directly beneath the load, where it is assumed that the surface deflection is due to deflections within all paving layers and the subgrade, and (b) a deflection at some radial distance from the load (in the case of ROADHOG, a distance equal to the pavement thickness), where it is assumed that the surface deflection is due entirely to deflection within the subgrade. It was suggested that the difference between these two deflections, termed "delta-D," could be used as a measure of pavement stiffness (*8*). AASHTO methodology assumes SN_{eff} to be a function of the pavement stiffness; using this assumption, SN_{eff} can be expressed in terms of delta-D.

The SN_{eff} of a number of conventional flexible pavement configurations to the deflection difference delta-D is given elsewhere (*8*). Deflection basins were generated using the ELSYM5 elastic layer model (*8*). SN_{eff} was estimated using component analysis, in which each paving layer was assigned a typical layer coefficient based on its input elastic modulus, and the structural number calculated according to Equation 1. Figure 1 shows the relationship between SN_{eff} and delta-D for various pavement thicknesses. Note the relationship shown in Figure 1 is primarily a function of total pavement thickness; subgrade resilient modulus is not explicitly considered.

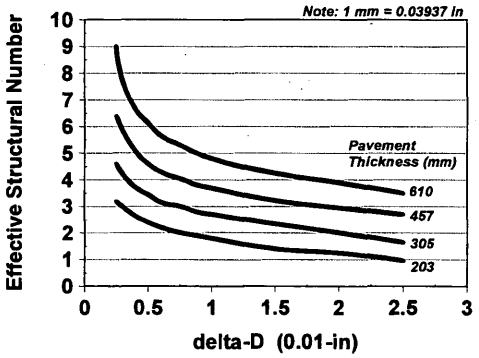

FIGURE 1 Delta-D/SN_{eff} relationship used in ROADHOG (*8*).

Determination of M_R

To calculate the SN required to carry future traffic (using AASHTO new pavement design procedures), an estimate must be provided of the roadbed soil (subgrade) resilient modulus. ROADHOG estimates M_R using a single pavement surface deflection, measured at 914 mm (36 in.) from the load. M_R is calculated by regression equations developed in a work by Elliott and Thompson from data generated by the ILLI-PAVE finite-element model (*9*). For illustrative purposes, the regression equation used for conventional flexible pavements with more than a 76-mm (3-in.) AC surface is shown as Equation 4.

$$E_{Ri} = 25.0 - 5.25 * D_{36} + 0.29 * D_{36}^2 \tag{4}$$

where

E_{Ri} is the breakpoint resilient modulus of the subgrade soil (ksi), and D_{36} is the pavement surface deflection at 36 in. (914 mm) from the load (mils).

FLEXIBLE OVERLAY DESIGN: AASHTO PROCEDURE

A complete description of the AASHTO flexible pavement overlay design procedure is found in the 1993 AASHTO guide (*3*). Additional information concerning the development of specific methodologies used in the AASHTO procedure can be found elsewhere (*2*). The AASHTO methodologies used for estimating SN_{eff} and M_R are briefly described here. Because M_R is used in the SN_{eff} determination, the procedure for estimating M_R is discussed first.

Determination of M_R

The procedure recommended by AASHTO for backcalculating the resilient modulus of the subgrade soil is based on a method proposed in a work by Ullidtz (*10*). The concept includes two basic assumptions: (a) at some radial distance from the load, the pavement deflection measured at the surface is equal to the deflection at the top of the subgrade, and (b) as radial distance from a load increases, the approximation of a distributed load by a point load

improves. These two assumptions allow a deflection to be estimated by the Boussinesq equation for a one-layer system. After rearranging the Boussinesq equation to solve for the elastic modulus and assuming a Poisson's ratio of 0.5 for the subgrade soil, the equation recommended in the 1993 AASHTO guide for estimating M_R is obtained.

$$M_R = \frac{0.24 * P}{d_r r} \quad (5)$$

where

M_R = resilient modulus of subgrade soil,
P = applied load,
d_r = deflection at radial distance r from load, and
r = radial distance from load.

Equation 5 is recommended only for deflections measured at radial distances greater than 0.7 times the effective radius of the stress bulb at the subgrade-pavement interface (a_e).

Determination of SN_{eff}

The AASHTO approach to determining the effective structural number of an existing pavement is based on the premise that the structural capacity of a pavement is implicitly related to the pavement's stiffness. The 1986 AASHTO guide (Appendix NN) uses this premise in developing an equal stiffness approach to determining SN_{eff} (*11*). The 1993 AASHTO guide follows a simplified version of this general approach. In the 1993 guide, SN_{eff} is related to the total pavement thickness and the effective modulus of the total pavement structure.

$$SN_{eff} = 0.0045 * D * \sqrt[3]{E_p} \quad (6)$$

where

SN_{eff} = effective structural number of pavement,
D = total pavement thickness (surface, base, subbase) (in.), and
E_p = effective modulus of pavement (psi).

Equation 7 is used to estimate the pavement's effective modulus (E_p). The method for estimating E_p is based on the Boussinesq deflection equation, with subsequent development by Odemark and Barber. A complete description of the development of Equation 7 is given elsewhere (*2*).

$$d_0 = 1.5pa \left\{ \frac{1}{M_R \sqrt{1 + \left(\frac{D}{a}\sqrt[3]{\frac{E_p}{M_R}}\right)^2}} + \left[1 - \frac{1}{\sqrt{1 + \left(\frac{D}{a}\right)^2}} \right] \frac{1}{E_p} \right\} \quad (7)$$

where

d_0 = maximum pavement surface deflection,
p = load plate pressure,
a = load plate radius,
M_R = resilient modulus of subgrade soil,
D = total pavement thickness, and
E_p = effective pavement modulus.

In the AASHTO method, the stiffness of the pavement (E_p) is a function of the stiffness of the subgrade (M_R), the loading characteristics (plate radius and pressure), the thickness of the pavement (D), and the maximum surface deflection. With a known surface deflection, an iterative process is performed to find the pavement modulus.

DATA ANALYSIS

Comparisons of the ROADHOG and AASHTO deflection-based overlay design procedures are performed using conventional flexible pavement configurations. Table 1 shows the parameters varied to establish the deflection data base. Pavement surface deflection basins are generated using the ILLI-PAVE finite-element model and the ELSYM5 elastic layer model. In the ELSYM5 model, all materials (AC, base, subgrade) are considered to be linear elastic, using the resilient modulus values shown in Table 1. The granular base and subgrade soil were modeled in ILLI-PAVE as stress dependent materials, using parameters taken from studies by Elliott and Thompson (*9*).

Overlay design factors directly compared include M_R and SN_{eff}. A brief presentation of the comparison results for each of the factors follows. The comparison of M_R backcalculation procedures is demonstrated using the results from only one pavement configuration [102-mm (4-in.) AC, 203-mm (8-in.) granular base]; the results presented are typical of the results obtained from the other conventional flexible pavement sections tested. The comparison of SN_{eff} algorithms is performed using a variety of conventional flexible pavement configurations.

Figure 2 shows backcalculated values of subgrade resilient modulus plotted versus input M_R values. Equation 4 is used to estimate M_R for the ROADHOG procedure, and Equation 5 is used for the AASHTO procedure. The points shown represent M_R values backcalculated from deflection basins generated by the ILLI-PAVE and ELSYM5 models.

The trends shown in Figure 2 are not surprising. Each backcalculation method provides relatively accurate estimates of M_R for deflection basins generated by the model on which the method is based. The ROADHOG procedure accurately estimates M_R for ILLI-PAVE-based deflections; Equation 4 (used in ROADHOG) is a regression equation developed from ILLI-PAVE-generated deflection data. The AASHTO procedure accurately estimates M_R for ELSYM5-based (elastic layer) deflections; Equation 5 is developed using elastic layer theory. Conversely, neither procedure estimates M_R accurately using deflections generated by the nonbasis model.

The points shown in Figure 2 raise the question of the accuracy with which each of the pavement models represents real-life pavements. Although it is beyond the scope of this paper to discuss the relative merits of the pavement models, it is worth noting that many researchers have recommended the use of stress-dependent models to represent unbound granular materials and subgrade soils (*12*). As used in this study, ILLI-PAVE models the nonlinear, stress-dependent behavior of paving materials and subgrade soils. ELSYM5 uses only linear elastic assumptions. Data generated from ILLI-PAVE are used for the comparisons that follow.

Based on the results obtained using the ILLI-PAVE-generated deflection basins, the AASHTO backcalculation method overestimates the subgrade resilient modulus, compared to the method used

TABLE 1 Parameters Varied To Establish Deflection Data Base

Material	Layer Coeff.	Thickness (in)	Thickness (mm)	Resilient Modulus (ksi)	Resilient Modulus (MPa)	AC Temp (deg C)
Asphalt Conc (surface)	0.44	2	51	1400	9660	5
		4	102	500	3450	20
		6	152	100	690	40
		8	203			
Crushed Stone (base #1)	0.14	6	152	30	207	
		8	203			
		10	254			
		12	305			
Gravel (base #2)	0.12	6	152	20	138	
		8	203			
		10	254			
		12	305			
Subgrade Soil				12	82.8	
				7.5	51.8	
				3	20.7	
				1	6.9	

in ROADHOG. Because M_R is used in the AASHTO effective structural number estimation procedure, an error in M_R may result in an error in SN_{eff}, directly affecting the resulting overlay thickness. Additional discussion of this point is provided in the comparison of SN_{eff} values.

Subgrade resilient modulus is also used to determine SN_f, the total structural number required to carry future traffic. SN_f is determined in the AASHTO and ROADHOG procedures using AASHTO new-pavement design concepts. For new-pavement design, a design value of M_R is needed. This design value should be obtained in a manner consistent with the assumptions underlying the development of the AASHTO flexible pavement design equation (*3*). The method of backcalculating M_R used in the ROADHOG method was developed to be consistent with the original AASHO Road Test soil (*7*). However, M_R values obtained using Equation 5 must be adjusted to make the values consistent with the laboratory measured value used for the AASHO Road Test soil (*2,3*). For conventional AC-surfaced pavements, the 1993 AASHTO guide recommends the M_R value obtained using Equation 5 be multiplied by a correction factor of 0.33 for use in design (*3*).

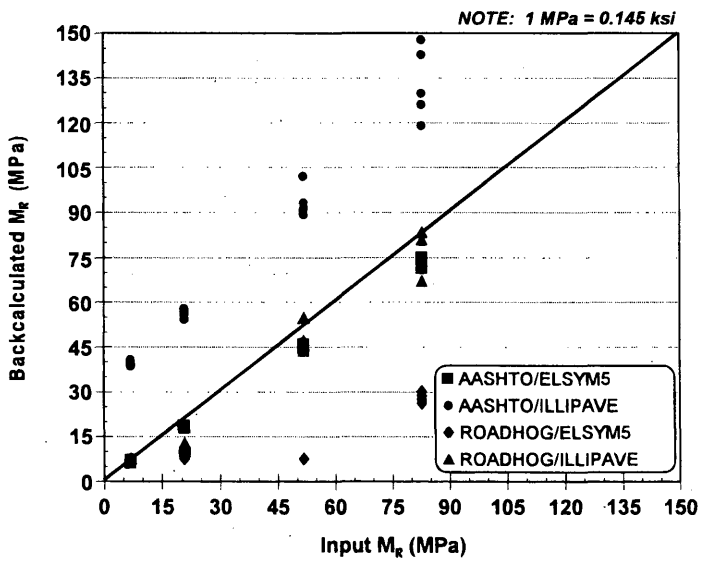

FIGURE 2 Comparison of backcalculated M_R with M_R values used in pavement models.

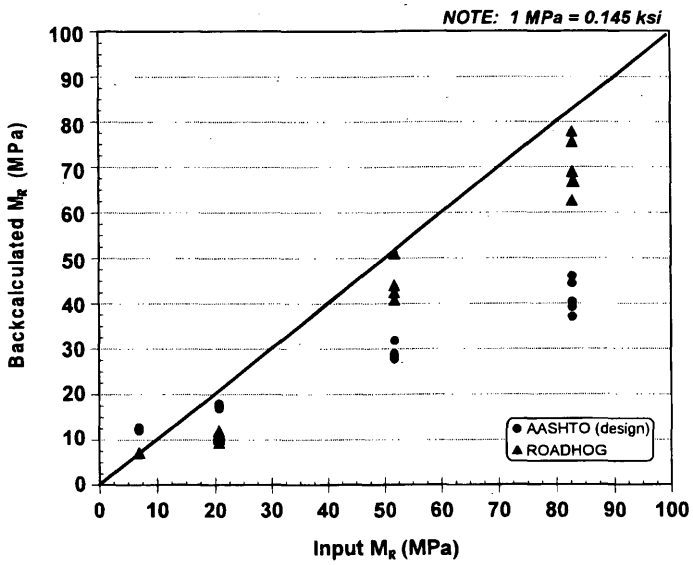

FIGURE 3 Comparison of AASHTO design M_R with M_R used in ILLI-PAVE model.

Figure 3 shows corrected design M_R values (using a correction factor of 0.33) for the AASHTO procedure and M_R values for the ROADHOG procedure plotted versus the input M_R values for the ILLI-PAVE-generated deflection basins. At lower stiffness levels, the design AASHTO M_R values reasonably reflect input values; however, the AASHTO method (using $C = 0.33$) underestimates M_R at higher stiffness levels.

The AASHTO flexible pavement design equation is sensitive to M_R, particularly for low M_R values. Underestimating the design subgrade resilient modulus has the general effect of increasing SN_f, while overestimating M_R generally decreases SN_f. This is illustrated in Figure 4, which shows SN_f values determined in the AASHTO and ROADHOG procedures plotted against SN_f values calculated using the input M_R values for ILLI-PAVE.

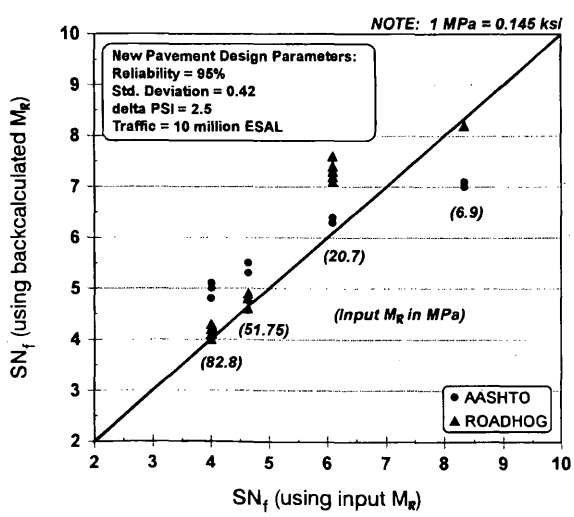

FIGURE 4 Comparison of SN_f from backcalculated M_R with SN_f from input M_R.

Effective Structural Number

To compare SN_{eff} values obtained from the AASHTO and ROADHOG procedures, some standard must be established to serve as a basis for comparison. For this research, the standard of comparison is the SN_{eff} value determined using component analysis (Equation 1). For each generated deflection basin, all paving layer thicknesses and modulus values are known. Layer coefficients are assigned to each material based on the material's modulus value and the relationships given in the 1993 AASHTO guide; layer coefficients used in this research are shown in Table 1. Two items regarding layer coefficients should be noted. The first is that layer coefficients used to determine the SN of the pavement section are selected with no consideration of material degradation—in other words, no reduced layer coefficients are used. The second item is that a single-layer coefficient is used for the asphalt concrete surface. The variation in AC modulus shown in Table 1 is related to temperature. Both the AASHTO and ROADHOG procedures adjust deflection data to a single reference temperature [approximately 20°C (68°F)]. The AC layer coefficient used (0.44) is typical for asphalt concrete at the reference temperature.

Figure 5 shows deflection-based SN_{eff} values (AASHTO and ROADHOG) plotted versus component analysis–based values for an input subgrade modulus equal to 51.75 MPa (7500 psi). Because of the large number of data points, individual values are not plotted. Instead, SN_{eff} data are plotted as trends determined by linear regression. The degree of fit as determined by the regression coefficient r^2 is shown for each regression line. For pavement configurations with lower SN_{eff} values both the AASHTO and ROADHOG methods adequately reflect component-based SN_{eff} values. At higher levels of SN_{eff}, the AASHTO method underestimates the pavement's effective structural number relative to component-based values. Underestimating SN_{eff} has the general effect of increasing overlay thickness.

One item to consider in the comparison shown in Figure 5 is the role of the subgrade resilient modulus on SN_{eff} values, particularly for

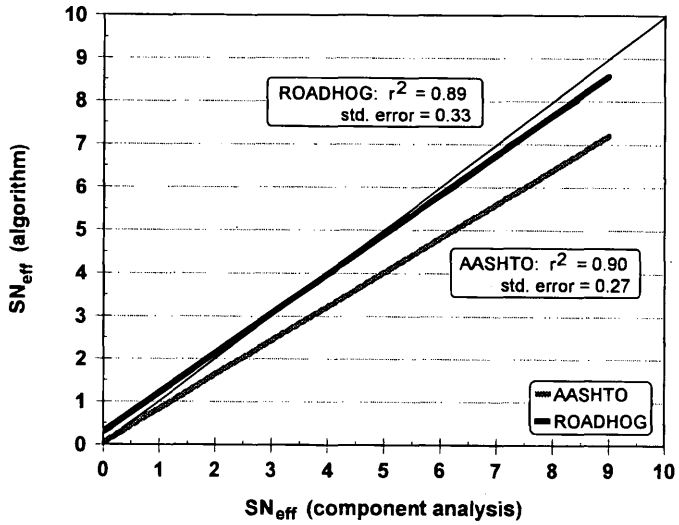

FIGURE 5 Comparison of ROADHOG and AASHTO SN_{eff} with SN_{eff} from component analysis.

AASHTO-based values. The ROADHOG SN_{eff} algorithm is relatively independent of M_R. In the AASHTO procedure, SN_{eff} and M_R are interdependent (see Equation 7). To adequately compare SN_{eff} procedures, it is necessary to distinguish the effect of M_R on the SN_{eff} estimate.

Figure 6 shows AASHTO-based SN_{eff} trends for four input levels of subgrade modulus. The SN_{eff} trends clearly reflect the effect of M_R, particularly for higher component analysis–based values of SN_{eff}. For any given component analysis–based SN_{eff} value (which denotes a single conventional flexible pavement configuration in this research), the AASHTO procedure estimates a range of SN_{eff} values, depending on the subgrade modulus used. It is apparent that the AASHTO SN_{eff} determination procedure provides an estimate that reflects the structural capacity of the total pavement system (paving layers plus subgrade soil), not of the pavement layers alone. This violates the basic definition of the AASHTO structural number in which SN is a function of the layer thicknesses and material properties (see Equation 1). For overlay design purposes, SN_{eff} should reflect only the structural capacity of the pavement layers. The effects of the subgrade will be reflected in the total SN required for the overlaid pavement.

Another complication in the AASHTO system and its use of M_R in determining SN_{eff} is that (for ILLI-PAVE-based deflections) the AASHTO procedure overestimates the subgrade modulus (Figures 2 and 3). This may help provide an explanation for why AASHTO underestimates SN_{eff}. For a given value of d_0 (refer to Equation 7), extremely high values of M_R (as seen in Figure 2) result in relatively low SN_{eff} values. An oversimplified explanation suggests that the AASHTO procedure gives too much credit to the subgrade soil and therefore discounts the structural capacity of the pavement structure, resulting in lower SN_{eff} values.

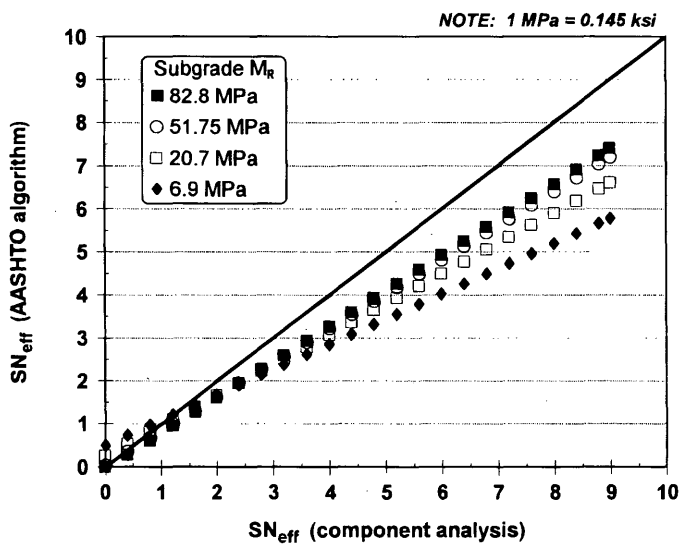

FIGURE 6 Comparison of AASHTO SN_{eff} at various M_R values with SN_{eff} from component analysis.

SUMMARY

The ultimate comparison between the two overlay design procedures is the recommended overlay thickness for a given pavement configuration and its associated deflection basin. Figure 7 shows a comparison of overlay thickness as determined by the AASHTO and ROADHOG methods for various conventional flexible pavement configurations. The AASHTO procedure generally recommends thicker overlays than does the ROADHOG procedure for pavements over stiffer subgrade soils; for pavements over soils with lower M_R values, the two procedures recommend similar overlay thicknesses. Overlay thickness is a direct function of SN_{ol}. The factors affecting SN_{ol} (and therefore overlay thickness) are SN_f and SN_{eff} (Equation 2).

It was established earlier that corrected design M_R values used in the AASHTO method generally underestimate the subgrade resilient modulus compared with the backcalculated modulus values used in ROADHOG. With all other new-pavement design factors constant, the SN_f values determined by AASHTO are higher than those determined by ROADHOG (Figure 4). Higher SN_f values will result in thicker overlays. It was also established that the AASHTO procedure generally underestimates SN_{eff} relative to the ROADHOG procedure, particularly for those pavement configurations having higher component analysis–based SN_{eff} values (Figure 5). Lower SN_{eff} values result in thicker overlays. The observed differences in recommended overlay thicknesses between AASHTO and ROADHOG can be traced, then, to both the SN_f and SN_{eff} estimates.

Because differences in the recommended overlay thickness exist, the question to be answered becomes, Which of the two overlay design procedures produces a more correct or realistic overlay thickness? The two quantities identified as affecting the overlay thickness are M_R and SN_{eff}. An independent basis of comparison is offered for each of these quantities: (a) the subgrade modulus value input into the pavement models, used for comparing M_R values backcalculated by each method, and (b) the component analysis–based structural number for each pavement configuration, used for comparing SN_{eff} values estimated by each method. In each case, the algorithms contained in the ROADHOG procedure produce values that compare more favorably with the standards used.

It becomes apparent through the analyses presented that the subgrade resilient modulus plays a crucial role in determining the overlay thickness, particularly in the AASHTO procedure. If stress-dependent, nonlinear material models, such as those used in ILLI-PAVE, produce more realistic pavement responses (e.g., surface deflections) than do linear elastic models, the apparent difficulty shown by the AASHTO procedure in estimating the subgrade modulus (particularly for stiffer subgrade soils) gives rise to concern about recommended overlay thicknesses.

CONCLUSIONS

Based on the analyses presented in this paper, the following conclusions are offered:

- For conventional flexible pavements overlying relatively stiff subgrades, the AASHTO overlay design procedure generally recommends thicker AC overlays than does the ROADHOG procedure. For pavements over subgrade soils with lower resilient modulus values, the two procedures recommend similar overlay thicknesses.
- For pavement sections having higher component analysis–based effective structural numbers, the AASHTO procedure underestimates SN_{eff} compared with the ROADHOG procedure.
- For higher values of subgrade resilient modulus, the AASHTO procedure generally overestimates SN_f compared with the ROADHOG procedure.
- The interdependence of SN_{eff} and M_R in the AASHTO procedure makes the subgrade modulus the primary factor in determining the required overlay thickness.

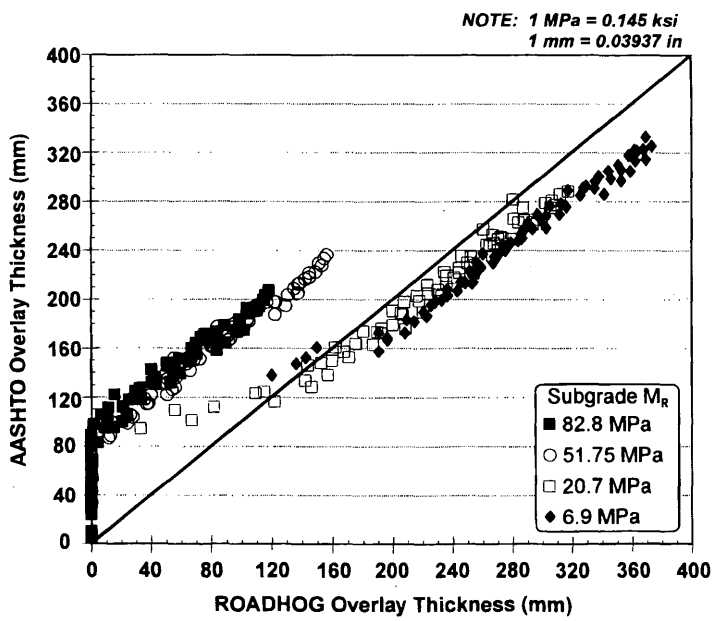

FIGURE 7 Comparison of AASHTO and ROADHOG recommended overlay analysis.

ACKNOWLEDGMENTS

This paper is based on Project TRC-9403, Reliability and Design Procedure Revisions to ROADHOG, conducted by the Department of Civil Engineering at the University of Arkansas. The project is sponsored by AHTD, the U.S. Department of Transportation, FHWA, and the Mack-Blackwell National Rural Transportation Study Center.

The authors gratefully acknowledge the assistance of Robert P. Elliott, Professor and Head of the Department of Civil Engineering at the University of Arkansas, during the preparation of this paper.

REFERENCES

1. *AASHTO Guide for Design of Pavement Structures.* American Association of State Highway and Transportation Officials, Washington, D.C., 1986.
2. Darter, M. I., R. P. Elliott, and K. T. Hall. *Revision of AASHTO Pavement Overlay Design Procedures, Appendix: Documentation of Design Procedures.* NCHRP Project 20-7/Task 39, June 1991.
3. *AASHTO Guide for Design of Pavement Structures.* American Association of State Highway and Transportation Officials, Washington, D.C., 1993.
4. Elliott, R. P., K. D. Hall, N. T. Morrison, and S. H. Kong. The Development of ROADHOG, A Flexible Pavement Overlay Design Procedure. *Final Report: TRC-8705, NDT Overlay Design.* Report UAF-AHTRC-90-001. Arkansas State Highway and Transportation Department, Little Rock, 1990.
5. *ILLI-PAVE: A Pavement Analysis Program Provided by the Transportation Facilities Group.* Department of Civil Engineering, University of Illinois at Urbana-Champaign, Urbana.
6. Kopperman, S., et al. *ELSYM5; Interactive Microcomputer Version User's Manual: IBM-PC and Compatible Version.* Report FHWA-TS-87-206. FHWA, U.S. Department of Transportation, 1986.
7. Hall, K. D., and R. P. Elliott. ROADHOG—A Flexible Pavement Overlay Design Procedure. In *Transportation Research Record 1374,* TRB, National Research Council, Washington, D.C., 1993.
8. Kong, S. H. *Determination of Effective Structural Number in Flexible Pavement Overlay Design.* Master's thesis, University of Arkansas, Fayetteville, 1989.
9. Elliott, R. P., and M. R. Thompson. *Mechanistic Design Concepts for Conventional Flexible Pavements.* Transportation Engineering Series No. 42. University of Illinois, Urbana, 1985.
10. Ullidtz, P. Overlay and Stage-by-Stage Design. *Proc. 4th International Conference on Structural Design of Asphalt Pavements,* Ann Arbor, Mich., 1977.
11. *AASHTO Guide for Design of Pavement Structures.* Vol. 2, Appendix NN. American Association of State Highway and Transportation Officials, Washington, D.C., 1986.
12. *Calibrated Mechanistic Structural Analysis Procedures for Pavements: Phase 2.* Volume II—Appendixes. NCHRP Project 1-26, Dec. 1992.

Publication of this paper sponsored by Committee on Flexible Pavement Design.

Inverted Flexible Pavement Response and Performance

EROL TUTUMLUER AND RICHARD D. BARKSDALE

An inverted section consists of an unstabilized crushed-stone base sandwiched between a lower cement-stabilized layer and the upper asphalt concrete (AC) surfacing. Two inverted full-scale instrumented pavement sections were tested to rutting or fatigue failure in a laboratory facility. One inverted section had a 152-mm (6-in.) cement-stabilized crushed-stone subbase and the other a 152-mm (6-in.) cement-treated silty sand subbase. The inverted sections were loaded up to 4.4 million load repetitions at failure. A 28.9-kN (6,500-lb) uniform circular loading was applied to the surface and systematically moved to prevent a punching failure. The inverted sections exhibited better performance compared to conventional and full-depth AC sections also tested. The inverted sections had lower vertical stresses on the subgrade and lower resilient surface deflections than the other sections. The rigid cement-stabilized subbase was effective in bridging a weak subgrade. The inverted section made optimum use of the compressive characteristics of the unstabilized aggregate base where stresses were compressive. A nonlinear finite-element program, GT-PAVE, was used to calculate the resilient pavement response. GT-PAVE did a reasonable job of simultaneously predicting the measured deformation and stress and strain response at six points in the different layers of the inverted sections. A sensitivity analysis indicates the use of a 152-mm (6-in.) unstabilized aggregate base and a 152- to 203-mm-thick (6- to 8-in.) cement-stabilized subbase to be an attractive inverted section design.

Today, more than 3.5 million km (2.2 million mi) of paved roads exist in the United States of which 94 percent consist of flexible pavements (*1*). Most of these flexible pavements have unstabilized aggregate bases or subbases. To achieve maximum economy in a pavement section, each material, including the unstabilized aggregate base, should be located to take full advantage of its best engineering properties. An inverted section consists of unstabilized aggregate base sandwiched between a lower cement-stabilized subbase and the upper asphalt concrete surfacing. An inverted section offers an interesting alternative to conventional flexible pavements with the inverted section making optimal use of the properties of each material.

This paper describes the behavior of two full-size inverted sections having (a) a cement-treated silty sand subbase and (b) a cement-stabilized aggregate subbase. These sections, as well as conventional ones, were constructed in the laboratory under carefully controlled conditions and tested to failure under cyclic loading. Stresses, strains, and deflections were measured at a number of locations in the different layers of the sections. A nonlinear finite-element program, GT-PAVE, was used to calculate pavement response and compare the theoretical values with the observed deformations, stresses, and strains. Pavement performance of the inverted sections was also directly compared with conventional and full depth asphalt concrete (AC) sections.

School of Civil and Environmental Engineering, Georgia Institute of Technology, Atlanta, Ga. 30332.

PREVIOUS STUDIES

The performance of inverted highway test sections has been reported in works by Johnson (*2*), and McGhee (*3*). An inverted test section subjected to aircraft loadings was studied (*4*). These inverted sections have all demonstrated good performance. On the basis of a 5-year study, an inverted section was found to be the most effective design and to exhibit the lowest overall cost of the sections included in the study (*3*). The subbase was constructed by stabilizing a residual micaceous silt and clayey silt subgrade with 10 percent cement by volume.

North Carolina State University researchers have recently found that among 24 full-scale flexible pavements tested, inverted sections having cement stabilized subgrades performed the best. These sections had unstabilized aggregate bases approximately 203 to 305 mm thick (8 to 12 in.) overlain by a 178-mm (7-in.) thick soil-cement subbase.

Asphalt concrete surface thicknesses of inverted sections have been relatively thin, varying from 38 to 76 mm (1.5 to 3 in.). The unstabilized aggregate base used in inverted sections has typically varied from 152 to 203 mm (6 to 8 in.) in thickness. A base having this range of thickness is relatively effective in eliminating or reducing reflection cracking. The subbase of two inverted highway sections (*2,3*) have both been 152 mm (6 in.) thick. The importance of using a high-quality cement-stabilized layer has been demonstrated through field performance (*5*).

Inverted sections are attractive in areas of low rainfall where there is no potential problem of water being trapped in the base above the low-permeability cement-stabilized layer. The successful use of inverted sections in Virginia (*3*), which is in a high rainfall area, suggests water being trapped in the base may not be a significant problem. When water is of concern, a free-draining base with provision for positive water collection should be provided.

The works of Maree et al. (*6,7*) and that of O'Neil et al. (*8*) have shown that an unstabilized aggregate layer, when confined in an inverted section or a granular overlay, develops large elastic moduli as high as 689 MPa (100 ksi). Criteria to give optimum performance for the unstabilized aggregates used in inverted sections have been developed (*9*). It was also found that an unstabilized aggregate layer, when used in an overlay between the old pavement and the resurfacing, reduces reflection cracking, which substantiates earlier experience in Arkansas (*8*).

The degree of saturation of an inverted section base has been found to increase because of cracks that form in the cement stabilized layer due to shrinkage or fatigue, or both (*7,9*). Rutting becomes greater and the elastic moduli decrease with the increase in base saturation. Even in wet conditions, a high-quality, well-constructed crushed-aggregate base, when used in an inverted section, is still quite resistant to rutting (*7,9*), with rutting in one instance observed to be one-half that of a conventional section (*9*).

MATERIAL PROPERTIES

The aggregate gradations and material properties used in the inverted test sections are summarized in Table 1. A Georgia Department of Transporation (DOT) B-binder asphalt concrete was used for the AC surfacing. The asphalt cement used in the mix was an AC-20 viscosity grade. The unstabilized aggregate base course consisted of crushed granitic gneiss prepared by blending in a small 0.096-m^3 (1/8-yd^3) Barber-Greene pugmill 20 percent by weight of No. 5 size aggregate, 25 percent of No. 57, and 55 percent of No. 810s. A low to moderate strength micaceous nonplastic silty sand subgrade, classified as an AASHTO A-4 soil, was used beneath the inverted test sections.

Equation 1 gives the observed resilient modulus variation as a function of bulk stress and deviator stress obtained from repeated load triaxial tests performed on the unstabilized aggregate base (*10*).

$$M_R(\text{MPa}) = 543.82\ \sigma_\theta^{0.61}\ \sigma_d^{-0.07} \quad r^2 = 0.95 \tag{1}$$

The foregoing resilient modulus model proposed in a work by Uzan (*11*) gives a much better fit of resilient modulus than does the more familiar K-θ model.

The nonlinear behavior of the silty sand subgrade was modeled using a bilinear approximation to give resilient modulus as a function of deviator stress (σ_d). The measured resilient modulus M_R (*12*), when corrected for soil suction effects, was as follows: $\sigma_d = 0$, M_R = 241 325 kPa (35,000 psi); σ_d = 17.2 kPa (2.5 psi), M_R = 40 681 kPa (5,900 psi), and σ_d = 68.9 kPa (10 psi), M_R = 39 302 kPa (5,700 psi).

INVERTED TEST SECTION CONSTRUCTION

Pavement testing was conducted in a facility consisting of a 2.4-m (8-ft) by 36.6-m (12-ft) in plan and 1.5-m (5-ft)-deep test pit. Cyclic load was applied by an air over oil pneumatic loading system attached to a heavy steel load frame. A 28.9-kN (6,500-lb) uniform dynamic load was applied to the surface of the test sections over a diameter of 231 mm (9.1 in.). Twelve large-scale pavement test sections were tested to evaluate pavement performance (*12*). Pavements tested in this facility consisted of two inverted sections, five conventional sections having crushed-stone bases, and five full-depth asphalt concrete sections (Table 2).

The two inverted test sections (Section 11 and Section 12, Table 2) consisted of 203 mm (8 in.) of unstabilized crushed-stone base sandwiched between 89 mm (3.5 in.) of asphalt concrete above and 152 mm (6 in.) of cement stabilized material below. The silty sand subgrade beneath the cement-stabilized subbase was 1118 mm (44 in.) deep. A concrete slab was located beneath the subgrade.

The silty sand subgrade was placed in 51-mm (2-in.) lifts up to a total thickness of 1 118 mm (44 in.) in the inverted sections. Each lift was compacted using a Wacker or a Jay 12 compactor to 98 percent of AASHTO T-99 standard proctor maximum dry density at a moisture content of 20.5 percent. A spring-loaded static penetrometer was used to ensure uniformity of the subgrade during construction. As-constructed density was determined using a thin wall drive tube sampler.

The 152-mm-(6-in.) thick cement-stabilized subbase of the inverted sections was constructed on top of the subgrade followed by the placement of the crushed-stone base. Base and subbase layers were placed in approximately 51-mm (2-in.) lifts. Compaction of the subbase and base was achieved using five to seven passes of the Jay 12 vibrating plate compactor. The unstabilized aggregate bases were compacted to 100 percent of the AASHTO T-180 modified proctor maximum dry density. Nuclear density measurements revealed that because of the presence of the underlying rigid cement-stabilized subbase, the compaction density in the unstabilized aggregate base was 105 percent of the T-180 maximum dry density.

The cement-stabilized layers were cured for 28 days. The B-binder asphalt concrete mix was then placed over the unstabilized base. The B-binder gives a strong asphalt concrete surface course to resist rutting in that layer under the heavy applied loading.

INVERTED TEST SECTION RESULTS

The full-scale laboratory tests conducted to failure permitted comparing the performance of the inverted sections with the full-depth asphalt concrete sections and the conventional sections having relatively thick layers of unstabilized crushed aggregate base (Tables 2 and 3). Test results for the conventional aggregate base and full-depth asphalt concrete sections have been previously described, as well as the instrumentation and loading scheme used in the study (*12,13*). A fatigue failure of the test sections was considered to occur when the surface cracks connected to form a grid-type pattern, usually over the loaded area. Only hairline cracks were allowed to develop. Before wider cracks formed, testing was terminated because of the large number of repetitions required to reach this state of deterioration.

A maximum rut depth of 13 mm (0.5 in.) was considered to constitute a rutting failure. The maximum rut depth was determined by averaging the rut depths measured at completion of testing at the primary load position and at completion of testing at the sixth secondary load position. The need for averaging the values of rutting was because of the varying amounts of creep and plastic flow of the asphalt concrete and base materials observed at the different load positions as the load was moved from one position to another.

Overall, the two inverted sections performed the best of all the sections studied (Table 2). The cement-stabilized crushed-stone subbase inverted section (Section 12) failed in combined fatigue and rutting after 4.4 million load repetitions, making it clearly the strongest section. The cement-treated silty sand subbase inverted section (Section 11) withstood 3.6 million repetitions giving this section the next best performance. The two inverted sections also exhibited lower vertical stress on the subgrade and lower resilient surface displacements than the other sections (Table 3).

The cement-treated silty sand subbase inverted section appeared to perform slightly better than the conventional 305-mm (12-in.) thick crushed-stone base section (Section 1), which failed at an estimated 3.5 million repetitions. Both sections had 89-mm (3.5-in.) AC surfacing. The inverted section, however, had a 203-mm (8-in.) crushed-stone base and 152-mm (6-in.) cement-treated subbase.

The performance of one section compared to another section is directly dependent on the specific properties of each section. Rutting failure of the asphalt concrete section occurred, to a significant extent, within the asphalt concrete. The asphalt concrete, as placed in the test sections, met the specifications for a Georgia DOT mix. Better-performing AC mixes could probably have been identified and used. The results, however, show that when a high-quality unstabilized aggregate base is constructed over a properly prepared subgrade, both the properties and performance of the AC become important and can become the weak link in the design.

TABLE 1 Aggregate Gradations and Material Properties Used In Flexible Pavement Test Sections[1]

SIEVES	Cumulative % Passing By Weight										Maximum Density (kN/m^3)	Opt. Water Content (%)
	38 mm (1.5 in.)	25 mm (1 in.)	19 mm (3/4 in.)	13 mm (1/2 in.)	10 mm (3/8 in.)	4.75 mm (No. 4)	2.00 mm (No. 10)	.425 mm (No.40)	0.25 mm (No. 60)	0.075 mm (No. 200)		
AC Aggregate Gradation: [2]	100	100	100	86	75	51	36	18	14	7	22.9	-
Base Aggregate Gradations:												
No. 5	100	96	37	5	2	-	-	-	-	-	-	-
No. 57	100	98	82	43	20	3	-	-	-	-	-	-
No. 810	100	100	100	100	100	77	56	27	19	8	-	-
Combined [3]	100	99	83	67	61	43	31	15	10	4	21.5 [5]	5.7
Subgrade Gradation:	100	100	100	100	100	100	99	85	70	39	16.5 [4]	18.5
CEMENT STABILIZED SUBBASE PROPERTIES :												
A. Soil - Cement Subbase: 5% by weight of Type I Portland cement added to the silty sand subgrade. (Section 11) Average 28-day unconfined compressive strength = 1476 kPa.											16.8 [5]	18.0
B. Aggregate - Cement Subbase: 4.5% by weight of Type I Portland cement added to the Combined base. (Section 12) Average 28-day unconfined compressive strength = 7902 kPa.											21.7 [5]	6.0

Notes:
1. 1 in. = 25.4 mm; 1 psi = 6.895 kPa; 1 lb = 4.448 kN
2. The B-binder AC had a 5.2% optimum asphalt content, 4 % voids in the total mix, Marshall mix stability of 10.2 kN (2300 lbs.), and a flow value of 2.3 mm (9.0/100.0 in.)
3. Maximum aggregate size = 38 mm
4. Determined by AASHTO T-99 test method
5. Determined by AASHTO T-180 test method

TABLE 2 Geometry and Performance Summary of Pavement Test Sections

Asphalt Concrete Thickness (mm)	Crushed Stone Thickness (mm)	Repetitions to Failure	Failure Mode	Comments
CRUSHED STONE BASE				
89.0	305.0	3,000,000	Fatigue/	
		3,500,000	Rutting	Tested to 2.4 million repetitions
				Failure Extrapolated
89.0	203.0	1,000,000	Rutting	
FULL DEPTH ASPHALT				
229.0	None	10,000,000	Rutting	Bad Asphalt:
			(25 mm)	AC Content: 5.9 %
				Flow: 3.9 mm
165.0	None	10,000	Rutting	Stability: 8318 kN
			(25 mm)	Dry Density: 22.8 kN/m^3
229.0	None	130,000	Rutting	Rutting Primarily in AC
165.0	None	440,000	Rutting	Rutting Primarily in AC
178.0	None	150,000	Rutting	
CRUSHED STONE BASE				
89.0	203.0	550,000	Rutting	
89.0	203.0	2,400,000	Fatigue	Permanent Deformation: 7 mm
89.0	203.0	2,900,000	Fatigue	Permanent Deformation: 9 mm
INVERTED SECTIONS				
89.0	203.0	3,600,000	Fatigue/	152 mm Soil Cement Subbase
			Rutting	
89.0	203.0	4,400,000	Fatigue/	152 mm Cement Stabilized
			Rutting	Subbase

Note: 1 in = 25.4 mm; 1 psi = 6.895 kPa; 1 lb = 4.448 kN

TABLE 3 Detailed Summary of Resilient Test Section Response

Section	Horizontal Tensile Strain (micro m/mm)		Vertical Stress (kPa)		Vertical Strain (micro m/mm)				Surface Deflection (mm)	
	Bottom AC	Bottom Base	Top Base	Top Subgrade	AC	Top Base	Bottom Base	Top Subgrade	254 mm from Centerline	368 mm from Centerline
CRUSHED STONE BASE										
1	0.465	0.597	-	23.4	-	-	-	1.700	0.76	0.38
2	0.674	0.754	-	-	11.000	21.300	-	13.100	0.48	0.25
FULL DEPTH ASPHALT										
3	Premature Failure - Excessive Asphalt Content									
4	Premature Failure - Excessive Asphalt Content									
5	0.319	-	-	60.0	0.850	-	-	1.380	0.30	0.18
6	0.460	-	-	86.9	-	-	-	1.500	0.51	0.30
7	0.410	-	-	88.9	0.650	-	-	2.200	0.48	0.33
CRUSHED STONE BASE										
8	0.300	0.375	-	82.1	-	0.560	0.110	1.850	0.51	0.33
9	0.280	1.080	62.0	76.5	-	0.560	0.340	1.750	0.56	0.33
10	0.400	1.025	54.0	46.9	-	0.620	0.400	2.500	0.43	0.25
INVERTED SECTION										
11	0.340	0.054	-	22.8	-	0.730	0.370	0.390	0.18	0.08
12	0.260	0.022	-	23.4	-	0.760	0.420	0.340	0.15	0.08

Note: "-" in a data field indicates data was not taken.
1 in = 25.4 mm; 1 psi = 6.895 kPa

Horizontal Tensile Strain

The resilient tensile strain occurring in the bottom of an AC surfacing, as shown by laboratory testing and field studies, is related to fatigue life of a flexible pavement. AC surface thickness was held constant in this study, although fatigue life decreases with increasing AC thickness for a given level of tensile strain.

The cement-stabilized crushed-stone subbase section experienced a measured horizontal radial tensile strain of about $260 * 10^{-6}$ mm/mm at the bottom of the AC surfacing. In contrast, the cement-treated silty sand subbase inverted section exhibited a larger horizontal tensile strain of about $340 * 10^{-6}$ mm/mm. The crushed-stone cement-stabilized subbase used in Section 12 was thus more effective in reducing the tensile strain in the asphalt concrete than the less rigid, cement-treated subbase of Section 11.

For comparison with the inverted sections, the tensile strains observed in the bottom of the AC surfacing of the conventional unstabilized aggregate base and full depth AC sections varied from $280 * 10^{-6}$ to $674 * 10^{-6}$ mm/mm with the average measured value being $413 * 10^{-6}$ mm/mm. The tensile strain of $260 * 10^{-6}$ mm/mm observed in the cement-stabilized aggregate subbase inverted section was slightly less than the $280 * 10^{-6}$ mm/mm measured in the best performing noninverted section (Section 1). This finding is in agreement with the observed fatigue performance.

In the inverted sections (Sections 11 and 12), the measured horizontal tensile strains between the crushed-stone base and the cement-treated layer were $54 * 10^{-6}$ and $22 * 10^{-6}$ mm/mm, respectively. These tensile strains were about 20 times smaller than the values measured in the conventional Sections 8, 9, and 10. These small observed strains in the inverted sections were due to the presence of the very stiff subbase beneath the interface at which the strain was measured. The small tensile strains are compatible with the theoretical finding that the lower portion of the unstabilized aggregate base is in a compressive stress state compared to a tensile stress state for a conventional aggregate base section. Because of the compressive stress state, a higher resilient modulus exists in the base of an inverted section than in a conventional base section.

Subgrade Stress

The average measured vertical stress on top of the subgrade of the inverted sections was 22.8 kPa (3.3 psi) for Section 11 and 23.4 kPa (3.4 psi) for Section 12 after 3.6 and 4.4 million load repetitions, respectively (Table 3). These subgrade stresses were up to three times smaller than the vertical stresses measured for the conventional crushed-stone base sections (Sections 8 and 9) and for the full-depth AC sections (Sections 6 and 7). These small vertical subgrade stresses in the inverted sections were caused by the rigid cement stabilized layer bridging the subgrade and greater depth. Section 1, which had the 305-mm (12-in.) thick unstabilized aggregate base and exhibited excellent performance, also had a measured vertical subgrade stress of 23.4 kPa (3.4 psi).

Vertical Displacement

Because a uniform load was applied to the surface using a flexible water-filled bladder, surface deflection could not be measured beneath the load using externally mounted linear variable differential transformers. The closest vertical resilient displacement to the centerline measured in the inverted sections was at a radial distance of 254 mm (10 in.) away from the centerline. Vertical resilient deformations measured in the inverted sections at this location were quite small and varied from 0.15 to 0.18 mm (0.006 to 0.007 in.) (Table 3). These deflections were up to four times smaller than the 0.3 to 0.76 mm (0.012 to 0.03 in.) measured at the same location in the conventional crushed-stone base sections and up to two times smaller than the 1.78 to 0.33 mm (0.07 to 0.013 in.) measured in the full-depth AC sections.

The inverted sections, which had a very rigid cement-stabilized subbase, were also effective in reducing permanent deformation in the subgrade compared to the other test sections. For example, only about 12 percent of the total permanent deformation occurred in the subgrade of the inverted sections compared with 68 percent in the subgrade of the conventional aggregate base sections (Sections 9 and 10). In the inverted sections, about 70 percent of the total permanent deformation occurred in the thin 89-mm (3.5-in.) thick asphalt concrete layer. The remaining 18 percent developed mostly in the upper half of the unstabilized crushed-stone base. The small relative amount of rutting in the base was at least partly because of the very high density obtained in that layer as a result of the presence of the rigid subbase on which the base was compacted. A high level of confinement provided by the rigid layer also accounts for some of the good performance of the crushed-stone base. Based on these findings, the inverted section is particularly attractive for use over a weak subgrade.

PREDICTION OF INVERTED SECTION RESPONSE

The recently developed nonlinear finite-element program GT-PAVE was used to predict the observed pavement resilient response (stresses, strains, and deformations) at different locations in the inverted sections (Table 3). Laboratory-evaluated material properties were used in the theoretical analysis except for the cement-stabilized subbase, which was estimated from correlations given in the literature. After finding reasonably good agreement between the predicted and observed response values in the inverted sections, a sensitivity analysis was performed for selected inverted pavement geometries using materials similar to those in the full-scale test study. The sensitivity analysis permitted determining optimum geometries for inverted sections and extending, at least approximately, the test section results to other conditions.

GT-PAVE Program Capabilities

The GT-PAVE nonlinear computer program uses isoparametric eight-node quadrilateral elements to analyze a flexible pavement as an axisymmetric solid consisting of either linear or nonlinear elastic layers. In the nonlinear elastic layers, a variation in response of the pavement with stiffness occurs as a result of using stress-dependent resilient moduli obtained from the material characterization models. A nonlinear analysis is performed in two stages: first, the gravity and initial stresses are calculated using 5 load increments, and then the wheel load is applied in 10 load increments. The no-tension modification approach in a work by Zienkiewicz et al. (*14*) is used in the granular base when it goes into tension.

Theoretical Analysis

A 140-element, 475-node axisymmetric finite-element mesh was used to analyze both inverted sections as nonlinear elastic layered

systems (Figure 1). The subgrade and the unstabilized aggregate base were treated as nonlinear elastic materials, and the AC surfacing and cement-stabilized subbase were modeled as linear elastic materials. The base was also given cross-anisotropic material properties. Use of an anisotropic characterization has been found to be necessary for correctly modeling the tension effect in the unstabilized granular bases (*15*). To model the tests, the wheel load was applied as a uniform pressure of 689 kPa (100 psi) over a circular area of radius 116 mm (4.55 in.) (Figure 1). A fixed boundary was assumed at the bottom of the 1118-mm (44-in.) thick subgrade where a concrete slab existed.

Linear elastic moduli used to model the cement-treated subbase were estimated from both charts and empirical correlations obtained from several sources (*16–20*). Resilient moduli in these correlations were related to the unconfined compressive strength of laboratory specimens prepared from cement-treated materials used in this study. For the soil-cement subbase of Section 11, the elastic moduli ranged from $3.5 * 10^3$ to $8.9 * 10^3$ MPa (507 to 1,300 ksi). Similarly, for the cement-stabilized crushed-stone subbase of Section 12, the moduli ranged from $8.3 * 10^3$ to $14.8 * 10^3$ MPa (1,200 to 2,000 ksi). After reviewing the variations in the moduli, a modulus of $4.14 * 10^3$ MPa (600 ksi) was assigned to the cement-treated silty sand subbase of Section 11, and $10.34 * 10^3$ MPa (1,500 ksi) to the cement-stabilized crushed-stone subbase of Section 12. The Poisson's ratio was assumed to be 0.2 for both sections (*20*).

The resilient modulus of the AC layer was taken (based on previous studies) to be $1.72 * 10^6$ kPa (250,000 psi) with a corresponding Poission's ratio of 0.35. To initiate the nonlinear analysis, initial estimates of the moduli must be input into the GT-PAVE program. The unstabilized crushed-stone bases were initially assigned vertical resilient moduli varying from 206,850 kPa (30 ksi) at the bottom to 413,700 kPa (60 ksi) at the top. The horizontal resilient moduli were taken to be 80 percent of the vertical moduli in the 203-mm (8-in.) thick anisotropic base. Similarly, an assumed Poisson's ratio of 0.43 in the vertical direction was reduced to 0.15 in the horizontal direction based on previous studies (*15*). After the first iteration of the first load increment, the material parameters of Uzan's model (Equation 1) were used for the nonlinear crushed-stone base. Material properties of the subgrade were modeled to be nonlinear isotropic as previously discussed, with a Poisson's ratio of 0.4. Initial moduli input to the program varied from 40 681 kPa (5900 psi) at the top to 103 425 kPa (15,000 psi) at the bottom of the subgrade.

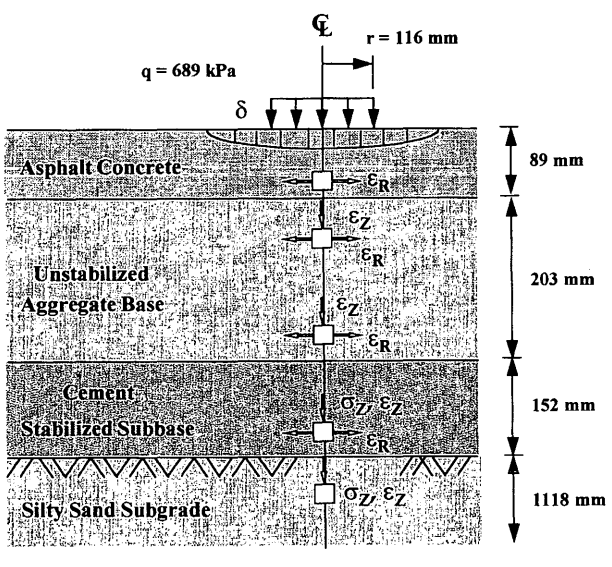

FIGURE 1 Typical cross section of inverted sections.

Table 4 compares the predicted GT-PAVE response variables with the measured ones. In general, finite-element predictions are in reasonably good agreement with the observed behavior of both inverted sections. Predictions were, however, in better agreement with observed response for Section 11 than for Section 12. The value of the vertical strain on top of the subgrade ($390 * 10^{-6}$ mm/mm) and the horizontal tensile strain at the bottom of the AC ($340 * 10^{-6}$ mm/mm) are essentially the same as the measured values in the cement-treated silty sand subbase (Section 11). In Section 12, the predicted value of the vertical stress on top of the subgrade [24.1 kPa (3.5 psi)] is in good agreement with the measured value of 23.4 kPa (3.4 psi). For this section, predicted tensile strain in the bottom of the AC was $340 * 10^{-6}$ mm/mm compared with a measured value of $260 * 10^{-6}$ mm/mm, which is still considered a reasonable prediction. Other predicted strains in this layer also differed from measured values in a similar manner. Strains in different layers are quite hard to predict with a high degree of accuracy.

The predictions summarized in Table 4 tend to verify the ability of nonlinear, anisotropic finite-element models such as GT-PAVE, to reasonably accurately predict a large number of measured stress, strain, and deflection response variables simultaneously. Such predictions are hard to achieve and indicate the model used is reasonably valid. This cannot be said for models that are verified by predicting only one or perhaps two measured response variables.

Figure 2 shows contours of horizontal radial stresses plotted on the top portion of the finite-element mesh for Section 12. The contours in Figure 2 show that the upper portion of the cement-treated subbase and almost all of the unstabilized crushed-stone base near the load are in horizontal compression. The bottom half of the subbase, as well as a thin layer on top of the subgrade, is in horizontal tension.

As a result of placing the cement-stabilized layer beneath the aggregate base, primarily horizontal compressive stresses of magnitudes ranging from 0 to 110 kPa (0 to 16 psi) are developed in the unstabilized crushed-stone base. This aggregate base performed well in the laboratory tests as indicated by the low measured permanent deformation (18 percent of total) and the high calculated values of resilient moduli (241 to 552 kPa; 35 to 80 ksi). Relatively high horizontal tensile stresses (up to 586 kPa; 85 psi under the load centerline) were predicted at the bottom of the stabilized subbase in Sections 11 and 12.

Sensitivity Analysis

A sensitivity analysis of inverted sections was performed using the GT-PAVE program for four different unstabilized aggregate base thicknesses varying from 76 to 406 mm (3 to 16 in.) and three different cement-treated subbase thicknesses varying from 102 to 254 mm (4 to 10 in.). The purpose of the sensitivity analysis was to find optimum design geometries for the inverted sections as defined by horizontal tensile strain in the bottom of the AC, vertical stress on the subgrade, and the tensile stress in the cement-stabilized subbase. Levels of subbase stabilization comparable to Section 11 and 12 were used corresponding to resilient moduli of $4.14 * 10^3$ MPa (600 ksi) and $10.34 * 10^3$ MPa (1,500 ksi), respectively. An impor-

TABLE 4 Comparison of Predicted and Measured Response Variables[1]

RESPONSE	TOP SUBGRADE		BOTTOM SUBBASE		BOTTOM BASE		TOP BASE	BOTTOM AC		SURFACE DEFLECTION		
	σ_z (kPa)	ε_z ($\frac{\mu m}{mm}$)	ε_R ($\frac{\mu m}{mm}$)	ε_z ($\frac{\mu m}{mm}$)	ε_R ($\frac{\mu m}{mm}$)	ε_z ($\frac{\mu m}{mm}$)	ε_z ($\frac{\mu m}{mm}$)	ε_R ($\frac{\mu m}{mm}$)	ε_z ($\frac{\mu m}{mm}$)	$\delta_{C.L.}$[2] (mm)	δ_{254}[3] (mm)	δ_{368}[3] (mm)
MEASURED (Section 11)	22.8	0.390	-	-	0.054	0.370	0.730	-0.340	-	0.48	0.18	0.08
PREDICTED (Section 11)	27.6	0.390	-0.079	0.045	0.051	0.317	1.050	-0.348	0.536	0.41	0.23	0.15
MEASURED (Section 12)	23.4	0.340	-	-	0.022	0.420	0.760	-0.260	-	0.41	0.15	0.08
PREDICTED (Section 12)	24.1	0.236	-0.046	0.025	0.035	0.362	1.047	-0.341	0.532	0.38	0.20	0.15

Notes: 1. A "-" in data field indicates no data was taken

2. Measured deflections at centerline $\delta_{C.L.}$ are extrapolated

3. Deflections measured at 254 mm and 368 mm radial distances away from centerline

4. 1 in = 25.4 mm; 1 psi = 6.895 kPa

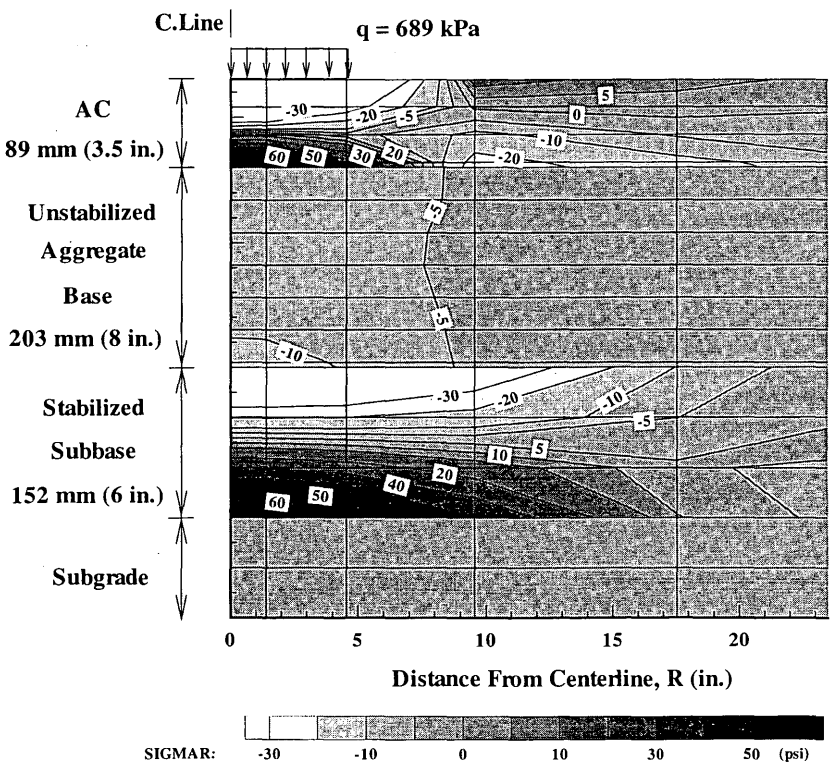

Notes: 1. 1 in. = 25.4 mm; 1 psi = 6.895 kPa

2. Tension is positive

FIGURE 2 Variation of radial tensile stresses throughout unstabilized aggregate base and cement stabilized subbase in Section 12.

tant factor in achieving good performance of an inverted section is to provide a subbase having sufficient strength to prevent fatigue- and durability-related failures.

The sensitivity analysis (Figure 3) indicates that increasing the thickness of the unstabilized aggregate base in the inverted sections causes an important increase in the horizontal strains at the bottom of the AC for stabilized subbase thicknesses of 102, 152, and 254 mm (4, 6, and 10 in.). Resilient surface deflections also increase with increasing base thickness although these results are not presented. For a base thickness equal to or greater than 152 mm, only a very small reduction occurs in the vertical subgrade stress with increasing base thickness (Figure 4). Therefore, inverted pavements having a 152-mm to 203-mm (6- to 8-in.) thick unstabilized crushed-stone base and also a similar thickness of cement-stabilized subbase appear to be a practical, economical design that minimizes tensile strain in the AC and vertical stress on the subgrade. Base or subbase thicknesses less than 152 mm (6 in.) are considered impractical to construct. This finding is in general agreement with the full-scale field tests recently conducted by North Carolina DOT.

Figure 5 shows the variation of horizontal radial tensile strain at the bottom of AC with increasing AC thicknesses for both inverted and conventional sections. The lower curve, which shows significant reductions in tensile strain compared to the conventional sections, is for inverted sections having a 152-mm (6-in.) thick base and subbase. For both sections, the horizontal radial tensile strain at the bottom of the AC decreases significantly with increasing AC thickness, suggesting the potential for improved fatigue life of the AC.

The variation of the horizontal radial tensile stress at the bottom of the stabilized subbase beneath the center of the load is shown in Figure 6 as a function of subbase thicknesses. In both the low-and high-moduli subbase inverted sections, an important decrease in tensile stress occurs with increasing subbase thickness. Fatigue life of the cement-stabilized subbase can therefore be improved by increasing subbase thickness.

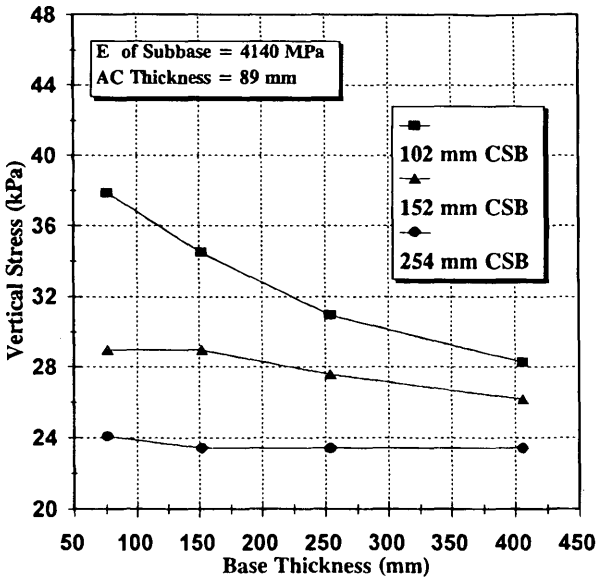

1. CSB: Cement Stabilized Subbase
1 in = 25.4 mm, 1 psi = 6.895 kPa

FIGURE 4 Variation of vertical stress on subgrade with base thickness in Section 11.

CONCLUSIONS

The full-scale test results show that cement-stabilized inverted sections having a subbase thickness of 152 to 203 mm (6 to 8 in.) can successfully withstand large numbers of heavy loadings better than both the conventional and full-depth AC sections used in this study. A full-depth AC section having better rut resistance would, of

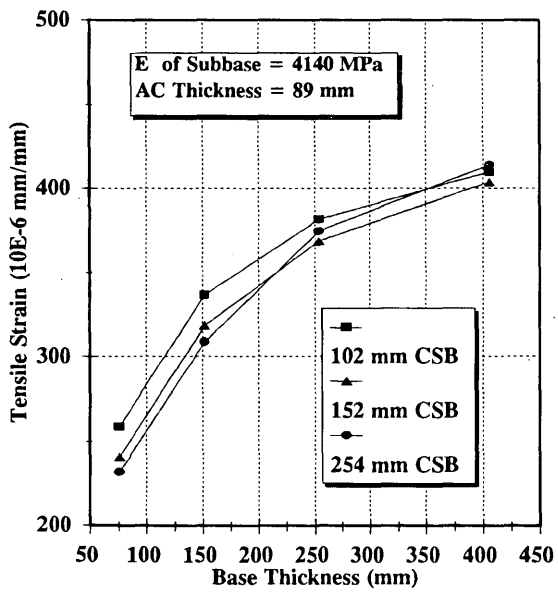

1. CSB: Cement Stabilized Subbase
1 in = 25.4 mm

FIGURE 3 Variation of horizontal tensile strain at bottom of AC with base thickness in Section 11.

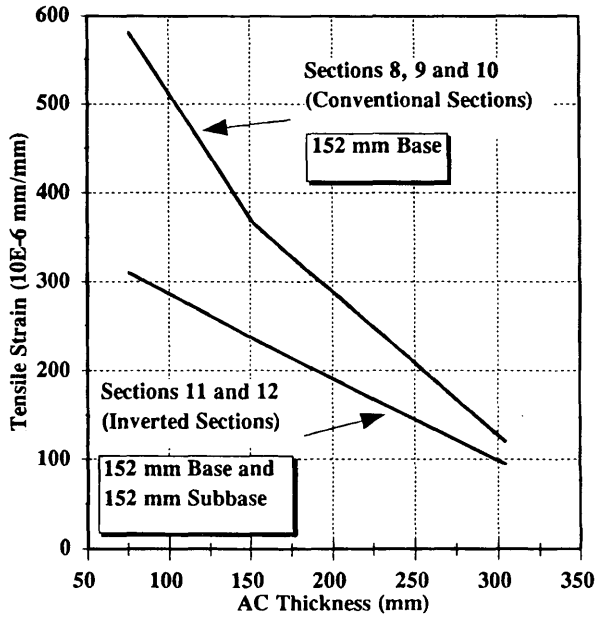

Note: 1 in = 25.4 mm

FIGURE 5 Variation of radial tensile strain at bottom of AC with AC thickness.

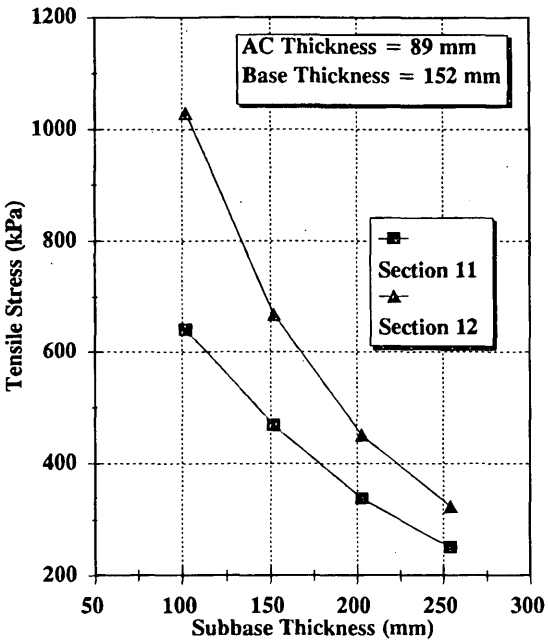

Note: 1 in = 25.4 mm, 1 psi =6.895 Kpa

FIGURE 6 Variation of radial tensile stress beneath centerline at bottom of cement stabilized subbase with subbase thickness.

course, perform better. The inverted sections also exhibit lower vertical stresses on the subgrade and lower resilient surface deflections than the other sections. The lower vertical stresses on the subgrade are caused primarily by the "beam" action of the stabilized subbase, which spreads the stress out. The significant reduction of vertical stress on the subgrade makes the use of an inverted section appealing for construction over a weak subgrade. The high-quality cement-stabilized crushed-stone subbase inverted section had the lowest tensile strain in the bottom of the AC of all 12 test sections studied. The low tensile strain in the AC and low vertical subgrade stress help explain why this section performed best.

Inverted sections make optimum use of the excellent compressive characteristics of unstabilized aggregate by placing it above the cement-stabilized layer where radial stresses are compressive. Better compaction of unstabilized materials placed over the stabilized layers is achieved. As a result of better confinement and a higher level of compaction, permanent deformations in the base are small. Reflection cracking is significantly reduced or eliminated since the cement-treated layer is placed deep in the section below the aggregate base.

Pavement response predictions for the two inverted sections made at six locations were in reasonably good agreement with observed values. This finding indicates the GT-PAVE nonlinear, cross-anisotropic program and the material characterization models used were valid. The theoretical sensitivity analysis performed using these models indicate an optimum and economical inverted pavement design placed on a weak to moderately strong subgrade would have an unstabilized aggregate base 152 mm (6 in.) thick and a 152-mm to 203-mm (6- to 8-in.) thick cement-stabilized subbase.

REFERENCES

1. *Highway Statistics, 1990.* FHWA U.S. Government Printing Office, Washington, D.C. 1990.
2. Johnson, V. W. Comparative Studies of Combinations of Treated and Untreated Bases and Subbases for Flexible Pavements. *Bulletin 289,* HRB, National Research Council, Washington, D.C., 1960, pp. 44–61.
3. McGhee, K. H. *Pavement Design Performance Studies.* Final Report on Phase C Research Report BHRC 70-R44, Virginia Council, 1971.
4. Grau, R. W. *Evaluation of Structural Layers of Flexible Pavements.* Miscellaneous Paper S-73-26. Waterways Experiment Station, 1973.
5. Tayabji, S. D., P. J. Nussbaum, and A. T. Ciolko. Evaluation of Heavily Loaded Cement Stabilized Bases. In *Transportation Research Record 839,* TRB, National Research Council, Washington, D.C., 1982, pp. 6–11.
6. Maree, J. H., N. J. W., van Zyl, and C. R. Freeme. Effective Moduli and Stress Dependence of Pavement Materials as Measured in Some Heavy-Vehicle Simulator Tests. In *Transportation Research Record 852,* TRB, National Research Council, Washington, D.C., 1982.
7. Maree, J. H., C. R. Freeme, N. J. W. van Zyl, and P. F. Savage. The Permanent Deformation of Pavements With Untreated Crushed-Stone Bases as Measured in Heavy Vehicle Simulator Tests. *Proc. 11th Australian Road Research Board Conference,* Melbourne, 1982.
8. O'Neil, D. J., J. P. Mahoney, and N. C. Jackson. *An Evaluation of Granular Overlays in Washington State.* Final Technical Report, Report No. FHWA-SA-92-042. Washington State Department of Transportation, 1992.
9. Horak, E., J. C. du Pisani, and C. J. van der Merwe. Rehabilitation Alternatives for Typical "Orange Free State" Rural Roads. *Proc. Annual Transportation Convention,* National Institute for Transport and Road Research, Perth, Australia, 1986.
10. Alba, J. L. *Laboratory Determination of Resilient Modulus of Granular Materials for Flexible Pavement Design.* Ph.D. dissertation. Georgia Institute of Technology, Atlanta, 1993.
11. Uzan, J. Characterization of Granular Materials. In *Transportation Research Record 1022,* TRB, National Research Council, Washington, D.C., 1985, pp. 52–59.
12. Barksdale, R. D., and H. A., Todres. *A Study of Factors Affecting Crushed Stone Base Performance.* Report SCEGIT-82-109, Georgia Institute of Technology, Atlanta, 1983.
13. Barksdale, R. D. Crushed Stone Base Performance. In *Transportation Research Record 954,* TRB, National Research Council, Washington, D.C., 1984, pp. 78–87.
14. Zienkiewicz, O. C., Y. K. Cheung, and K. G. Stagg. Stress Analysis of Rock as a "No Tension" Material. *Geotechnique,* Vol. 18, 1968, pp. 56–66.
15. Barksdale, R. D., S. F. Brown, and F. Chan. *NCHRP Report 315: Potential Benefits of Geosynthetics in Flexible Pavements.* TRB, National Research Council, Washington, D.C., 1989.
16. Felt, E. J., and M. S. Abrams. Strength and Elastic Properties of Compacted Soil-Cement Mixtures. *ASTM Special Technical Publication,* No. 206, 1957, pp. 152–173.
17. Jones, R. Measurement of Elastic and Strength Properties of Cemented Materials in Road Bases. In *Highway Research Record 128,* HRB, National Research Council, Washington, D.C., 1966, pp. 101–111.
18. Williams, R. I. T. Properties of Cement Stabilized Materials. *The Journal of the Institution of Highway Engineers,* Vol. 19, No. 2, 1972, pp. 5–19.
19. Hadley, O. W. Material Characterization and Inherent Variation Analysis of Soil-Cement Field Cores. In *Transportation Research Record 1295,* TRB, National Research Council, Washington, D.C., 1991, pp. 23–36.
20. *Soil Stabilization In Pavement Structures—A User's Manual.* Vol. 1 and 2. Report FHWA-IP-80-2. Office of Development Implementation Division, FHWA, U.S. Department of Transportation, 1979.

Publication of this paper sponsored by Committee on Flexible Pavement Design.

Sensitivity Analysis of Input Parameters for Pavement Design and Reliability

BRIAN M. KILLINGSWORTH AND DAN G. ZOLLINGER

The reliability of a certain pavement design can be related directly to the variation of the input parameters and loading conditions the design process incorporates. To compare different designs using different materials that meet the same design criteria, it is important that the design process evaluate variability between designs in the same manner. It is under this premise that a rational, mechanistic pavement design process for different pavement types is required and hence introduced. These mechanistic pavement design approaches lend themselves well to probabilistic concepts, particularly in light of calibration procedures that can be used to significantly improve the accuracy of design results and desired levels of reliability. When design alternatives that evaluate reliability consistently are compared, it is important to know which variable inputs have the most impact on the range of any given level of reliability. A sensitivity analysis can be useful in assessing the effect on any given input parameter on the resulting design (i.e., mean value and increase in distress for a given level of reliability). This type of exercise will identify design values that must be carefully selected and that can have a signifcant impact on the design result. This will ensure that consistent levels of reliability are maintained in the design process and that reasonable judgments will be made with respect to the most cost-effective pavements.

The principal objective of any engineering design process is to produce a system that performs its intended function in a clear, concise, and accurate manner. To achieve reliability in design, the design process must correctly address, identify, and account for appropriate areas of variability. Because there is uncertainty associated with any engineering design process, an appropriate measure of reliability can be based on probability. This statement is corroborated by Ang and Tang (*1*), who state: "consistent levels of . . . reliability may be achieved if the criteria for design are based on such probabilistic measures of reliability."

A standard engineering definition of reliability is "the probability of an object (item or system) performing its required function adequately for a specified period of time under stated conditions" (*2*). Four essential elements of this definition are further identified, (*2*):

1. Reliability is expressed as a probability.
2. A quality of performance is expected.
3. The performance of the object is expected for a period time.
4. The object is expected to perform under specified conditions.

To compare different designs using different materials that meet the same design criteria, it is important that the design process evaluate variability between designs in the samer manner. This can be accomplished by consistently applying probabilistic concepts that will provide comparable levels of reliability in a format in which all design results are equitably accounted for in the system analysis.

Reliability-based design using probability concepts has been found to be useful in pavement design procedures. In the past, mechanistic design procedures were largely deterministic in that few design inputs were explicitly associated with a mean and a variance. A concept that has outlived its usefulness is the inclusion of some associated variance by applying a factor of safety to certain design inputs. This approach can account for some of the variance, but such empirical modifications only result in overly confounded estimates of design reliability. Consequently, there is no way to reasonably assess what level of reliability is achieved by such a factor.

It has been shown that the mechanistic pavement design approach lends itself well to probabilistic concepts, particularly in light of calibration procedures that can be used to significantly improve the accuracy of design results and desired levels of reliability. Because of this particular feature, a calibrated mechanistic-empirical design process allows the same criteria to be applied in any region, with any soil and climate condition, in the design of a suitable pavement structure. In addition, pavement designs for different pavement types can be compared because a consistent approach to reliability can be applied to the two pavement types.

Quantifying and analyzing variability of pavement materials and design inputs are fundamental concerns in developing a probabilistic-based design that evaluates reliability.

> Design reliability is an indelible aspect of the pavement design process and needs to be genuinely considered and weighted equally with other design factors included in the design procedure. Design reliability . . . positively reinforces and enhances every component of a design procedure in such a manner that the associated and inherent component variability is directly related to the overall probability of pavement failure. Design reliability is the key to realistically, mathematically, and logically accounting for the material and pavement design variabilities (*3*).

Reliability is important in pavement design because of the variance or uncertainty involved in every facet of the pavement process. Factors such as planning, design, construction, use, and maintenance are inherently variable in nature and affect the ability to predict what will happen.

If uncertainty is correctly accounted for and design criteria and inputs are comparable, equitable pavement designs for different pavement types can be achieved and can provide a basis for life-cycle cost analysis. Mechanistic-empirical pavement design models are tools by which this process can be accomplished on a total design systems basis. This type of approach can simultaneously consider paving materials, environment, and loading conditions, while also considering the associated variances for each.

B. M. Killingsworth, Brent Rauhut Engineering, Inc., 8240 North Mopac, Ste. 220, Austin, Tex. 78759. D. G. Zollinger, Texas A&M University, CE/TTI Tower, Room 402D, College Station, Tex. 77843.

FRAMEWORK FOR COMPARABLE PAVEMENT DESIGN

Reliability in mechanistic design approaches is based on engineering mechanics and probability theory formulated so that characteristic distribution parameters can be calibrated with information available in field and performance data bases. However, these parameters also are a function of an individual site or a regional characteristic that not only calibrates the mean level of distress but also the variance associated with the distress. The calibration process, therefore, fine tunes the reliability factors that are associated with the distress distributions and that can characterize the variability of unaccountable influences such as environment, material, and traffic effects (*4*).

Design factors usually incorporated in mechanistic designs include design life, environment, traffic prediction and loading, subgrade strength, and paving material characterization. If pavement designs are developed under the same premise and design reliability is applied identically, the designs can be considered consistent and can provide a basis for determining the most cost-effective pavement structure.

The following section describes one form of inputs and models that can be considered for each pavement type when developing the analytical framework for a mechanistic-empirical design procedure for pavements. Development of a flexible pavement design system is summarized in a Texas Transportation Institute (TTI) research report (*5*) that explains the theory behind a flexible pavement design program. Readers are encouraged to refer to this report for information and details not covered in this paper.

With the advent of high-speed personal computers, intricate mechanistic and empirical design models for various distresses can be incorporated into a single design framework that takes a systems approach to design and considers multiple modes of failure. Computer design algorithms, developed for different pavement types, that (*a*) consider appropriate design inputs and (*b*) incorporate design reliability consistently can be used as input to determine the most cost-effective pavement structure. Two pavement design frameworks that meet these criteria will demonstrate how the design of two pavement types—flexible and rigid—can be compared (*5,6*). The flexible pavement design procedure considers the following failure modes:

- Fatigue cracking (square meters per 1000 m^2 of pavement),
- Rutting, and
- Serviceability or roughness in terms of the present serviceability index (PSI).

The rigid pavement design procedure considers these failure conditions:

- Fatigue cracking (percent midslab cracks),
- Faulting (millimeters on the joint),
- Spalling (number of spalls/per km), and
- Serviceability or roughness in terms of PSI.

The cracking models for these pavement types incorporate reliability concepts using Miner's hypothesis (*7*) to accumulate fatigue damage to predict the mean level of pavement cracking under load and environment stresses. The mechanistic, load-induced cracking model for the flexible pavement system requires the following general inputs:

- Specific traffic loading,
- Resilient moduli of pavement materials,
- Fatigue law of asphalt materials, and
- Variances of resilient moduli, layer thicknesses, and fatigue law parameters.

The mechanistic, load-induced cracking model for the rigid pavement system requires the following inputs:

- Specific traffic loading,
- Modulus of rupture for the concrete,
- Subgrade strength,
- Layer thicknesses,
- Joint spacing,
- Fatigue law of the portland cement concrete mixture, and
- Associated variances of some of the listed variables.

The fatigue life of both pavement types is calculated in terms of the total number of load reptitions to failure, denoted N_f. The allowable loads to failure in asphalt pavements is a function of the maximum tensile stress at the bottom of the asphalt layer, and in concrete pavements it is a function of the total edge stress developed in the pavement slab. The form of the fatigue law used to predict fatigue cracking life in the flexible design program (*8*) is:

$$\log N_f = k_1 - k_2 \cdot \log \epsilon_t - k_3 \cdot \log E \quad (1)$$

where:

ϵ_t = maximum tensile strain at bottom of asphalt layer,
E = resilient modulus (stiffness) of asphalt layer, and
k_i = parameters of fatigue law ($k_i = k_1$ or k_2; $i = 1$, 2, or 3).

The form of the fatigue law used to predict fatigue cracking in the rigid pavement design program (*9*) is:

$$\log N_f = k_1 - k_2 \cdot \frac{\sigma_{tot}}{MR} \quad (2)$$

where

σ_{tot} = total pavement stress (combination of σ_{wls} and σ_{ELS}),
σ_{wls} = wheel load stress,
σ_{ELS} = environmental load stress,
MR = modulus of rupture for concrete, and
k_i = parameters of fatigue law.

The Miner law of cumulative damage has been adopted by both pavement design procedures to accumulate damage due to load and environmental effects. The general form of the law is

$$D_j = \sum_{i=1}^{j} \frac{n_i}{N_{fi}} \quad (3)$$

where

D_j = relative accumulated damage caused to surface layer during j periods,
n_i = actual number of traffic repetitions applied to pavement during period i, and
N_{fi} = total number of traffic repetitions that can be applied to pavement during period i.

If traffic repetitions are in terms of axle load groups, damage can be accumulated over the summation of the load groups as well as over the period. Damage can be accumulated over the summation of a thermal gradient if one is used for curl analysis in the concrete pavement system.

The variance of damage (D_j) is calculated using Cornell's first-order, second-moment method based on the variabilities of the pertinent inputs for both pavement design processes. The computations assume that the mean values of D_j for the different periods are additive. This is equivalent to the assumption that the different damage accumulation periods are independent of each other.

After the expected (or mean) value and variance of the damage function are computed, the percent of cracked area or slabs cracked is computed as the probability that the damage function reaches or surpasses a critical value, which is normally assumed to be 1. This is shown by the following:

$$\%\overline{C} = 100 \cdot \text{prob}\,(D_j \geq D_c) \tag{4}$$

where

$\%\overline{C}$ = percent cracking, which can be converted into cracked area by multiplying by 10 for asphalt pavements or the percentage of slabs cracked in concrete pavements;
D_j = computed accumulated damage; and
D_c = critical damage level, normally equal to 1 according to Miner's hypothesis.

DEVELOPMENT OF STRESS-STRAIN CALCULATION MODELS

The fatigue life analysis for flexible and rigid pavement structures depends on the pavements' capability to sustain repeated loading for a specified period of time. As mentioned previously, this is the maximum tensile strain at the bottom of the asphalt layer for flexible pavements and the total stress on the edge of the concrete slab for rigid pavements.

The tensile strain at the bottom of the asphalt layer is expressed in a precise form based on analysis using the BISAR (*10*) program to develop regression algorithms for the data. The strain was computed for a dual wheel with a contact area radius equal to 114.3 mm and a center-to-center distance between wheels equal to 343 mm. The BISAR program was used to calculate the strains at two points in the upper layer and second layer, if one is present, of the pavement structure: under one wheel of the dual and between the wheels. The radial and tengential strains were computed for specific ranges of pavement layer thicknesses and moduli. The maximum strain between the radial and tangential strains was chosen for the regression analysis, which usually turns out to be the tangential strain. The regression algorithms developed from the BISAR output were used to adjust the wheel load strain calculated by the WESLAY model for different soil conditions and to adjust layer moduli as input by the design engineer.

The tensile strain at the bottom of the asphalt concrete layer is expressed as a Langrangian interpolation polynomial as follows:

$$\frac{E_{sg}\epsilon(x^k)}{P} = \sum_{i=\min}^{\min+d} L_i(x^k)\,\frac{E_{sg}\epsilon(x_i^k)}{P}\bigg|_{x_l} \qquad k \not\equiv 1 \tag{5}$$

where

$$L_i(x^k) = \prod_{\substack{j=\min \\ j\neq 1}}^{\min+d} \frac{(x^k - x_j^k)}{(x_i^k - x_j^k)}$$

and

i = min, min + 1, . . . , min + d (min = 1);
d = degree of polynomial;
E_{sg} = subgrade elastic modulus;
P = applied pressure;
x^k = variables that equal ratios of layer thicknesses to contact area and layer moduli to subgrade modulus; and
$\epsilon(x)$ = tensile strain at bottom of asphalt layer.

The TTI report (*5*) explains the process for the final strain calculation by stating that Equation 5

> . . . is an n[th] degree Langrangian interpolating polynomial which establishes the value of E_{sg}/P for all values within the allowable ranges of the layer thicknesses and modulus of elasticity. The tensile strain for a given pavement structure is interpolated over min + d values of strain associated with a single variable x_i^k in which the values of the x^1 variables are held constant at each strain.

The report (*5*) continues by stating that Equation 5

> is repetitively solved for each combination of x^k variables in accordance to the pavement structure and layer moduli. Following this process, the design program develops a smaller table of strain values generated from interpolation over the layer thickness and layer moduli. The final strain value is determined when all the variables (x^k) for a given pavement structure have been accounted for in the interpolation process. The interpolation polynomial is regenerated for each new pavement structure or when the pavement structure is modified.

The total edge stress calculated for a specified concrete pavement structure is based on the summation of the wheel load stress, curl stress, and stress due to erosion beneath the slab. Wheel load stress is calculated by regression equations developed from numerous Illi-Slab (*11*) runs. Each regression equation is in the form of

$$s = a_1 + a_2 \cdot \ell + a_3 \cdot \ell^2 \tag{6}$$

where

$$s = \text{dimension stress in form of } \frac{\sigma_{wls} \cdot h^2}{P}$$

σ_{wls} = wheel load stress;
h = slab thickness;
P = wheel load;
ℓ = radius of relative stiffness, which is equal to

$$\sqrt[4]{\frac{E_c \cdot h^3}{12 \cdot (1 - \nu^2) \cdot k_{sg}}}$$

E_c = elastic modulus of concrete slab;
ν = Poisson's ratio for concrete slab; and
k_{sg} = foundation modulus of subgrate reaction.

The regression equations developed for dimensionless stress are affected by three design factors input by the design engineer: the

degree of bond between the subbase and the surface slab, the shoulder type used in the design, and the axle configuration. An equation in the form of Equation 6 has been developed for every combination of these design factors.

Because all design factors are directly or indirectly predetermined from model inputs, the wheel load stress can be determined by rearranging the dimensionless stress equation to (*12*)

$$\sigma_{wls} = \frac{P \cdot s}{h^2} \tag{7}$$

Curl stress is calculated by considering the temperature differential that occurs within the slab due to daytime heating and nighttime cooling. The initial curl stress is calculated by Westergaard's analysis, and the stress is then corrected for slab length by the inclusion of a coefficient that considers the effect of L/ℓ. The following formulas mathematically describe total curl stress (*13*):

$$\sigma_{curl} = c_1 \cdot \sigma_0 \tag{8}$$

where

$$\sigma_0 = \frac{E_c \alpha \Delta t}{2(1 - \nu)}$$

and

$$c_1 = 1 - \frac{2 \cos \lambda \cosh \lambda}{\sin 2\lambda + \sinh 2\lambda} \cdot (\tan \lambda + \tanh \lambda)$$

where

$$\lambda = \frac{L}{\ell\sqrt{8}}$$

where

σ_{curl} = curl stress corrected for curvature,
σ_0 = Westergaard's uncorrected curl stress,
c_1 = curl correction for $L/1$,
α = coefficient of thermal contraction/expansion
Δt = temperature differential between top and bottom of slab, and
L = slab length.

The passing of axle loads over a concrete slab may sometimes cause erosion, which is the loss of underside slab support. Erosion can have a substantial effect on the total stress that develops on the slab edge. Erosion in the rigid pavement design program is incorporated by multiplying the total stress by an erosion factor, which is equal to 1 if there is no erosion, or a factor greater than 1 when erosion occurs. The erosion factor is based on the following equation:

$$\beta = 1.000 + 0.109 \cdot \left(\frac{\rho_s}{\ell}\right) + 0.034 \cdot \left(\frac{\rho_s}{\ell}\right)^2 \tag{9}$$

where β is the correction for erosion, and ρ_s is the rate of erosion.

The total stress can now be shown mathematically (*14*) as

$$\sigma_{tot} = (\sigma_{wls} + \alpha\sigma_{curl}) \cdot \beta \tag{10}$$

where α is a curl correction factor introduced to allow combination of the wls and the curl stress (*14*). However, it was set equal to 1 for this analysis because of favorable comparisons to other calculated total pavement stresses.

The methods described herein predict a single value for fatigue life in terms of N_f. This does not mean, however, that only one value of N_f exists for each specific pavement structure. Instead, N_f is probabilistically distributed. Because N_f is probabilistic, there exists for each pavement an expected value of N_f and an associated variance that describes the distribution N_f will follow. The variation affiliated with N_f results from the fact that the values used to calculate N_f are not exact values but are distributed over a range of values. As noted previously, most distribution parameters can be calibrated with field data. N_f is a parameter that fits into this category; however, N_f is sensitive to each specific pavement site, and the calibration can be different depending on the site.

LOAD-INDUCED CRACKING SUBSYSTEM FOR ASPHALT CONCRETE PAVEMENTS

As noted previously, the mean area of cracking is based on the damage function that relates allowable traffic to the tensile strain at the bottom of the asphalt layer. The cracked area is obtained from Equation 4, which states that the cracked area is given by the probability that the damage reaches or exceeds a value of 1. If a normal distribution for damage is assumed, the probability can be found from the following:

$$\text{prob}\,(D_j \geq 1) = \frac{1}{\sqrt{2\pi}\,\sigma_j} \int_1^\infty \exp\left[-\frac{1}{2}\left(\frac{t - \overline{D_j}}{\sigma_j}\right)^2\right] dt \tag{11}$$

where

$D_j = \sum n_i/N_{fi}$, damage function accumulated up to the jth period;
n_j = number of 18 Kip SAL repetitions during period i ($ESAL_i$);
N_{fi} = fatigue number of 18 Kip SAL repetitions that material can withstand to failure, given by Equation 1;
t = dummy variable of integration; and
σ_j = standard deviation of damage function.;

By using Cornell's first-order, second-order moment theory, the average damage function and its variance can be determined for the damage function. The TTI report assumes that the periods are independent one of the other, and thus the covariance terms in Equation 14 are nil (*5*). The mean damage or the expected value then can be computed using

$$\overline{D_j} = \sum_{i=1}^{j} \frac{\overline{n_i}}{\overline{N_{fi}}} = \sum_{i=1}^{j} \overline{\Delta D_i} \tag{12}$$

and the variance from

$$\text{Var}(D_j) = \text{Var}\left(\sum_{i=1}^{j} \Delta D_j\right) = \sum_{i=1}^{j} \text{Var}(\Delta D_i) \tag{13}$$

where

$$\text{Var}(\Delta D_i) = \sum_k \left(\frac{\partial \Delta D_i}{\partial X_k} \Big| \overline{x}_k \sigma_{x_k}\right)^2 + \left(\sum_l \sum_{k \neq l} \sum_k \frac{\partial \Delta D_i}{\partial X_k} \Big| \overline{x}_l \sigma_{x_l}\right) \rho_{kl} \tag{14}$$

where ρ_{kl} is the correlation coefficient between X_k and X_l.

The variables denoted X_k are all the variables of which ΔD_i is a function, with the exception of n_i (or the load repetitions), because the variance of the cracked area with respect to traffic is calculated separately from the variance of the cracked area because of pavement material parameters. Therefore, the computed cracked area as explained by the TTI report will be the area which corresponds to a given number of load repetitions (*5*). The derivative of ΔD_i with respect to X_k can then be shown as

$$\frac{\partial \Delta D_i}{\partial X_k} = \frac{\partial\left(\frac{1}{N_{fi}}\right)}{\partial X_k} \tag{15}$$

showing ϵ_i and N_{fi} as

$$\epsilon_i = \frac{p}{E_{sg}} \cdot F$$

$$-1n\left(\frac{1}{N_{fi}}\right) = k_1 \mathrm{Ln}10 + k_2 \mathrm{Ln}\left(\frac{\epsilon_i}{10^{-6}}\right) + k_3 \mathrm{Ln}\left(\frac{E_i}{1000}\right)$$

where F is a function of layer thicknesses and moduli, and k_i is parameter of fatigue law.

The derivatives then can be shown by the following expressions:

$$\frac{\partial\left(\frac{1}{N_{fi}}\right)}{\partial k_1} = -\frac{1}{N_{fi}} \mathrm{Ln}10 \tag{16}$$

$$\frac{\partial\left(\frac{1}{N_{fi}}\right)}{\partial k_2} = -\frac{1}{N_{fi}} \cdot \mathrm{Ln}\left(\frac{\epsilon_i}{10^{-6}}\right)$$

$$\frac{\partial\left(\frac{1}{N_{fi}}\right)}{\partial k_3} = -\frac{1}{N_{fi}} \cdot \mathrm{Ln}\left(\frac{E_i}{1000}\right)$$

$$\frac{\partial\left(\frac{1}{N_{fi}}\right)}{\partial T_l} = -\frac{1}{N_{fi}} \cdot \frac{k_2}{\epsilon_i} \cdot \frac{p}{E_{sg} a} \cdot \frac{\partial F}{\partial\left(\frac{T_l}{a}\right)} \qquad l = 1, 2, 3$$

$$\frac{\partial\left(\frac{1}{N_{fi}}\right)}{\partial E_l} = -\frac{1}{N_{fi}} \cdot \frac{k_2}{\epsilon_i} \cdot \frac{p}{E_{sg}^2} \cdot \frac{\partial F}{\partial\left(\frac{E_l}{E_{sg}}\right)} - \frac{1}{N_{fi}} \frac{k_3}{E} \delta_{ml}$$

$$l = 1, 2, 3; m = 1 \text{ or } 2$$

$$\frac{\partial\left(\frac{1}{N_{fi}}\right)}{\partial E_{sg}} = -\frac{1}{N_{fi}} \cdot \frac{k_2}{\epsilon_i} \cdot \frac{p}{E_{sg}} \cdot \left[-\frac{F}{E_{sg}} + \sum_{l=1}^{3} \frac{\partial F}{\partial\left(\frac{E_l}{e_{sg}}\right)} \cdot \left(-\frac{E_l}{E_{sg}^2}\right)\right]$$

where δ_{ml} is Kronecker's Delta.

The derivatives of F are calculated by the Langrangian interpolation regression equations that are discussed in the TTI report and shown by Equation 5 in this paper.

In the TTI report it is stated that by knowing the average value of the damage D_j and its variance at the end of the period j, the average cracked area for a given number of repetitions can be computed (*5*).

Variance of Cracked Area with Respect to Number of Repetitions

The determination of the variance of the cracked area for the flexible pavement design system is divided into two components: (*a*) the variance with respect to the number of load applications up to and including the present period and (*b*) the variance with respect to the pavement parameters. The TTI report proceeds through the derivation of the variance of the cracked area with respect to the number of load applications by expressing the cracked area as

$$C = \frac{1000}{\sqrt{2\pi}} \int_1^{\infty} \frac{1}{\sigma_j} \exp\left[-\frac{1}{2}\left(\frac{t-\overline{D}_j}{\sigma_j}\right)\right] dt \tag{17}$$

The variance of cracking due to the variability in the number of load repetitions is shown by using the Taylor series approximation.

$$\mathrm{Var}(C) = \left(\frac{\partial C}{\partial N} \Big|_{\overline{N}}\right)^2 \cdot \mathrm{Var}(N) \tag{18}$$

where

$$D_j = \sum_{i=1}^{j} \frac{n_i}{N_{fi}}$$

and the variance is expressed as

$$\sigma_j = \sigma = \sum_{i=1}^{j} \sum_{k} \left[\frac{\left(\frac{1}{N_{fi}}\right)}{\partial x_k} \Big| \overline{x}k\right]^2 \cdot \mathrm{Var}(X_k) \cdot n_i^2 = \sum_{i=1}^{j} c_i n_i^2$$

The TTI report continues with the rest of the derivation by the following equations and using the transformation

$$\frac{t - D}{\sigma} = T \qquad dt = \sigma dT$$

with the limits

$$t = \infty \qquad T = \infty$$

$$t = 1 \qquad T = T_1 = \frac{1 - D}{\sigma}$$

This gives the error function

$$C = 1000\left[\frac{1}{\sqrt{2\pi}} \int_1^{\infty} \exp\left(-\frac{1}{2} T^2\right) dT\right] \tag{19}$$

Then taking the derivative with respect to load repetitions gives

$$\frac{\partial C}{\partial N} = \frac{1000}{\sqrt{2\pi}} \int_{T_1}^{\infty} -T \exp\left(-\frac{1}{2} T^2\right) \frac{\partial T}{\partial N} dT \tag{20}$$

Using these above definitions,

$$\frac{\partial T}{\partial N} = -\frac{1}{\sigma}\frac{\partial D}{\partial N} - \frac{T}{\sigma}\frac{\partial \sigma}{\partial N} = -DN - T \cdot SN$$

$$\frac{\partial D}{\partial N} = \sum_{i=1}^{j} \frac{1}{N_{fi}}\frac{\partial n_i}{\partial N} = \sigma \cdot DN$$

$$\frac{\partial \sigma}{\partial N} = \frac{1}{\sigma}\sum_{i=1}^{j} c_i n_i \frac{\partial n_i}{\partial N} = \sigma \cdot SN$$

$$N = N_j = \sum_{i=1}^{j} n_i$$

where N is N_j, the number of load repetitions (ESALs) accumulated during j periods.

Substituting $\frac{\partial T}{\partial N}$ Equation (20) gives

$$\frac{\partial C}{\partial N} = \frac{1000}{\sqrt{2\pi}} \int_{T_1}^{\infty} (DN \cdot T + SN \cdot T^2) \exp\left(-\frac{1}{2} T^2\right) dT$$

This function is integrated by parts to give

$$\frac{\partial C}{\partial N} = \frac{1000}{\sqrt{2\pi}} (DN + SN \cdot T_1) \exp\left(-\frac{1}{2} T_1^2\right) + SN \cdot C$$

The TTI report details the derivative $\frac{\partial n_i}{\partial N}$ as shown in these definitions as evaluated from the traffic growth as follows (Figure 1):

$$\frac{\partial n_j}{\partial N_j} = \frac{\frac{\partial n_j}{\partial y}}{\frac{\partial N_j}{\partial y}} = \frac{\left(\frac{BL - AL}{20}\right)(y_j - y_{j-1})}{AL + \left(\frac{BL - AL}{20}\right) y_j} \quad (21)$$

The report also discusses how the variance of traffic affects the variance of the cracked area,

> Since the cracked area increases sharply with the number of repetitions after cracking has initiated, the Var[C] with respect to N may be very large. The flexible pavement design model implements a Var[log N] = 0.0355. After transformation, one gets Var[N] = 0.188^2 (or a standard deviation of $0.43N$).
>
> The variance of N is due to the variation of several factors such as design ADT, the percent of trucks in the traffic mix, axle load equivalency factors, and the distribution of the axle loads. Variation in ADT may be considered to be a between project variation and should not be included in the Var[N] term. However, the remaining factors do have a contribution to within project variation and should be included in the Var[N] (5).

Variance of Cracked Area with Respect to Pavement Parameters

The second portion of the variance of the cracked area deals with the pavement parameters. The initial portion of the derivation is similar to that shown in the derivation of the variance of the cracked area with respect to the number of load applications. The variance of the cracked area with respect to the pavement parameters is shown mathematically as the following:

$$\text{Var}(C) = \sum \left(\frac{\partial C}{\partial x_k}\Big|_{\bar{x}_k}\right)^2 \text{Var}(x_k) + \left(\sum_{\ell}\sum_{\substack{k \\ k \neq \ell}} \frac{\partial C}{\partial x_k}\Big|_{\bar{x}_k} \sigma x_k \frac{\partial C}{\partial X_l}\Big|_{\bar{x}_\ell} \sigma x_\ell\right) \rho_{k\ell} \quad (22)$$

By taking the derivative of Equation 19 with respect to the pavement parameters, the following is obtained:

$$\frac{\partial C}{\partial x_k} = \frac{1000}{\sqrt{2\pi}} \int_{T_1}^{\infty} -T \exp\left(-\frac{1}{2} T^2\right) \frac{\partial T}{\partial x_k} dT$$

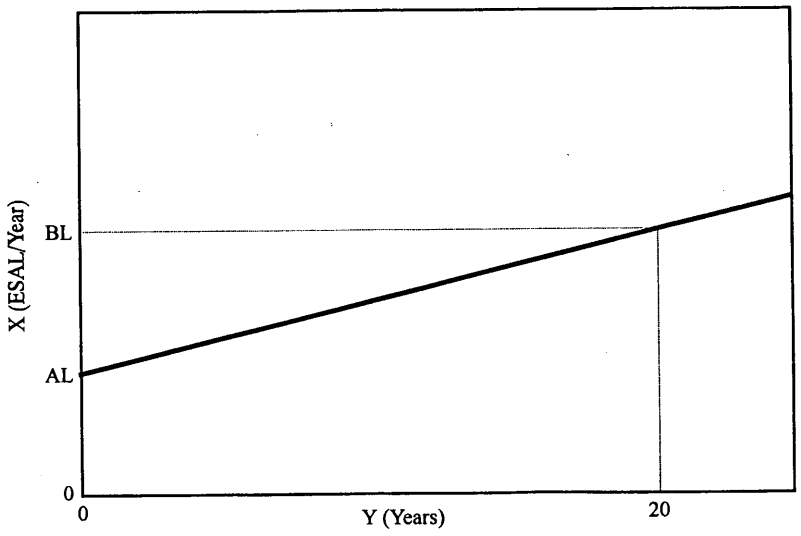

FIGURE 1 Traffic characterization in flexible pavement design system.

with

$$\frac{\partial T}{\partial x_k} = -\frac{1}{\sigma}\frac{\partial D}{\partial x_k} - \frac{T}{\sigma}\frac{\partial \sigma}{\partial x_k} = -DD - DS \cdot T$$

By following the same steps as before, the following is obtained:

$$\frac{\partial C}{\partial x_k} = \frac{1000}{\sqrt{2\pi}} \int_{T_1}^{\infty} (DD \cdot T + DS \cdot T^2) \exp\left(-\frac{1}{2} T^2\right) dT$$

Integration by parts gives

$$\frac{\partial C}{\partial X_k} = \frac{1000}{\sqrt{2\pi}} \cdot \frac{1}{\sigma}\frac{\partial D}{\partial X_k} \exp\left(-\frac{1}{2} T_1^2\right) + \frac{1}{\sigma}\frac{\partial \sigma}{\partial X_k}\left[\frac{1000}{\sqrt{2\pi}} T_1 \exp\left(-\frac{1}{2} T_1^2\right) + C\right] \quad (23)$$

Recalling the damage function

$$D = \sum_{i=1}^{j} \frac{n_i}{N_{fi}}$$

the variance of the damage with respect to the pavement parameters can be obtained as

$$\sigma^2 = \sum_{i=1}^{j}\left[\sum_{\ell}\left(\frac{\partial\left\{\frac{1}{N_{fi}}\right\}}{\partial X_\ell}\Big|_{\bar{x}_\ell}\right)^2 \mathrm{Var}(X_\ell)\right] n_i^2$$

$$\frac{\partial D}{\partial X_k} = \sum_{i=1} \frac{\partial\left(\frac{1}{N_{fi}}\right)}{\partial X_k} n_i = \sum_i \frac{\partial \Delta D_i}{\partial X_k}$$

$$\frac{1}{\sigma}\frac{\partial \sigma}{\partial X_k} = \frac{1}{2\sigma^2}\sum_{i=1}^{j}\left\{\sum_{\ell} 2 \cdot \left(\frac{\partial\left\{\frac{1}{N_{fi}}\right\}}{\partial X_\ell}\Big|\bar{x}l\right) \cdot \left(\frac{\partial^2\left(\frac{1}{N_{fi}}\right)}{\partial X_k \partial X_\ell}\Big|\bar{x}_k, \bar{x}_\ell\right) \mathrm{Var}(X_\ell) n_i^2\right\} \quad (24)$$

The determination of σ is explained in the TTI report by the following statements:

> It seems that the variance of C is due to two causes: (a) the variation of D with respect to the value of one (shifting of the density distribution curve), and (b) the variation of σ (flatness of the bell shape of the curve). The contribution of σ is very complex to evaluate because it involves the evaluation of mixed derivatives. Therefore, the term with σ was dropped, assuming that its contribution is negligible (*5*).

Substituting Equations 23 and 24 into 22 and assuming the contribution of σ is negligible,

$$\mathrm{Var}(C) = \sum_{i=1}^{j} \frac{10^6}{2\pi}\frac{1}{\sigma^2}\left\{\exp\left[-\frac{1}{2}\left(\frac{1 - D_i}{\sigma_i}\right)^2\right]^2\right\} * \sum_k \left(\frac{\partial \Delta D_i}{\partial X_k}\Big|\bar{x}_k\right) \mathrm{Var}(X_k) + \left(\sum_{\ell}\sum_{\substack{k \\ k \neq \ell}} \frac{\partial \Delta D_i}{\partial X_k}\Big|\bar{x}_k \sigma x_k \frac{\partial \Delta D_i}{\partial X_l}\Big|\bar{x}_\ell \sigma x_\ell\right) \rho_{k\ell} \quad (25)$$

> The variance of cracking with respect to pavement parameters and the variance of cracking with respect to number of repetitions is combined into an overall variance of cracking (Var[C]) leading to the determination of the level of cracking corresponding to various levels of reliability . . . (*5*).

LOAD-INDUCED CRACKING SUBSYSTEM FOR PORTLAND CEMENT CONCRETE PAVEMENTS

The development of a fatigue crack in a concrete slab can be defined as the probability that the accumulated fatigue damage exceeds a critical level of fatigue damage ($D_c = 1$), as stated previously. Hence, the variance of cracking and mean level of cracking are related to variance and mean level of fatigue damage, as is the case with the asphalt concrete system. Accordingly, the percent mean cracking level is the probability that some critical level of damage has been surpassed, as shown by Equation 4.

The average damage function and its variance are computed in the same manner as in the asphalt concrete system in that Cornell's first-order, second-moment method is used and the assumptions are identical. The variance of damage is computed using the following equations:

$$\mathrm{Var}(D_i) = \sum \mathrm{Var}(\Delta D_i)$$

$$\mathrm{Var}(\Delta D_i) = \sum \left(\frac{\partial \Delta D_i}{\partial x_k}\right)^2 \mathrm{Var}(X_k)$$

where i corresponds to each time period.

The variance of the incremental damage for the asphalt concrete system is shown by Equation 14, and the only changes that would occur for the portland cement concrete (PCC) system are the variables X_k, which are involved with the computation of ΔD_i. The fatigue law for the PCC system is stated in Equation 2. Equation 10 shows that the total stress is an accumulation of the wheel load stress, curl stress, and stress induced from the loss of underside support. Accordingly, the percentage of midslab cracks computed will be a direct function of the number of load repetitions to which the pavement is subjected. The derivative of ΔD_i with respect to X_k is given by Equation (15) and is the same for the PCC pavement design system as it is for the asphalt concrete pavement design system. The respective PCC pavement derivatives of $1/(N_f)$ with respect to X_k are given as the following:

$$\frac{\delta\left(\frac{1}{N_f}\right)}{\delta k_1} = -\frac{b}{N_f}$$

$$\frac{\delta\left(\frac{1}{N_f}\right)}{\delta k_2} = \frac{br}{N_f}$$

$$\frac{\delta\left(\frac{1}{N_f}\right)}{\delta Mr} = -\frac{bk_2\sigma}{N_f Mr^2}$$

$$\frac{\delta\left(\frac{1}{N_f}\right)}{X_k} = \frac{bk_2}{N_f \cdot Mr} \cdot \frac{\delta \sigma}{\delta X_k}$$

where $X_k = h$, k_{sg}, E_c, ν, and a. The derivatives $\delta\sigma/\delta X_k$ equal the following:

$$\frac{\delta\sigma}{\delta X_k} = \frac{\delta\beta}{\delta X_k}(\sigma_{wls} + \sigma_{curl}) + \frac{\delta(\sigma_{wls} + \sigma_{curl})}{\delta X_k}\beta \quad (26)$$

where the derivatives of $\delta\beta/\delta X_k$ can be developed from the equations given previously.

Field data for damage suggest that their density function almost matches the Weibull distribution. Therefore, in the concrete pavement design procedure, the general form of damage distribution (or probability density function) can be approximated by

$$\text{pdf}(D_i) = \frac{\beta}{\alpha}\left(\frac{D_i}{\alpha}\right)^{\beta-1}\exp\left[-\left(\frac{D_i}{\alpha}\right)^{\beta}\right] \quad \text{for } D_i > \nu_s$$

where

ν_s = 0 for damage calculations,
D_i = accumulated fatigue damage up to period i, and
β, α = shape and scale parameters for the Weibull distribution, respectively.

If $\xi = (D_i/\alpha$ and $d\xi = 1/\alpha$ are substituted with $\xi^{\beta} = \nu$ and $\beta\xi^{l-1} = d\nu$,

$$\text{pdf}(D_i) = \frac{\beta}{\alpha}\xi^{\beta-1}e^{\xi^{\beta}}$$

The probability that the accumulated damage (D_i) is less than the critical damage (D_c) is

$$\text{prob}(D_i < D_c) = \int_0^{D_c} f(D_i)\,dD_i$$

$$= \frac{\beta}{\alpha}\int_0^{\xi_c} \xi^{\beta-1}e^{\xi^{\beta}}\alpha\,d\xi$$

$$= \int_0^{\nu_c} e^{-\nu}\,d\nu$$

with $\nu_c = \xi_c^{\beta} = \left(\frac{D_c}{\alpha}\right)^{\beta}$ and the previous substitutions. However, recall that

$$\%C = \text{prob}(D_i > D_c)$$

Therefore,

$$\%C = 100 - 100\int_0^{\nu_c} e^{-\nu}\,d\nu = \frac{100}{e^{\nu_c}} \quad (27)$$

The variance of cracking can be developed from Equation 28 and comprises the same two components as shown in the asphaltic concrete system: (a) variance of cracking due to variance in material parameters (X_k) and (b) variance of cracking due to variance in traffic (N). Mathematically, the total variance is expressed as

$$\text{Var}(C) = \text{Var}(C)_{x_k} + \text{Var}(C)_N$$

Variance of Cracking Due to Material Parameters

The material parameters (X_k) affecting the variance of slab cracking are identified as pavement thickness (h), subgrade k value (k_{sg}), concrete modulus of elasticity (E_c), concrete modulus of rupture (Mr), Poisson ratio (ν), and the fatigue parameters k_1 and k_2. Another term that can be included but is not a material property is the radius of the load area (a). The variance of cracking due to the material parameters is

$$\text{Var}(C)_{x_k} = \sum\left(\frac{\partial C}{\partial X_k}\right)^2\text{Var}(X_k) + \sum\sum\left(\frac{\partial C}{\partial X_k}\sigma_{x_k}\frac{\partial C}{\partial X_l}\sigma_{x_l}\right)\rho_{kl} \quad (28)$$

where ρ_{kl} is the correlation coefficient between X_k and X_l.

The partial differentiation of cracking with respect to material parameters, X_k, $(\{\partial C\}/\{\partial X_k\})$ is determinated by differentiating Equation 27:

$$\frac{\partial C}{\partial X_k} = 100\int_0^{\nu_c}\frac{\partial \nu}{\partial X_k}e^{-\nu}\,d\nu$$

$$\text{where } \frac{\partial \nu}{\partial X_k} = \frac{\partial[(\xi)^{\beta}]}{\partial X_k} = \beta(\xi)^{\beta-1}\frac{1}{\alpha}\left[\frac{\partial D_i}{\partial X_k}\right]$$

which can be further reduced to

$$\frac{\partial C}{\partial X_k} = -100\cdot\frac{\beta}{\alpha}\cdot\left(\frac{\partial D_i}{\partial X_k}\right)\int_0^{\nu_c}(\xi)^{\beta-1}e^{-\nu}\,d\nu$$

$$= -100\cdot\frac{e}{\alpha}\cdot\left(\frac{\partial D_i}{\partial X_k}\right)\int_0^{\nu_c}\nu^r e^{-\nu}\,d\nu$$

$$= -100\cdot\frac{\beta}{\alpha}e^{-\nu_c}(\nu_c^r)\left(\frac{\partial D_i}{\partial X_k}\right)$$

Therefore

$$\frac{\sigma C}{\sigma X_k} = -\%C\cdot\frac{\beta}{\alpha}\nu_c^r\left(\frac{\partial D_i}{\partial X_k}\right)$$

$$\text{where } r = \frac{\beta - 1}{\beta}$$

The derivative of cracking with respect to the material parameters can be substituted in Equation 28 to obtain the variance of cracking due to the material parameters. Note the following derivatives for damage with respect to the pavement parameters:

$$\frac{\sigma D_i}{\sigma X_k} = \frac{\partial\left(\frac{1}{N_f}\right)}{\partial X_k}n_i \quad (29)$$

The derivatives of Equation 29 are shown previously in this section.

Variance of Cracking Due to Traffic

The variance of cracking due to traffic (N) is expressed as the following:

$$\text{Var}(C)_N = \left\{ \frac{\partial C}{\partial N} \Big|_{\bar{N}} \right\}^2 \text{Var}(N)$$

which is the same for asphalt concrete pavements. By using the probability density function for the Weibull distribution to express the percent of midslab cracks from Equation 27, the derivative $\delta C/\delta N$ can be evaluated as

$$\frac{\sigma C}{\sigma N} = 100 \cdot \int_0^{\nu_c} \frac{\delta \nu}{\delta N} e^{-\nu} \delta \nu$$

$$\text{where } \frac{\delta \nu}{\delta N} = \frac{\beta}{\alpha} \left[\frac{D_i}{\alpha} \right]^{\beta - 1} \frac{\delta D_i}{\delta N}$$

and

$$\frac{\delta D_i}{\delta N} = \sum_{i=1}^{j} \frac{1}{N_f} \frac{\delta n_i}{\delta N}$$

The derivative $\delta D_i/\delta N$ is evaluated from the traffic growth, and the derivative $\delta n_i/\delta N$ is the same as in Equation 21 for the asphalt concrete pavements. Substituting and completing the integration for the evaluation of $\delta C/\delta N$ results in the following equation:

$$\frac{\delta C}{\delta N} = 100 \cdot \frac{\beta}{\alpha} e^{-\nu_c} \nu_c^r \frac{\delta D_i}{\delta N} = -\bar{C} \frac{\beta}{\alpha} \nu_c^r \frac{\delta D_i}{\delta N}$$

where

β = Weibull distribution shape parameter,
α = Weibull distribution scale parameter,
$\nu_c = (D_c/\alpha)^\beta$, and D_c is a calibration term and equals 1 for these purposes, and
$r = (\beta - 1)/\beta$.

Therefore, the derivatives for cracking with respect to the material parameters and with respect to traffic as well as the variance for each of the material parameters (by assuming a coefficient of variation for each parameter) have been defined. However, the variance due to traffic is yet to be determined.

The variance of traffic, or Var(N), is influenced by several factors previously discussed in the asphalt concrete pavements section on the variance of cracking due to traffic. These factors include, but are not exclusive to, the distribution of axle loads, axle equivalency factors, and the percentage of trucks in the design traffic. Design traffic repetitions do not necessarily have to be in terms of equivalent loads, ESALs, to compute appropriate distress, but can be expressed in terms of axle load groups as an alternative. The design engineer will determine which method is most appropriate for the project design. With the availability of high-speed personal computers, this type of traffic expression can be achieved without increasing computing time excessively.

SENSITIVITY ANALYSIS OF SELECTED DESIGN INPUTS FOR TWO KENTUCKY PAVEMENTS

When comparing design alternatives that evaluate reliability consistently, it is important to know which variable inputs have the most impact on the range of any given level of reliability. This stems from the notion that errors that do occur in the assessment of design reliablity can manifest themselves in two ways: (a) an incorrect prediction of the mean level of distress and (b) an incorrect prediction of the increase in the amount of distress for a given level of design reliability. If, for any reason, one or both of these incorrect predictions occur in the design process, a biased prediction of pavement life and reliability will cause one pavement type to have an advantage over or to be at a disadvantage to the other in terms of life-cycle cost predictions. A consistent comparison between the two designs, therefore, cannot be achieved.

A sensitivity analysis can be useful in assessing how any given input parameter affects the resulting design (i.e., mean value and the increase in distress for a given level of reliability). This type of exercise will identify design values that must be carefully selected and that can have a significant impact on the design result. In addition, the exercise will ensure that consistent levels of reliability are maintained in the design process and that reasonable judgments will be made with respect to the most cost-effective pavement.

Two pavements in Kentucky with different design criteria have been chosen as an example. A sensitivity study is concluded on various design inputs to determine which inputs have the greatest effect on the prediction of design life. A sensitivity study is conducted by varying the chosen design inputs by plus and minus the assigned coefficients of variation from the mean level of the design inputs. The design inputs used in the sensitivity study of these two pavements are the subgrade strength with a coefficient of variation of 30 percent, the traffic level in ESALs per year with a coefficient of variation of 20 percent, the surface layer modulus with a coefficient of variation of 20 percent, and the input surface thickness with a coefficient of variation of 10 percent. Change in the value of the coefficient of variation for a design variable does not necessarily have a significant effect on the overall calculated variance. Therefore, if a coefficient is assumed for a design value that is not known, the effect on the calculated variance should not be significant.

Pavement site A has a relatively weak subgrade (41,370 Kilopascals) and low traffic (3 million ESALs). Its design includes a granular base layer in both pavement systems. The sensitivity analysis for the flexible pavement indicated that as subgrade strength was varied by its coefficient of variation, a substantial percent change in thickness occurred (Figure 2). The percent change in thickness as traffic varied was slightly smaller but followed the same pattern. The pattern reversed somewhat for the surface modulus and surface thickness but stayed consistent. As surface thickness varied, the percent change was measured in allowable traffic. This analysis indicates that with low traffic and a weak subgrade, the flexible pavement design is moderately sensitive to changes in subgrade modulus, allowable traffic, and surface modulus; however, it is much less sensitive to changes in surface thickness.

The sensitivity analysis for the portland cement concrete pavement indicates that as subgrade modulus varied by its coefficient of variation, no difference was measured in the required thickness, and essentially the same was indicated as traffic varied by its coefficient (Figure 3). As the PCC surface modulus varied, some change in surface thickness was indicated; however as the surface thickness varied by its coefficient of variation, there was considerable change in

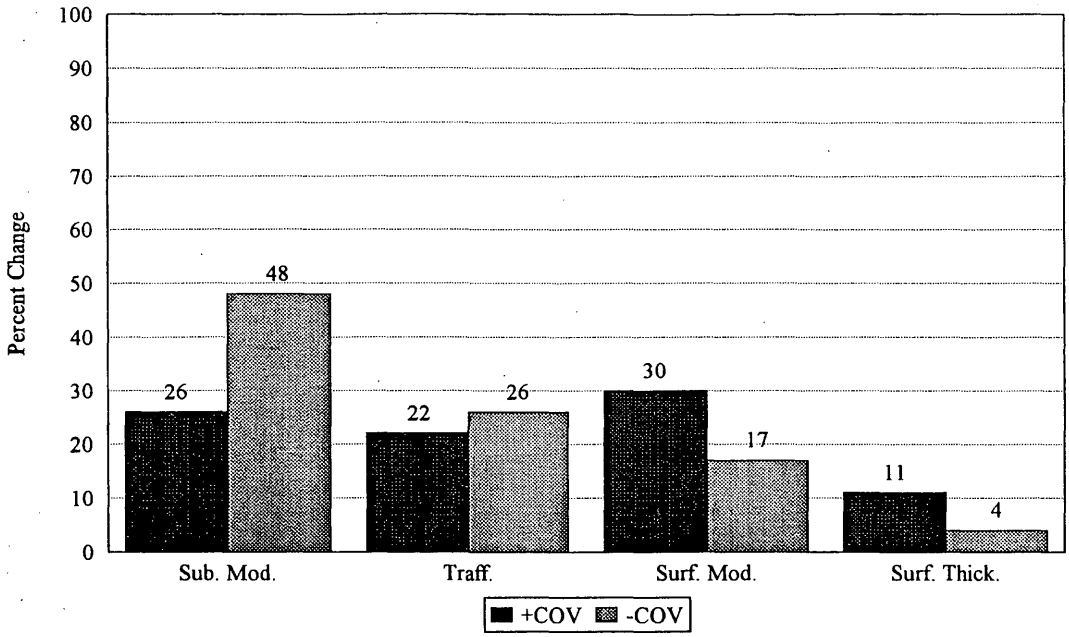

FIGURE 2 Percent change from mean input for asphalt concrete design, pavement site A.

the allowable traffic. This indicates that at lower traffic levels and subgrade strength, concrete pavements cannot be sensitive to subgrade modulus and allowable traffic, but are sensitive to the input surface thickness.

The sensitivity analysis for pavement site B, which consisted of a high traffic level (88 million ESALs) and a moderately strong subgrade (113,767 Kilopascals), generally followed the same type of trends as pavement site A for both pavement types.

For this design, the flexible pavement seemed to be less sensitive to variations in subgrade modulus, traffic, and surface modulus and more sensitive to variations in surface thickness (Figure 4). This indicates that as required thickness and allowable traffic increase, other design parameters become less of a factor.

The analysis of the PCC design for higher traffic indicates that all design parameters are somewhat sensitive to variations in their design values (Figure 5). The large differences between pavement

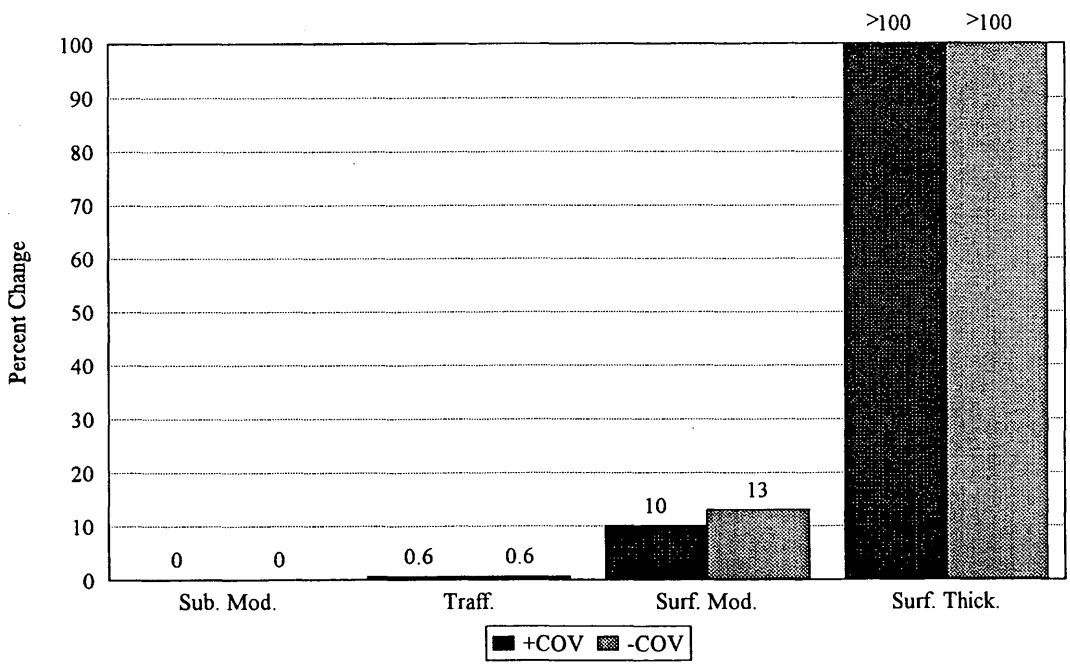

FIGURE 3 Percent change from mean input for PCC design, pavement site A.

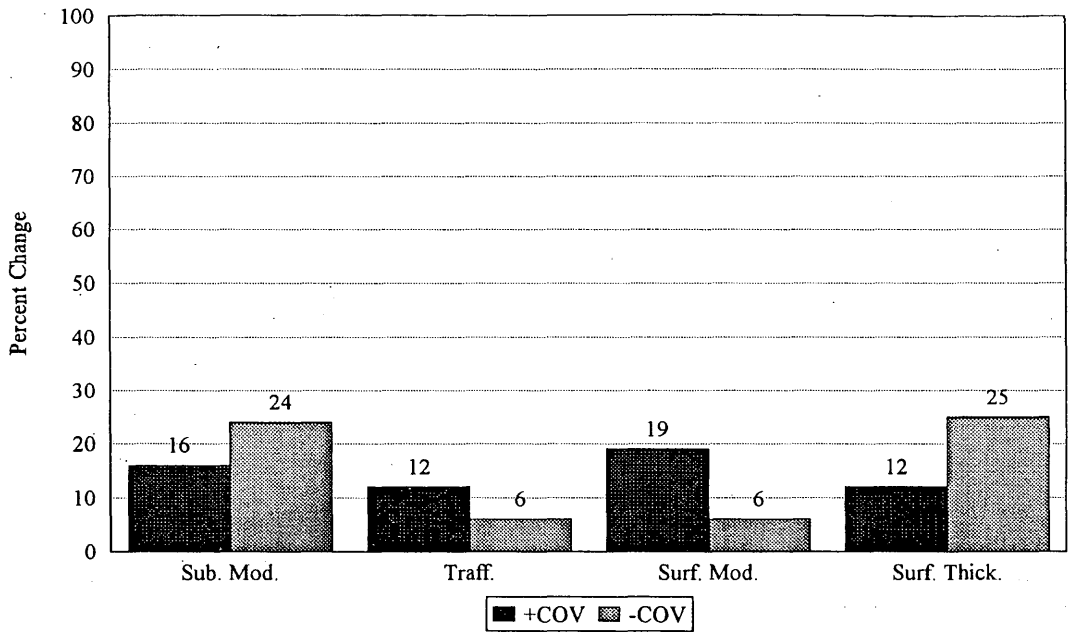

FIGURE 4 Percent change from mean input for asphalt concrete design, pavement site B.

sites A and B occurred as traffic and surface thickness varied. This indicates that as required thickness and allowable traffic increase, the rigid pavement design system becomes more sensitive to changes in subgrade modulus and input traffic and considerably less sensitive to variations in surface thickness. The two rigid pavement designs have approximately the same sensitivity to variations in surface modulus.

The conclusions that can be drawn from this sensitivity analysis follow:

- As traffic level and subgrade modulus differ, design parameter sensitivity changes in both pavement types, but to a lesser extent in PCC pavements.
- The trends in percent change for the flexible pavement design as predicted by the previously described design process are consistent with other studies on design parameter sensitivity.
- The trends in percent change for the rigid pavement design indicate that PCC pavements are not sensitive to small changes in subgrade strength or levels of traffic.

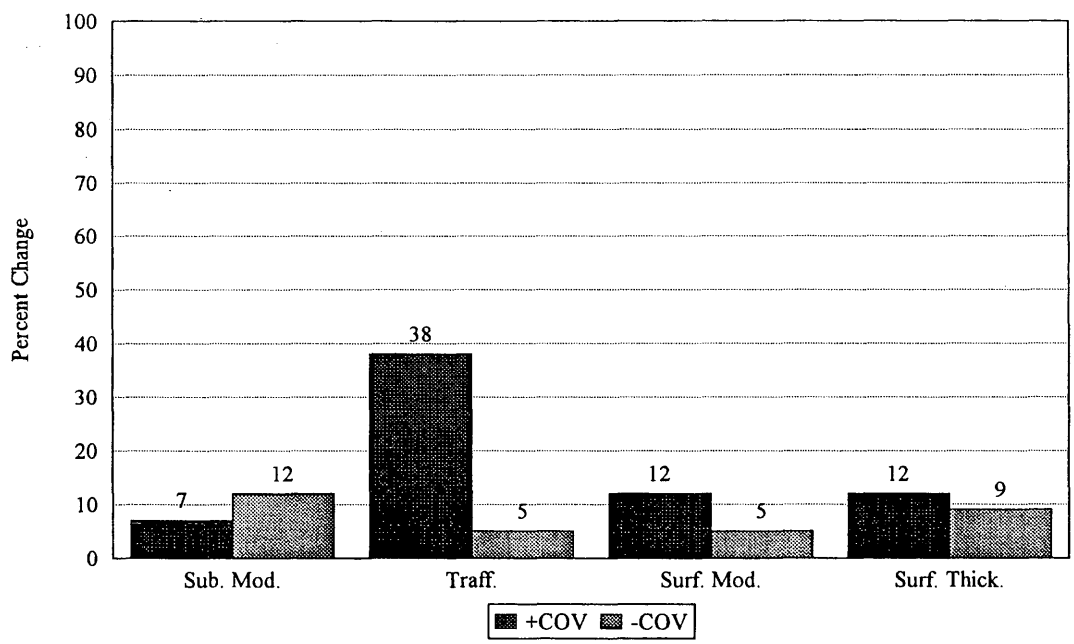

FIGURE 5 Percent change from mean input for PCC design, pavement site B.

CONCLUSIONS

The inclusion of reliability in pavement designs, or in any design of this type, is an important and required step to ensure safety and quality, while meeting economic considerations. Therefore, the design reliability must be quantifiable and based on proven mathematical concepts and statistics. Mechanistic/empirical pavement designs are tools with which sound reliability-based designs can be accomplished. One such approach that addresses many of the challenges facing pavement designers today has been presented. A rational attempt was made at applying reliability concepts consistently to designs of differing pavement types so that a fair and equitable judgment can be made between designs on a life-cycle cost basis.

Although many challenges have been addressed, there are still hurdles to overcome with these types of designs. One hurdle exists in the assignment of coefficients of variation to design inputs. Currently, there are limited data available for quantification of variations associated with construction activities, environment, traffic loadings, and materials testing. Therefore, previous experience, along with the available data, is used to assign coefficients of variation, which immediately introduces a possible bias when attempting to compare pavement designs.

A second challenge to overcome relates to the comparison between pavement types when designs have been completed. Every attempt was made to apply design concepts consistently between pavement types; however, no two pavement designs will be alike because of inherent differences in theory. For example, How is a designer to know whether the estimates of serviceability between two pavement types have equivalent variabilities? An even more complicated question arises: How is a designer to know whether the estimates of variability of rutting for the flexible pavement design are the same as estimates of variability of faulting and other distresses for the rigid pavement design? This question, which presents a very complex issue, currently has no answer.

Another bias along these same lines that can be introduced is in the assignment of failure criteria for condition measurements. Again, How is the design engineer supposed to know that the predicted performance between two pavement designs is equivalent? For example, if the flexible pavement design fails in rutting, which is specified at ½ in., and the rigid pavement design fails in fatigue cracking, which is specified at 20 percent failed slabs, how does the design engineer know that the predicted performance between the two pavement types is equivalent?

Even with these shortcomings, the mechanistic/empirical pavement designs introduced in this paper are a positive step toward improving today's pavement designs. With the help of personal computers and climatic effects models, mechanistic/empirical designs that incorporate consistent approaches to design reliability should produce suitable pavement systems for both pavement types, and reasonable judgments that show appropriate sensitivity to typical variations in pavement design parameters can be made.

REFERENCES

1. Ang, A. H. S., and W. H. Tang. Probability Concepts in Engineering Planning and Design. Vol. 1, *Basic Principles.* John Wiley & Sons, Inc., New York, 1975.
2. Harr, M. E. *Reliability Based Design in Civil Engineering.* McGraw-Hill, New York, 1987.
3. Zollinger, D. G., and R. L. Lytton. *Engineering Reliability in the Mechanistic/Empirical Design of Highway Pavements.* Unpublished report prepared for the National Coalition for Mechanistic Design. Nov. 1991.
4. Zollinger, D. G., and B. F. McCullough. Development of Reliability Factors and Analysis for the Calibration of Pavement Design Models Using Field Data. Presented at the Transportation Research Board 73rd Annual Meeting, Washington, D.C., 1993.
5. Uzan, J., D. G. Zollinger, and R. L. Lytton. *The Texas Flexible Pavement System (TFPS) Mechanistic/Empirical Model.* FHWA/Tx-91/455-1. Texas Transportation Institute, Research Report 2455-2, College Station, Nov. 1990.
6. Zollinger, D. G., and B. K. Killingsworth. *The Rigid Pavement Design System (RPDS) Mechanistic/Empirical Model.* Texas Transportation Institute, College Station, March 1992.
7. Miner, M. A. Cumulative Damage in Fatigue. *Transactions, American Society of Mechanical Engineers,* Vol. 67, 1945, pp. A159–A164.
8. Finn, F., C. Saraf, R. Kulkarni, K. Nair, W. Smith, and A. Abdullah. The Use of Distress Prediction Subsystems for the Design of Pavement Structures. *Proc., 4th International Conference on Structural Design of Asphalt Pavements,* Ann Arbor, Mich., Vol. 1, 1977, pp. 3–38.
9. Zollinger, D. G., and E. J. Barenberg. A Mechanistic Based Design Procedure for Jointed Concrete Pavements. Presented at 4th International Conference on Concrete Pavement Design and Rehabilitation, Purdue University, West Lafayette, Indiana, 1989, pp. 95–97.
10. *BISAR: Layered System Under Normal and Tangential Loads.* Shell-Koninilijke/Shell Laboritorium, Amsterdam, The Netherlands, 1972.
11. *A Computerized Two-Dimensional Finite Element Slab Analysis Model.* Illi-Slab, Update. University of Illinois, 1983.
12. Ioannides, A. M., and R. A. Salsilli-Murua. Temperature Curling in Rigid Pavements: An Application of Dimensional Analysis. In *Transportation Research Record 1127,* TRB, National Research Council, Washington, D.C., 1987, pp. 1–11.
13. Westergaard, H. M. Analysis of Stress in Concrete Pavement Due to Variations in Temperature. *Public Roads,* Vol. 8, No. 3, May 1927, pp. 54–60.
14. Darter, M. I. *Design of Zero-Maintenance Plan Jointed Concrete Pavement: Vol. I, Development of Design Procedures.* Technical report to FHWA. [University of Illinois, Champaign, June 1977].

Publication of this paper sponsored by Committee on Flexible Pavement Design.

Assessment of Computer Programs for Analysis of Flexible Pavement Structure

DAR-HAO CHEN, MUSHARRAF ZAMAN, JOAKIM LAGUROS, AND ALAN SOLTANI

Five computer programs were reviewed and evaluated to establish the most appropriate one for routine pavement structural analysis, including two 2-D axisymmetric finite-element programs (ILLI-PAVE and MICH-PAVE), one 3-D finite-element program (ABAQUS), and two multilayered elastic-based programs (DAMA and KENLAYER). The most commonly used criteria for pavement design—the maximum surface deflection, tensile (radial) strain at the bottom of the asphalt concrete (AC) layer, and compressive strain at the top of subgrade—were used as the basis for selection. The effects due to treatment of dual-wheel and single-wheel loading and idealization of linear and nonlinear on pavement structure responses were also investigated. For linear and nonlinear analyses, only DAMA and MICH-PAVE satisfy the natural boundary conditions in which the vertical stresses equal the imposed contact pressure of 689 kPa (100 psi). For linear analysis, MICH-PAVE gives the intermediate maximum surface deflection, compressive strain, and tensile strain; for nonlinear analysis, DAMA yields the intermediate maximum surface deflection, compressive strain, and tensile strain. The natural boundary condition is also satisfied in DAMA, and dual-wheel loading can also be considered in computations. The results from ABAQUS yield the lowest tensile strain compared with other programs. The stress-dependant behavior of the material within each layer can be represented using MICH-PAVE and DAMA only when the thickness of the AC layer (h1) is about 22.86 cm (9 in.) or more. The difference between dual-wheel and single-wheel loading is more prominent when h1 is thin (with a maximum difference of 40.5 percent when h1 is 7.62 cm). This suggests that DAMA is probably the most appropriate computer program, among the five computer programs investigated, to use for routine structural analyses of flexible pavements.

More and more flexible pavement designs are being based on a mechanistic approach. In a mechanistic design procedure, a structural analysis tool or computer program is required to predict the stress-strain and displacement response of pavements. A number of computer programs based on the Finite-Element (FE) or the multilayered elasticity (MLE) method have been developed and used for structural analysis of flexible pavement (*1–5*). Overall, the MLE-based procedures are more widely used (*6*) because of their simplicity, but they may suffer from the inability to evaluate the stress-dependant behavior of soil and granular materials and may yield tensile stresses in granular material, which do not occur in the field. In this study, the pavement system is considered a three-layer system, including the subgrade, granular base, and surface asphalt concrete (AC). It is well known that a comprehensive analysis of flexible pavements should include the stress-dependant behavior of granular base course and the cohesive subgrade, the geostatic force of the pavement itself (gravity load), finite width of the AC pavement, multiple wheel loading at any location of the given domain being analyzed, and partial bonding between the AC and the granular layer. However, none of the structural models or computer programs is capable of incorporating all these parameters in analysis simultaneously. Also, the results may vary among analysts because of the assumptions made in each procedure and the different input assigned by individual analysts. Thus, selection of an appropriate computer program for structural analysis of flexible pavements is a challenge for the pavement engineers. A number of structural analysis programs are available, namely, ILLI-PAVE, MICH-PAVE, DAMA, KENLAYER, ABAQUS, CHEVRON, BISAR, ELSYM5, VESYS, and WESLEA (*6*). Of these, the first five programs have been selected to understand better the accuracy and consistency of the structural responses and the results relative to comparison are presented in this paper.

ILLI-PAVE (*5*) developed at the University of Illinois and MICH-PAVE (*3*) developed at the Michigan State University are the two FE computer programs devoted to the structural analysis of flexible pavements capable of accounting for stress-dependant characterization of granular materials and subgrade soils through an iterative scheme. These two programs consider the pavement as an axisymmetric solid of revolution and divide it into a number of finite elements, each as a section of concentric rings. The computer program DAMA (*2*) was developed at the University of Maryland and was used to obtain the structural design charts included in the ninth edition of the Asphalt Institute's MS-1 manual. The nonlinear characterization of granular materials in DAMA was achieved by using an approximate equation that was obtained from a multiple regression analysis. The computer program KENLAYER (*4*) was developed at the University of Kentucky for flexible pavement design and analysis, and and it can be applied to a multilayered system under stationary or moving multiple wheel loads with each pavement layer being either linear elastic, nonlinear elastic, or viscoelastic. ABAQUS, a 3-D finite-element program, has been used successfully in structural analysis of pavement (*7*) and was used in this study to compare and verify its results with those from the 2-D FE programs (ILLI-PAVE and MICH-PAVE) and those from the MLE programs.

OBJECTIVE

The main objective of this study was to identify and select the most appropriate computer program for the routine structural analysis of flexible pavements. The maximum surface deflection, tensile (radial) strain at the bottom of the AC layer, and compressive strain at the top of subgrade are the most commonly used criteria for pave-

D.-H. Chen, Texas Department of Transportation, 125 E. 11th Street and Bull Creek Road, Suite 37, Austin, Tex. 78701. M. Zaman, J. Laguros, and A. Soltani, School of Engineering and Environmental Science, University of Oklahoma, Norman, Okla. 73019.

ment design (*4,6,8*) and were used in this study as the basis for selecting the most appropriate computer program. The specific tasks of the study were to:

1. Investigate the differences between linear and nonlinear (i.e., the stress-dependant behavior of soil and granular materials) analyses;
2. Investigate the effect of dual-wheel and single-wheel loading on the structural response of pavements (maximum surface deflection, tensile or radial and compressive strains); and
3. Identify a computer program that is most applicable for analysis of flexible pavements, including the influence of such factors as dual-wheel or single-wheel loading and of stress dependency of the associated materials.

COMPUTER PROGRAMS INVESTIGATED

ILLI-PAVE and MICH-PAVE

In general, the FE methods–based procedures can analyze the nonlinear pavement systems more realistically than other structural models by considering the variation of modulus within each layer (*4*). The stress-dependant properties in the form of resilient modulus (RM) and the failure criteria for granular materials and fine-grained soils were incorporated in ILLI-PAVE (*5*) and MICH-PAVE (*3*). The principal stresses in the granular and subgrade layers are modified at the end of each iteration in a way whereby they do not exceed the strength of the materials, as defined by the Mohr-Coulomb failure envelope. However, the validity of this method for modifying the principal stresses to satisfy the Mohr-Coulomb failure criterion is questionable (*4*). Because the stresses in one element are adjusted in this algorithm, they must be redistributed to the adjoining elements. Thus, the adjusted stresses in each element without considering the overall equilibrium do not appear to be theoretically correct (*4*). Another limitation of ILLI-PAVE and MICH-PAVE is the representation of wheel loading by a single interior circular area in which dual-wheel and edge loading cannot be taken into account. Although the actual contact area is not circular, the circular loaded area was assumed to enable the axisymmetric idealization in ILLI-PAVE and MICH-PAVE.

ILLI-PAVE and MICH-PAVE use the same method to characterize granular materials and fine-grained soils and the same Mohr-Coulomb failure criterion to adjust the state of stresses. A major difference between ILLI-PAVE and MICH-PAVE is that MICH-PAVE uses a flexible boundary at a limited depth beneath the subgrade instead of a rigid boundary at a greater depth (50 times the radius of the applied load) below the subgrade. The flexible boundary, which accounts for displacements that occur beneath it, enables the bottom boundary to be placed at any depth below which displacements and stresses are of no interest. The use of the flexible boundary greatly reduces the number of degrees of freedom (DOF) required and thus reduces the computation time. The half-space below the flexible boundary is assumed to be homogeneous and linear elastic. To account for the coupling between the flexible boundary and the finite elements, the stiffness matrix of the half-space, which corresponds to the DOF along the boundary, is obtained from the inverse of the flexibility matrix because of its simplicity (*3*). The radial boundaries of ILLI-PAVE and MICH-PAVE are located at a distance of 12 times and 10 times the radius of the applied load, respectively.

Nonlinear Analysis in MICH-PAVE and ILLI-PAVE

To determine the stresses, strains, and deflections in the pavement system, it is necessary to have a proper constitutive model to address the stress-dependant behavior of granular materials and the subgrade soils. The stress-dependant characteristics of untreated granular materials in Equation 1 is most commonly used by researchers (*4,9–12*), and it is used in MICH-PAVE and ILLI-PAVE. However, it should be noted that one drawback of this model is that the stress path is limited in which the material constants were derived through laboratory compressive stress tests that do not cover an adequate range of stress paths encountered in the field. Brown and Pappin (*13*) also reported that the K-θ model in Equation 1 has been found to fit the laboratory shear strain data well, but it does not handle the volumetric strains properly.

$$RM_2 = K_1\theta^{K2} \tag{1}$$

where K_1 and K_2 are two material constants determined from laboratory testing. The ranges of K_1 and K_2 are well documented (*11,12*). The model is also discussed in the report by Laguros et al. (*9*), who investigated six types of aggregates by using the testing procedures T294-92I and T292-91I suggested by AASHTO in 1991 (*14*) and 1992 (*15*), respectively.

For a cohesive subgrade soil, the RM is expressed through a bilinear relationship, as given in Equations 2 and 3.

for $K_1 > (\sigma_1 - \sigma_3)$

$$RM_3 = K_2 + K_3 [K_1 - \sigma_1 + \sigma_3] \tag{2}$$

and for $K_1 < (\sigma_1 - \sigma_3)$

$$RM_3 = K_2 + K_4[\sigma_1 - \sigma_3 - K_1] \tag{3}$$

in which K_1, K_2, K_3, and K_4 are material constants.

Abaqus

ABAQUS, a 3-D FE program (*1*), has been used successfully in structural analysis of pavement (*7*) and was used here to provide a more realistic representation of a pavement system and to verify the FE programs based on an axisymmetric idealization and the MLE-based programs. An attempt was made to find the difference between the results obtained from the 3-D analysis and those from 2-D FE and MLE programs and to investigate whether the 3-D FE analyses are necessary or even beneficial in the routine design. The 3-D infinite element was used in the vertical direction to reduce the number of elements required in the idealization and thus reduce the computation time. The infinite element was located 152.4 cm below the pavement surface. An example of the mesh used in this study is shown in Figure 1. The mesh presented in Figure 1 has 3,825 nodes and 3,072 elements. The computing time was approximately 1 to 2 hr for a VAX 6520-VMX machine at the University of Oklahoma, not including preparation of input data. In the present study, the geostatic forces due to self-weight were considered and the material models for the granular base and the subgrade layer were assumed to be linear elastic. Also, the equivalent area concept was

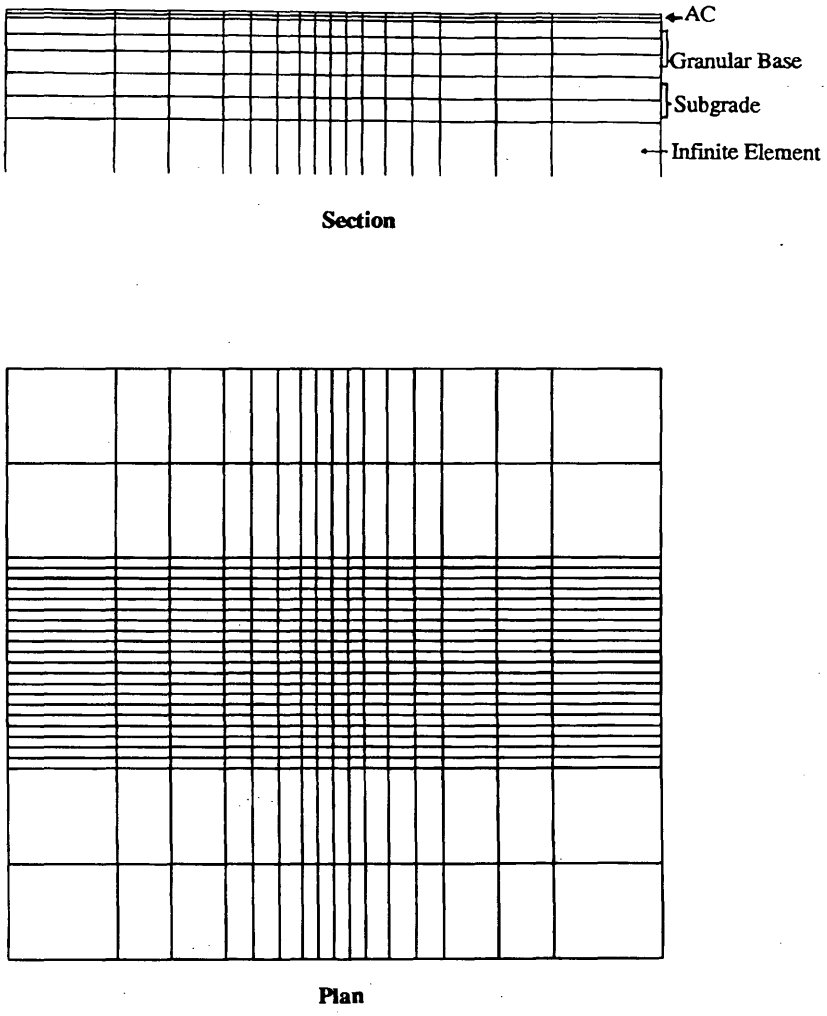

FIGURE 1 Typical FE mesh for ABAQUS.

used to obtain the rectangular loaded area for ABAQUS. For example, a 40.45-kN single loaded radius of 13.589 cm, with a 689-kPa contact pressure, is equivalent to the rectangular loaded area of 29.03 × 20 cm having the same contact pressure of 689 kPa.

MLE Model

MLE- and FE-based models are used extensively in flexible pavement analysis procedures. Overall, the MLE-based procedures are more widely used (*6*). The historical development and general description of various MLEs can be found elsewhere (*3,8*). However, in general, the MLE programs have the following drawbacks:

- They could not model the nonlinear resilient behavior of granular and cohesive soils in a realistic manner.
- The layers are in full contact.
- They may yield tensile stresses in a granular material, which do not occur in the field.

DAMA

The computer program DAMA (*2*) was developed at the University of Maryland for developing the structural design charts used in the ninth edition of the Asphalt Institute's MS-1 manual (*16*). DAMA is an elastic-layered pavement analysis program that can be used to analyze a multilayered elastic pavement structure by cumulative damage techniques induced by single- or dual-wheel loading.

Nonlinear Analysis in DAMA

In DAMA, the subgrade and AC layers are considered linear elastic and the untreated granular base nonlinear elastic. Considering the subgrade a linear elastic material is a reasonable approximation because the variation of modulus from the change of subgrade stresses is usually small and a reasonable subgrade modulus can be assumed. Instead of using a more accurate method of iterations to determine the RM of the granular layer, the following predictive

TABLE 1 Case Study

RM Values	h1=3"	h1=6"	h1=9"
RM1 =250 ksi	Case 1	Case 2	Case 3
RM1 =500 ksi	Case 4	Case 5	Case 6
RM1 =750 ksi	Case 7	Case 8	Case 9

inch = " = 2.54 cm

equation based on multiple regression is used to account for stress dependency (*2,17*):

$$RM_2 = 10.447 h_1^{-0.471} h_2^{-0.041} RM_1^{-0.139} RM_3^{0.287} K_1^{0.868} \quad (4)$$

where

RM_1, RM_2, and RM_3 = moduli of the asphalt layer, granular base, and subgrade, respectively;
h_1 and h_2 = thickness of the asphalt layer and the granular base, respectively; and
K_1 = nonlinear constant in Equation 1 with the exponent K_2 equal to 0.5.

KENLAYER

KENLAYER (*4*) treats the flexible pavement structure as an elastic multilayer system under a circular loaded area. For multiple wheels, the superposition principle is applied directly in KENLAYER for a linear system. In a nonlinear elastic system, the superposition principle is also applied but with a method of successive approximations. First, the system is considered linear, and the stresses due to multiple-wheel loads are superimposed. Based on the stresses computed, a new modulus is determined. Then, the system is considered linear again, and the process is repeated until the modulus converges to a specified tolerance.

Nonlinear Analysis in KENLAYER

Two methods can be applied in KENLAYER to account for the nonlinearity in the granular layers (*4*). In Method 1, the nonlinear granular layer is subdivided into a number of layers and the stresses at the middepth of each layer are used to determine RM. If the horizontal stress, including the geostatic stress, is negative, it is set to zero. This modification helps avoid negative bulk stress. In Method 2, the layers of granular materials are considered a single layer and a point, normally between the upper quarter and the upper third of the layer, and they are selected to compute the RM.

KENLAYER uses the stresses at a single point in each nonlinear layer to compute the modulus of the layer, which is not theoretically correct. As the stresses vary with the radial distance from the load, the modulus should also change with the radial distance and is not uniform throughout the layer. It is important to note that even in nonlinear analysis, both DAMA and KENLAYER consider each horizontal layer having a constant modulus material. However, in the nonlinear analysis in ILLI-PAVE and MICH-PAVE, the moduli vary with elements even for the same horizontal layer.

CASE STUDY

By varying the thickness of the AC layer (h1) and its modulus (RM1), while keeping the thickness and properties of the other layers constant, it is possible to identify a matrix of nine different cases, as given in Table 1. In practice, it is rare to have AC thickness less than 7.62 cm. Also, the effect on the structural response from the variation of the thickness of the granular base layer (h2) and its modulus (RM2) is found to be minimum (*4*). Therefore, they were not included. The material properties used in this case study are presented in Table 2 and Figure 2.

Current FE methodology has advantages over layered-elastic solutions because it provides greater flexibility in realistically modeling the nonlinear response characteristics of granular base layer and subgrade soil. The use of MLE programs and the ILLI-PAVE finite-element program for the development of future AASHTO design guides was recommended (*6*). It was suggested to use the modulus-depth relationship obtained from ILLI-PAVE to establish the various moduli for the MLE, thus capitalizing on the stress-dependent feature of the ILLI-PAVE and the multiple-wheel capability of MLE (*6*). However, in general, the results from MICH-PAVE are more accurate and realistic than those from the ILLI-PAVE because of MICH-PAVE's use of a flexible boundary as apposed to the rigid boundary in ILLI-PAVE (*4*). Furthermore, a study by Harichandran et al. (*18*) found the use of an equivalent layer resilient modulus (ELRM) (obtained from MICH-PAVE) for each layer by averaging the moduli of the finite elements in the layer that lie within an assumed 2:1 load distribution zone can be adequately used to reflect the stress-dependent variation of the modulus within the layer. Hence, MICH-PAVE was

TABLE 2 Material Constants Used

Layer	Poisson's ratio	Unit Weight (pcf)	k0	k1	k2	k3	k4	C (psi)	ϕ (degree)
AC	0.35	150	0.7						
Base	0.38	140	0.6	5000	0.5			0	45
Soil	0.45	115	0.8	5.2	3021	1110	-178	6	0

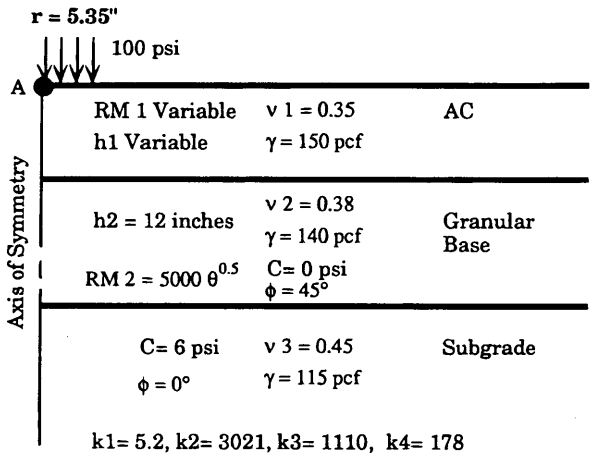

FIGURE 2 Problem description (single wheel).

selected in this study to compute ELRM. The computed ELRM for the aforementioned nine cases are given in Table 3, wherein the values were obtained by fixing the flexible boundary at 114.3 cm below the surface of the subgrade soil. Harichandran et al. (*3*) recommended that the position for flexible boundary is at least 91.44 cm below the surface of the subgrade soil. The ELRMs for subgrade soil are the same (60 MPa or 8,694 psi), indicating that treating the subgrade as a linear elastic medium is a fair assumption.

COMPARISON OF RESULTS FOR LINEAR ANALYSIS

Contact Stress (Natural Boundary Condition)

For linear analysis, a comparison of vertical stress obtained from different computer programs at Point A in Figure 2 is presented in Table 4. The ELRM values obtained from MICH-PAVE, as given in Table 3, were used as the moduli in the granular layer and subgrade soil. From Table 4, it can be inferred that only DAMA and MICH-PAVE satisfy the natural boundary condition in which the vertical stresses equal the imposed contact pressure 689 kPa (100 psi).

Maximum Surface Deflection, Tensile Strain, and Compressive Strain

A comparison of the maximum surface deflection, tensile (radial) strain at the bottom of the AC layer and compressive strain at the top of the subgrade soil obtained from different computer programs is illustrated in Table 5A, B, and C. It was reported that the conventional analyses may overestimate the tensile (radial) strain at the bottom of AC layer when comparing it with 3-D linear elastic FE analysis (*19*). This phenomenon is confirmed in this study. In fact, even the 2-D axisymmetric FE models (ILLI-PAVE and MICH-PAVE) overestimate the tensile (radial) strain at the bottom of the AC layer. Examination of Table 5A, B, and C indicates the following:

- In all cases, ILLI-PAVE gave the lowest maximum surface deflection due to the fixed boundary at a certain depth.
- In most cases (seven out of nine), KENLAYER yielded the highest maximum surface deflections.
- In all cases, ABAQUS gave the lowest tensile strain.
- In all cases, the tensile strains obtained from DAMA and KENLAYER had close agreement, and the latter gave the highest tensile strain.
- In all cases, DAMA provided the highest compressive strain.
- In all cases, the maximum surface deflections obtained from ABAQUS had a close agreement with those obtained from MICH-PAVE.
- The variability of tensile strain was lower than that in compressive strain.

TABLE 3 ELRM from MICH-PAVE for Cases 1 to 9

Layer	ELRM h1=3" (psi)	ELRM h1=6" (psi)	ELRM h1=9" (psi)
Case	(1)	(2)	(3)
AC	250000	250000	250000
Base	25630	17464	13745
Soil	8694	8694	8694
Case	(4)	(5)	(6)
AC	500000	500000	500000
Base	23317	14770	12860
Soil	8694	8694	8694
Case	(7)	(8)	(9)
AC	750000	750000	750000
Base	21598	13922	12462
Soil	8694	8694	8694

1 psi = 6.89 kPa; inch = 2.54 cm

TABLE 4 Comparison of Vertical (Compressive) Stresses of Figure 2 by Using Linear Analysis

Cases	Programs	Vertical Stress (psi)
Case 4	DAMA	100
	ILLIPAVE	87
	KENLAYER	140
	MICHPAVE	100
	ABAQUS	57
Case 5	DAMA	100
	ILLIPAVE	91
	KENLAYER	100
	MICHPAVE	100
	ABAQUS	61
Case 6	DAMA	100
	ILLIPAVE	98
	KENLAYER	74
	MICHPAVE	100
	ABAQUS	62

1 psi = 6.89 kPa

TABLE 5 Comparison [by Using Nonlinear (NL) and Linear (L) Analysis] of Maximum Surface Deflections (milli in.) at Axis of Symmetry (*top*), Compressive Strains (microstrain) at Top of Subgrade (*middle*), and Tensile (Radial) Strains (microstrain) at Bottom of AC Layer (*bottom*)

		DAMA		ILLI		KENL		MICH		ABAQ
RM1	h1	NL	L	NL	L	NL	L	NL	L	L
250	3"	37.69	35.35	42.93	29.98	42.56	35.79	38.11	33.58	32.90
(ksi)	6"	27.84	27.16	27.67	21.96	39.26	27.41	26.87	25.39	26.28
	9"	21.55	21.38	20.41	16.96	26.67	21.70	20.24	19.98	21.00
500	3"	34.58	32.95	36.58	26.57	38.31	32.91	34.28	30.57	29.50
(ksi)	6"	23.30	19.08	21.57	17.59	30.29	23.12	21.74	21.24	21.92
	9"	17.13	15.46	15.60	12.79	20.09	16.81	16.05	16.05	16.29
750	3"	32.48	31.08	32.43	24.35	35.48	31.16	31.64	28.68	27.54
(ksi)	6"	20.84	20.76	18.51	15.13	26.34	20.56	19.14	18.83	19.29
	9"	14.99	14.84	13.52	10.91	17.21	14.79	14.41	14.33	13.93

		DAMA		ILLI		KENL		MICH		ABAQ
RM1	h1	NL	L	NL	L	NL	L	NL	L	L
250	3"	1004	954	1334	757	828	698	944	783	663
(ksi)	6"	587	582	623	451	623	478	507	465	464
	9"	359	360	343	279	275	326	274	269	311
500	3"	902	868	1034	660	745	651	815	699	603
(ksi)	6"	452	406	418	332	460	397	356	344	372
	9"	250	256	211	188	261	242	178	177	226
750	3"	825	804	867	589	676	617	721	638	560
(ksi)	6"	377	377	317	266	384	341	280	275	310
	9"	197	200	164	145	211	198	136	134	182

		DAMA		ILLI		KENL		MICH		ABAQ
RM1	h1	NL	L	NL	L	NL	L	NL	L	L
250	3"	604	543	537	502	622	543	489	527	351
(ksi)	6"	418	404	394	366	464	404	370	367	280
	9"	262	259	249	239	369	258	225	224	185
500	3"	481	445	442	399	484	444	416	423	286
(ksi)	6"	275	207	252	240	291	272	243	241	184
	9"	161	137	147	143	165	158	132	132	117
750	3"	400	378	368	333	395	378	358	357	214
(ksi)	6"	207	207	186	178	218	206	181	180	138
	9"	118	116	104	102	121	117	94	94	81

- As h1 and RM1 increased, the difference in maximum surface deflections, tensile strains, and compressive strains among the programs decreased.
- Among all programs investigated in this study, the MICH-PAVE gave the intermediate maximum surface values for deflection, compressive strain, and tensile strain.

Deflection Profile

The surface deflection profiles for Cases 4, 5, and 6, respectively, are given in Figure 3. It was observed that ILLI-PAVE gives the lowest surface deflection along the radial direction. MICH-PAVE and ABAQUS provided the closest deflection profiles for all three

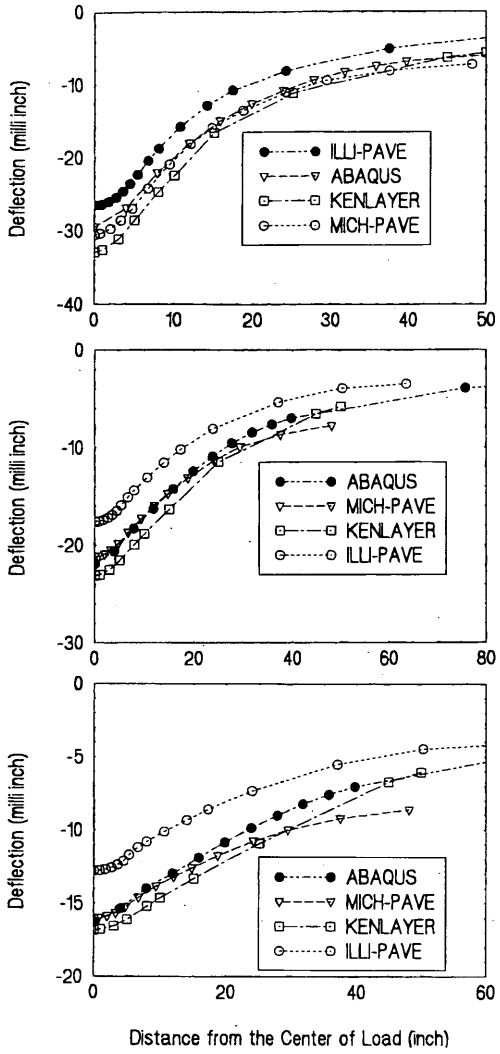

FIGURE 3 Comparison of surface deflection profiles from various computer programs for L analysis: Case 4—RM1 = 500 ksi, h1 = 3 in. (*top*); Case 5—RM1 = 500 ksi, h1 = 6 in. (*middle*); Case 6—RM1 = 500 ksi, h1 = 9 in. (*bottom*).

cases investigated. The computer program DAMA did not give the deflection along a radial direction; consequently, it was not included in the comparison.

COMPARISON OF RESULTS FOR NONLINEAR ANALYSES

Contact Stress (Natural Boundary Condition)

Similar to linear analysis, only DAMA and MICH-PAVE satisfy the natural boundary conditions in which the vertical stresses equal the imposed contact pressure of 689 kPa, as shown in Table 6. Note that in the present study, linear elastic idealization was used in ABAQUS's analysis and thus it was not included in the comparison.

TABLE 6 Comparison of Vertical (Compressive) Stresses at Point A of Figure 2 by Using NL Analysis

Cases	Programs	Vertical Stress (psi)
Case 4	DAMA	100
	ILLIPAVE	89
	KENLAYER	130
	MICHPAVE	100
Case 5	DAMA	100
	ILLIPAVE	91
	KENLAYER	74
	MICHPAVE	100
Case 6	DAMA	100
	ILLIPAVE	98
	KENLAYER	74
	MICHPAVE	100

1 psi = 6.89 kPa

Maximum Surface Deflection, Tensile Strain, and Compressive Strain

The maximum surface deflection, tensile (radial) strain at the bottom of the AC layer, and compressive strain at the top of the subgrade from different computer programs for nonlinear analyses are compared in Table 5, indicating a wide dissimilarity in results obtained from these programs. In view of Table 5, the following observations are made:

- In most cases (eight out of nine), KENLAYER gave the highest maximum surface deflections.
- In most cases (eight out of nine), the maximum surface deflections from DAMA, ILLI-PAVE, and MICH-PAVE had a close agreement.
- In all cases, the compressive strains from DAMA and ILLI-PAVE had a close agreement, and DAMA gave higher values compared with MICH-PAVE.
- In all cases, KENLAYER yielded the highest tensile strain.
- In all cases, MICH-PAVE gave the lowest tensile strain.
- Among all programs investigated in this study, DAMA provided the intermediate maximum surface deflections and compressive and tensile strains.

COMPARISON OF LINEAR AND NONLINEAR ANALYSIS

Comparison of Maximum Surface Deflection, Tensile Strains, and Compressive Strains Between Linear and Nonlinear Analyses in MICH-PAVE

It is noteworthy to identify the differences between the results obtained from the nonlinear analysis and those from the linear analysis (using the ELRM computed from nonlinear analysis) using the same computer program (MICH-PAVE). A comparison of maximum surface deflection, compressive strain at the bottom of the AC layer, and tensile (radial) strain at the top of the subgrade is presented in Table 7. The differences between nonlinear and linear

TABLE 7 Comparison of Maximum Surface Deflections, Tensile (Radial) Strains at Bottom of AC Layer, and Compressive Strains at Top of Subgrade for MICH-PAVE by Using NL and L Analysis

Cases	Conditions	DEF. (milli inch)	C (microstrain)	T
Case 1	Nonlinear	38.11	944	489
	Linear	33.58	783	527
	Difference (%)	13.5	20.6	7.2
Case 2	Nonlinear	26.87	507	370
	Linear	25.39	465	367
	Difference (%)	5.8	9.0	0.8
Case 3	Nonlinear	20.24	274	225
	Linear	19.98	269	224
	Difference (%)	1.3	1.9	0.4
Case 4	Nonlinear	34.28	815	416
	Linear	30.57	699	423
	Difference (%)	13.1	16.6	1.7
Case 5	Nonlinear	21.74	356	243
	Linear	21.24	344	241
	Difference (%)	2.4	3.5	0.8
Case 6	Nonlinear	16.16	178	132
	Linear	16.05	177	132
	Difference (%)	0.7	0.6	0
Case 7	Nonlinear	31.64	721	358
	Linear	28.68	638	357
	Difference (%)	10.3	13.0	0.3
Case 8	Nonlinear	19.14	280	181
	Linear	18.83	275	180
	Difference (%)	1.6	1.8	0.6
Case 9	Nonlinear	14.41	136	94
	Linear	14.33	134	94
	Difference (%)	0.6	1.5	0

inch = 2.54 cm

analysis are also given in this table. Table 7 illustrates that, as RM1 and h1 increases, the difference between the results from the nonlinear and linear analyses decreases. The maximum difference of 20.6 percent for compressive strains for Case 1 (h1 = 7.62 cm) indicates that the ELRM could be used satisfactorily to represent the stress-dependant behavior of the materials within each layer. Because the stress-dependant behavior of granular base and subgrade soil could be approximated by the use of ELRM, it may also be approximated by Equation 4. This explains why the results for nonlinear analysis from DAMA, MICH-PAVE, and ILLI-PAVE had a close agreement.

Comparison of Surface Deflection Profile Between Linear and Nonlinear Analyses by MICH-PAVE

The surface deflection profiles for the nine cases, using the MICH-PAVE for nonlinear analysis and linear analysis, were obtained and are presented in Figure 4. In view of these figures, a similar trend is

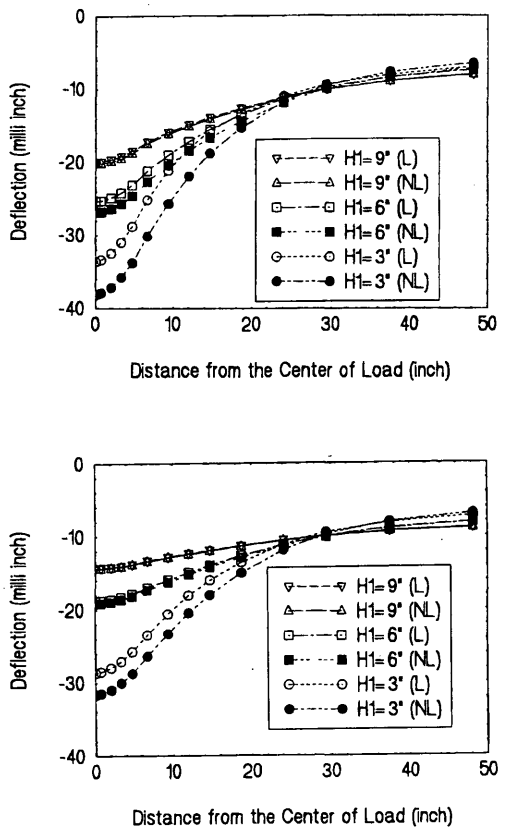

FIGURE 4 Comparison of surface deflection profiles between NL and L analysis from MICH-PAVE: Cases 1 to 3—RM1 = 250 ksi, h1 = 3, 6, 9 in. (*top*); Cases 7 to 9—RM1 = 750 ksi, h1 = 3, 6, 9 in. (*bottom*).

observed for the surface deflection profiles and those for maximum surface deflection and tensile and compressive strains (i.e., as RM1 and h1 increase, the difference between nonlinear and linear analysis decreases, as expected).

Comparison of Surface Deflection Profile Between Linear and Nonlinear Analysis

The surface deflection profiles obtained from the linear analysis using ILLI-PAVE, ABAQUS, and MICH-PAVE and from the nonlinear analysis using ILLI-PAVE and MICH-PAVE were grouped and are presented in Figure 5. Only Cases 4, 5, and 6 were investigated here because an AC modulus of 3 445 MPa (500 ksi) is most commonly used in design, and the effect of AC thickness on the structural response is more significant than the effect due to the AC modulus. It was observed that as h1 increases, the difference in the deflection based on ABAQUS (linear), MICH-PAVE (linear and nonlinear), and ILLI-PAVE (nonlinear) decreases. In fact, the surface deflection profiles for ABAQUS (linear) and MICH-PAVE (linear and nonlinear) for Case 6 are approximately the same [Figure 5 (*bottom*)], indicating that when h1 is thick (22.86 cm = 9 in.) the nonlinear behavior is less dominant. This observation

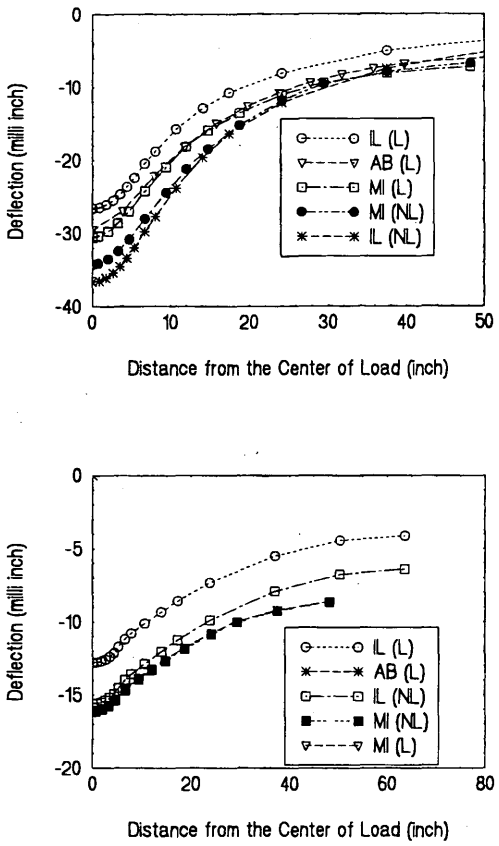

FIGURE 5 Comparison of surface deflection profiles between NL and L analysis among programs: Case 4—RM1 = 500 ksi, h1 = 3 in. (*top*); Case 6—RM1 = 500 ksi, h1 = 9 in. (*bottom*).

supports the use of the ELRM concept in MICH-PAVE for satisfactorily computing the surface deflections.

Comparison of Maximum Surface Deflection, Tensile Strain, and Compressive Strain Between Linear and Nonlinear Analyses

A comparison of nonlinear and linear analyses for maximum surface deflection, tensile strain, and compressive strain is presented in Table 5. A close examination of the results presented indicates the following:

- By using the same program, as h1 and RM1 increase, the difference between the linear and the nonlinear analysis decreases.
- For both the nonlinear and linear analyses, as h1 and RM1 increase, the difference in results obtained from the different programs decreases.
- As expected, the nonlinear analysis gave higher values of maximum surface deflection, tensile strain, and compressive strain than those from linear analysis.
- In terms of increment ratios, to reduce the level of maximum surface deflection, tensile strain, and compressive strain more effectively is to increase the thickness of h1 than to increase the modulus of RM1.

DUAL WHEEL VERSUS SINGLE WHEEL

The three programs—ABAQUS, DAMA, and KENLAYER—investigated in this study can consider the effect of dual wheel on the pavement structure, as shown in Figure 6. The moduli of granular layer and subgrade are the ELRM values obtained from MICH-PAVE, as given in Table 3. The comparison of dual-wheel linear analysis among these three programs is presented in Table 8 and the following observations are made:

- In all three cases, ABAQUS gave the lowest tensile strain.
- In all three cases, DAMA provided the lowest compressive strain.
- In all three cases, DAMA yielded the lowest and KENLAYER gave the highest maximum surface deflection, respectively.
- DAMA gave the intermediate tensile strains.

Because DAMA gave the intermediate surface deflection, compressive strain, and tensile strain in the nonlinear analysis, it was decided to study the difference in results for the single-wheel and dual-wheel idealization for both the linear and nonlinear analyses. The differences between the single-wheel nonlinear and the dual-wheel nonlinear analysis were computed and are given in Table 9. The following observations are made:

- Single-wheel nonlinear analysis gave the highest maximum surface deflection and compressive and tensile strains.
- Dual-wheel linear analysis gave the lowest maximum surface deflection and compressive and tensile strains.
- As h1 increases, the difference between single-wheel nonlinear and dual-wheel nonlinear analysis decreases for both the maximum surface deflection and compressive strain but not for the tensile strain.
- A maximum difference of 40.5 percent in compressive strain was observed between the single-wheel and dual-wheel nonlinear analyses, when h1 was equal to 3 in.

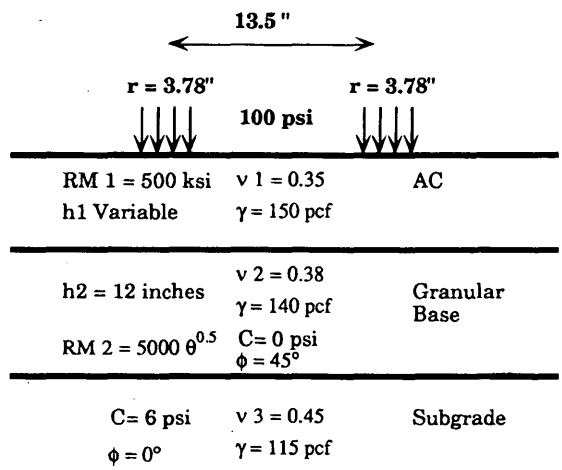

FIGURE 6 Problem description (dual wheel).

TABLE 8 Comparison of Maximum Surface Deflections at Center of Dual Wheel, Tensile (Radial) Strains at Bottom of AC Layer, and Compressive Strains at Top of Subgrade by Using L Analysis

Cases	Programs	DEF. (milli inch)	C (microstrain)	T
Case 4	DAMA	18.38	383	183
	KENLAYER	26.76	513	296
	ABAQUS	23.38	484	175
Case 5	DAMA	17.2	320	166
	KENLAYER	20.78	350	212
	ABAQUS	19.61	335	128
Case 6	DAMA	14.53	215	111
	KENLAYER	15.67	222	133
	ABAQUS	14.85	210	84

inch = 2.54 cm

ASSESSMENT OF NUMBER OF VARIABLES AND TESTING TIME

Some of the variables in the programs may be used only for certain problems. For example, KENLAYER can consider, among others, multiple wheel loads and viscoelastic analysis. Thus, when comparing programs it is better to consider the number of variables required as input for the same problem. The same problem in Figure 2 was selected for this purpose. Table 10 shows a comparison of the number of variables required as input for the five programs investigated. It was observed that DAMA required the least input variables, followed by MICH-PAVE, and ABAQUS needed the most input variables.

To compare the running time for the computer programs considered, an example (Case 4, RM1 = 3445 MPa, h1 = 7.62 cm) was used. The approximate time to run this example is shown in Table 10. A 386 PC (25 MHz) with a math coprocessor was used in this study (except for ABAQUS). Note that the input preparation time was not included and only the running time is given in Table 10. The data in Table 10 show that the running time for KENLAYER is the least, followed by MICH-PAVE, and the 3-D FE general-purpose program ABAQUS required maximum time, as expected.

CONCLUSIONS

Two 2-D axisymmetric FE programs (ILLI-PAVE and MICH-PAVE), one 3-D FE program (ABAQUS), and two multilayered elastic-based programs (DAMA and KENLAYER) were reviewed, evaluated, and compared in this study. The contact stress (nature boundary condition), maximum surface deflection, tensile (radial) strain, and compressive strain were used as the evaluation criteria. The effects from treatment of dual-wheel and single-wheel loading and linear and nonlinear idealization on pavement structure responses were investigated. From the analysis of the results presented in the preceding sections, the following observations and conclusions were made:

- For both linear and nonlinear analyses, only DAMA and MICH-PAVE satisfied the natural boundary condition in which the vertical stresses equal the imposed contact pressure of 689 kPa.
- For linear analysis, MICH-PAVE gave the intermediate maximum surface deflection, compressive strain, and tensile strain.
- For linear analysis, ABAQUS gave the lowest tensile strain, as reported in the literature.

TABLE 9 Comparison of Single and Dual Wheel for DAMA by Using L and NL Analysis

Cases	Programs	DEF. (milli inch)	C (microstrain)	T
Case 4	Single-wheel (L)	32.95	868	445
	Dual-wheel (L)	18.38	383	183
	Single-wheel (NL)	34.58	902	481
	Dual-wheel (NL)	27.89	642	402
	difference* (%)	**24.0**	**40.5**	**19.7**
Case 5	Single-wheel (L)	19.08	406	207
	Dual-wheel (L)	17.2	320	166
	Single-wheel (NL)	23.3	452	275
	Dual-wheel (NL)	20.59	360	222
	difference (%)	**13.16**	**25.6**	**23.9**
Case 6	Single-wheel (L)	15.46	256	137
	Dual-wheel (L)	14.53	215	111
	Single-wheel (NL)	17.13	250	161
	Dual-wheel (NL)	16.0	210	130
	difference (%)	**7.1**	**19.0**	**23.8**

inch = 2.54 cm

*
The computed differences were the differences between Single-wheel (NL) and Dual-wheel (NL)

TABLE 10 Comparison of Number of Variables Required as Input and Testing Time

Program	DAMA	ILLI-PAVE	KENLAYER	MICH-PAVE	ABAQUS
Vaiables	20	34	47	29	more than 50
Running Time	36 Sec. 386 PC	332 Sec. 386 PC	21 Sec. 386 PC	33 Sec. 386 PC	519 Sec. (CPU time for VAX6520 Computer)

- The surface profiles from ABAQUS and MICH-PAVE had a close agreement.
- For nonlinear analysis, DAMA gave the intermediate maximum surface deflections and compressive and tensile strains.
- As h1 and RM1 increase, the difference in results between linear and nonlinear analyses decreases.
- When h1 is thick [22.86 cm (9 in.)], ELRMs from MICH-PAVE and Equation 4 in DAMA were used satisfactorily to represent stress-dependent behavior of the materials within each layer.
- The results from the 3-D FE program ABAQUS indicate that the surface profiles from ABAQUS and the 2-D axisymmetric FE program MICH-PAVE had a close agreement, but the results from ABAQUS yield the lowest tensile strain compared with other programs. Also, the computing time is approximately 1 to 2 hr for a VAX 6520-VMX machine. Thus, for a thin AC section, ABAQUS may be used for verification purpose but not for routine pavement structural analysis.
- In terms of increment ratios, to reduce the level of maximum surface deflection, tensile strain, and compressive strain more effectively, it is necessary to increase the thickness of h1 instead of RM1.
- The dual-wheel loading always gave less maximum surface deflection, tensile strain, and compressive strain than those obtained from single-wheel loading.
- The maximum difference between single-wheel and dual-wheel analyses was found to be 40.5 percent when h1 is 7.62 cm (3 in.). As h1 increases, the difference in results between single-wheel and dual-wheel analyses decreases.
- Because DAMA gave the intermediate maximum surface deflection, compressive strain, and tensile strain in nonlinear analysis; satisfied the natural boundary condition; required the least input variables; and has the capacity to consider dual-wheel loading, it suggests that DAMA is probably the best one to use in routine pavement design.

ACKNOWLEDGMENTS

Financial support for this study was provided by FHWA in cooperation with the Oklahoma Department of Transportation and by the Oklahoma Center for Advancement of Technology and Science.

REFERENCES

1. ABAQUS, Finite Element Computer Program. Version 5.2. Hibbitt, Karlsson, and Sorensen, Inc., Pawtucket, N.Y., 1992.
2. Computer Program DAMA (CP-1/1991 Revision)—Pavement Structural Analysis Using Multi-Layered Elastic Theory. Asphalt Institute, Lexington, Ky., 1991.
3. Harichandran, R. S., M. S. Yeh, and G. Y. Baladi. *MICH-PAVE User's Manual.* Final Report, FHWA-MI-RD-89-032. Department of Civil and Environmental Engineering, Michigan State University, East Lansing 1989.
4. Huang, Y. H. *Pavement Analysis and Design.* Prentice-Hall, Englewood Cliffs, N.J., 1993.
5. *ILLI-PAVE PC Version USER'S MANUAL.* NCHRP 1-26. Transportation Faculties Group, University of Illinois at Urbana-Champaign, 1990.
6. Thompson, M., et al. *Calibrated Mechanistic Structural Analysis Procedures for Pavement.* NCHRP Report 1-26. 1992.
7. Zaghloul, S., and T. White. Use a Three-Dimensional, Dynamic Finite Element Program for Analysis of Flexible Pavement. In *Transportation Research Record 1388*, TRB, National Research Council, Washington, D.C., 1993, pp. 60–69.
8. Monismith, C. L. Analytically Based Asphalt Pavement Design and Rehabilitation: Theory to Practice, 1962–1992. In *Transportation Research Record 1354,* TRB, National Research Council, Washington, D.C., 1992, pp. 5–26.
9. Laguros, J., M. M. Zaman, and D.-H. Chen. *Resilient Modulus of Select Aggregate Bases and Their Correlations With Other Engineering Properties.* Report 2189, ORA 125-6073. School of Civil Engineering and Environmental Science, University of Oklahoma, Norman, 1993.
10. Zaman, M. M., J. Laguros, and R. Danayak. Assessment of Resilient Modulus Testing Methods and Their Application to Design of Pavements. Report FHWA/OK 91(08). University of Oklahoma, Norman, 1991.
11. Zaman, M. M., D.-H. Chen, and J. G. Laguros, Resilient Modulus Testing of Granular Material and Their Correlations With Other Engineering Properties. *Journal of Transportation Engineering*, ASCE, Vol. 120, No. 6, November–December 1994, pp. 967–988.
12. Chen, D.-H., M. M. Zaman, and J. G. Laguros. Characterization of Base/Subbase Materials Under Repetitive Loading. *Journal of Testing and Evaluation*, ASTM, Vol. 23, No. 3, May 1995, pp. 180–188.
13. Brown, S. F., and J. W. Pappin. Analysis of Pavements With Granular Bases. In *Transportation Research Record 810*, TRB, National Research Council, Washington, D.C., 1981, pp. 17–23.
14. *AASHTO Designation T292-91I: Interim Method of Test for Resilient Modulus of Subgrade Soils and Untreated Base/Subbase Materials.* AASHTO, Washington, D.C., 1991.
15. *AASHTO Designation T294-92I: Interim Method of Test for Resilient Modulus of Unbound Granular Base/Subbase Materials and Subgrade Soils-SHRP Protocol P46.* AASHTO, Washington, D.C., 1992.
16. *Thickness Design—Asphalt Pavements for Highways and Streets,* Manual Series 1 (MS-1), Asphalt Institute, Lexington, Ky., 1991.
17. Witczak, M. W., and B. E. Smith. Prediction of Equivalent Granular Base Moduli Incorporating Stress Dependent Behavior in Flexible Pavements. *Transportation Journal*, ASCE, Vol. 107, No. TE6, 1981, pp. 635–652.
18. Harichandran, R. S., M. S. Yeh, and G. Y. Baladi. MICH-PAVE: A Nonlinear Finite Element Program for Analysis of Flexible Pavements. In *Transportation Research Record 1286*, TRB, National Research Council, Washington, D.C., 1990, pp. 123–131.
19. Saraf, C., K. Marshek, H. Chen, R. Connell, and W. R. Hudson. The Effect of Truck Tire Contact Pressure Distribution on the Design of Flexible Pavements. *Proc., 6th International Conference on Structure Design of Asphalt Pavements,* Vol. 1, Nottingham, England, 1987, pp. 180–190.

Publication of this paper sponsored by Committee on Flexible Pavement Design.